COMPUTATIONAL MODELLING STUDIES OF PRECIOUS MIXED METALS SULPHIDES

by

MAMOGO ADOLPHINA MASENYA

RESEARCH DISSERTATION

Submitted in fulfillment of the requirements for the degree of

MASTER OF SCIENCE

in

Physics

in the

FACULTY OF SCIENCES & AGRICULTURE

(School of Physical & Mineral Sciences)

at the

UNIVERSITY OF LIMPOPO (Turfloop Campus)

SUPERVISOR: Prof. P.E. Ngoepe

2016

Declaration

I declare that the dissertation hereby submitted to the University of Limpopo (Turfloop Campus) for the degree of Master of Science in Physics has not previously been submitted by me for a degree at this or any other university, that it is my own work both in design and execution, and that all material contained herein has been duly acknowledged.

Ms. M. A. MASENYA **Date**

Dedications

This work is dedicated to my mother Esther Masenya, my brother Peter Seabela and my son Hlompho Masenya.

Acknowledgements

I would like to take this time and express my deepest gratitude to my supervisor Prof P.E. Ngoepe, who undertook to act as my supervisor despite his many other academic and professional commitments. His wisdom, knowledge and commitment to the highest standards inspired and motivated me. I would like to thank the Materials Modelling Centre members for their inputs and the support they have given me throughout the years. I would also like to acknowledge National Research Foundation for financial assistance.

I would like to thank God for the wisdom and perseverance that he has been bestowed upon me during this research project, and indeed, throughout my life: "I can do everything through him who gave me strength. My fellow brothers and sisters in Christ for their continual support and encouragement throughout the years.

Lastly I would like to thank Khomotso Maenetja and Ruth Masenya for their continuous support they showed me throughout the years of my study.

Abstract

The stabilities of PtS to PdS and PdS to PtS were investigated using density functional theory within the generalized gradient approximation. Their structural, electronic and mechanical properties were determined to show their stability and the effect of pressure on different compositions. We found good correlation of calculations with available experimental data. The lattice parameters were observed to fluctuate with increasing concentration for both systems. Furthermore, heats of formation were calculated to determine the relative structural stability of the systems. They predict that the most stable structure is $Pd_{50}S_{50}$ $P4_2/mmc$ and $Pt_{25}Pd_{25}S_{50}$ $P4_2/mmc$ being the least stable. $Pd_{12.5}Pt_{37.5}S_{50}$ $P4_2/m$ is the most stable and $Pd_{50}S_{50}$ $P4_2/m$ being the least stable structure. The $Pt_{37.5}Pd_{12.5}S_{50}$ P_1 was said to be the most stable structure and $Pd_{50}S_{50}$ P_1 being the least stable. The phonon dispersion calculations show that $Pt_{50}S_{50}$ $P4_2/mmc$, $Pd_{50}S_{50}$ $P4_2/mmc$, $Pd_{12.5}Pt_{37.5}S_{50}$ $P4_2/m$ and $Pt_{50}S_{50}$ P_1 (derived from $P4_2/mmc$) are mechanically stable, consistent with calculated elastic constants. The $Pt_{25}Pd_{25}S_{50}$ $P4_2/mmc$ show soft modes, which are due to vibrations of Pt and Pd atoms in the x - y plane which suggests the instability of the structure, in agreement with C_{66} being negative, and consistent with heats of formation. The lattice parameters decreased steadily with increasing pressure. An anomaly was observed in $Pt_{50}S_{50}$ P_1 (derived from $P4_2/mmc$), where the c lattice parameter was found to increase with increasing pressure. The electronic density of states (DOS) were performed on all compositions. The DOS were subjected to pressure and it was generally noted that the band gap increases with increasing pressure. It was observed that the smaller the band gap, the more stable the structure. Furthermore, phonon dispersions under pressure show that compounds with the $P4_2/mmc$ and P_1 (from $P4_2/mmc$) symmetries display the mixing of lower and upper energy bands at pressures above 30 GPa.

Table of contents

List of figures

List of tables

Chapter 1

Introduction

1.1. General introduction

Precious materials like cooperite (PtS), braggite (Pt, Pd, Ni)S, vysotskite (PdS) and sperrylite ($PtAs_2$) are the most important sources of platinum in the world's largest deposits of platinum-group minerals (PGMs) [1, 2]. Cooperite, braggite, and vysotskite are the only sulphide minerals with ideal compositions in the system containing Pt and Pd [3]. The members of cooperite, sperrylite and braggite series belong to the most abundant PGMs in many platinum group elements (PGE) deposits such as the Merensky reef, UG2 chromitite layer, Bushveld Igneous Complex [4]. The Merensky Reef is the rock in North of South Africa which contains the most of Platinum Group Metals [5]. The rock is situated in Bushveld Igneous Complex. Geologically, platinum is found in thin layers of metal ores called sulfides. Platinum sulphide is a platinum bearing mineral, as such, its properties relevant to platinum extraction are of interest to the mining industry, especially as economic mineral deposits become increasingly difficult to discover [6]. Pt and Pd sulphides are of great importance in the mining industries for extraction of useful precious minerals. In particular, their structural, electronic, magnetic, optical and thermodynamic properties are of interest since these affect ore formation, mineral processing and environmental mineralogy [7]. Furthermore, these sulphides play an important role as catalysts in the petroleum refining industry, and are used as active components in automotive industry [8, 9]. They represent the only known class of stable catalytically active phases for strongly sulpho-reductive hydroprocessing conditions and are usually active ingredients in automotive catalysts. PGMs, together with gold and silver form the family of precious metals [10]. They are used in chemotherapy, particularly to fight leukemia. These PGMs are an excellent hydrogenation and dehydrogenation

catalyst, they can be alloyed and used in jewellery [4]. The metal is used in dentistry, electrical contacts and in making surgical instruments.

1.2. Structural Aspects

The crystal structure of PtS is tetragonal with space group $P4_2/mmc$ (131), with the lattice parameters a = 3.470 Å, c = 6.100 Å and α = β = γ = 90°. The positions of the atoms are generated by Pt(2c): $(0, \frac{1}{2}, 0)$, $(\frac{1}{2}, 0, \frac{1}{2})$, S(2e): $(0, 0, \frac{1}{4})$, $(0, 0, \frac{3}{4})$ [11]. In cooperite, platinum is coordinated by four sulphurs in a square planar arrangement. The sulphurs are tetrahedrally coordinated by four platinum ions [6]. Braggite (Pt, Pd, Ni)S is found significantly varying metal rations (all with Pt, Ni > Pd) in the ore deposit [3]. It was reported by Bannister [11] as being isomorphus with the structure of palladium sulphide. The mineral braggite has a composition close to PdS (Pd > Pt, Ni) was reported by Genkin and Zvyagintsev [12] to be iso-structural with PdS and vysotskite.

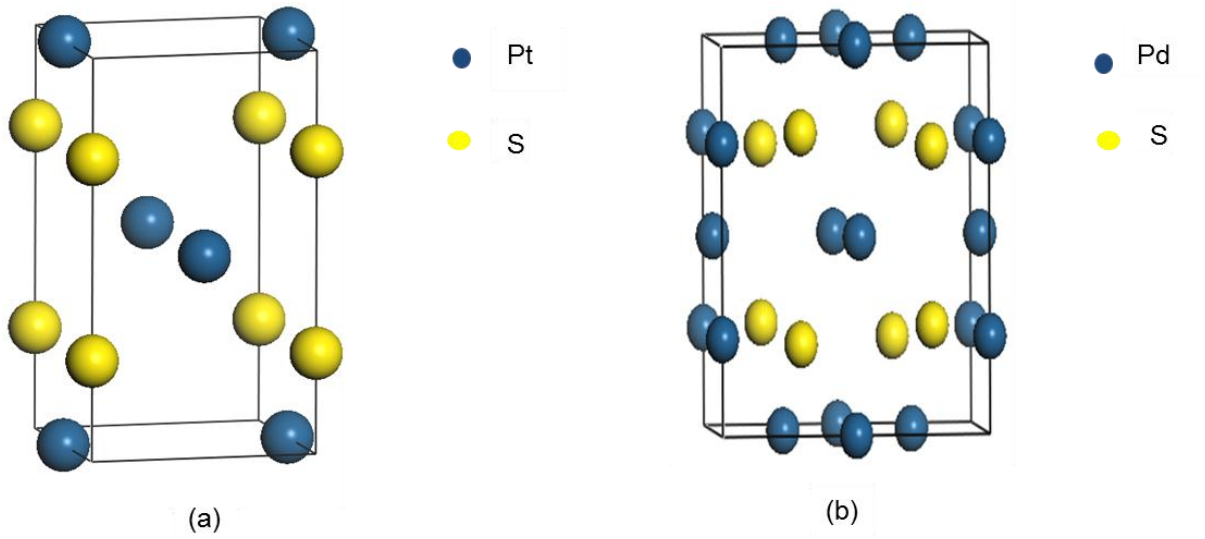

Figure 1.1. The crystal structure of (a) PtS with space group $P4_2/mmc$ and (b) PdS with space group $P4_2/m$

The crystal structure of PdS is tetragonal with a space group $P4_2/m$, it has lattice parameters a = 6.429 Å, c = 6.611 Å and α = β = γ = 90^o. Pd(1) atom sits in a slightly ruffled square of S atoms, while a rectangular plane coordinates atom Pd(2) and atom Pd(3) are both bend out of the plane and coordinated rectangularly. Four Pd atoms in a distorted tetrahedron coordinate each S atom [13].

1.3. Review of Properties

1.3.1. Structural Properties

Louis et al (1978) reported the detailed mineralogical analyses of cooperite, braggite and vysotskite. The identity of cooperite (PtS; $P4_2/mmc$), braggite (Pt, Pd)S and vysotskite (PdS) to be nickeloan members of an isormophous solid-solution series (Pd, Pt)S ($P4_2/m$). Cooperite approaches an ideal Ni-free composition more closely than braggite and vysotskite do and no difficulty or uncertainty clouds its identity. From their analyses, it appears that braggite and vysotskite contains a minimum of about 10 mole percent Ni replacing the other metals. Thus, vysotskite can be defined as all members of the braggite solid-solution series containing less than 10 mole percent [12, 14, 15, 16]. Cabri et al determined the cooperite ($Pt_{0.96}Pd_{0.03}Ni_{0.12}S_{1.01}$) with space group $P4_2/mmc$ to have lattice parameters a = 3.465 Å, c = 6.104 Å, braggite ($Pt_{0.63}Pd_{0.24}Ni_{0.12}S_{1.01}$) space group $P4_2/m$ with lattice parameters a = 6.367 Å, c = 6.561 Å and vysotskite ($Pd_{0.89}Pt_{0.1}Ni_{0.09}S_{1.01}$) space group $P4_2/m$ with a = 6.368 Å, c = 6.562 Å using X-ray powder diffraction pattern. They concluded that Ni is not an essential element in the formation of cooperite, braggite or vysotskite, since each of the phases can be prepared, Ni-free. Braggite and vysotskite are compositional variants end member composition of PdS, which has not been found in nature. The study suggested that the family of minerals be called the braggite series and that all composition containing less than 10 mole percent PtS be called vysotskite. And also, since it is possible to distinguish cooperite from braggite, it is impossible to differentiate between braggite and vysotskite by X-ray methods because of the very similar cell dimensions [4].

1.3.2. Electronic properties

Electronic properties of a material help us to consider the material under three main groups, namely, metals, semiconductors and insulators. The existence and size of the energy gap (the gap between the highest occupied orbitals and the lowest unoccupied orbital) determines the type of material. In the case of a metal there is no gap as there is overlap of the orbitals, but for semiconductors and insulators there is a gap but is large in insulators. Density of states, phonon density of states and elastic constants are used to determine the stability of the structure. Electronic properties of PtS and PdS have been studied by Nguyen-Manh et al [7].

1.3.3. Mechanical Properties

The mechanical properties of materials, their strength, rigidity and ductility are of vital importance in determining their fabrication and possible practical applications. Mechanical properties are used to help to classify and identify materials. Most structural materials are anisotropic, which means their material properties vary in orientation. It is common to see mechanical properties listed by the directional grain structure of the material. These properties are not constant and they change often as a function of pressure, temperature, rate of loading and other conditions [17, 18]. Moduli of elasticity and ductility may increase or decrease with increasing pressure and temperature [19].

1.3.4. Vibrational properties

The phonon spectrum of solid is important in evaluating physical quantities such as specific heat, thermal expansion coefficient and electron-phonon interactions [20]. With the advent of computational techniques, calculations of phonon frequencies within the local density approximation (LDA) became possible [21]. Structural transformation and vibrational properties of BaO_2 have been studied from phonon spectra [22]. Calculated phonon dispersions and phonon density of states will be used in the current study.

1.4. Motivation

In the current study attention will be paid to different phases of precious metal sulphides, such as PtS and PdS, residing in mineral ores. Such ores are usually grinded and milled in the process of extracting constituent compounds and the latter, (such as PtS) are subjected to high pressures which could change their stabilities and properties. First-principles calculations have previously been successfully used to study such properties in different compounds and were validated experimentally [8, 23]. The current study will employ such methods to investigate changes in structural properties, such as lattice parameters of the $(Pt_{50-x}Pd_x)S_{50}$ system. The stability of these compounds will be deduced from a combination of heats of formation, electronic, mechanical and lattice dynamics at ambient and high pressures.

1.5. Outline

In this study, density functional theory will be employed to study our systems.

In Chapter 1, the background to the study is introduced, together with structural properties and literature review on precious metal sulphides. The chapter is concluded with motivation and an outline of the study.

In Chapter 2, we discuss the DFT methods that were employed in this study, including related approximations.

In Chapter 3, we present and discuss the results generated in the current study, mainly using the VASP code. The results include structural, electronic, mechanical and lattice dynamics properties of $Pt_{50-x}Pd_xS_{50}$ compounds at ambient and high pressures

Chapter 4, we give the summary and conclusions of the results. Finally, the bibliography which helps in giving the insight to the analysis of the work listed.

Chapter 2

Theoretical techniques

Introduction

Simulation methods are an ideal tool to understand and predict the properties of materials using computers. Computational techniques have been used to successfully verify experimental observations and they are able to bring new insights and clarifications to the experimental findings at the atomic level. The knowledge obtained from computers and experiments are complimentary to each other. The success of the computer simulations of materials rests upon an accurate modelling of how atoms interact with each other. The commonly known computational technique is based on ab initio method.

2.1. Density Functional Theory

Density functional theory was developed by Hohenberg and Kohn in 1964 [24]. Kohn and Sham [25], proved that the total energy including the exchange and correlation of an electron gas is a unique functional of the electron density. DFT has been effectively used as the most important first-principles quantum mechanical approach in solid state physics and is known as the unified approach that provides accurate structural, energetic and electronic properties for solids and surfaces, as well as molecules [26]. The theory is based on concepts by Thomas [27] and Fermi [28], who introduced the idea of expressing the total energy of a system as a functional of the total electron density. The accuracy of the early attempts was far from satisfactory because of the simple treatment of the kinetic energy term. Later on, Slater motivated the search for practical electronic structure calculations [29]. Furthermore, an approach was developed which later became the X_α method [30], which was originally intended as an approximation to Hartree-Fock theory. The X_α is generally viewed as a simplified form or precursor of DFT. In contrast to the Hartree-Fock picture, which begins conceptually with a description of in-

dividual electrons interacting with nuclei and all other electrons in the system, DFT starts with a consideration of the entire system. The total energy of a system is expressed as a functional of the total electron density, which in turn depends on the positions of the atoms

$$E = E[\rho(r), R_\alpha] \,, \tag{2.1}$$

where R_α denotes the positions of all atoms, α, in the system under consideration. The Born-Oppenheimer approximation amounts in separating the electronic and nuclear degree of freedom. The electronic mass is smaller compared to the nuclei, and the electrons respond instantaneously to change in the position of the nuclei. This approximation is good, since the electrons are always in their good state as the atoms vibrate thermally. This depicts that the positions of the nuclei are parameters which appears in the potential of Schrödinger's equation defining the wave functions of the electrons. This enabled Kohn and Sham to derive an effective one electron Schrödinger equation by expressing the functional as the sum of three terms written as

$$E[\rho] = T_0[\rho] + U[\rho] + E_{xc}[\rho], \tag{2.2}$$

where T_0 is the kinetic energy, U is the Coulomb energy due to a classical electrostatic interactions among all charged particles in the system and E is the exchange correlation energy. The coulomb energy U which is purely classical contains the electrostatic energy arising from the columbic attraction between electrons and nuclei, the repulsion between all electronic charges, and the repulsion between nuclei. It can be written as

$$U[\rho] = U_{en}[\rho] + U_{ee}[\rho] + U_{ion-ion} \,. \tag{2.3}$$

The set of wave functions that are used in the Kohn-Sham energy functional are given by the self-consistent solutions of the equation:

$$\left[-\frac{\hbar^2}{2m}\nabla^2 + V_{ion}(r) + V_H(r) + V_{XC}(r)\right]\psi_i(r) = \varepsilon_i\psi_i(r) \,, \tag{2.4}$$

where ψ_i is the wave function of electronic state i, ε_i is the Kohn-Sham eigenvalue, V_{ion} is the static total electron-ion potential and V_H is the Hartree potential of the electron which is given by

$$V_{H(r)} \int \frac{\rho(r')}{|r-r'|} dr' \tag{2.5}$$

and the exchange-correlation potential, V_{XC}, is given by

$$V_{XC}(r) = \frac{\delta E_{XC}[\rho(r)]}{\delta \rho(r)} \tag{2.6}$$

The electron density, $\rho(r)$, is given by

$$\rho(r) = 2 \sum_i \int |\psi_i(r)|^2 \tag{2.7}$$

Hence, the Kohn-Sham total energy functional is written as

$$E = 2 \sum_{occ} \varepsilon_i + U_{ion-ion} - \frac{e^2}{2} \iint \frac{\rho(r)\rho(r)}{|r-r'|} dr dr' + E_{XC}\,[\rho(r)] - \int \rho(r)\, V_{XC} dr \tag{2.8}$$

The exchange-correlation energy potential cannot be obtained explicitly, since the exact exchange-correlation energy is unknown. Therefore, approximation methods are needed to solve the problem. The known approximation methods are LDA and GGA, which will be discussed in the next section.

2.3. Approximation methods

2.3.1. Local Density Approximation

The Hohenberg-Kohn theorem provides motivation for using approximate methods to describe the exchange-correlation energy as a function of the electron density. To apply the Kohn-Sham equations, the energy-functional $E[\rho(r)]$, has to be known. Unfortunately, the Hohenberg-Kohn theorem does not yield the density functional. Thus, approximations for the exchange-correlation functional, which is the only unknown part of the energy-functional, $E[\rho(r)]$, have to be made. The simplest method of describing the exchange-correlation energy is to use the local-density approximation (LDA) [25], which assumes that the exchange correlation energy per electron at a point r in the electron gas, $\varepsilon_{xc}(r)$, is equal to the exchange-correlation energy per electron in a homogeneous electron gas that has the same density as the electron gas at point r. Thus

$$\varepsilon_{XC}^{LDA}[\rho(r)] = \varepsilon_{XC}^{hom}\big(\rho(r)\big) \tag{2.9}$$

The exchange-correlation energy of an electronic system in local density approximation uses only the electron density, $\rho(r)$ at spatial point r to determine the exchange-correlation energy density at that point. It is taken to be that of a uniform electron gas of the same density. The exchange part of the functional is defined as the exact expression derived for a uniform electron gas [27]. Thus, the exchange-correlation energy can be written as

$$E_{xc}[\rho(r)] = \int \varepsilon_{xc}(r)\rho(r)d^3r\,, \tag{2.10}$$

where $\varepsilon_{xc}(r)$ is equal to the exchange-correlation energy per electron in a homogeneous gas that has the same density as the electron gas at point r. The potential is calculated as

$$V_{XC}^{LDA}[\rho(r)] = \frac{\delta E_{XC}^{LDA}[\rho(r)]}{\delta\rho(r)} = \frac{\partial[\rho(r)\varepsilon_{XC}^{LDA}(\rho(r))]}{\partial\rho(r)} \tag{2.11}$$

In the local density approximation, the exchange-correlation energy per electron at a point r in the inhomogeneous electron gas is equal to the exchange-correlation energy per electron in a homogeneous electron gas that has the same density as the inhomogeneous electron gas at point r. The exchange-correlation energy of the homogeneous gas can be obtained with great accuracy using quantum Monte Carlo simulation [31, 32]. The local-density approximation assumes that the exchange-correlation energy functional is purely local. So the only information needed is the exchange-correlation energy of the homogeneous gas as a function of density.

2.3.2 Generalized Gradient Approximation

In recent years, the generalized gradient approximation (GGA) was considered a possible improvement over LDA. The GGA has found to be improving the description of total energies, ionization energies and electron affinities of atoms, atomization energies of molecules and some solid state properties. The introduces dependence of the ex-

change-correlation functional on the local gradient $\nabla\rho(r)$ of the density for the exchange energy, and has the form

$$E_x^{GGA}[\rho] = \int d^3r \varepsilon_{xc}^{unit}\left[\rho(r)F_X\left(s(r)\right)\right], \quad (2.12)$$

where $\varepsilon_x^{unit}(\rho)$ is the exchange energy density of a uniform electron gas (proportional to $\rho^{\frac{4}{3}}$) and $s = |\nabla_\rho| \,/\, (2k_F\rho)$ is the dimension-less density gradient and $k_F = (3\pi^2\rho)^{\frac{1}{3}}$ is the Fermi wave vector, $F_x(s)$ is the exchange enhancement factor characterising the precise form of the GGA. The GGA functionals that are commonly used in physics includes Perdew, Burke and Ernzerhof (PBE) [33] and Perdew-Wang from 1991 (PW91) [34], and are parameters free. The PBE presents a more elegant derivation of the functional using exact properties of the exchange-correlation energy. Generalized gradient approximation is known to produce the correct ground state for magnetic transition metals.

2.4 Plane Wave Pseudopotential Method

The pseudopotential plane wave method has become one of the most widely used methods for calculating ground state properties of extended systems within the framework of density functional theory. The simplicity of plane waves leads to very efficient numerical schemes for solving the Kohn–Sham equations, and employing pseudopotentials guarantees that the wave functions can be expanded in a relatively small set of plane waves.

2.4.1. Plane-Wave Basis Sets

Plane-wave basis sets are common solutions for free electrons with boundary conditions that restrict the periodicity of the wave function. In principle, the Kohn-Sham single-particle wave functions [35] may be represented in terms of any complete basis set. Kohn-Sham equations are difficult to solve since they are an integral-differential problem, therefore it is necessary to transform them into a solvable equation, which can be

done in expanding the electronic wavefunction with a basis set. Bloch's theorem states that the electronic wavefunction at each k point can be expanded in terms of a discrete plane-wave basis set. In a periodic system, the Kohn-Sham eigenfunctions can be written using Bloch'sTheorem as

$$\psi_{i,k}(r) = e^{i(k.r)}u_{i,k}(r), \tag{2.13}$$

where, $u_{i,k}(r)$, is a cell-periodic term, and the range of k can be restricted to one primitive cell of the reciprocal lattice, which usually is chosen to be the Brillouin zone. Moreover, $u_{i,k}(r)$, can be Fourier transformed into a sum using the planewave basis set with wave vectors that are reciprocal lattice vectors indexed by G, where the electronic wave functions at a k-point in the Brillouin zone are written in the form

$$\psi_{i,k}(r) = \sum_G c_{i,k}(G)e^{i(G+k).r} \tag{2.14}$$

In principle, an infinite plane-wave basis set is required to expand the electronic wavefunctions. However, the coefficient, $c_{i,K+G}$, for plane-waves with small kinetic gy, $(\frac{\hbar^2}{2m})|K+G|^2$, which are more important than those with large kinetic energy.

2.4.2. Pseudo Potentials Approximation

It has been shown by the use of Bloch's theorem that the electronic wave function can be expanded using a discrete set of plane waves. Unfortunately a plane wave basis set is usually very poorly suited to expanding the electronic wavefunctions because a very large number are required to accurately describe the rapidly oscillating wavefunctions of electrons in the core region. Large plane-wave basis set are required to perform an all-electron calculations and an amount of computational time is required to calculate the electronic wave functions.

It is well known that most physical properties of solids are much dependable on the valence electrons than that of the tightly bound core electrons, that's where the pseudopotential approximation is introduced [36, 37, 38]. This approximation uses this fact to re-

move the core electrons and the strong nuclear potential and replace them with a weaker pseudopotential which acts on a set of pseudo wavefunctions rather than the true valence wavefunctions. An ionic potential, valence wave function and the corresponding pseudopotential and pseudo wave function are shown in the figure below. The valence wave function oscillates rapidly in the region occupied by the core electrons due to the strong ionic potential in this region. Orthogonality between the core wave functions and the valence wave functions is maintained by these oscillations, which is required by the exclusion principle. The pseudopotential is constructed in such a way that there are no radial nodes in the pseudo wave function in the core region and that the pseudo wavefunctions and pseudopotential are identical to all the electron wavefunction and potential outside a radius.

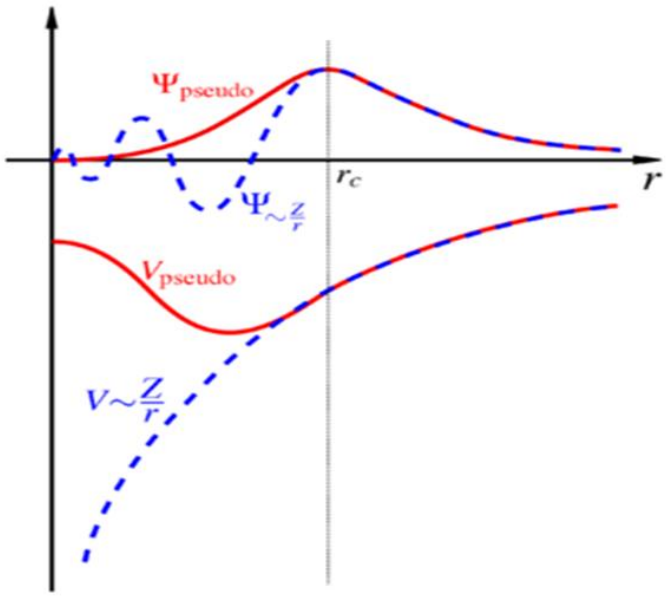

Figure 2. 1. Comparison of a wavefunction in the Coulomb potential of the nucleus (blue) to the one in the pseudopotential (red). The real and the pseudo wavefunction and potentials match above a certain cutoff radius r_c.

The pseudopotential is constructed in such a way that its scattering properties or phase shifts for the pseudo wavefunctions are identical to the scattering properties of the ion and the core electrons for the valence wavefunctions, but in such a way that the pseudo wavefunctions have no radial nodes in the core region. The phase shift produced by the ion core is different for each angular momentum component of the valence wave func-

tion and so the scattering from the pseudopotential must be angular momentum dependent. The most general form for pseudopotential is

$$V_{NL} = \sum_{lm} |lm\rangle V_l \langle lm| \,, \tag{2.14}$$

where $|\boldsymbol{lm}\rangle$, are thespherical harmonics and $\boldsymbol{V_l}$,is the pseudopotential for angular momentum $\boldsymbol{l}$ [39]. The majority of the pseudopotentials currently used in electronic structure are generated from all electron atomic calculations. Howewver, a pseudopotential that uses the same potential for all the angular momentum components of the wave function is called a local pseudopotential. The norm-conserving pseudopotential are an example of the non-local pseudopotential and uses a different potential for each angular momentum components of the wave function.

2.5. k-sampling

Electronic states are allowed only at a set of k-points determined by the boundary conditions that apply to the bulk solid. The density of allowed k-points is proportional to the volume of the solid. The infinite numbers of electrons in the solid are accounted for by an infinite number of k-points and only a finite number of electronic states are occupied at each k-point.

The Bloch theorem changes the problem of calculating an infinite number of electronic wavefunctions to one of calculating a finite number of k-points. The occupied states at each k-point contribute to the electronic potential in the bulk solid so that in principle an infinite number of calculations are needed to compute this potential. However the electronic wavefunctions at k-points that are very close are identical. Hence it is possible to represent the electronic wavefunctions over a region of k space by the wavefunctions at the single k-point. In this case the electronic states at only a finite number of k-points are required to calculate the electronic potential and hence determine the total energy of the solid.

Methods have been devised for obtaining very accurate approximations to the electronic potential from a filled electronic band by calculating the electronic wavefunctions at special sets of *k*-points. The two most common methods are those of Chadi and Cohen [40] and Monkhorst and Pack [41]. Using these methods, the electronic potential and the total energy of an insulator can be obtained by calculating the electronic states at a very small number of k-points. A denser set of k-points are required to calculate the electronic potential and the total energy of a metallic system in order to define the Fermi surface precisely.

However, the computational cost of performing a very dense sampling of k space increase linearly with the number of k-points in the Brillouin zone (BZ). Density functional codes approximate these k space integrals with a finite sampling of k-points. Special k-points schemes have been developed to use the fewest possible k-points for a given accuracy, thereby reducing the computational cost. The most commonly used scheme is that of Monkhorst and Pack [41].

2.6. Planewave pseudopotential code VASP

2.6.1. VASP Code

The Viena Ab initio Simulation Program (VASP) [42] is a package for performing *ab-initio* quantum-mechanical molecular dynamics (MD) simulations using pseudopotential or the projector-augmented wave method and a plane wave basis set [43]. The approach implemented in VASP is based on the (finite-temperature) local density approximation with the free energy as vibrational quantity and an exact evaluation of the instantaneous electronic ground state at each MD time step. This package uses efficient matrix diagonalisation scheme and efficient Pulay/ Broyden [44, 45]. The technique avoids all problems possibly occurring in the original Car-Parinello metod [46], which is based on the simultaneous integration of electronic and ionic equations of motion. The interaction between ions and electrons is described by ultra-soft Vanderbilt (US-PP)

[47]. Forces and stresses can be easily calculated with VASP and used to relax atoms into their instaneous ground state.

2.7. PHONON Code

A phonon is an elementary excitation in the quantum mechanical treatment of vibrations in a crystal lattice or the quantum unit of a crystal lattice vibration [48]. Phonons play a major role in physical properties of condensed matter, such as thermal conductivity and electrical conductivity. Its study is an important part of condensed matter physics. The phonons are considered a qusi-particle, because it only exists in solids as a consequence of vibrational motions, since they do not propagate in vacuum. A phonon is often classified as a “quasiparticle” which means it can be observed as a phenomenon but not specifically extracted as an individual object.

Phonons do not behave as independent particles, but instead it interacts with other phonons within an object. This interaction causes groups of phonons to form chains or lattice structures. One phonon is able to transfer its energy to the next one in the chain, a long lattice is able to transfer continuous energy in the form of electricity or heat [49]. They are considered harmonic oscillators; since they are consist of wave properties. The vibrations of atoms in a crystal lattice of a solid around their equilibrium position can be decomposed into a linear composition of normal modes, which have their origin in crystal symmetry. Every normal mode is characterized by a frequency υ and a wave vector k, a boson with energy $E = h.\upsilon,$ and momentum $p = h.k,$ can be associated to each of them. These bosons are called phonons, and they represent the quanta of energy of lattice vibrations [50].

2.8. Theoretical Background of the Calculated Properties

2.8.1. Heats of Formations

The heat of formation is the heat released or absorbed during the formation of a pure substance from its elements. Heat of formation is one of the prime thermodynamic ingredient in free energy to determine phase diagrams, the other being entropy. It's associated with entropies which provide a fundamental understanding on stabilities and phase diagrams constructions. The heat of formation is given by

$$\Delta H_f = E_c - \sum_i x_i E_i , \tag{2.16}$$

where $E_{c,}$ the total energy of the compound is, E_i , is the calculated total energy of the element $i,$ in the compound. The formation energy is accountable for the reactive stability of phases at low temperatures, where entropic contributions are considered not important. These relative stabilities of different phases are determined through a common tangent rule [51]. The results of lattice parameters, heats of formation will be discussed in Chapter 3.

2.8.2. Elasticity

In the science of materials, numbers that quantify the response of a particular material to elastic or non-elastic deformation when a stress load is applied to that material are known as elastic constants. Both stress and strain have three tensile and three shear components, giving six components in total. Elastic constants have vital information regarding the strength of the materials against an extremely applied strain and also act as stability criteria to study structural transformation. Elastic properties are very important to understand solid-state physical, chemical and mechanical properties. Elastic constants are defined by means of Taylor expansion of the total energy $U(V, \varepsilon)$ for the system with respect to a lattice strain ε of the primitive cell volume V. The energy of a strained system is expressed as

$$U(V,\varepsilon) = U(V_0,0) + U(V_0,0)\left[\sum_i \tau_i\, \varepsilon_i \xi_i + \frac{1}{2}\sum_{ij} C_{ij}\varepsilon_i \xi_i \xi_j\right], \qquad (2.17)$$

where $U(V_0,0)$, the energy of unstrained system with equilibrium volume is V_0, τ_i, is an element in the stress tensor, ξ_i and ξ_j, are the factors to take care of Voigt index. Mechanical stability of homogeneous crystals has long been a subject of extensive theoretical and computational investigation. Born initiated the systematic study of a crystal stability under load [52]. Born has stability criteria which are set for conditions on the elastic constants (C_{ij}), which are related to the second-order change in the internal energy of a crystal under deformation. It has been suggested recently that the Born conditions are valid only for the stability analysis of an unstressed lattice and not for the stressed lattice [53]. The elastic constant of a material describes its response to an applied stress or conversely the stress required to kaintain a given deformation. Both stress and strain have three tensile and three shear components, giving six components in total. The linear elastic constants form a 6x6 symmetric matrix having 27 different components, such that $\sigma_i = C_{ij}\varepsilon_j$, for small stresses, σ, and strains, ε, [54], where i and j are the indices attaining values from 1, 2, 3, ….8. Any symmetry in the structure can make some of these components equal, and or some strictly zero. A cubic crystal has only three different symmetry elements (C_{11}, C_{12}, C_{44}) with each representing three equal elastic constants ($C_{11} = C_{22} = C_{33}$, $C_{12} = C_{23} = C_{31}$ and $C_{44} = C_{55} = C_{66}$). A single strain with non-zero first and fourth components can give stresses relating to all three of these coefficients, yielding a very efficient method of obtaining elastic constants for cubic system. Nye [55] gives a full account of the symmetry of stress, strain and elastic constants. Elasticity describes the response of a crystal under external strain and provides information of the strength of the material, characterized by bulk modulus (B), shear modulus (C'), Young's modulus €, Poisson's ratio (υ) and shear anisotropy factor (A) [56]. Quadratic dependence of the crystal energy E on the strain is expected for small deformations. The elastic moduli are defined as follows

$B = \frac{1}{3}(C_{11} + 2C_{12}),$ $\quad C' = \frac{1}{2}(C_{11} - C_{12}),$ $\quad \upsilon = \frac{C_{12}}{C_{11}+C_{12}}$ and $\quad A = \frac{2C_{44}}{C_{11}-C_{12}}$.

For a cubic crystal under hydrostatic pressure, the generalized elastic stability criteria [53] in analogy to the conductional criteria are $C_{11}+2C_{12}>0$, $C_{44}>0$, $C_{11}-C_{12}>0$. The single crystal moduli for the {100} plane along [010] direction and for {110} plane along the

[110] direction in a cubic crystal are given by C_{44} and C'. Orthorombic deformation is related to the shear constant C_{44}, whereas the tetragonal deformation is related to C' and its size reflects the degree of stability of the crystal with respect to a tetragonal shear [57]. There are six independent elastic constants in the contacted matrix notation, C_{11}, C_{12}, C_{13}, $C_3$3, C_{44} and C_{66}, for a crystal with tetragonal structure. The elastic moduli that can be derived from these elastic constants are:

$B = \frac{1}{9}(2C_{11} + C_{33} + 4C_{13} + 2C_{12}),\quad C' = \frac{1}{15}(2C_{11} + C_{33} - C_{12} - 2C_{13} + 6C_{44} + 3C_{66}),$

$E = C_{33} - 2\upsilon C_{13},\quad \upsilon = \frac{C_{13}}{C_{11}+C_{12}}$ and $A_1 = \frac{2C_{66}}{C_{11}-C_{12}}$ (on basal plane)

$A_2 = \frac{4C_{44}}{C_{11}+C_{33}-2C_{13}}$ (on (010) plane).

The corresponding mechanical stability criteria for tetragonal crystal are $C_{11} - C_{12} > 0$, $C_{11} + C_{33} - 2C_{13} > 0$, $C_{11} > 0$, $C_{33} > 0$, $C_{44} > 0$, $C_{66} > 0$, $2C_{11} + C_{33} + 2C_{12} + 4C_{13} > 0$.

A hexagonal crystal has six different symmetry elements C_{11}, C_{12}, C_{13}, C_{44} and C_{66}, with five of them been independent since $C_{66} = (C_{11} - C_{12}) / 2$. For hexagonal system, there are two different strain patterns, one with non-zero and fourth component and the other with a non-zero third component which gives stresses that are related to all five independent elastic coefficients [58, 59, 60]. The stability condition for orthorhombic crystal should satisfy the Born stability criteria [61].

$(C_{11} + C_{22} - 2C_{12}) > 0$, $(C_{11} + C_{33} - 2C_{13}) > 0$, $(C_{22} + C_{33} - 2C_{23}) > 0$, $C_{11} > 0$, $C_{22} > 0$, $C_{33} > 0$, $C_{44} > 0$, $C_{55} > 0$, $C_{66} > 0$, $(C_{11} + C_{22} + C_{33} + 2C_{12} + 2C_{13} + 2C_{23}) > 0$.

In metals and alloys (a partial or complete solid solution of one or more elements in a metallic matrix) behaving like isotropic media, the young's modulus is proportional to the bulk modulus when the Poisson's ratio is close to 1/3.

2.8.3. Densities of States

The density of states is described as the number of states per interval of energy at each energy level which are available for occupation by electrons. A high DOS at a specific

energy level means there are states available for occupation and DOS at zero implies that no states can be occupied at that energy level. In general, a DOS is an average over the space and time doins occupied by the system. Integrating the density of states over a range of energy will produce a number of states [62].

$$N(E) = \int_{E}^{\Delta E} g(E)dE$$

Thus $g(E)dE$, represents the number of states between E and dE.

Density of stetes allows integration with respect to the electron to be used instead of the integration over the Brillioun zone. The DOS is a useful mathematical concept which allows integration with respect to electron energy to be used instead of integration over the Brillioun zone. It is often used for quick visual analysis of the electronic structure. Characteristics such as the width of the valence band, the energy gab in insulators, the number of intensity of the main features are helpful interpreting experimental spectroscopic data. DOS analysis helps in understanding the changes in electronic structure caused by external pressure. Various numerical techniques are used for evaluating the DOS and the simplest is based on Gaussian smearing of the energy levels of each band and the other technique is histogram sampling. This method does not reproduce good results. More accurate methods are based on linear or quadratic interpolations of band energies between the reference points in the Brillioun zone. The most popular and reliable technique is based on the tetrahedron interpolation, is unfortunately not well suited to the Monkhorst-Pach grid of special points. CASTEP [40] uses a simplified linear interpolation scheme. The method is based on linear interpolation in parallelepipeds formed by the points of the Monkhorst-Pack set, which is followed by the histogram sampling of the resultant set of band energies.

Chapter 3

Structural, Mechanical, Electronic and Vibrational Properties of the (Pt,Pd)S

In this chapter we present the DFT calculations results at different concentrations of $Pt_{50-x}Pd_xS_{50}$. Structural properties i.e. lattice parameters, heats of formation, electronic, mechanical and vibrational properties will be discussed. The effect of pressure on such properties will be determined at pressures, ranging from 0 - 50 GPa. We further compare the calculated results with the experiments, where available. The PtS with space group $P4_2/mmc$, and PdS with space group $P4_2/m$ were used in this study. Since the PtS $P4_2/mmc$ has limited sites for obtaining a wide range of concentrations, a supercell was created with P_1 symmetry. The PdS $P4_2/m$ has sufficient sites for insertion of different Pt concentrations.

3.1 Convergence of cut-off energy and k-points sampling

3.1.1. Energy cutoff

In order to determine precise cutoff energy for both PtS and PdS, single point energy calculations were performed for different kinetic energy at default number of k-points for each system. Figure 3.1.1 shows the curve of total energy per atom against cutoff energy for the PtS and PdS. The energy cutoffs of 364 eV were chosen for both our systems, respectively since it was sufficient to converge our structures.

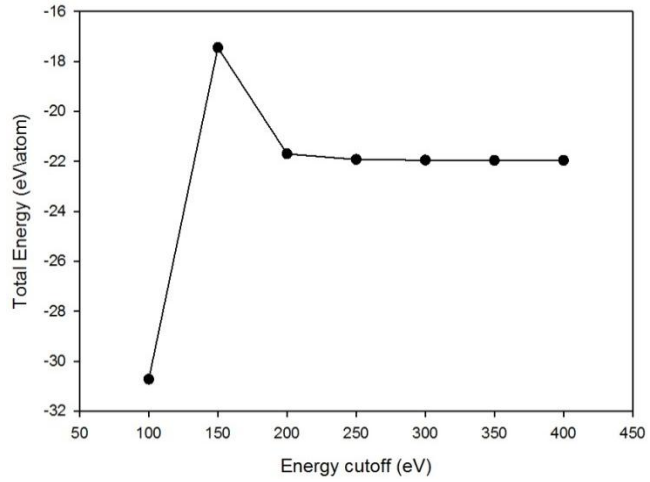

(i)

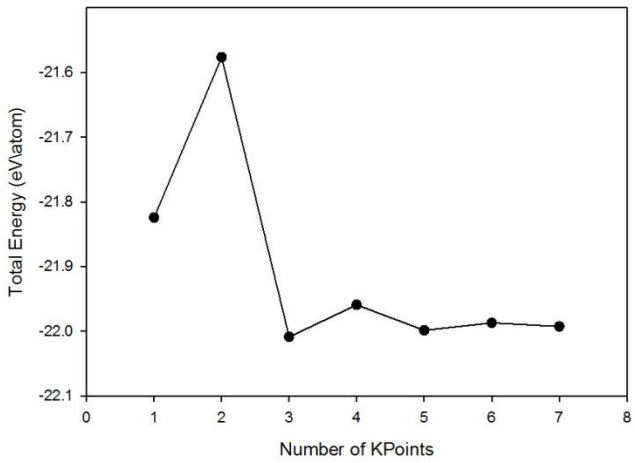

(ii)

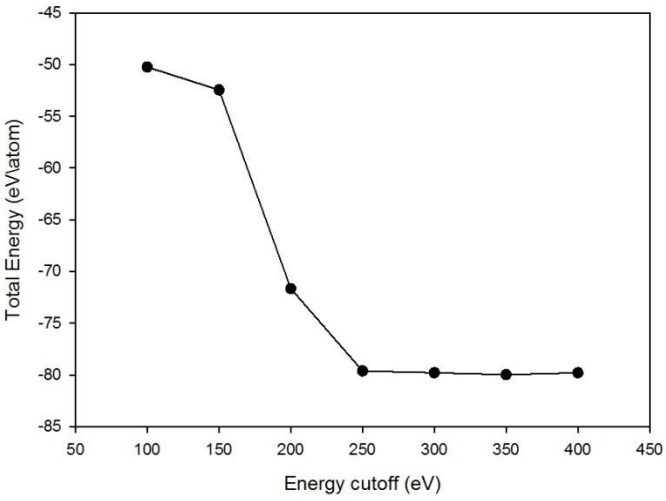

(iii)

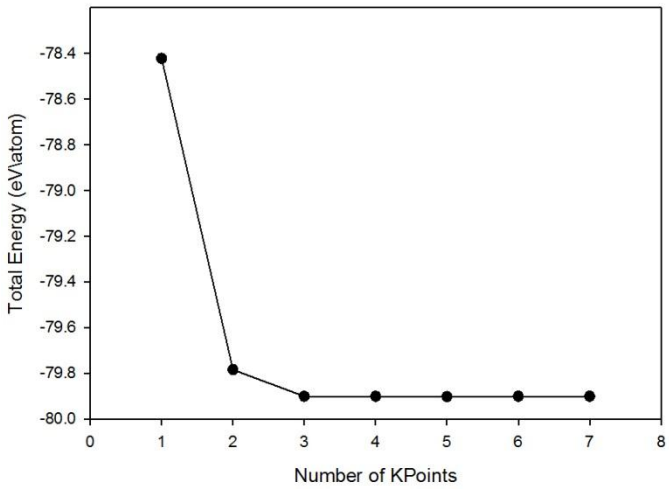

(iv)

Figure 3.1. 1. The graph of (i), (iii) total energy (eV/atom) against cutoff (ii), (iv) total energy (eV/atom) against number of k-points for PtS and PdS.

3.1.2. K-points sampling

After a suitable kinetic energy cut-off has been obtained, it is crucial to also determine the appropriate number of k-points to use in plane-wave pseudopotential calculations. Several methods have been suggested for special k-points sampling in the Brillouin zone [40, 63, 64, 41]. The methods help in obtaining the accurate approximation for the total energy by calculating the electronic state at a very small number of k-points. The Monkhorst-Pack scheme of the k-points sampling was used to select an optimal set of special k-points of the Brillioun zone in a way that the greatest possible accuracy is achieved from the number of k-points used [24, 25]. The total energy with respect to the number of k-points was considered converged when the energy change per atom was within 1 meV. The k-points were found to be 4x4x3 for both PtS and PdS, respectively.

3.2. Structural Properties for $Pt_{50-x}Pd_xS_{50}$ and $Pd_{50-x}Pt_xS_{50}$

Table 3.2.1, shows the results of equilibrium lattice constants and heats of formation for $Pt_{50-x}Pd_xS_{50}$ with $P4_2/mmc$ symmetry. The results are in good agreement with the available experimental values. Only three concentrations were generated from PtS pure structure with the same symmetry. $Pt_{25}Pd_{25}S_{50}$ is said to be unstable since it has a positive heat of formation. The instability of this composition will be seen in phonon density of states which will be discussed later.

Table 3.2. 1. Results of the lattice parameters and the heats of formation energy for the $(Pt_{50-x}Pd_x)S_{50}$

Composition	Space group	Lattice parameters a (Å) c (Å)	Exp a (Å) c (Å)	Energy of formation (eV/atom)
$Pt_{50}S_{50}$	$P4_2/mmc$	3.539 6.114	3.470 6.110 [1]	-0.345
$Pt_{25}Pd_{25}S_{50}$	$P4_2/mmc$	5.008 8.671	-	3.902
$Pd_{50}S_{50}$	$P4_2/mmc$	3.546 6.163	-	-0.577

Tables 3.2.1 and 3.2.2 shows the results of lattice constants and heats of formation. From table 3.2.2 the results show that lattice parameters fluctuate with increasing concentration of platinum. One of the stable structures is $Pd_{37.5}Pt_{12.5}S_{50}$, since it has a very low heat of formation and it corresponds with the structure of braggite. Moreover, supercell approach was used in table 3.2.3 where results show that lattice parameters increase steadily with increasing concentration of palladium. The results for lattice parameters against Pt composition are plotted in figure 3.2.1 and 3.2.2 respectively. Lattice parameters for $Pt_{50}S_{50}$ and $Pd_{50}S_{50}$ are more or less the same because $Pd_{50}S_{50}$ retains the same structure of $Pt_{50}S_{50}$ since they have the same symmetry.

Table 3.2. 2. Results of the lattice parameters and the heats of formation energy for the $(Pd_{50-x}Pt_x)S_{50}$

Composition	Space group	Lattice parameters a (Å) c (Å)	Exp a (Å) c (Å)	Energy of formation (eV/atom)
$Pd_{50}S_{50}$	$P4_2/m$	6.512 6.702	6.429 6.611 [13]	-0.567
$Pd_{37.5}Pt_{12.5}S_{50}$	$P4_2/m$	6.515 6.673	-	-2.343
$Pd_{25}Pt_{25}S_{50}$	$P4_2/m$	6.510 6.689	-	-1.184
$Pd_{12.5}Pt_{37.5}S_{50}$	$P4_2/m$	6.488 6.661	6.370 6.540 [65]	-2.374
$Pt_{50}S_{50}$	$P4_2/m$	6.496 6.676	-	-0.599

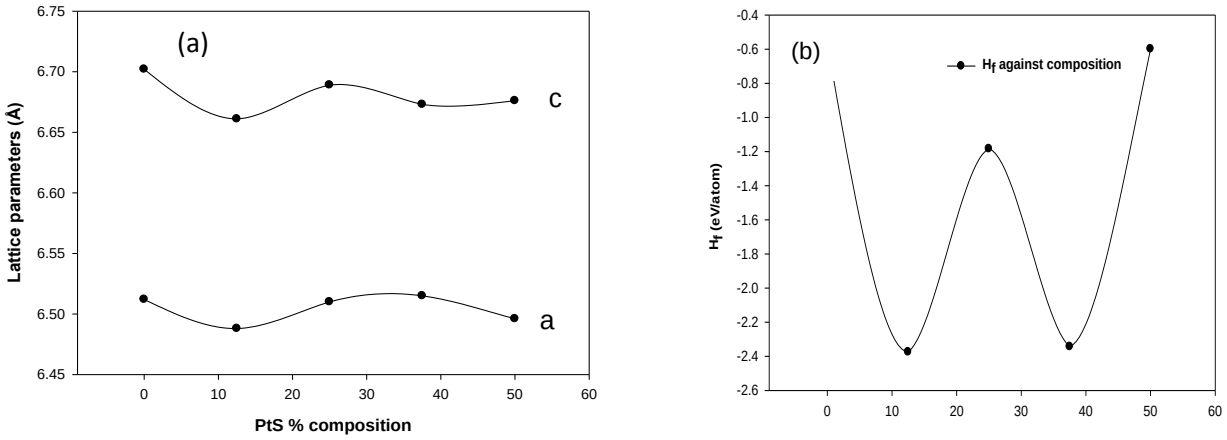

Figure 3.2. 1. The graph of (a) lattice parameters against composition (b) formation energy against composition

Table 3.2. 3. Results of the lattice parameters and the heats of formation energy for the $(Pt_{50-x}Pd_x)S_{50}$ supercell

Composition	Space group	Lattice parameters a (Å) c (Å)	Energy of formation (eV/atom)
$Pt_{50}S_{50}$	$P_1/P4_2/mmc$	7.071 12.223	-0.687
$Pt_{37.5}Pd_{12.5}S_{50}$	$P_1/P4_2/mmc$	7.071 12.258	-2.640
$Pt_{25}Pd_{25}S_{50}$	$P_1/P4_2/mmc$	7.083 12.291	-1.265
$Pt_{12.5}Pd_{37.5}S_{50}$	$P_1/P4_2/mmc$	7.088 12.308	-2.411
$Pd_{50}S_{50}$	$P_1/P4_2/mmc$	7.101 12.310	-0.571

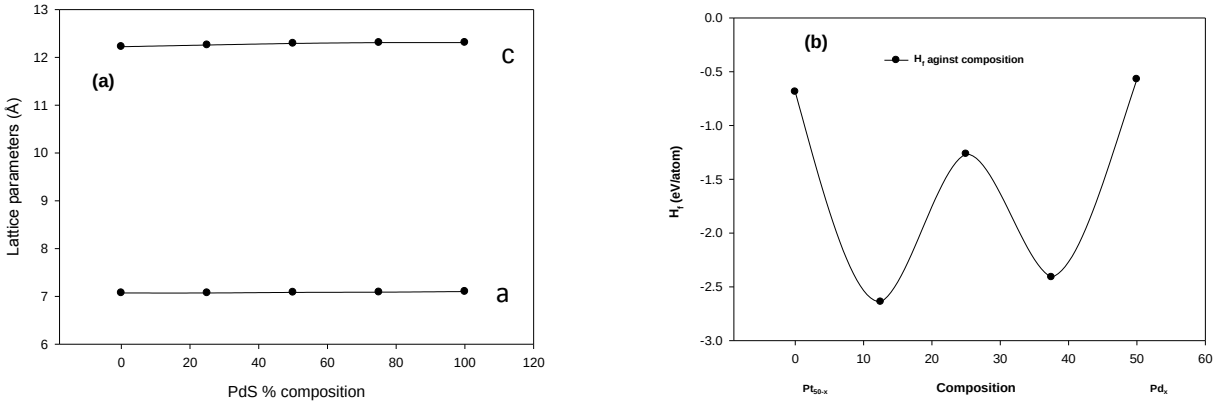

Figure 3.2. 2. The graph of (a) lattice parameters against composition (b) formation energy against composition.

As we replace some of the platinum by palladium, both a and c lattice parameters fluctuate, where a decrease was observed at $Pt_{37.5}Pd_{12.5}S_{50}$ then increases at $Pt_{25}Pd_{25}S_{50}$ for both lattice parameters. For $Pt_{12.5}Pd_{37.5}S_{50}$, as c lattice parameter decreases, the lattice parameter increases, then decreases at $Pt_{50}S_{50}$ whereas c increases. The heats of formation fluctuate with an increase of platinum concentration and the stable concentration was found to be $Pt_{12.5}Pd_{37.5}S_{50}$ since it has the lowest value of formation energy. Lattice parameters increases steadily with increasing concentration for both a and c lattice parameters. The formation energy fluctuates with increasing concentration of palladium. $Pt_{37.5}Pd_{12.5}S_{50}$ is said to be stable since it has the lowest value of formation energy.

3.3. Mechanical properties, phonon dispersion and density of states of the (Pt, Pd)S

3.3.1. Elastic properties of $Pt_{50-x}Pd_xS_{50}$ and $Pt_{50-x}Pd_xS_{50}$

From the perspective of materials physics, the elastic constants C_{ij} contain some of the more important information that can be obtained from ground-state total-energy calculations. A given crystal structure cannot exist in a stable or metastable phase unless its elastic constants obey certain relationships. The C_{ij} also determines the response of the crystal to external forces, as characterized by the bulk modulus, shear modulus, Young's modulus, and Poisson's ratio, and so plays an important role in determining the strength of a material [66]. First-principles calculations that use periodic boundary conditions assume the existence of a single crystal, so all elastic constants can be determined by direct computation.

Table 3.3. 1. Results of the elastic constants of $(Pt_{50-x}Pd_x)S_{50}$ and $(Pd_{50-x}Pd_x)S_{50}$

	Space group	C_{11} GPa	C_{12} GPa	C_{13} GPa	C_{33} GPa	C_{44} GPa	C_{66} GPa	Bulk modulus GPa	Shear modulus GPa
$Pt_{50}S_{50}$	$P4_2/mmc$	190.26	62.80	115.73	288.43	28.34	12.34	138.92	38.92
$Pt_{25}Pd_{25}S_{50}$	$P4_2/mmc$	507.73	49.16	96.67	697.22	287.89	-50.32	244.19	203.10
$Pd_{50}S_{50}$	$P4_2/mmc$	143.92	44.19	96.05	224.58	15.69	8.56	109.44	26.39
$Pd_{50}S_{50}$	$P4_2/m$	162.61	91.27	88.25	185.53	29.02	51.70	116.25	38.15
$Pd_{37.5}Pt_{12.5}S_{50}$	$P4_2/m$	179.64	94.93	96.87	182.70	34.78	57.95	124.37	42.39
$Pd_{25}Pt_{25}S_{50}$	$P4_2/m$	186.53	97.30	95.75	186.24	40.14	59.98	126.32	46.09
$Pd_{12.5}Pt_{37.5}S_{50}$	$P4_2/m$	200.99	115.22	105.28	231.94	38.66	62.96	142.83	48.60
$Pt_{50}S_{50}$	$P4_2/m$	233.84	139.11	130.14	266.85	48.46	68.12	170.37	55.35

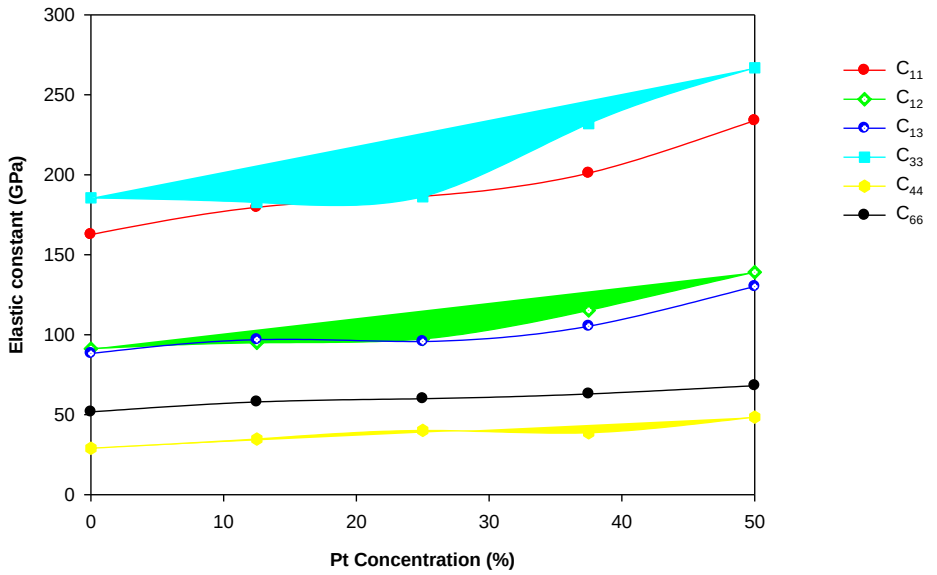

Figure 3.3. 1. Variation of elastic constants of $Pd_{50-x}Pt_xS_{50}$ against Pt concentration ($P4_2/m$)

Table 3.3. 2. Results of the elastic constants of $(Pt_{50-x}Pd_x)S_{50}$ (P_1/ $P4_2$/mmc)

Composition	C_{11} GPa	C_{12} GPa	C_{13} GPa	C_{33} GPa	C_{44} GPa	C_{66} GPa	Bulk modulus GPa	Shear modulus GPa
$Pt_{50}S_{50}$	191.40	62.55	116.13	289.09	31.06	12.10	140.17	39.98
$Pt_{37.5}Pd_{12.5}S_{50}$	175.48	58.36	108.71	264.30	26.90	10.93	129.64	35.62
$Pt_{25}Pd_{25}S_{50}$	160.54	54.72	103.27	249.97	25.02	10.09	122.19	32.16
$Pt_{12.5}Pd_{37.5}S_{50}$	152.46	48.52	98.79	234.47	20.87	9.15	114.62	29.64
$Pd_{50}S_{50}$	143.79	43.42	92.94	216.80	17.37	8.27	107.00	26.94

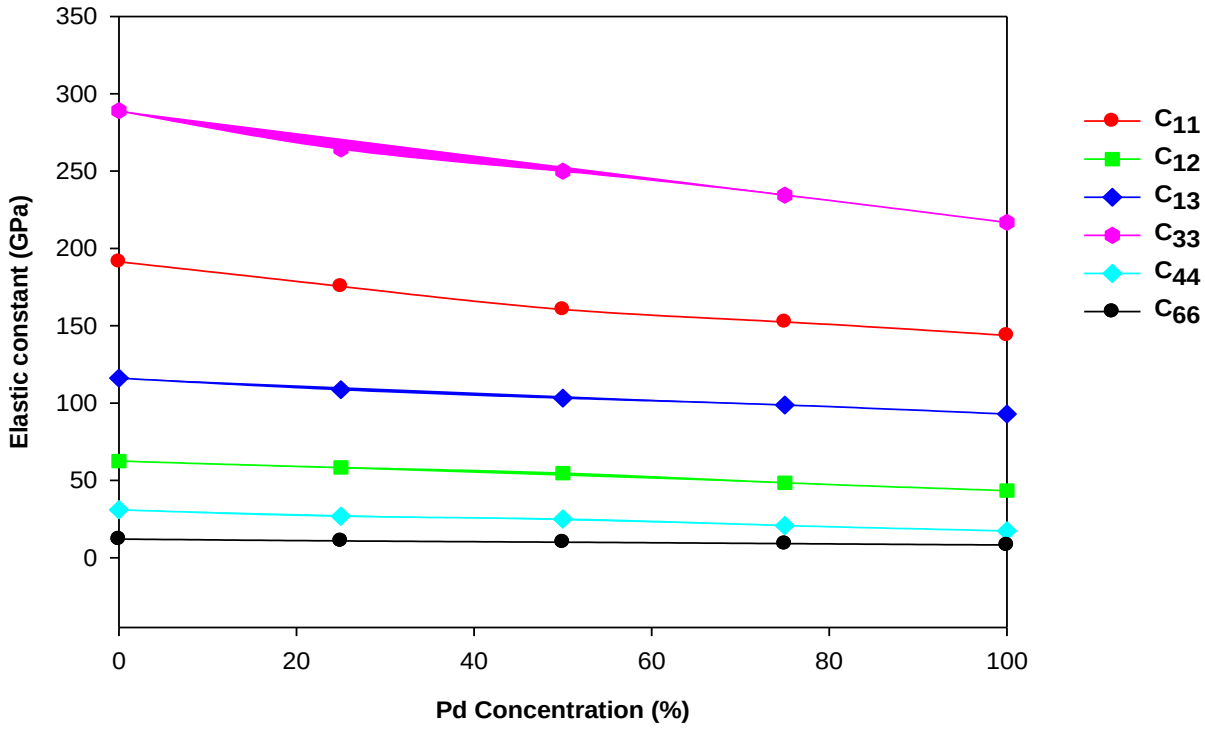

Figure 3.3. 2. Variation of elastic constants of $Pt_{50-x}Pd_xS_{50}$ against Pd concentration (P_1/ $P4_2$/mmc)

The results obtained in Table 3.3.1 with symmetry $P4_2/m$ and 3.3.2 with symmetry P_1 (from $P4_2/mmc$) show that all compounds meet the requirements for a crystal to be stable under any homogeneous elastic deformation, the requirements are $C_{11} - C_{22} > o$, $C_{11} + C_{33} - 2C_{13} > 0$, $C_{11} > 0$, $C_{33} > 0$,$C_{44} > 0$, $C_{66} > 0$, $(2C_{11} + C_{33} + 2C_{12} + 4C_{13}) > 0$. Figure 3.3.1.1, shows variation of elastic constants of $Pd_{50-x}Pt_xS_{50}$ with Pt content. An increase of elastic constants was noticed with increasing Pt content. A decrease in elastic constants was observed in figure 3.3.2 with increasing concentration of Pd. C_{12}, C_{13}, C_{44} and C_{66} show a linear decrease as Pd is introduced to the system. $C_{11}$and C_{33}, whilst decreasing near linearly with increasing Pd at higher concentrations, shows a slight curvature at lower concentrations. As Pd is introduced to the system, elastic constants decrease with increasing concentration of Pd.

3.4. Phonon dispersions for $Pt_{50-x}Pd_xS_{50}$ and $Pd_{50-x}Pt_xS_{50}$

Phonon dispersions of $Pt_{50-x}Pd_xS_{50}$ and $Pd_{50-x}Pt_xS_{50}$ calculations were performed at different concentrations, used for heats of formation and elastic properties. In Fig. 3.4.1 phonon dispersion curve of $Pt_{50}S_{50}$ $P4_2/mmc$ were plotted along with partial phonon density of states, depicting contributions of the elements. There are no imaginary phonon frequencies detected in this structure.

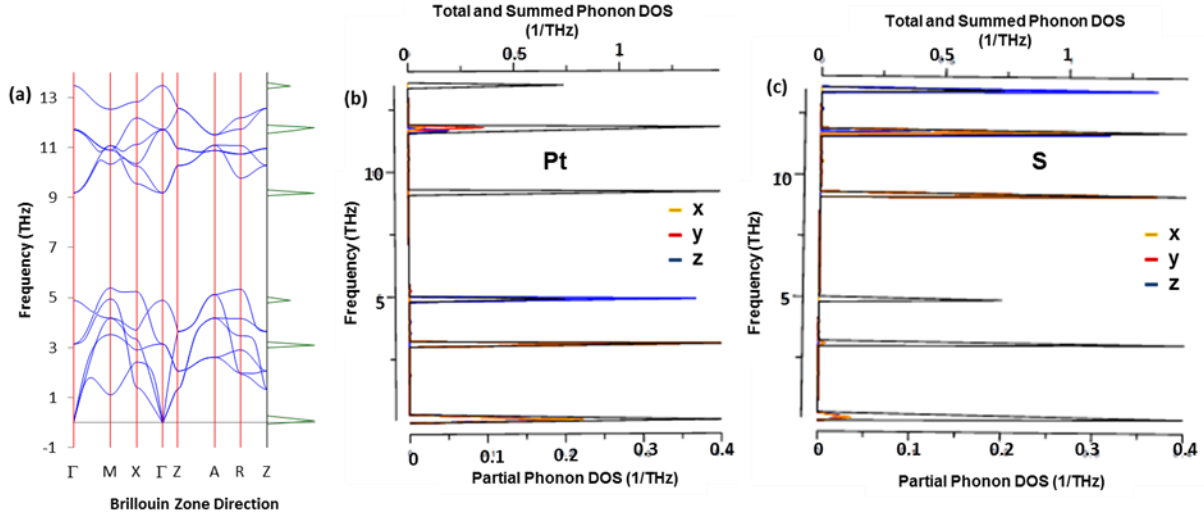

Figure 3.4. 1. (a) Phonon dispersions for $Pt_{50}S_{50}$ $P4_2/mmc$, Phonon density of states for $Pt_{50}S_{50}$ (b) Pt contribution and (c) S contribution

Both platinum and sulphur atoms contribute to the acoustic branches and optical branches. In Figure 3.4.2, phonon dispersions show a negative frequency which is associated with a positive value for energy of formation and is regarded as been unstable for $Pt_{25}Pd_{25}S_{50}$ structure. The negative frequency corresponds to C_{66} being negative which indicates instability, and emanate from vibrations of Pt, Pd and S.

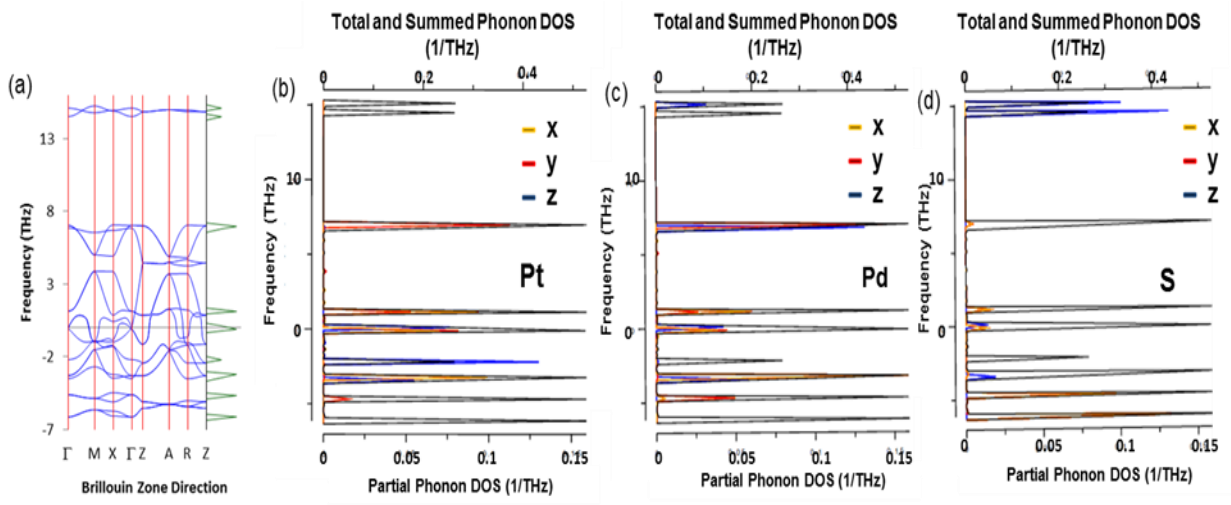

Figure 3.4. 2. Phonon dispersions for $Pt_{25}Pd_{25}S_{50}$ $P4_2/mmc$ (a) Phonon density of states for $Pt_{25}Pd_{25}S_{50}$ (b) Pt contribution, (c) Pd contribution and (d) S contribution.

Since figure 3.4.2 alludes to structural instability, different structures were extracted from the $Pt_{25}Pd_{25}S_{50}$ $P4_2/mmc$ structure and were optimized. Phonon dispersions were calculated to locate stable structures. A stable structure was $Pt_{25}Pd_{25}S_{50}$ with a space group P_2/c in figure 3.3.3 and lattice parameters a = 6.961, b = 6.924 and c = 8.163 Å.

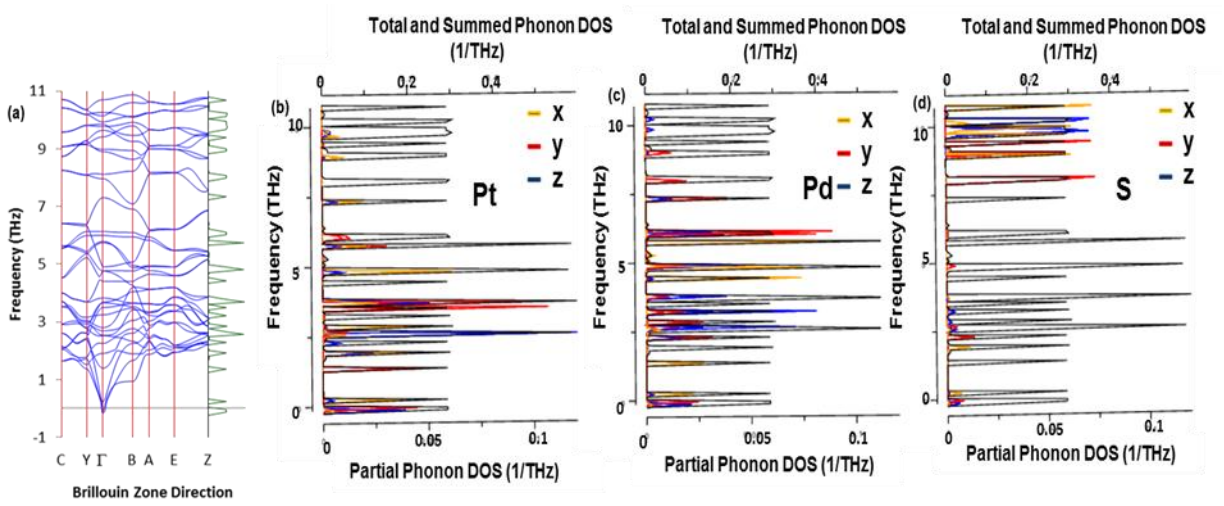

Figure 3.4. 3. (a) Phonon dispersions for $Pt_{25}Pd_{25}S_{50}$ P_2/c, Phonon density of states for $Pt_{25}Pd_{25}S_{50}$ (b) Pt contribution, (c) Pd contribution and (d) S contribution.

Figure 3.4.3 shows the phonon spectra with limited soft modes along Γ of the Brillioun zone. The phonon spectra consists of two bands which nearly overlap, the upper band which consist of optical branches and the lower band which consist of acoustic and optical branches The partial DOS shows that Pt and Pd atoms contributes towards the soft modes, with x - y component being dominant. S atoms contribute minimal to the soft modes. It is observed that the bands have mixed due to sulphur atoms vibrating at lower frequencies. The soft modes are due to C_{66} being negative. The optical branches in the upper band are mainly emanating from the S atoms.

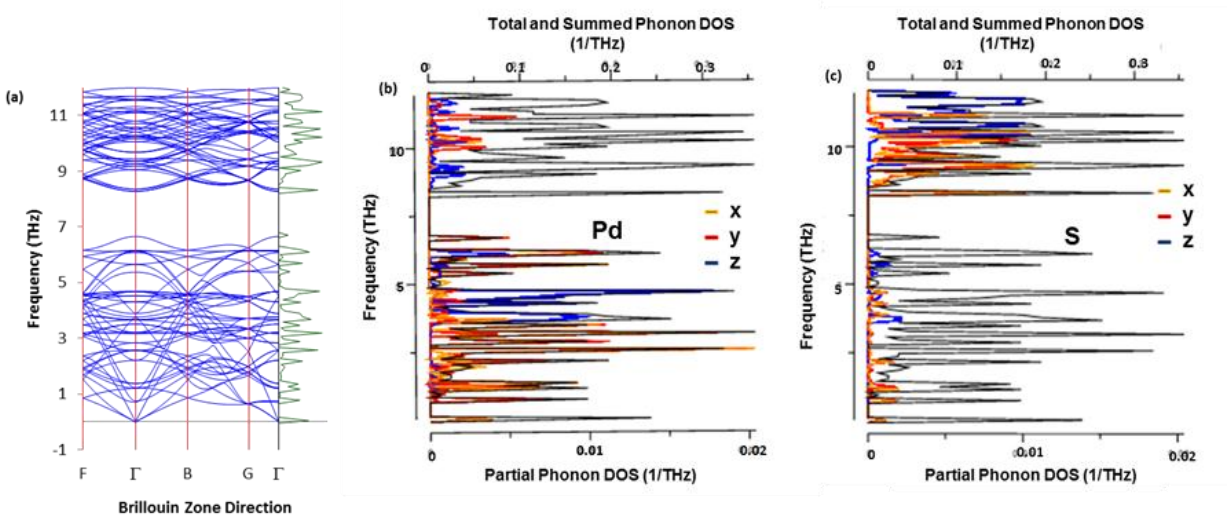

Figure 3.4. 4. (a) The phonons dispersion curve for $Pd_{50}S_{50}$ $P4_2/mmc$, Phonon density of states (b) Pt contribution and (c) S contribution.

No soft modes were observed, all branches are positive. Looking at the PDOS, it is observed that Pd and S atoms are responsible for the acoustic and optical branches in the lower band, and x - y being dominant. The S and Pd atoms are mainly responsible for the optical branches in the upper band. The $Pd_{50}S_{50}$ $P4_2/mmc$ structure has many branches compared to $Pt_{50}S_{50}$ and $Pt_{25}Pd_{25}S_{50}$ $P4_2/mmc$ structures.

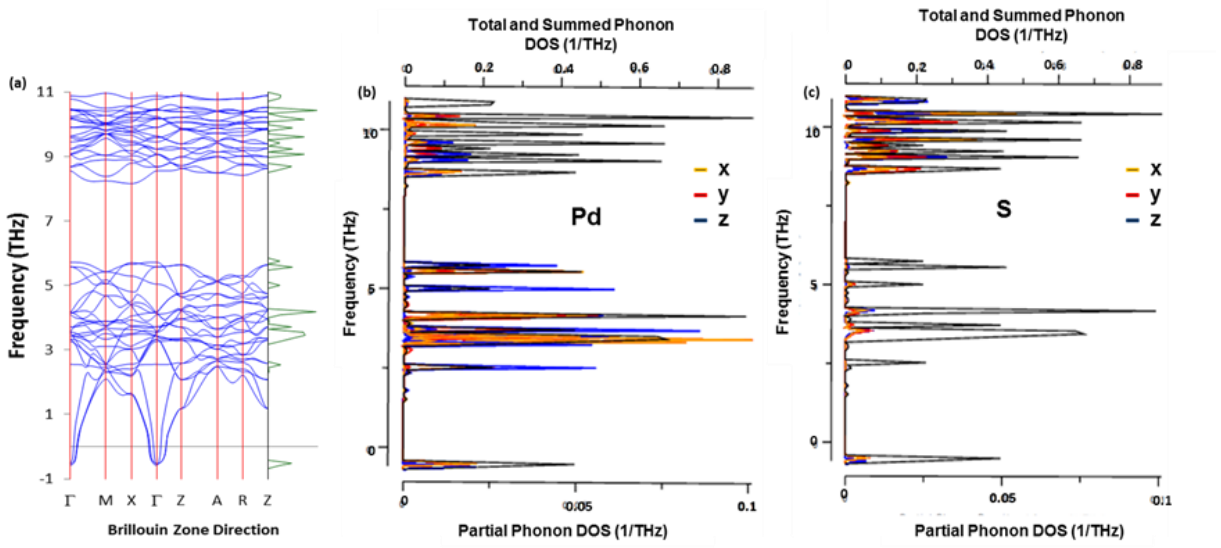

Figure 3.4. 5. (a) The phonon dispersions curve for $Pd_{50}S_{50}$ $P4_2/m$, Phonon density of states (b) Pd contribution and (c) S contribution.

Figure 3.4.5, shows phonon spectra with negative frequency at point Γ of the Brillioun zone. The partial DOS shows that Pd and S atoms are responsible for the negative frequencies, with Pd being more dominant. The x - z component is dominant in the optical branches of the lower band. Both S and Pd contribute to the optical branches in the upper band, with S atoms being dominant.

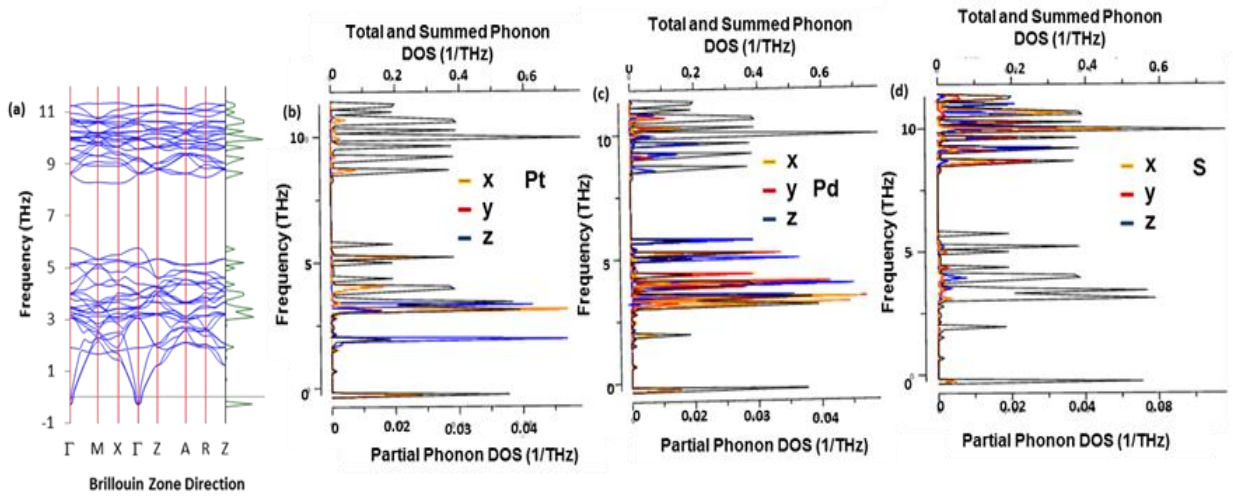

Figure 3.4. 6. (a) The phonon dispersions curve for $Pd_{37.5}$ $Pd_{12.5}S_{50}$ $P4_2/m$, Phonon density of states (b) Pt contribution (c) Pd contribution and (d) S contribution.

The phonon spectra show soft modes at point Γ of the Brillioun zone. The partial DOS indicate that Pt, Pd and S atoms contribute towards the soft modes, though the latter is insignificant. It is noted that Pt and Pd contributions are dominant in the lower band whilst Pd and S atoms are responsible for the optical branches in the upper band, where the Pt contribution is limited.

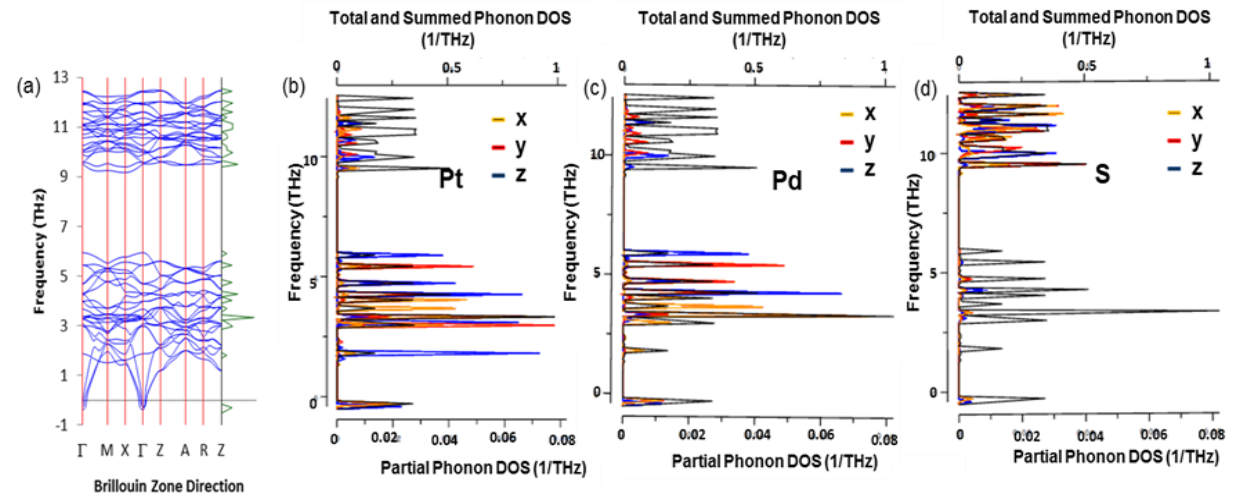

Figure 3.4. 7. (a) The phonon dispersions curve for $Pd_{25}Pt_{25}S_{50}$ $P4_2/m$, Phonon density of states (b) Pt contribution, (c) Pd contribution and (d) S contribution.

Figure 3.4.7, shows phonon spectra with 25% of Pt, where slight soft modes were detected at point Γ of the Brillioun zone. The PDOS shows that Pt, Pd and S atoms vibrate at lower frequencies, below 0 THz. It is evident that x - z components of Pt and Pd are mainly responsible for the soft modes. Pt and Pd contribute dominantly to the lower band consisting of acoustic and optical branches whilst the optical branches in the upper band are due Pt, Pd and S atoms. Sulphur atoms vibrate at higher frequencies, greater than 9.0 THz in the upper band.

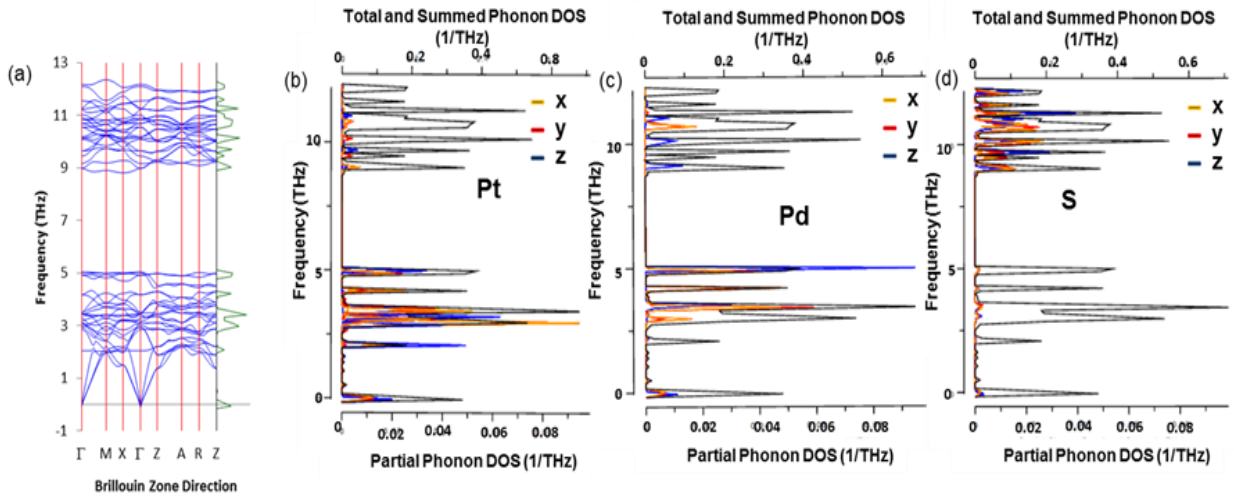

Figure 3.4. 8. (a) The phonon dispersions curve for $Pd_{12.5}Pt_{37.5}S_{50}$ $P4_2/m$, Phonon density of states (b) Pt contribution, (c) Pd contribution and (d) S contribution.

The phonon dispersions for $Pd_{12.5}Pt_{37.5}S_{50}$ $P4_2/m$ are given in Fig 3.4.8 and no soft modes are observed. The lower band is associated with the Pt and Pd atoms, and mainly the y - z components. The optical branches in the upper band emanate from the Pt, Pd and S atoms with the latter being dominant.

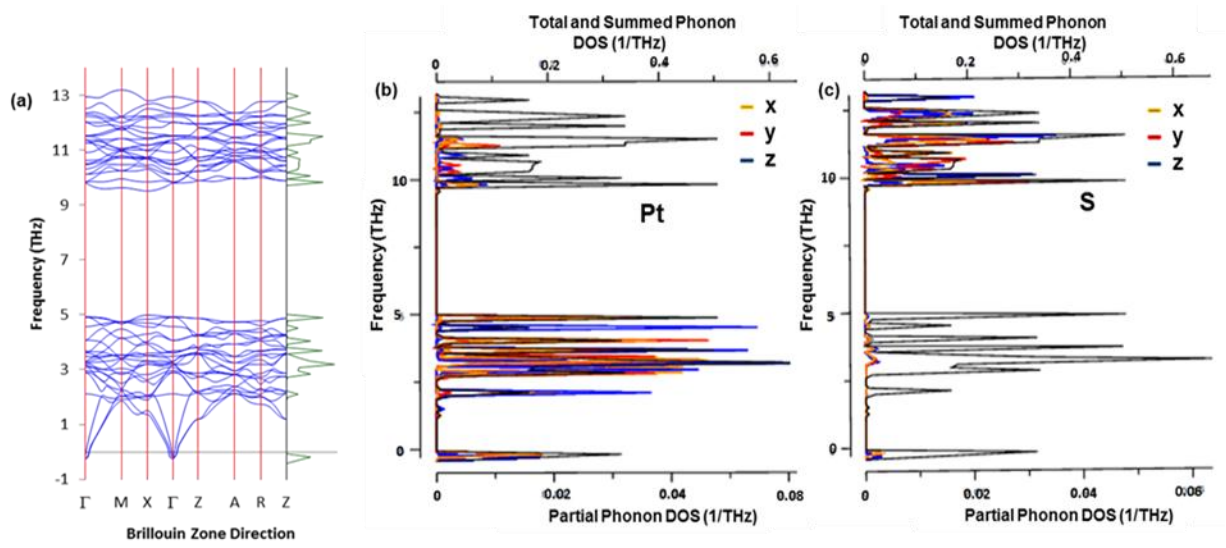

Figure 3.4. 9. (a) The phonon dispersions curve for $Pt_{50}S_{50}$ $P4_2/m$. Phonon density of states (b) Pt contribution and (c) S contribution.

Figure 3.4.9, shows phonon spectra for $Pt_{50}S_{50}$ $P4_2/m$ with limited soft modes in the Γ direction of the Brillioun zone. Pt and S atoms are responsible for the soft modes. The x - z components contribute to the soft modes. It was observed that Pt contributes towards the acoustic and optical branches in the lower band and Pt and S, with the latter dominating, contribute to the optical branches in the upper band

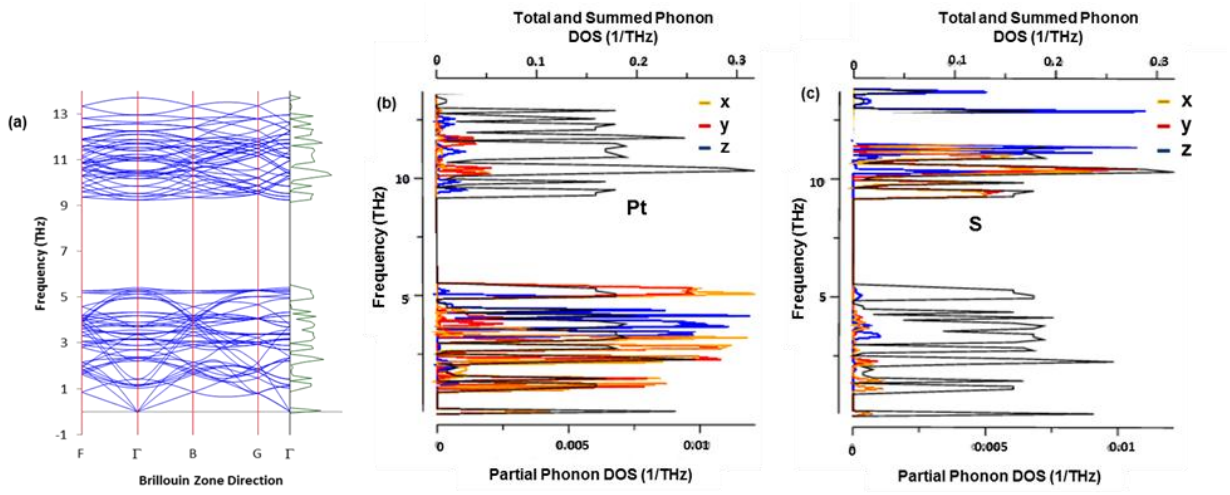

Figure 3.4. 10. (a) The phonon dispersions curve for $Pt_{50}S_{50}$ P_1, Phonon density of states (b) Pt contribution and (c) S contribution.

Figure 3.4.10, shows phonon dispersion curve of PtS supercell, with a P_1 deduced from $P4_2/mmc$ symmetry where all phonon branches are positive. Pt atoms contribute predominantly to frequencies in the lower band and S atoms to the upper band.

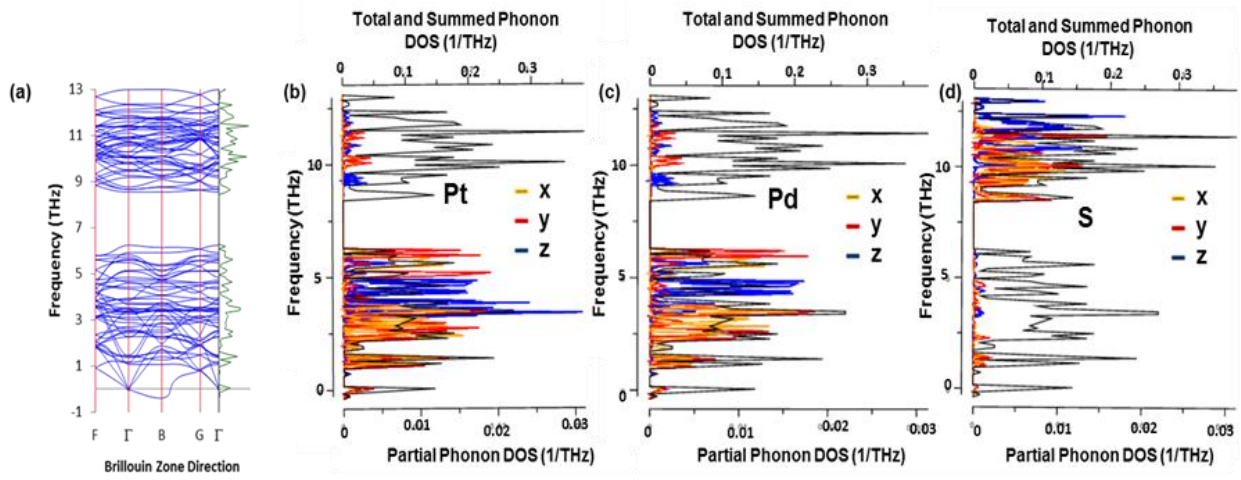

Figure 3.4. 11. (a) The phonon dispersions curve for $Pt_{37.5}Pd_{12.5}S_{50}$ P_1, Phonon density of states (b) Pt contribution (c) Pd contribution and (d) S contribution.

Figure 3.4.11, shows that as palladium is introduced to the system, the structure becomes unstable since soft modes are noted in the F - B direction of the Brillioun zone. From the PDOS, it is observed that Pt and Pd atoms vibrate at lower frequencies, below 0 THz. Pt and Pd atoms contributes in towards the lower band and S atoms contribute to the upper band.

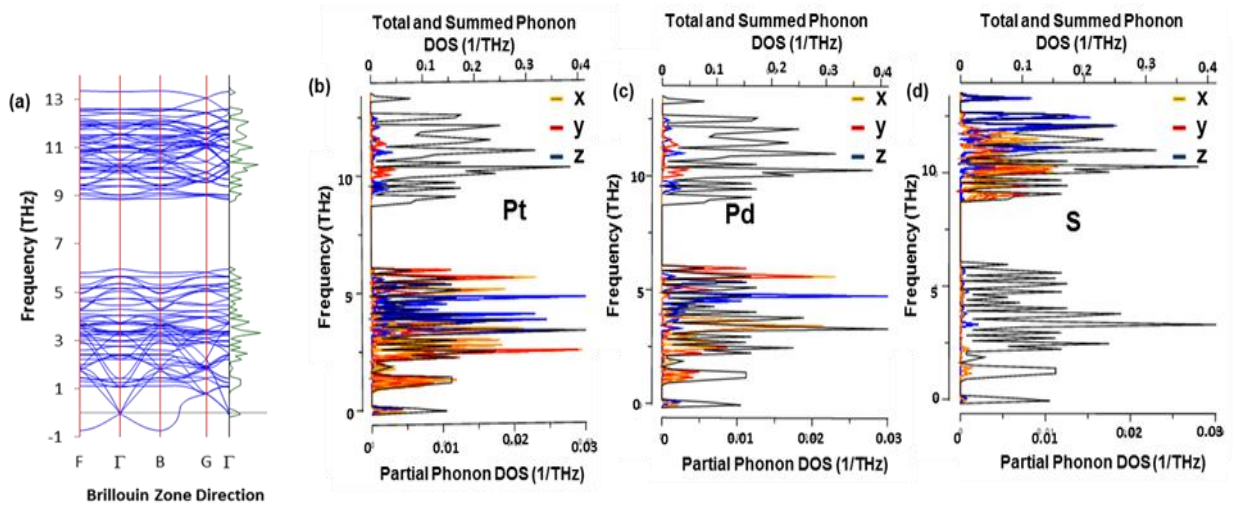

Figure 3.4. 12. (a) The phonon dispersions curve for $Pt_{25}Pd_{25}S_{50}$ P_1, Phonon density of states (b) Pt contribution, (c) Pd contribution and (d) S contribution.

Figure 3.4.12, shows phonon spectra of $Pt_{25}Pd_{25}S_{50}$ P_1 with soft modes in the Γ- B direction of the Brillioun zone. Pt and Pd atoms are mainly responsible for soft modes. Pt and Pd atoms contribute to the lower band and S atoms predominantly to the upper band.

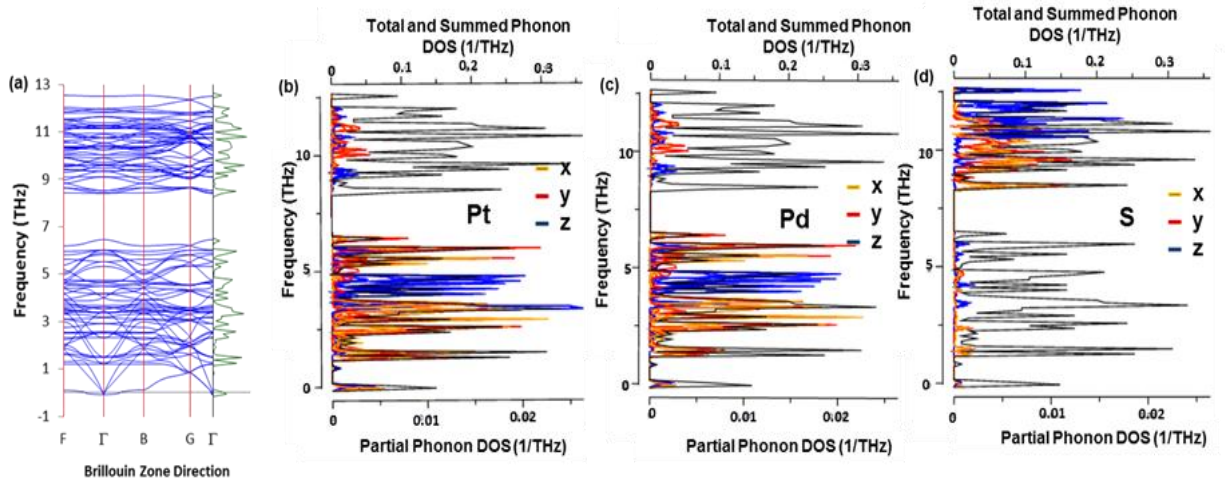

Figure 3.4. 13. (a) The phonon dispersion curve for $Pt_{12.5}Pd_{37.5}S_{50}$ P_1, Phonon density of states (b) Pt contribution, (c) Pd contribution and (d) S contribution.

Figure 3.4.13, shows phonon dispersion curve $Pt_{12.5}Pd_{37.5}S_{50}$ P_1 where all branches are positive. The Pt and Pd atoms contribute mainly to the lower band and S atoms to the upper band.

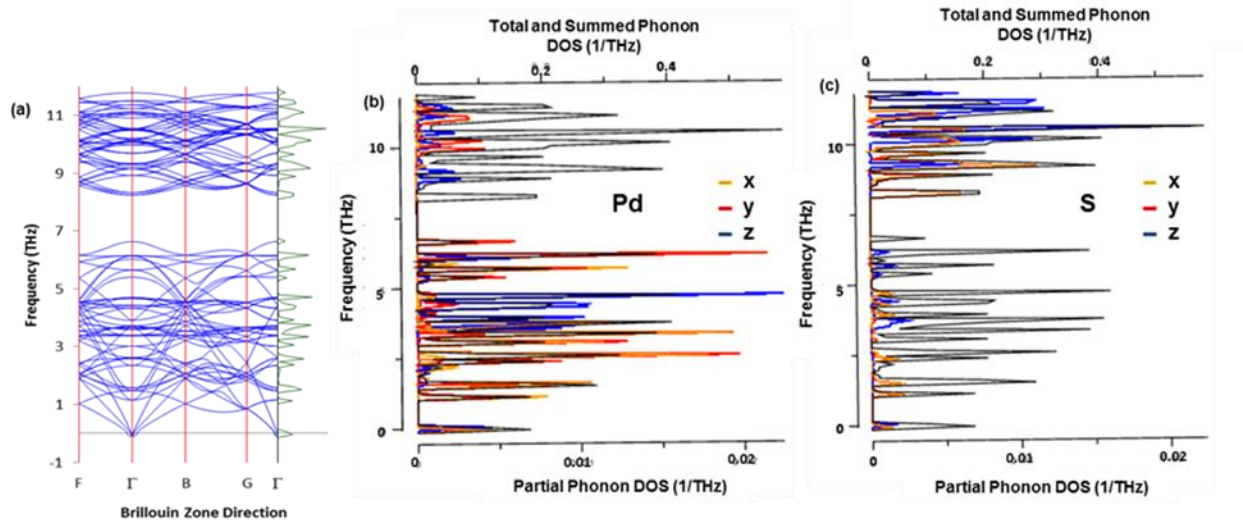

Figure 3.4. 14. (a) The phonon dispersions curve for $Pd_{50}S_{50}$ P_1, Phonon density of states (b) Pt contribution, (c) Pd contribution and (c) S contribution.

Figure 3.4.14, gives the phonon spectra with no soft modes, all branches are positive which suggests stability of structure. The Pd atoms contribute to the lower band and S atoms, and Pd to a limited extent, contribute to the upper band.

3.5. Density of states

The density of states (DOS) shows the contribution of states from platinum (Pt) and sulphur (S) atoms, and these contributions are analyzed from the partial density of states. Structural instabilities in metals are typically related to details of the Fermi surface. In order to better examine the differences in electronic structures of different crystal structures, we plot their density of states (DOS). The DOS is expressed in the number of states per atom per energy interval. Raybaund et al. [19] reported that the formation of a deep pseudogap at the Fermi level is the driving electronic mechanism for stabilization of the PtS and PdS.

3.5.1. Density of states for $Pt_{50-x}Pd_xS_{50}$ and $Pd_{50-x}Pt_xS_{50}$

Total and partial density of states for $Pt_{50-x}Pd_xS_{50}$ and $Pd_{50-x}Pt_xS_{50}$ at 0 GPa will be presented in this section. Figure 3.5.1 shows the total and partial density of states of PtS with $P4_2/mmc$ structure. It was observed that the d-orbital contributes more to the total DOS. Figure 3.5.2 shows total and partial DOS for $Pt_{25}Pd_{25}S_{50}$ where a metal behaviour was noticed. As Pd is introduced to the system, the structure becomes a metal. The d-orbital of Pd contributes towards the total and S has less contribution. Figure 3.5.3 shows total and partial DOS of PdS, where an indirect band gap was noted and estimated as 0.9 eV. The peak ranging from -6 eV to VBM mainly comes from the S (3p) and Pd (4d). The more palladium is added the more the structure becomes stable.

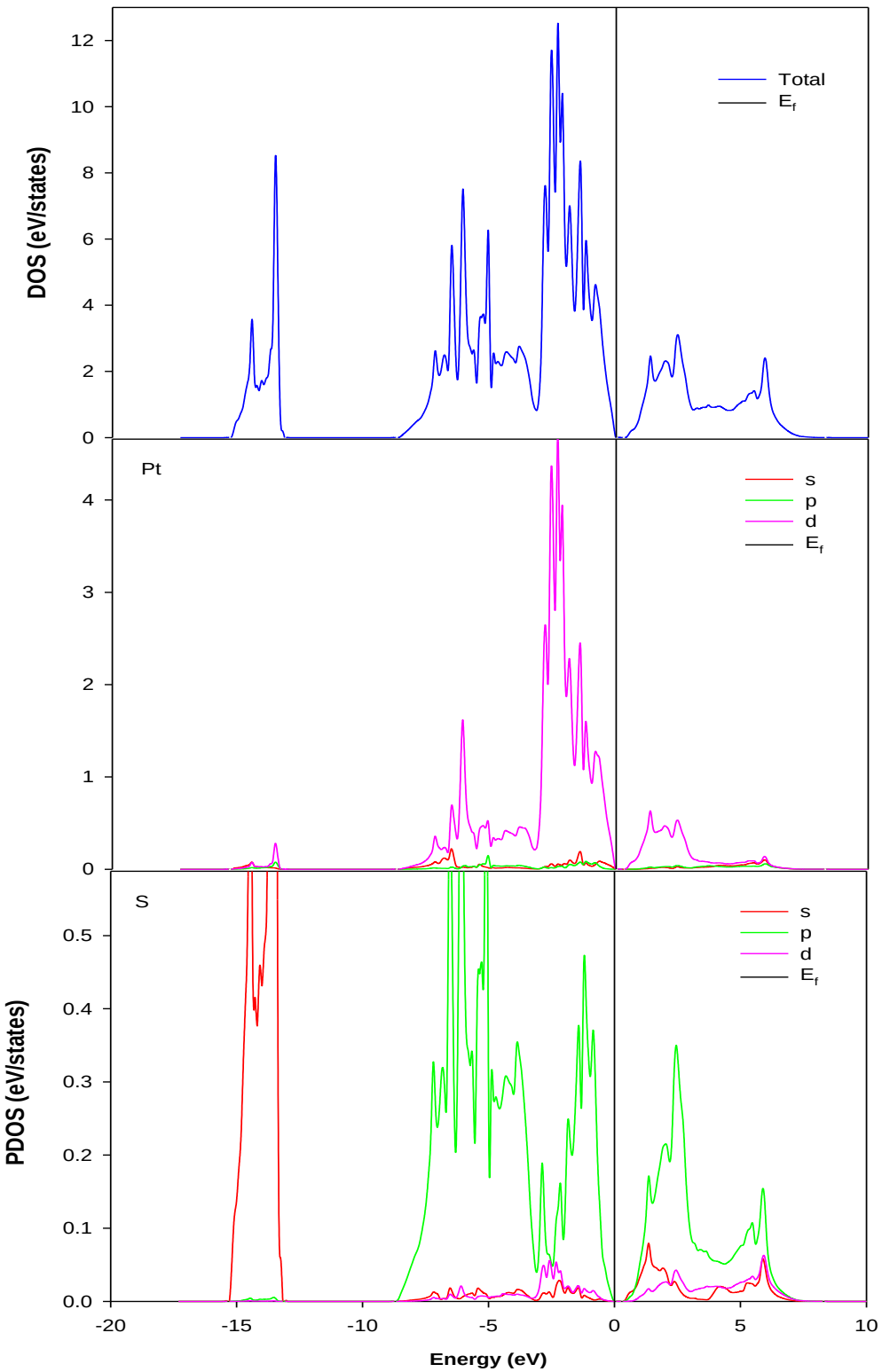

Figure 3.5. 1. Total and partial density of states for $Pt_{50}S_{50}$ $P4_2/mmc$ structure

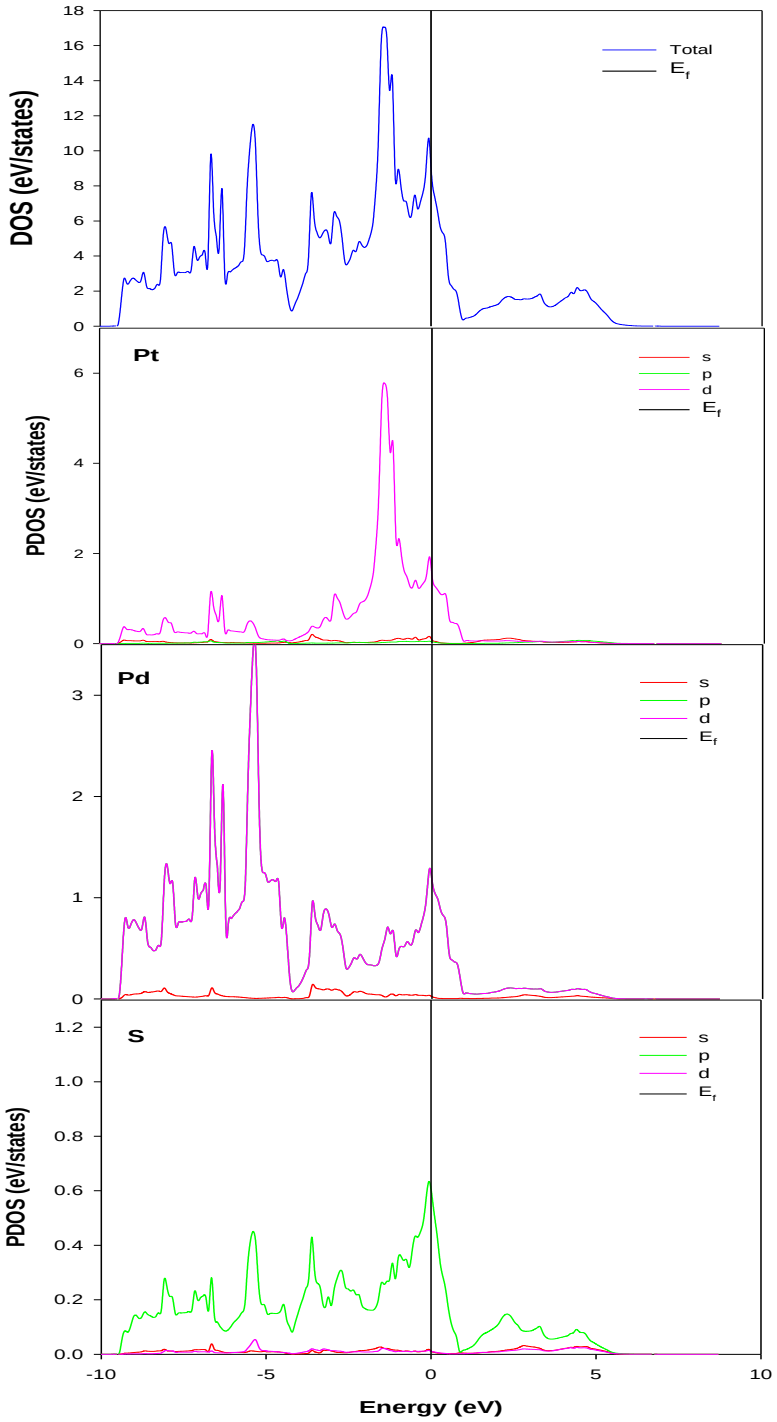

Figure 3.5. 2. Total and partial density of states for Pt_{25} $Pd_{25}S_{50}$ $P4_2/mmc$ structure

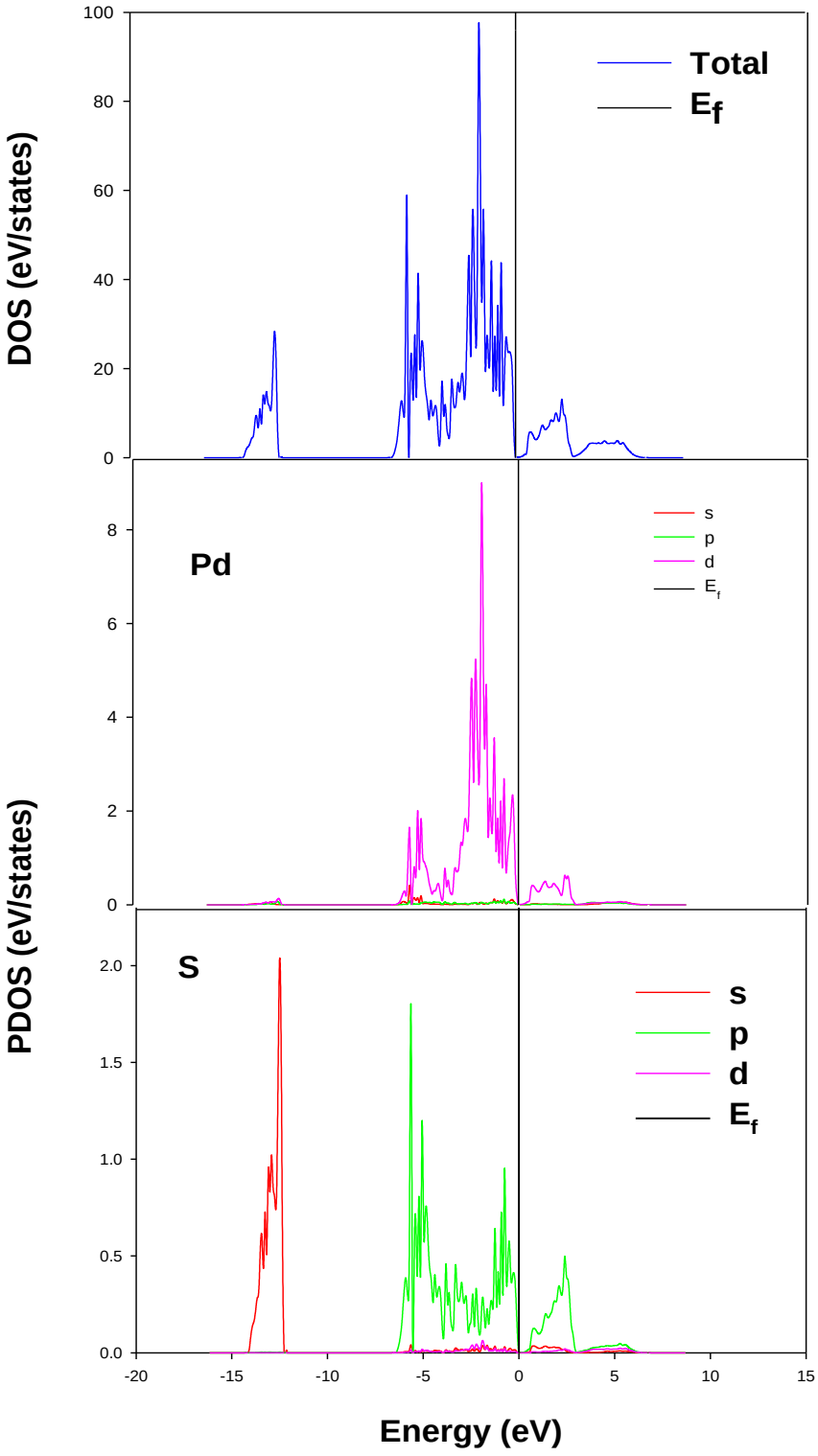

Figure 3.5. 3. Total and partial density of states for $Pd_{50}S_{50}$ $P4_2/mmc$ structure

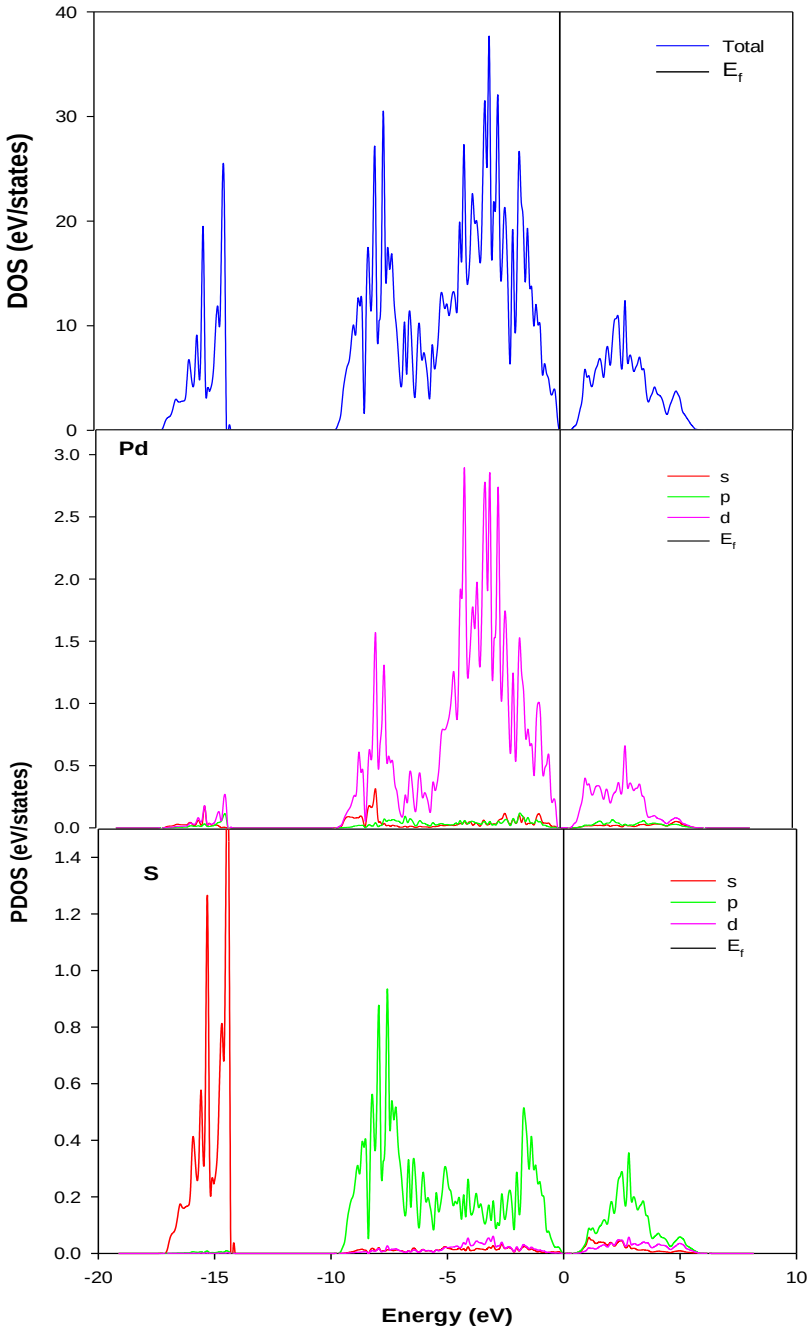

Figure 3.5. 4. Total and partial density of states for $Pd_{50}S_{50}$ $P4_2/m$ structure

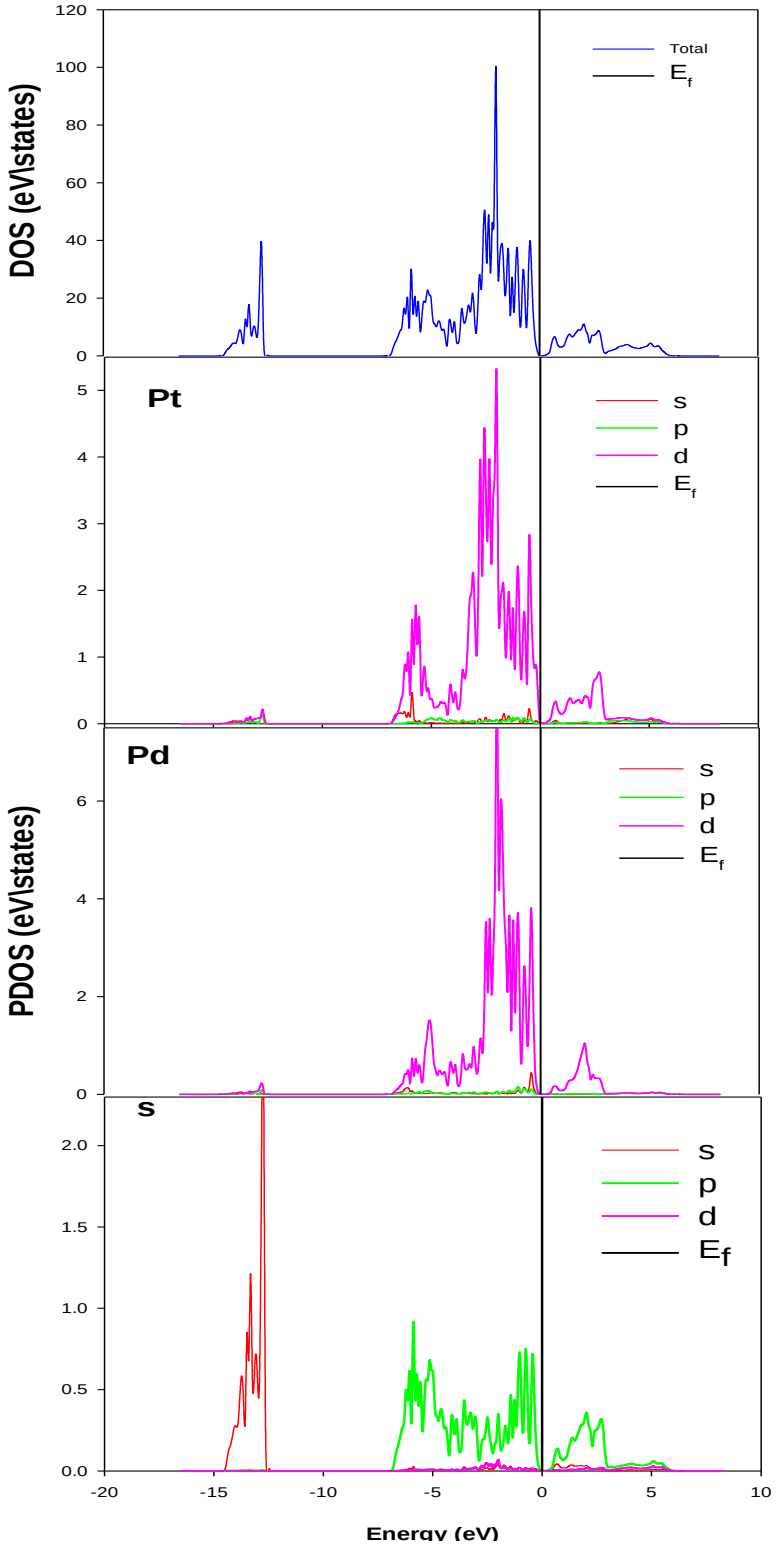

Figure 3.5. 5. Total and partial density of states for $Pd_{37.5}Pt_{12.5}S_{50}$ $P4_2/m$ structure

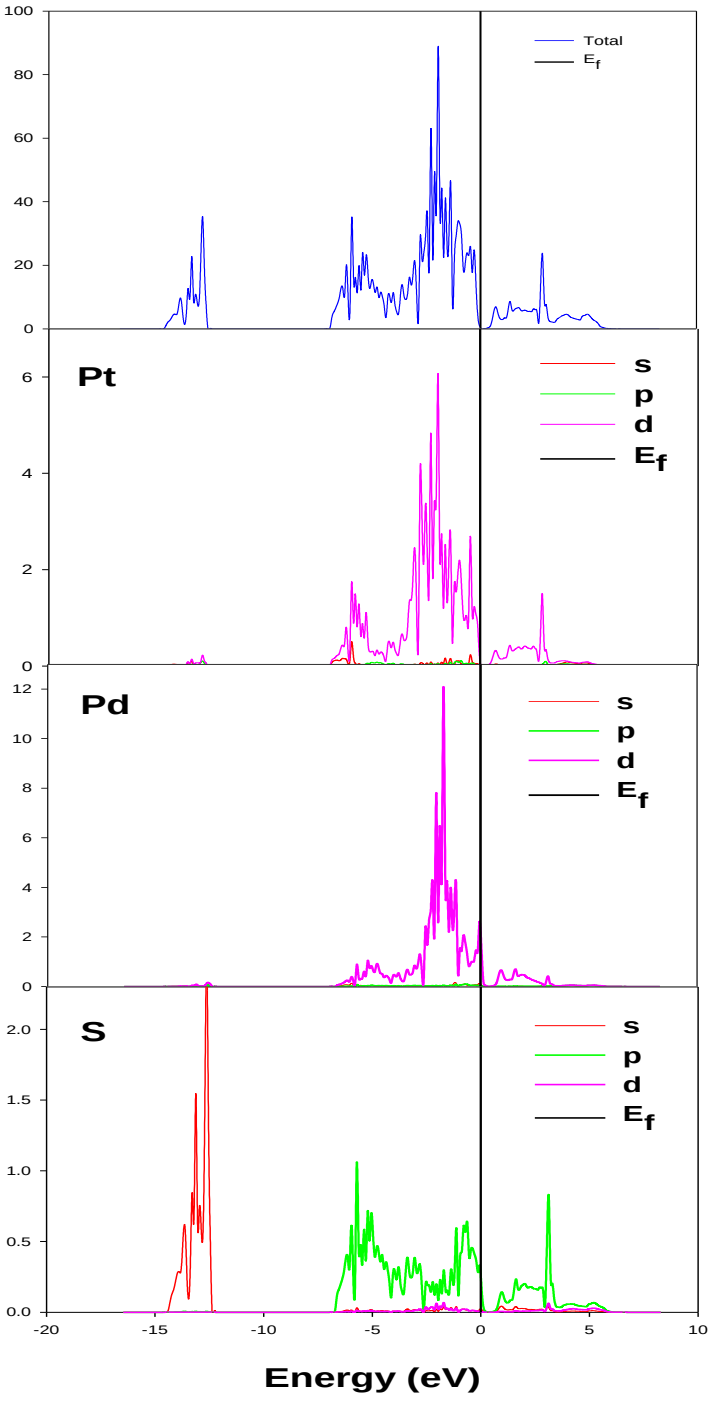

Figure 3.5. 6. Total and partial density of states for $Pt_{25}Pd_{25}S_{50}$ $P4_2/m$ structure

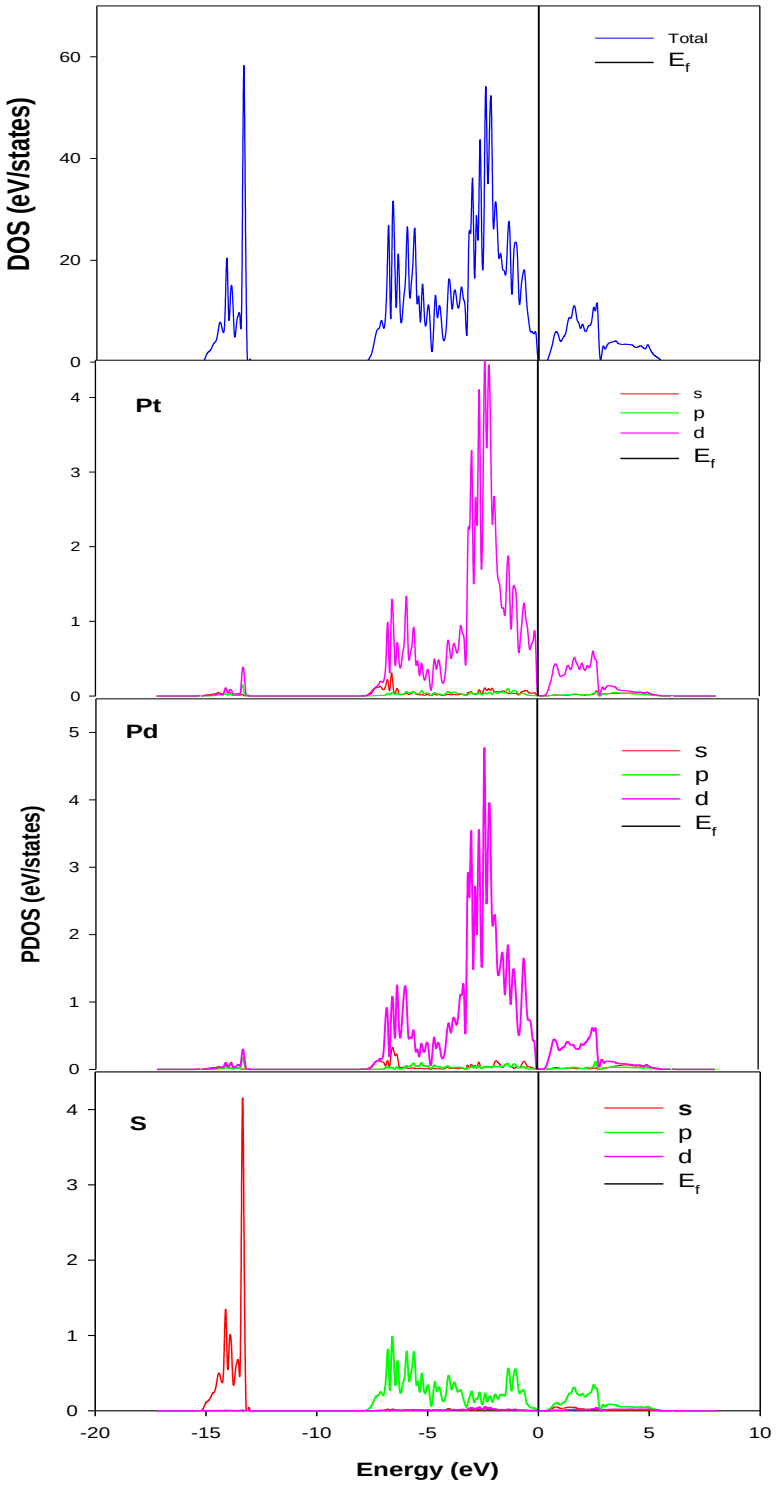

Figure 3.5. 7. Total and partial density of states for $Pd_{12.5}Pt_{37.5}S_{50}$ $P4_2/m$ structure

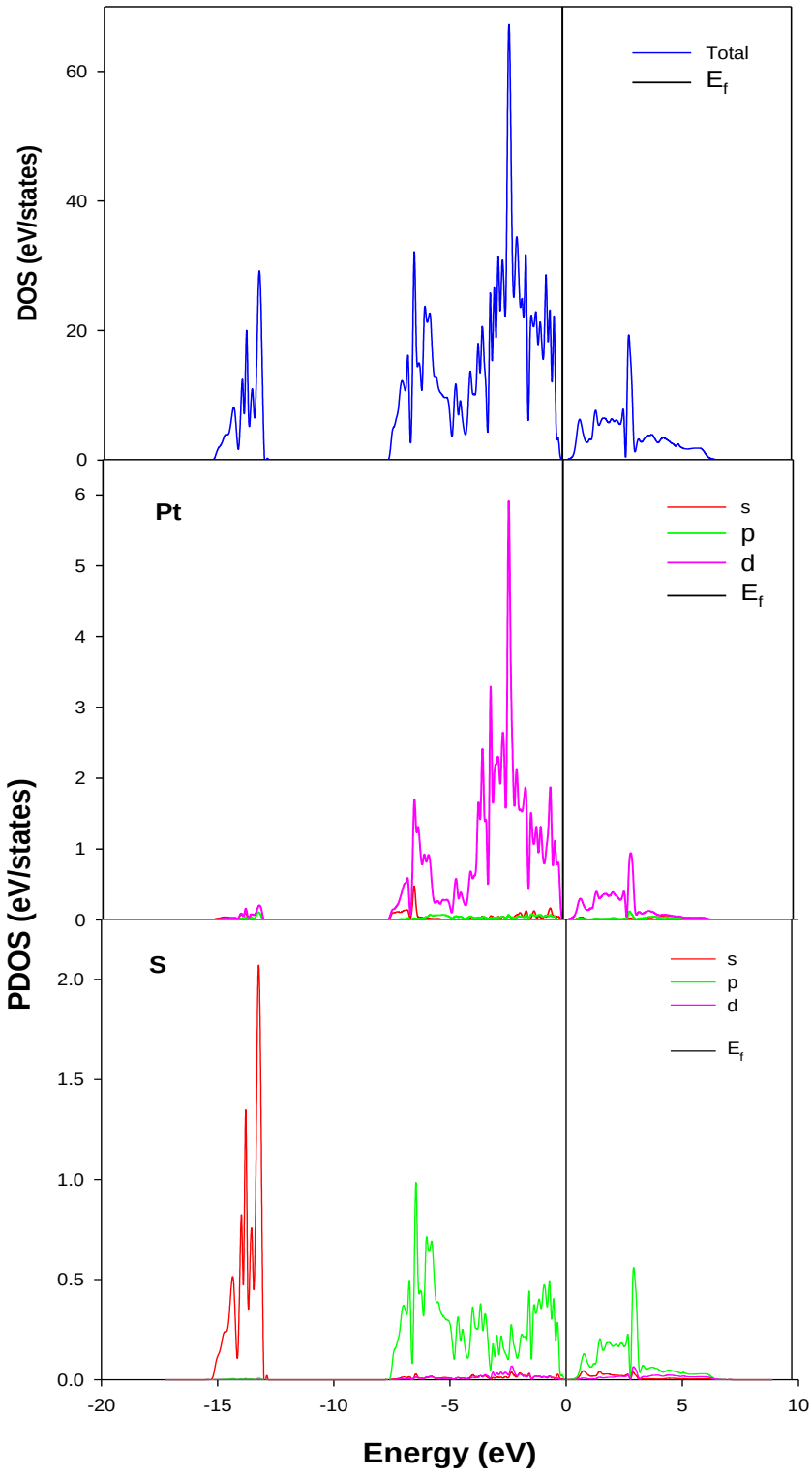

Figure 3.5. 8. Total and partial density of states for $Pt_{50}S_{50}$ $P4_2/m$ structure

Figure 3.4.4, shows the total and partial density of states (PDOS) for $Pd_{50}S_{50}$ $P4_2/m$ structure. PdS has an indirect band gap of 0.5 eV, which is in agreement with other measured energy gaps, that range from 0.002 eV to 3 eV [67, 68, 69, 8]. The 4d states of Pd contribute more to the total DOS and the s and p states contribution is minimal. The peak ranging from -14 eV to -12 eV emanates mainly from the 3s states of S. The broader distribution between -6.5 eV and valence band (VB) emanates predominately from the 3p states of S and the dominant of 4d states of Pd. Figure 3.4.5, shows the total DOS and PDOS of $Pd_{37.5}Pt_{12.5}S_{50}$ $P4_2/m$. A bandgap of 0.3 eV was noted. The 3s states of S are dominant in the peak ranging from -14.7 eV to -13.5 eV. The 3p states of S and 4d states of Pd are dominant in the peak ranging from -7eV and VB. Figure 3.4.6 shows the total DOS and PDOS of $Pd_{25}Pt_{25}S_{50}$ composition. An indirect band gap was observed and was estimated as 0.7 eV. The 5d and 4d states of Pt and Pd respectively contribute more to the total DOS and the s and p states contribution is very minimal. The peak ranging from -14.5 eV to -13 eV emanates mainly from the 3s states of S. The broader distribution between -6.5 eV and VB emanates predominately from the 3p states of S and 5d and 4d states of Pt and Pd respectively. The conduction band consists of the anti-bonging of the d states of Pt and Pd and the p states of S. Figure 3.4.7 gives the total DOS and PDOS of $Pd_{12.5}Pt_{37.5}S_{50}$ composition. The valence part of the DOS consists of three isolated peaks positioned from -15 eV to -14 eV, and the broader distribution extending from -6.5 eV up to the VB. The d states of both Pt and Pd contribute more to the DOS. Figure 3.4.8 shows the total DOS and PDOS of $Pt_{50}S_{50}$ $P4_2/m$ concentration. The 5d states of Pt contribute more to the DOS. The peak ranging from -15 eV to -14.5 eV emanates from the 3s states of S. The broader distribution between -7 ev and VB is associated with the S (3p) and Pt (5d) states. The calculated band gap is 0.4 eV. The conduction band consists of the anti-bonding of the d states of Pt and the p states of S.

3.5.2. Density of states for the supercell approach

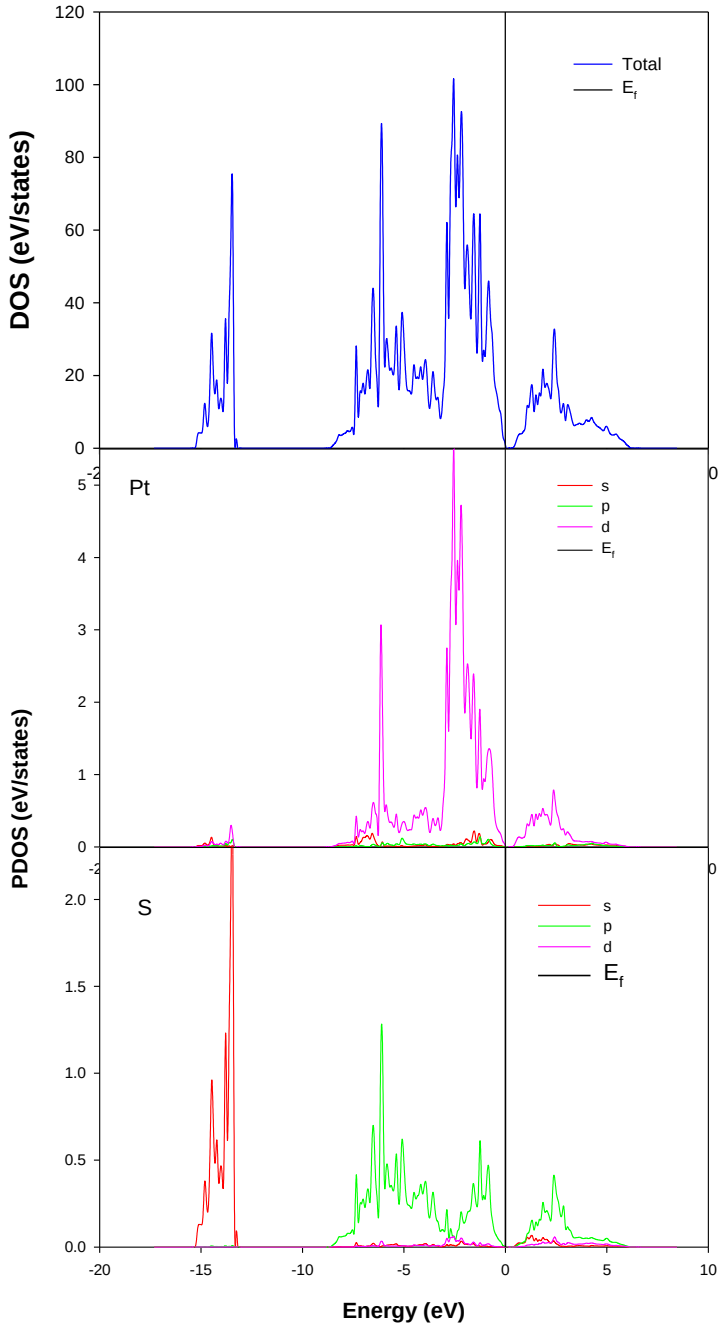

Figure 3.5.2. 1. Total and partial density of states for $Pt_{50}S_{50}$ P_1 structure (from $P4_2/mmc$)

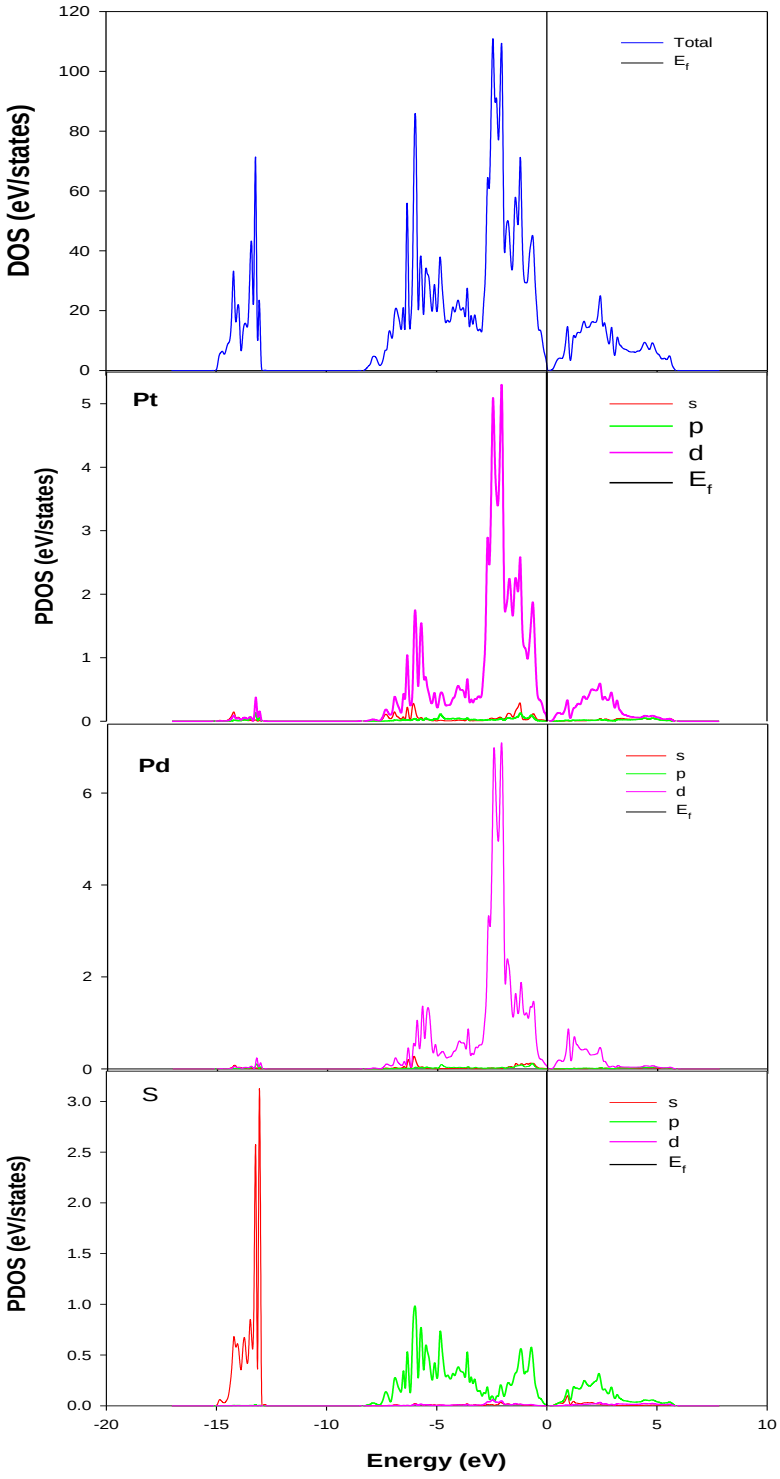

Figure 3.5.2. 2. Total and partial density of states for $Pt_{37.5}Pd_{12.5}S_{50}$ P_1 structure (from $P4_2/mmc$)

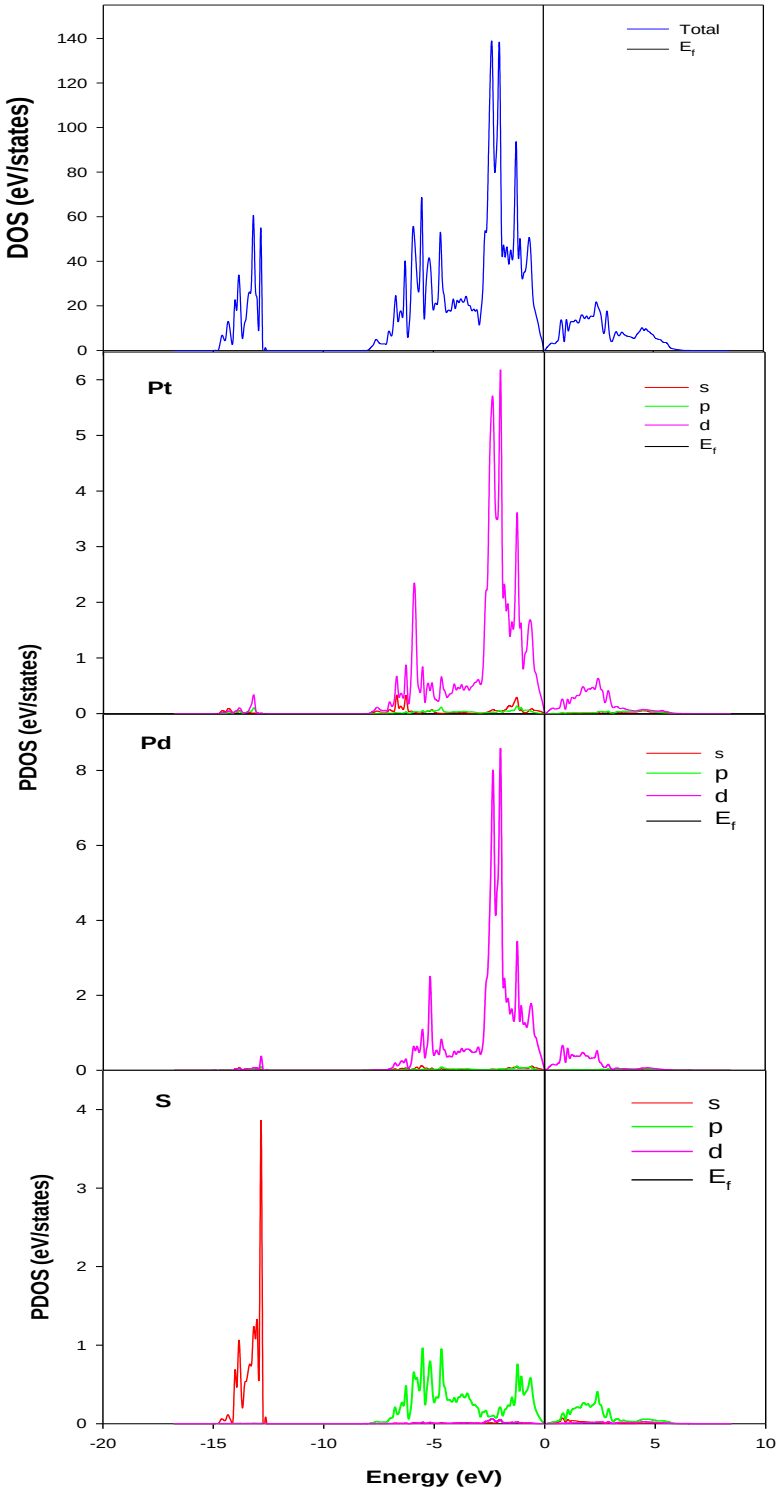

Figure 3.5.2. 3. Total and partial density of states for $Pt_{25}Pd_{25}S_{50}$ P_1 structure (from $P4_2/mmc$)

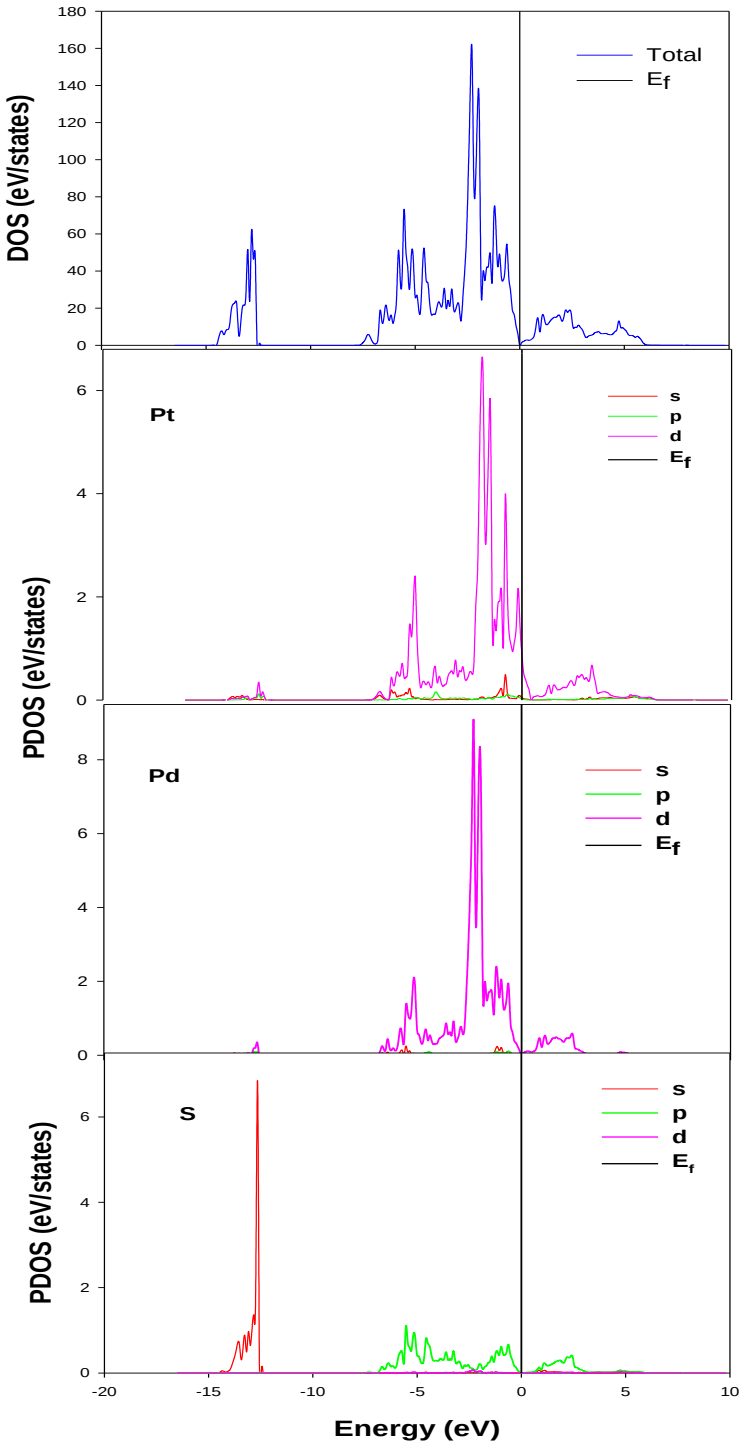

Figure 3.5.2. 4. Total and partial density of states for $Pt_{12.5}Pd_{37.5}S_{50}$ P_1 structure (from $P4_2/mmc$)

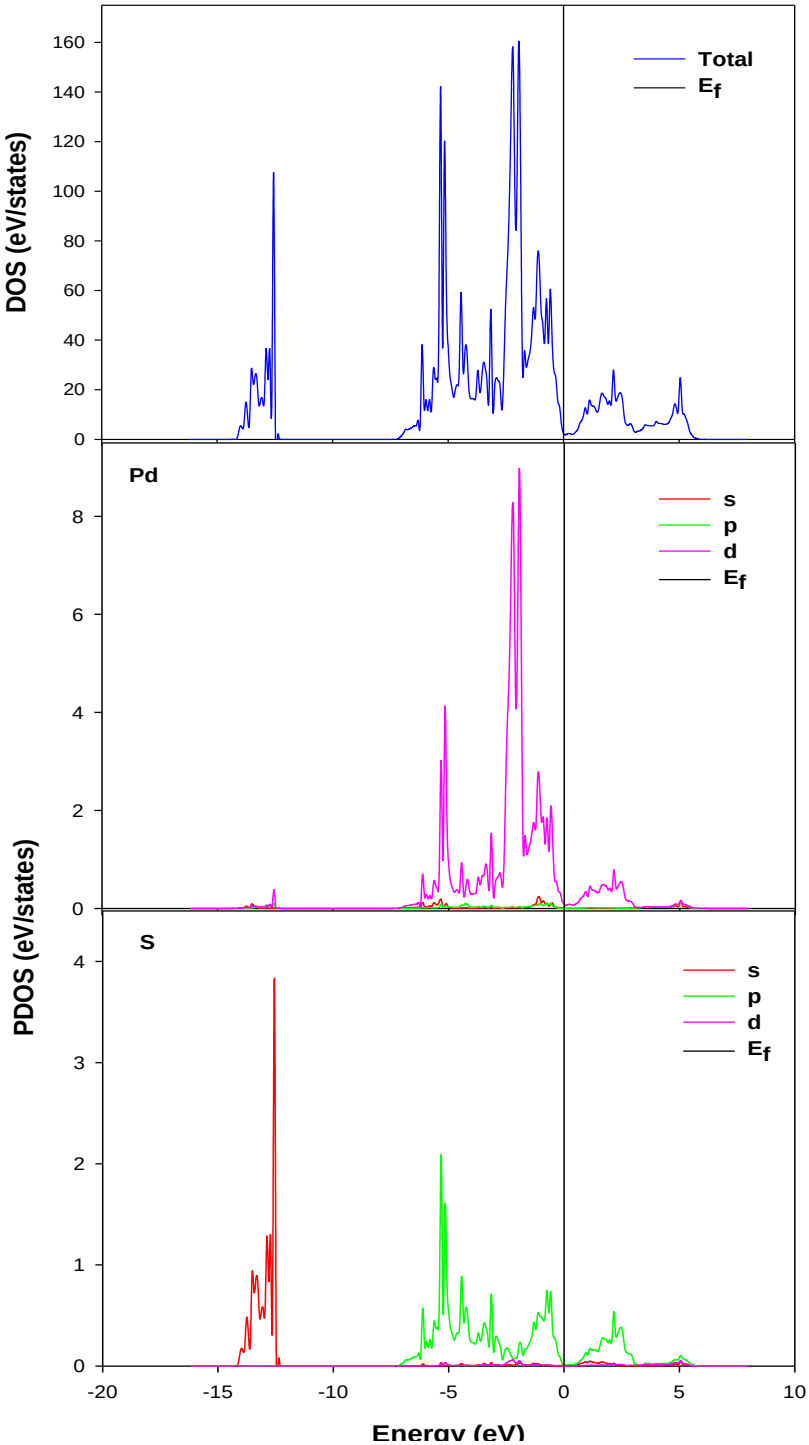

Figure 3.5.2. 5. Total and partial density of states for $Pd_{50}S_{50}$ P_1 structure (from $P4_2/mmc$)

Figure 3.5.2.1, shows the total DOS and PDOS of $Pt_{50}S_{50}$ composition with symmetry P_1/ $P4_2$/mmc. The valence part of the DOS consists of isolated peaks positioned from -15 eV to -14 eV is related mainly to the S 3s state, and the broader distribution extending from -7 eV to the VB is associated with the S 3p and Pt 5d states. The 4d states of Pt contribute more to the DOS and the s and p states' contribution is minimal. The band gap was 0.5 eV. Figure 3.5.2.2 gives the total DOS and PDOS of $Pt_{37.5}Pd_{12.5}S_{50}$ composition. A bandgap was estimated as 0.6 eV. The 5d and 4d states of both Pt and Pd respectively contribute more to the total DOS. The peak ranging from -15 eV to -13.5 eV emanates mainly from the 3s states of S. The broader distribution between -7 eV and VB emanates predominately from the 3p states of S and the dominant of 5d of Pt and 4d of Pd. The conduction band consists of the ant-bonding of d states of Pt and Pd and the p states of S. Figure 3.5.2.3, shows the total DOS and PDOS of $Pt_{25}Pd_{25}S_{50}$ concentration. A bandgap was noted, which was estimated as 0.7 eV. The d states of Pt and Pd contribute more to the total DOS. The s and p states are dominant at the peak ranging from -7 eV to VB. The s states were observed to be dominant in S. Figure 3.5.2.4 gives the total DOS and PDOS of $Pt_{12.5}Pd_{37.5}S_{50}$ composition. The peak ranging from -14.5 eV to -13 eV emanates mainly from S (3s) states. The broader distribution between -6.5 eV and VB emanates predominately from the S (3p), Pt (5d) and Pd (4d) states. The calculated bandgap is 0.8 eV. Figure 3.5..2.5 gives the total DOS and PDOS of $Pd_{50}S_{50}$ composition and the bandgap is 0.6 eV. The d states of Pt contribute more to the total DOS. The peak ranging from -14.5 eV to -13.5 eV emanates mainly from the 3s states of S, 5d and 4d states of Pt and Pd respectively. The conduction band consists of the anti-bonding of the d states of Pd and the p states of S. It was observed that as the concentration increases, the bandgap increases, and then decreases.

3.6. Pressure variation on structural, electronic and mechanical properties

Table 3.6. 1. Pressure dependence of the $(Pt_{50-x}Pd_x)S_{50}$ and $(Pd_{50-x}Pt_x)S_{50}$

	Space group	10GPa	20 GPa	30 GPa	40 GPa	50 GPa
$Pt_{50}S_{50}$	$P4_2/mmc$	a=3.426, c=6.101	a=3.328, c=6.121	a=3.243, c=6.153	a=3.112, c=6.318	a=3.035, c=6.385
$Pt_{25}Pd_{25}S_{50}$	$P4_2/mmc$	a=4.661, c=8.474	a=4.468, c=8.364	a=4.339, c=8.266	a=4.251, c=8.162	a=4.191, c=8.045
$Pd_{50}S_{50}$	$P4_2/mmc$	a=3.386, c=6.194	a=3.247, c=6.277	a=3.013, c=6.687	a=4.251, c=8.162	a=2.633, c=7.520
$Pd_{50}S_{50}$	$P4_2/m$	a=6.346, c=6.567	a=6.232, c=6.445	a=6.129, c=6.392	a=6.054, c=6.306	a=5.980, c=6.259
$Pd_{37.5}Pt_{12.5}S_{50}$	$P4_2/m$	a=6.364, c=6.528	a=6.247, c=6.431	a=6.153, c=6.359	a=6.074, c=6.298	a=6.003, c=6.249
$Pd_{25}Pt_{25}S_{50}$	$P4_2/m$	a=6.375, c=6.541	a=6.256, c=6.444	a=6.164, c=6.372	a=6.085, c=6.313	a=6.015, c=6.260
$Pd_{12.5}Pt_{37.5}S_{50}$	$P4_2/m$	a=6.355, c=6.552	a=6.243, c=6.463	a=6.156, c=6.397	a=6.082, c=6.340	a=6.017, c=6.294
$Pt_{50}S_{50}$	$P4_2/m$	a=6.353, c=6.551	a=6.253, c=6.468	a=6.168, c=6.399	a=6.096, c=6.343	a=6.033, c=6.294
$Pt_{50}S_{50}$	$P_1/P4_2/mmc$	a=6.855, c=12.196	a=6.663, c=12.226	a=6.492, c=12.292	a=6.291, c=12.491	a=6.075, c=12.769
$Pt_{37.5}Pd_{12.5}S_{50}$	$P_1/P4_2/mmc$	a=6.835, c=12.241	a=6.624, c=12.296	a=6.428, c=12.421	a=6.695, c=12.094	a=5.712, c=14.455
$Pt_{25}Pd_{25}S_{50}$	$P_1/P4_2/mmc$	a=7.084, b=7.062 c=12.292	a=6.810, b=6.808 c=12.306	a=6.576, b=6.574 c=12.402	a=6.366, b=6.362 c=12.554	a=7.633, b=6.079, c=12.743
$Pt_{12.5}Pd_{37.5}S_{50}$	$P_1/P4_2/mmc$	a=7.088, c=12.308	a=6.793, c=12.338	-	-	-
$Pd_{50}S_{50}$	$P_1/P4_2/mmc$	a=6.781, c=12.366	a=6.497, c=12.539	a=5.653, c=14.477	a=5.433, c=14.818	a=5.292, c=14.977

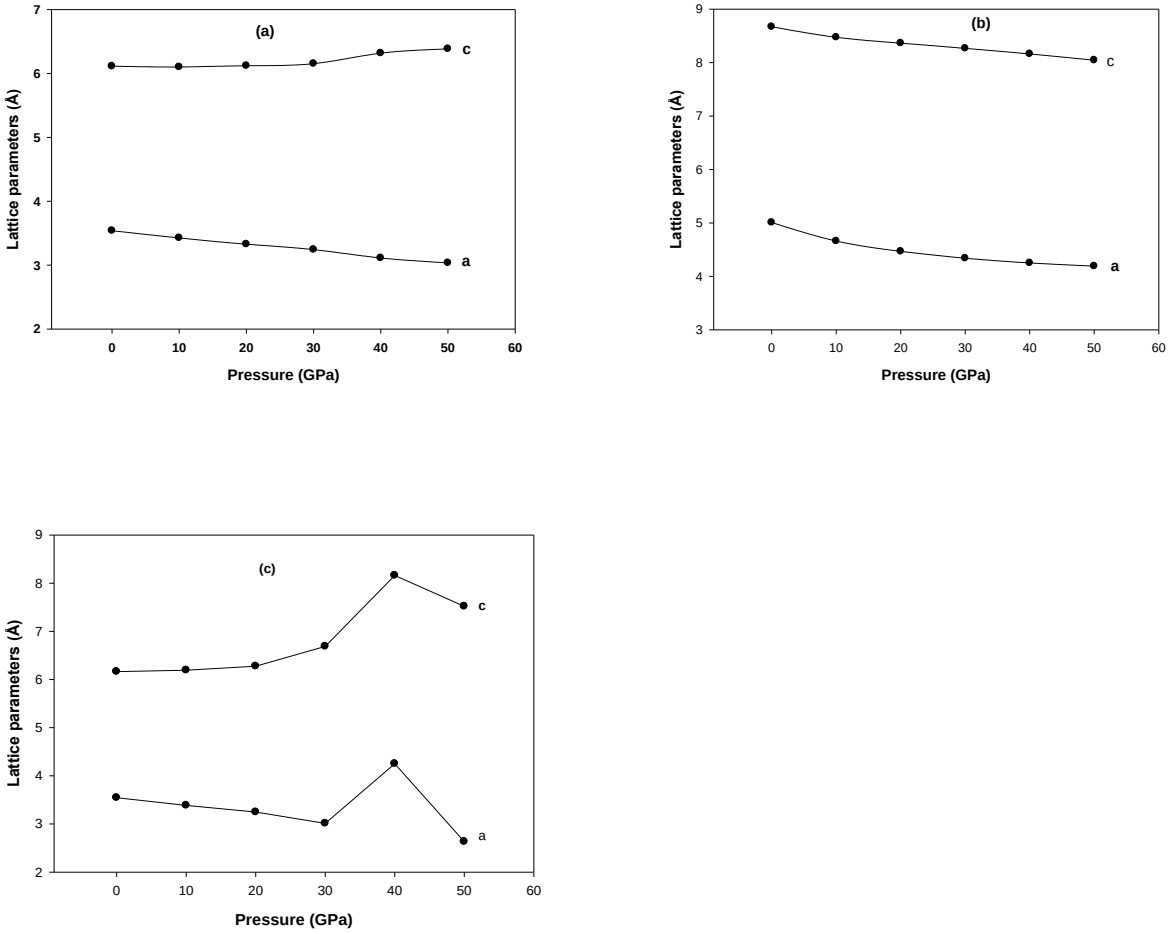

Figure 3.6. 1. The graphs of lattice parameters (Å) against pressure (GPa) (a) $Pt_{50}S_{50}$ (b) $Pt_{25}Pd_{25}S_{50}$ and (c) $Pd_{50}S_{50}$ $P4_2/mmc$

Pressure was varied from 10 – 50 GPa on different concentrations. From the plot (a) in figure 3.6.1, a lattice parameter of $Pt_{50}S_{50}$ was observed to be decreasing with increasing pressure, whereas lattice parameter c increases with increasing pressure. In plot (b), lattice parameters of $Pd_{25}Pt_{25}S_{50}$ decreases with increasing pressure. Anomaly was observed in figure 3.6.1 (a) and (c), and also in figure 3.6.3 (a), (b) and (c) plots, where the c lattice parameter increased with increasing pressure. This striking feature is the increase of c parameter of the PtS with increasing pressure. Similar behaviour was noted in negative linear compressibility, where the material was submitted to hydrostatic

pressure, contrary to intuition, it does not contract in all directions but expand in at least one other direction [17].

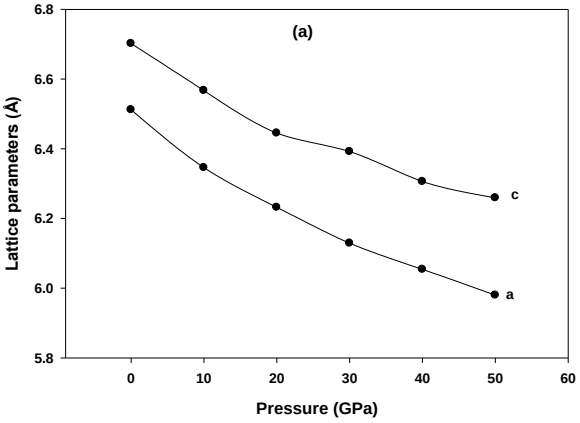

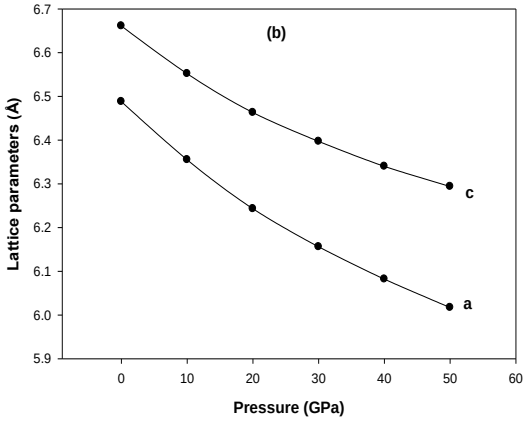

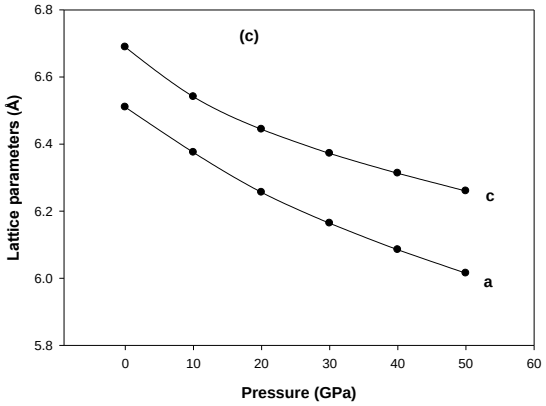

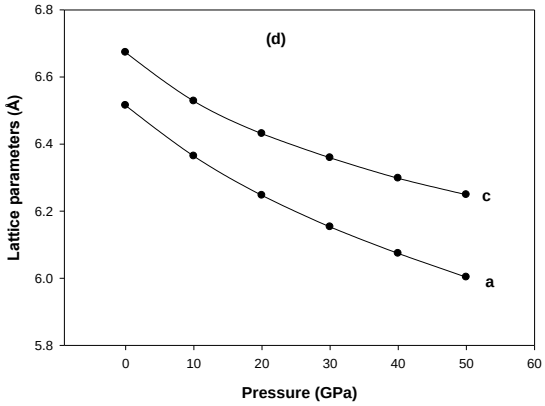

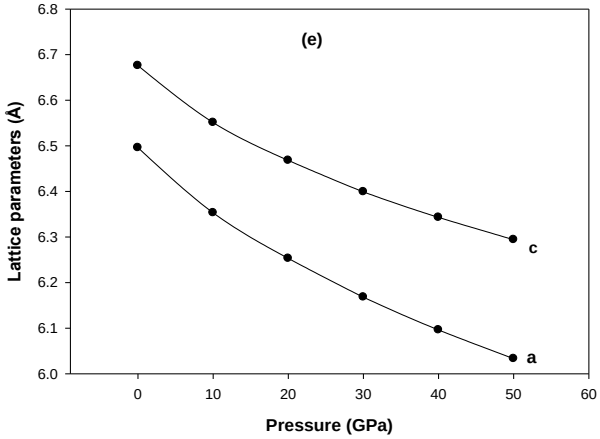

Figure 3.6. 2. The graphs of lattice parameters (Å) against pressure (GPa) (a) $Pd_{50}S_{50}$, (b) $Pd_{37.5}Pt_{12.5}S_{50}$, (c) $Pd_{25}Pt_{25}S_{50}$, (d) $Pd_{12.5}Pt_{37.5}S5_0$ and (e) $Pt_{50}S_{50}$ $P4_2/m$

The results in figure 3.6.2 show that all lattice parameters of $Pd_{50}S_{50}$, $Pd_{37.5}Pt_{12.5}S_{50}$, $Pd_{25}Pt_{25}S_{50}$, $Pd_{12.5}Pt_{37.5}S_{50}$ and $Pt_{50}S_{50}$ $P4_2/m$. decrease with increasing pressure, with the a lattice parameter changing faster. The results plotted in figure 3.6.3, show that as pressure increases the a lattice parameters of $Pd_{50}S_{50}$, $Pd_{37.5}Pt_{12.5}S_{50}$, $Pd_{25}Pt_{25}S_{50}$ and $Pt_{50}S_{50}$ P_1 (from $P4_2/mmc$) decreases. A possible transformation was observed on $Pt_{25}Pd_{25}S_{50}$ in (c) where a ǂ b ǂ c. From the plot, both a and b lattice parameters decreases with increasing concentration whereas c increases with increasing pressure. In plot (d), lattice parameters fluctuate with increasing pressure. At 30 GPa, it was noticed that a decreases, while c increases with pressure.

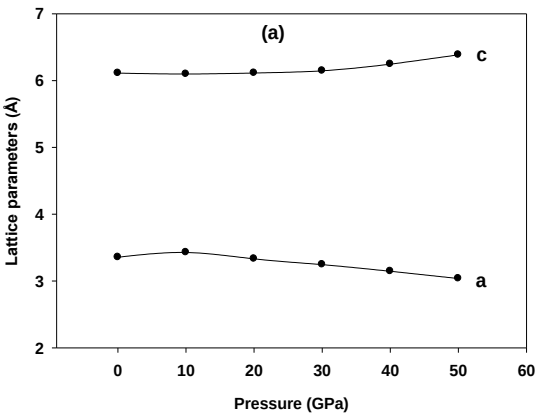

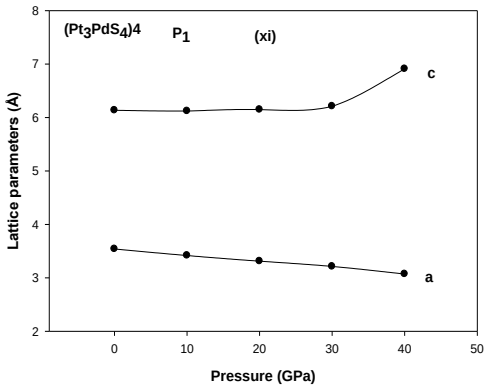

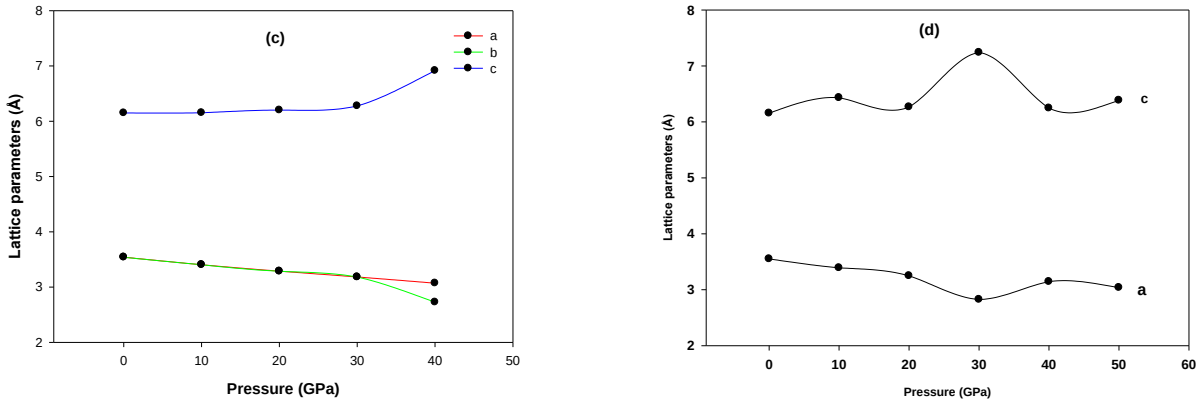

Figure 3.6. 3. The graphs of lattice parameters (Å) against pressure (GPa) (a) $Pd_{50}S_{50}$, (b) $Pd_{37.5}Pt_{12.5}S_{50}$, (c) $Pd_{25}Pt_{25}S_{50}$, and (d) $Pt_{50}S_{50}$ P_1 (from $P4_2/mmc$)

3.6.1. Pressure dependence on elastic properties of $(Pt_{50-x}Pd_x)S_{50}$ and $(Pd_{50-x}Pt_x)S_{50}$

Table 3.6.1. 1. Elastic constants of $(Pt_{50-x}Pd_x)S_{50}$ and $(Pd_{50-x}Pt_x)S_{50}$ at 10 GPa

	Space group	C_{11} GPa	C_{12} GPa	C_{13} GPa	C_{33} GPa	C_{44} GPa	C_{66} GPa	Bulk modulus GPa	Shear modulus GPa
$Pd_{50}S_{50}$	$P4_2/m$	213.53	139.75	133.63	242.62	26.32	42.81	164.34	36.60
$Pd_{37.5}Pt_{12.5}S_{50}$	$P4_2/m$	231.87	140.30	145.04	240.82	30.30	46.09	182.70	39.62
$Pd_{25}Pt_{25}S_{50}$	$P4_2/m$	235.88	141.71	144.28	243.34	38.00	53.82	173.1	44.95
$Pd_{12.5}Pt_{37.5}S_{50}$	$P4_2/m$	254.58	165.97	149.83	290.38	37.72	55.53	192.51	48.45
$Pt_{50}S_{50}$	$P4_2/m$	262.10	165.07	151.69	295.04	46.63	63.11	197.41	54.66

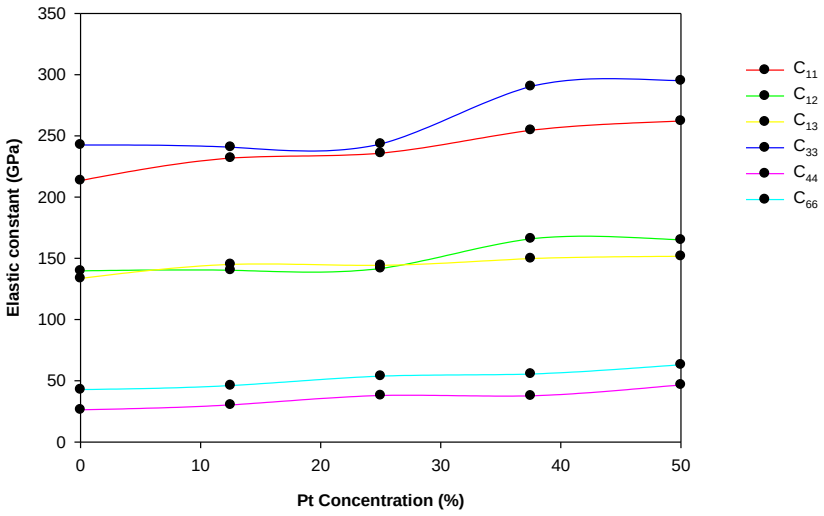

Figure 3.6.1. 1. Variation of elastic constants of $Pd_{50-x}Pt_xS_{50}$ against Pt concentration $P4_2/m$ at 10 GPa

Table 3.6.1. 2. Results of the elastic constants of $(Pt_{50-x}Pd_x)S_{50}$ and $(Pd_{50-x}Pt_x)S_{50}$ at 20 GPa

	Space group	C_{11} GPa	C_{12} GPa	C_{13} GPa	C_{33} GPa	C_{44} GPa	C_{66} GPa	Bulk modulus GPa	Shear modulus GPa
$Pd_{50}S_{50}$	$P4_2/m$	260.34	185.43	180.82	22.91	291.92	14.05	40.76	211.86
$Pd_{37.5}Pt_{12.5}S_{50}$	$P4_2/m$	279.37	182.86	187.25	24.10	306.96	19.48	42.64	220.05
$Pd_{25}Pt_{25}S_{50}$	$P4_2/m$	284.98	187.09	189.55	24.71	307.27	25.70	49.97	223.29
$Pd_{12.5}Pt_{37.5}S_{50}$	$P4_2/m$	302.75	208.87	195.94	28.24	359.12	28.61	54.84	240.68
$Pt_{50}S_{50}$	$P4_2/m$	313.66	214.96	194.28	30.00	370.31	37.41	64.23	244.96

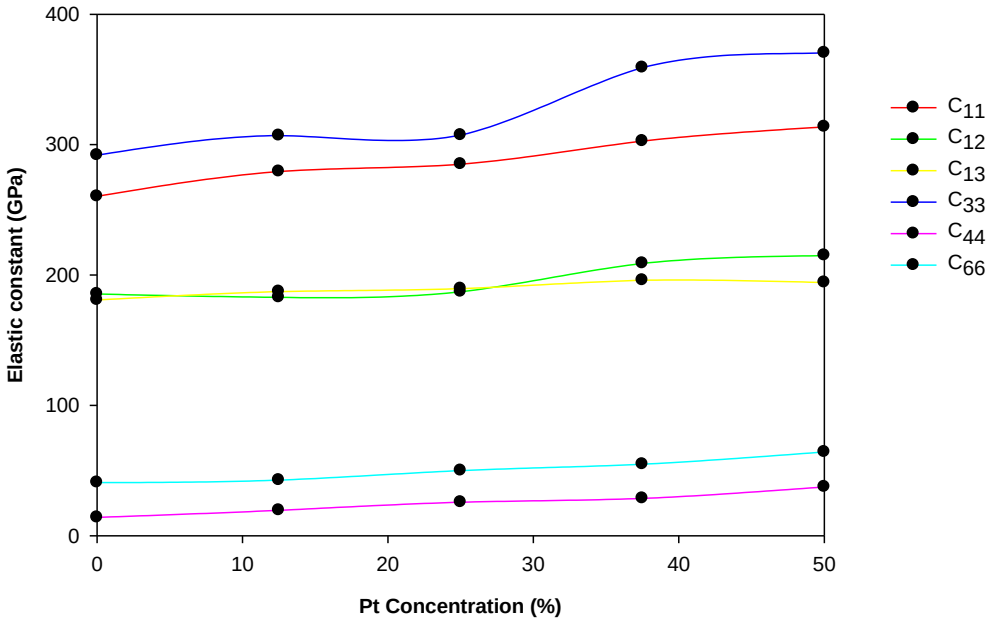

Figure 3.6.1. 2. Variation of elastic constants of $Pd_{50-x}Pt_xS_{50}$ against Pt concentration $P4_2/m$ at 20 GPa

Table 3.6.1. 3. Results of the elastic constants of $(Pt_{50-x}Pd_x)S_{50}$ and $Pd_{50-x}Pt_xS_{50}$ at 30 GPa

Composition	Space group	C_{11} GPa	C_{12} GPa	C_{13} GPa	C_{33} GPa	C_{44} GPa	C_{66} GPa	Bulk modulus GPa	Shear modulus GPa
$Pd_{50}S_{50}$	$P4_2/m$	303.69	228.88	223.61	341.14	6.02	36.09	255.64	27.79
$Pd_{37.5}Pt_{12.5}S_{50}$	$P4_2/m$	321.06	229.88	226.31	360.65	12.65	35.04	263.08	33.42
$Pd_{25}Pt_{25}S_{50}$	$P4_2/m$	325.99	230.96	231.18	362.94	20.66	47.58	266.84	39.22
$Pd_{12.5}Pt_{37.5}S_{50}$	$P4_2/m$	346.99	254.13	240.41	410.15	24.27	51.70	286.00	44.66
$Pt_{50}S_{50}$	$P4_2/m$	359.36	258.93	239.95	422.17	32.06	61.70	290.95	51.97

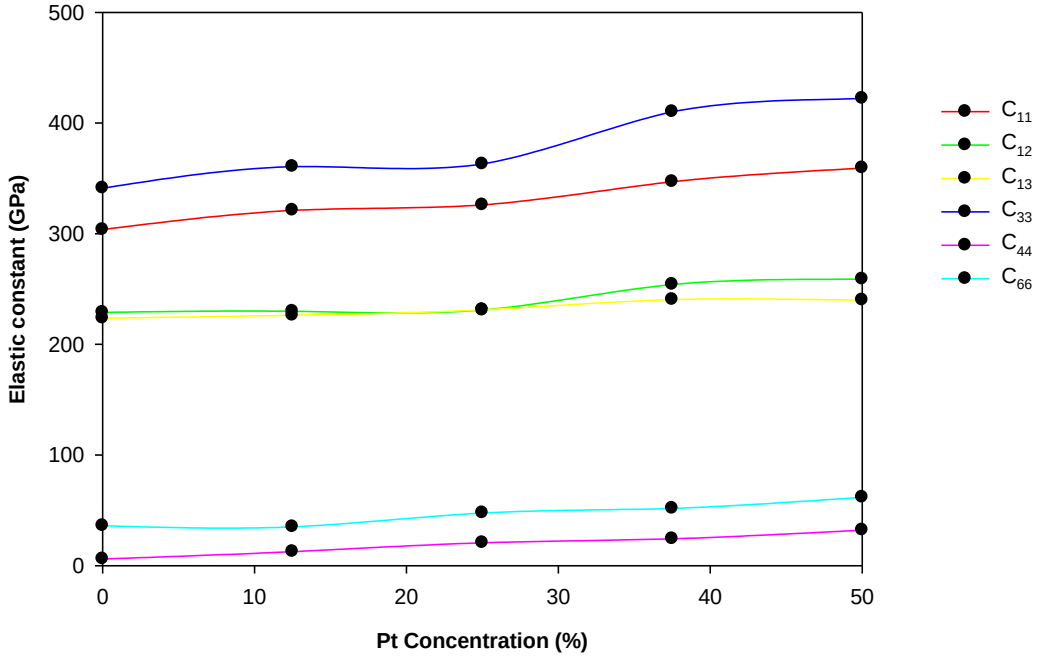

Figure 3.6.1. 3. Variation of elastic constants of $Pd_{50-x}Pt_xS_{50}$ against Pt concentration $P4_2/m$ at 30 GPa

Table 3.6.1. 4. Results of the elastic constants of $(Pt_{50-x}Pd_x)S_{50}$ and $(Pd_{50-x}Pt_x)S_{50}$ at 40 GPa

Composition	Space group	C_{11} GPa	C_{12} GPa	C_{13} GPa	C_{33} GPa	C_{44} GPa	C_{66} GPa	Bulk modulus GPa	Shear modulus GPa
$Pd_{50}S_{50}$	$P4_2/m$	343.57	271.97	264.16	382.40	-2.31	25.61	296.68	22.15
$Pd_{37.5}Pt_{12.5}S_{50}$	$P4_2/m$	362.62	274.47	269.11	407.96	5.89	31.39	306.51	30.00
$Pd_{25}Pt_{25}S_{50}$	$P4_2/m$	366.69	275.81	269.56	407.90	13.74	37.02	307.90	34.66
$Pd_{12.5}Pt_{37.5}S_{50}$	$P4_2/m$	384.89	300.22	282.97	453.38	16.48	43.76	328.38	39.14
$Pt_{50}S_{50}$	$P4_2/m$	397.42	302.79	282.19	466.05	26.55	51.42	332.80	47.15

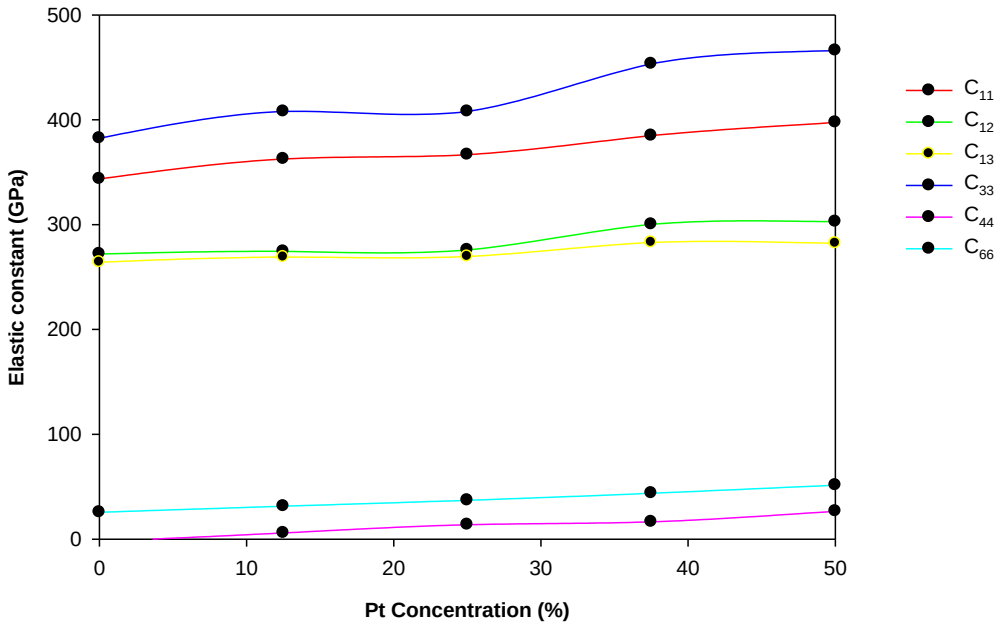

Figure 3.6.1. 4. Variation of elastic constants of $Pd_{50-x}Pt_xS_{50}$ against Pt concentration $P4_2/m$ at 40 GPa

Table 3.6.1. 5. Results of the elastic constants of $(Pt_{50-x}Pd_x)S_{50}$ and $(Pd_{50-x}Pt_x)S_{50}$ at 50 GPa

	Space group	C_{11} GPa	C_{12} GPa	C_{13} GPa	C_{33} GPa	C_{44} GPa	C_{66} GPa	Bulk modulus GPa	Shear modulus GPa
$Pd_{50}S_{50}$	$P4_2/m$	382.96	311.50	307.10	425.36	-15.06	21.41	338.08	15.96
$Pd_{37.5}Pt_{12.5}S_{50}$	$P4_2/m$	402.26	324.78	300.91	454.06	-10.09	23.32	345.76	22.76
$Pd_{25}Pt_{25}S_{50}$	$P4_2/m$	410.17	319.15	311.96	451.73	0.76	33.84	350.91	29.01
$Pd_{12.5}Pt_{37.5}S_{50}$	$P4_2/m$	424.67	341.53	323.48	496.31	2.17	41.48	369.18	32.97
$Pt_{50}S_{50}$	$P4_2/m$	434.37	345.68	322.91	506.87	9.34	49.67	373.18	39.28

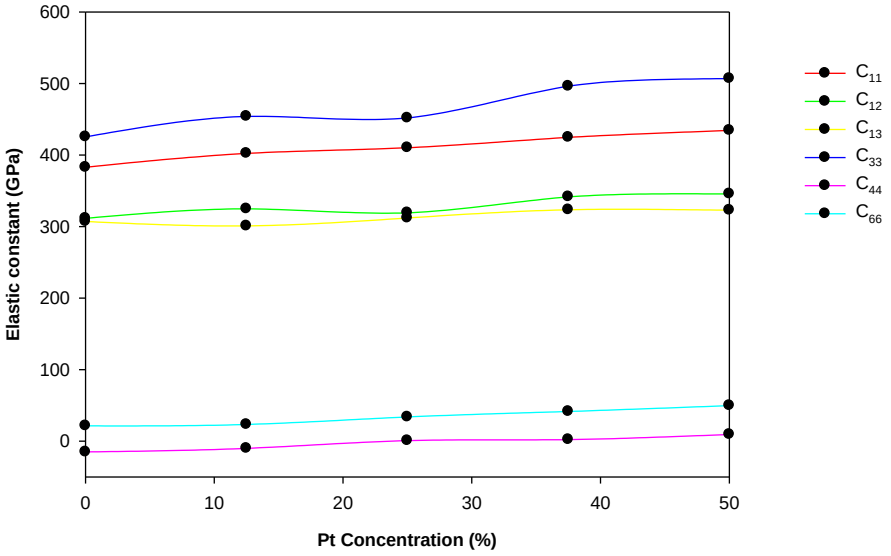

Figure 3.6.1. 5. Variation of elastic constants of $Pd_{50-x}Pt_xS_{50}$ against Pt concentration $P4_2/m$ at 50 GPa

Figure 3.6.1.1 and Table 3.6.1.1 show the plot on variation of elastic constants of $Pd_{50-x}Pt_xS_{50}$ against Pt concentration at 10 GPa. An increase in all elastic constants was noted as the Pt content concentration increases. At low pressures C_{12} and C_{33} tend to be constant below 25% Pt and reflect a marked increase above 25% Pt which levels off above 40% Pt. At higher pressures, i.e. 20 to 50 GPa, depicted in Figures 3.6.1.2 to 3.6.1.5 respectively, C_{33} shows a gentle increase at low Pt concentrations whilst indicating a similar behavior as at 10 GPa for higher Pt concentrations. The other elastic constants, C_{11}, C_{13}, C_{44} and C_{66} increase steadily with increasing Pt content. However, C_{44} is negative at lower Pt concentrations, i.e. for $Pd_{50}S_{50}$ at 40 and 50 GPa and for $Pd_{37.5}Pt_{12.5}S_{50}$ at 50 GPa. Hence, it may be concluded that except for mechanical instability observed in these concentration and pressure ranges, the $Pd_{50-x}Pt_xS_{50}$ satisfies the necessary tetragonal mechanical stability conditions for all other studied ranges, i.e. $C_{11}-C_{22}>o$, $C_{11}+C_{33}-2C_{13}>0$, $C_{11}>0$, $C_{33}>0$, $C_{44}>0$, $C_{66}>0$, $(2C_{11}+C_{33}+2C_{12}+4C_{13})>0$.

3.6.2. Pressure dependence on elastic properties of $(Pt_{50-x}Pd_x)S_{50}$ with P_1 (from $P4_2/mmc$)symmetry

Table 3.6.2. 1. Results of the elastic constants of $(Pt_{50-x}Pd_x)S_{50}$ at 10 GPa

Composition	C_{11} GPa	C_{12} GPa	C_{13} GPa	C_{33} GPa	C_{44} GPa	C_{66} GPa	Shear modulus GPa	Bulk modulus GPa
$Pt_{50}S_{50}$	244.78	89.63	169.78	368.72	21.16	4.84	37.73	190.74
$Pt_{37.5}Pd_{12.5}S_{50}$	225.63	87.12	163.19	342.36	17.44	4.14	33.13	180.07
$Pt_{25}Pd_{25}S_{50}$	206.08	87.35	156.86	323.00	11.20	2.81	27.62	171.53
$Pt_{12.5}Pd_{37.5}S_{50}$	190.73	87.49	154.85	315.94	1.76	1.68	21.06	165.75
$Pd_{50}S_{50}$	178.39	84.68	147.44	299.23	5.41	0.57	20.70	157.24

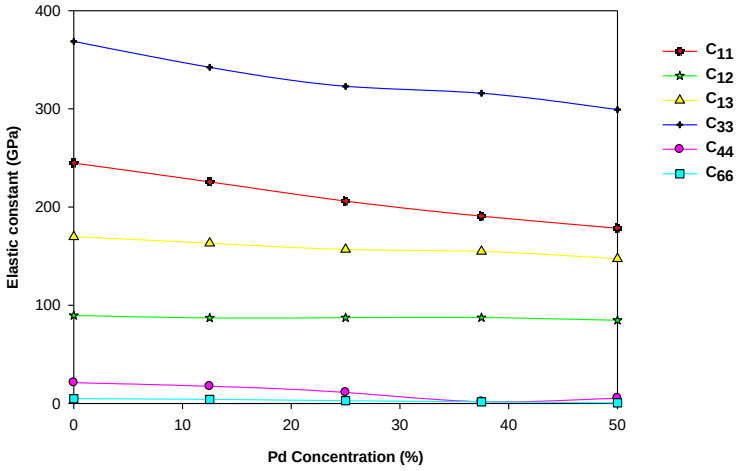

Figure 3.6.2. 1. Variation of elastic constants of $Pt_{50-x}Pd_xS_{50}$ against Pd concentration P_1 (from $P4_2/mmc$), 10 GPa.

Table 3.6.2. 2. Results of the elastic constants of $(Pt_{50-x}Pd_x)S_{50}$ at 20 GPa

Composition	C_{11} GPa	C_{12} GPa	C_{13} GPa	C_{33} GPa	C_{44} GPa	C_{66} GPa	Shear modulus GPa	Bulk modulus GPa
$Pt_{50}S_{50}$	284.95	122.71	220.26	443.96	7.60	-2.97	32.49	237.82
$Pt_{37.5}Pd_{12.5}S_{50}$	266.48	117.68	217.48	421.79	7.52	-4.44	28.91	228.89
$Pt_{25}Pd_{25}S_{50}$	245.57	117.90	209.07	395.74	0.85	-4.89	22.59	218.07
$Pt_{12.5}Pd_{37.5}S_{50}$	226.32	119.91	209.15	391.46	-6.99	-5.81	16.52	213.39
$Pd_{50}S_{50}$	195.53	132.50	205.42	377.30	-9.44	-7.53	9.70	206.12

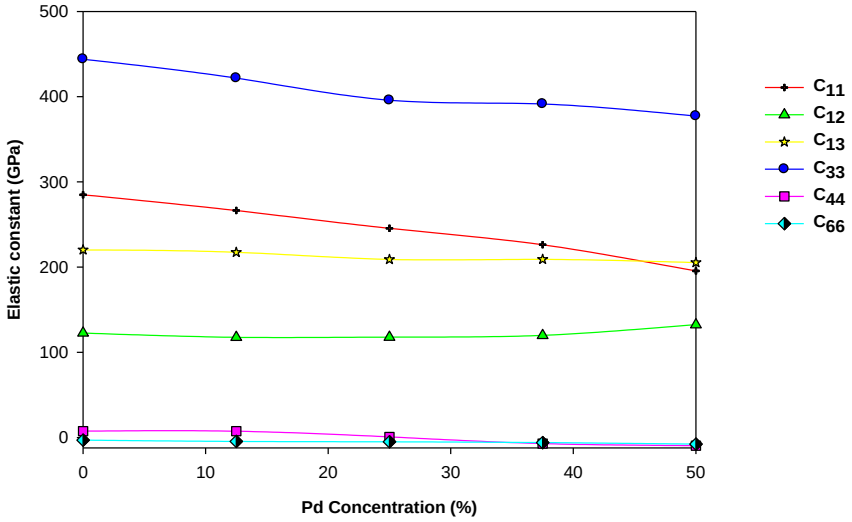

Figure 3.6.2. 2. Variation of elastic constants of $Pt_{50-x}Pd_xS_{50}$ against Pd concentration P_1 (from $P4_2/mmc$), 20 GPa

Table 3.6.2. 3. Results of the elastic constants of $(Pt_{50-x}Pd_x)S_{50}$ at 30 GPa

Composition	C_{11} GPa	C_{12} GPa	C_{13} GPa	C_{33} GPa	C_{44} GPa	C_{66} GPa	Shear modulus GPa	Bulk modulus GPa
$Pt_{50}S_{50}$	306.47	137.62	277.61	516.54	-4.29	-12.28	-24.95	279.46
$Pt_{37.5}Pd_{12.5}S_{50}$	266.48	117.68	217.48	495.35	-6.66	-12.47	21.94	272.75
$Pt_{25}Pd_{25}S_{50}$	274.58	148.55	260.21	471.31	-8.48	-13.10	16.90	262.73
$Pt_{12.5}Pd_{37.5}S_{50}$	-	-	-	-	-	-	-	-
$Pd_{50}S_{50}$	205.23	174.84	261.64	519.10	9.87	-2.32	18.92	258.42

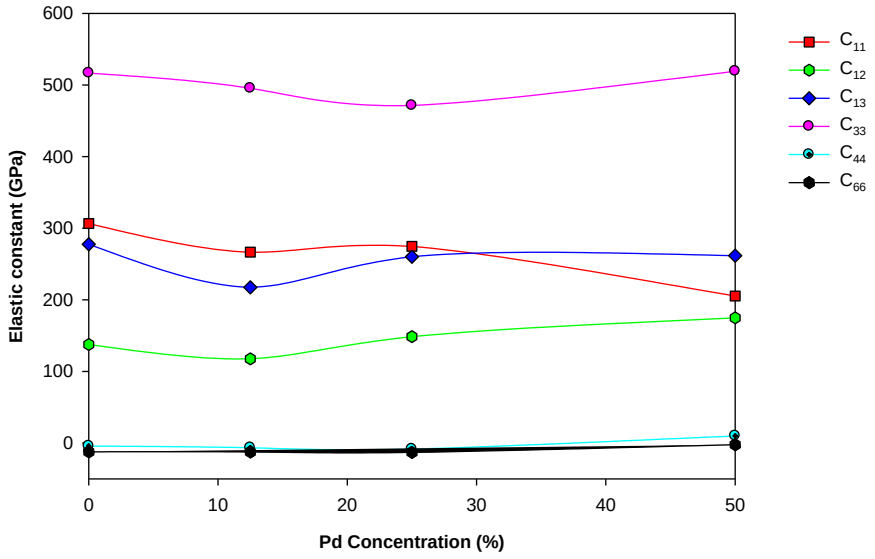

Figure 3.6.2. 3. Variation of elastic constants of $Pt_{50-x}Pd_xS_{50}$ against Pd concentration P_1 (from $P4_2/mmc$), 30 GPa

Table 3.6.2. 4. Results of the elastic constants of $(Pt_{50-x}Pd_x)S_{50}$ at 40 GPa

Composition	C_{11} GPa	C_{12} GPa	C_{13} GPa	C_{33} GPa	C_{44} GPa	C_{66} GPa	Shear modulus GPa	Bulk modulus GPa
$Pt_{50}S_{50}$	356.96	189.20	317.25	602.55	-7.56	-16.43	26.53	329.31
$Pt_{37.5}Pd_{12.5}S_{50}$	409.98	237.84	338.91	374.69	151.31	82.78	99.47	328.74
$Pt_{25}Pd_{25}S_{50}$	293.29	182.27	307.50	566.29	20.31	-8.91	17.31	310.70
$Pt_{12.5}Pd_{37.5}S_{50}$	-	-	-	-	-	-	-	-
$Pd_{50}S_{50}$	298.19	186.78	290.48	599.25	-32.02	-11.07	13.15	303.45

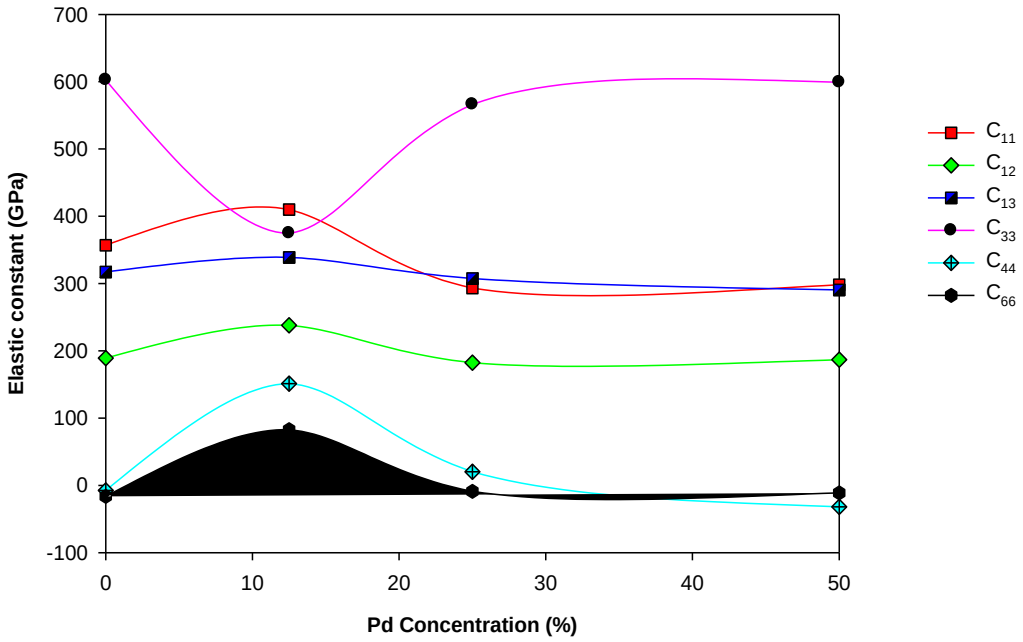

Figure 3.6.2. 4. Variation of elastic constants of $Pt_{50-x}Pd_xS_{50}$ against Pd concentration P_1 (from $P4_2/mmc$), 40 GPa.

Table 3.6.2. 5. Results of the elastic constants of $(Pt_{50-x}Pd_x)S_{50}$ at 50 GPa

Composition	C_{11} GPa	C_{12} GPa	C_{13} GPa	C_{33} GPa	C_{44} GPa	C_{66} GPa	Shear modulus GPa	Bulk modulus GPa
$Pt_{50}S_{50}$	335.23	193.30	360.51	666.67	-16.91	-23.01	16.82	351.75
$Pt_{37.5}Pd_{12.5}S_{50}$	392.56	296.91	350.48	441.94	99.59	51.79	63.19	354.94
$Pt_{25}Pd_{25}S_{50}$	342.93	241.41	257.62	451.96	52.57	57.19	61.20	309.94
$Pt_{12.5}Pd_{37.5}S_{50}$	-	-	-	-	-	-	-	-
$Pd_{50}S_{50}$	399.87	179.81	311.51	685.60	-15.22	-21.33	35.61	344.06

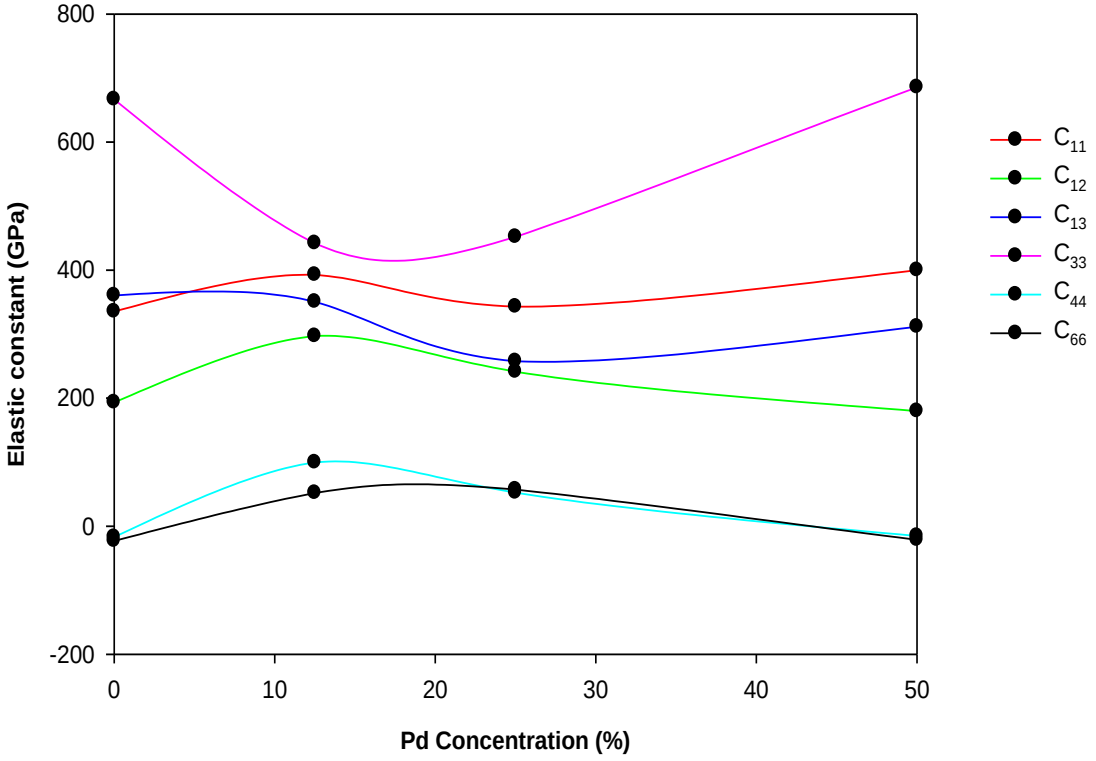

Figure 3.6.2. 5. Variation of elastic constants of $Pt_{50-x}Pd_xS_{50}$ against Pd concentration P_1 (from $P4_2/mmc$), 50 GPa

Figure 3.6.2.1 shows a graph of $Pt_{50-x}Pd_x S_{50}$ against Pd concentration at 10 GPa and the necessary conditions for stability, C_{11}-C_{22}>o, C_{11}+C_{33}-2C_{13}>0, C_{11}>0, C_{33}>0, C_{44}>0, C_{66}>0, (2C_{11}+C_{33}+2C_{12}+4C_{13})>0 are satisfied. Generally, it is observed that as the pressure increases, the elastic constants decrease including the shear and bulk moduli. C_{44} follows the same trend except that the value corresponding to $Pt_{12.5}Pd_{37.5}S_{50}$ is smaller than that of $Pt_{50}S_{50}$. Figure 3.6.2.2 and Table 3.6.2.2 show the plot on variation of elastic constants with Pd concentration at 20 GPa. All compositions are mechanically unstable since their values of C_{66} are negative. In addition the most unstable compositions are $Pt_{12.5}Pd_{37.5}S_{50}$ and $Pd_{50}S_{50}$ since both C_{44} and C_{66} are negative, which was depicted in the phonon dispersion curves. The same argument applies to almost all compositions of $Pt_{50-x}Pd_xS_{50}$ at 30 GPa as depicted in Figure 3.6.2.3 and Table 3.6.2.3, where both C_{44} and C_{66} plots are negative. Gentle minima are noted for C_{11}, C_{12} and C_{13} at $Pt_{37.5}Pd_{12.5}S_{50}$ and at $Pt_{25}Pd_{25}S_{50}$ for C_{33} and all elastic constants, except C_{11}, tend to increase above the latter composition. It can be deduced from Table 3.6.2.4 and Figure 3.6.2.4, related to elastic constants variation at 40 GPa, that $Pt_{37.5}Pd_{12.5}S_{50}$ is the only stable composition and all elastic constant plots reflect a maximum at that composition except for C_{33} which shows a minimum and whose value is less than that of C_{11}. It was observed that C_{12}, C_{44} and C_{66} fluctuate with increasing pressure. Figure 3.6.2.5 and Table 3.6.2.5 show elastic constants variation at 50 GPa and $Pt_{37.5}Pd_{12.5}S_{50}$ and $Pt_{25}Pd_{25}S_{50}$ appear to be stable compositions. The curve for C_{33}, with a U shape, is different from those of other elastic constants which reflect a gentle maximum at lower Pd concentrations. Elastic constants calculations related to the composition $Pt_{12.5}Pd_{37.5}S_{50}$ did not even converge above 20 GPa.

3.7. Variation of pressure on phonon dispersions

Pressure was applied to phonon dispersion curves at different concentration in the range 10 - 50 GPa. It was observed that pressure reduces the imaginary frequencies to a certain level, and if too much pressure is applied the structure changes its form. $Pd_{50}S_{50}$ $P4_2/mmc$ and $Pt_{37.5}Pd_{12.5}S_{50}$ changed their form at 50 GPa, where they did not converge. Also in $Pt_{25}Pd_{25}S_{50}$ P_1, a transformation occurred and in $Pd_{50}S_{50}$ P_1 the structure did not converge at 40 & 50 GPa. The PtS $P4_2/mmc$, PdS $P4_2/m$ and PtS P_1 were used for this study. PtS P_1 structure was chosen since PtS $P4_2/mmc$ has limited sites to insert different concentrations. The PtS P_1 has many sites where different concentrations can be inserted. The $P4_2/m$ has enough sites.

3.7.1. Pressure variation of Phonon Dispersions – $Pt_{50}S_{50}$– Phonon Density of States ($P4_2/mmc$)

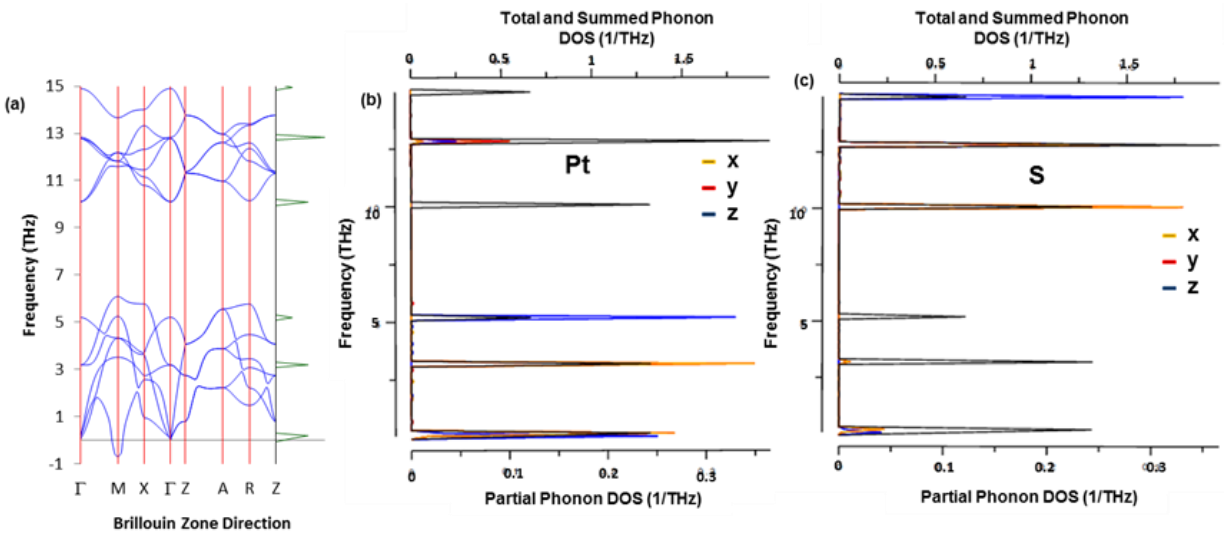

Figure 3.7.1. 1. (a) Phonon dispersion for $Pt_{50}S_{50}$ $P4_2/m$ at (10 GPa), Phonon density of states (b) Pt contribution and (c) S contribution

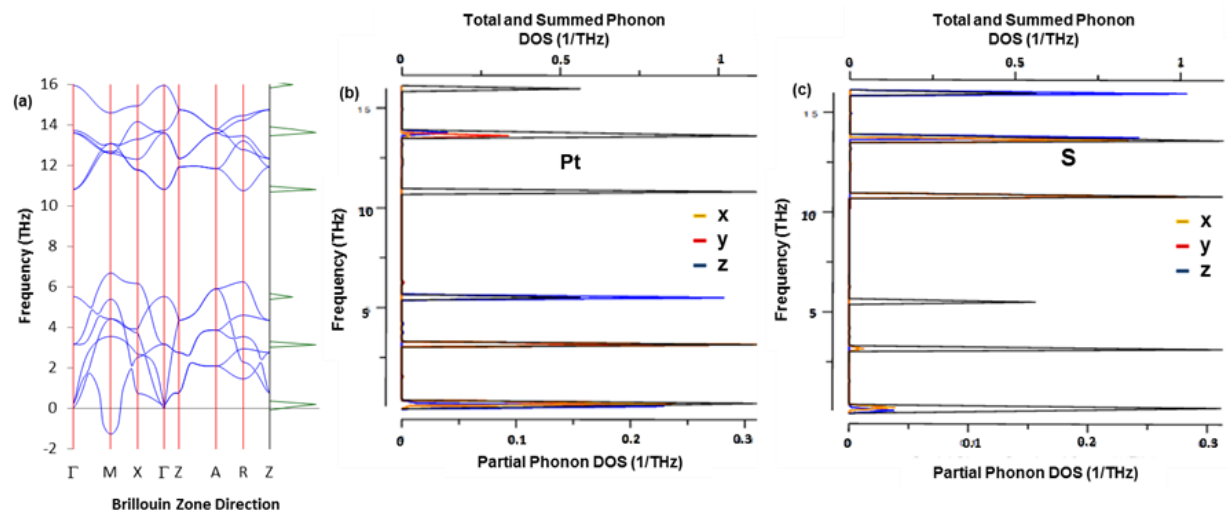

Figure 3.7.1. 2. (a) Phonon dispersion for $Pt_{50}S_{50}$ $P4_2/mmc$ at (20 GPa), Phonon density of states (b) Pt contribution and (c) S contribution

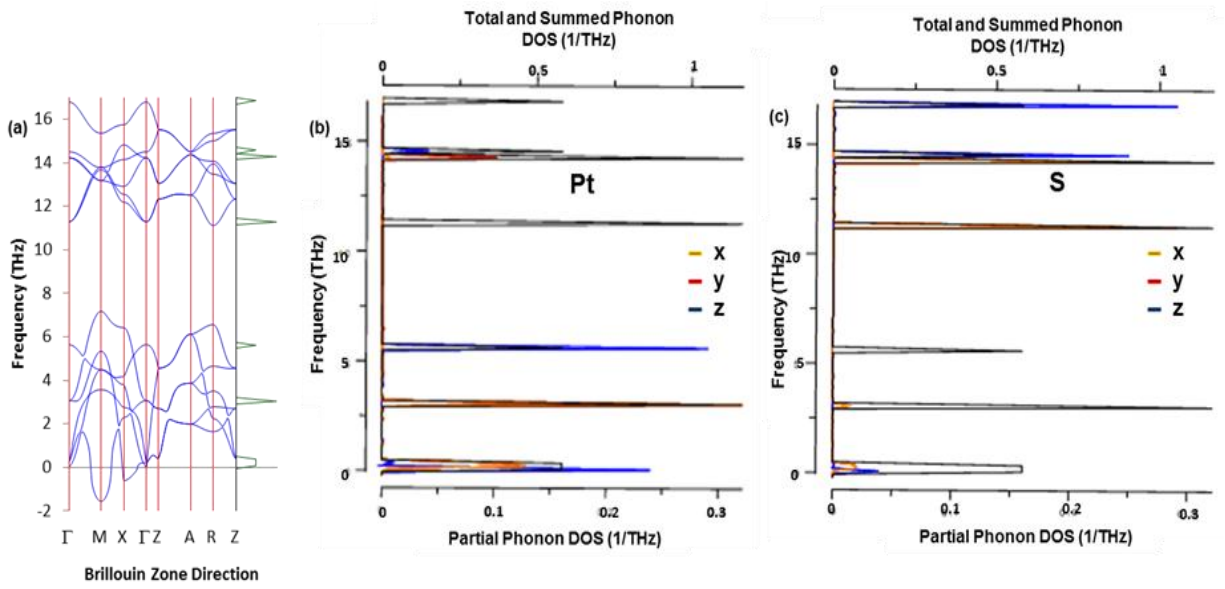

Figure 3.7.1. 3. (a) Phonon dispersion for $Pt_{50}S_{50}$ $P4_2/mmc$ at (30 GPa), Phonon density of states (b) Pt contribution and (c) S contribution

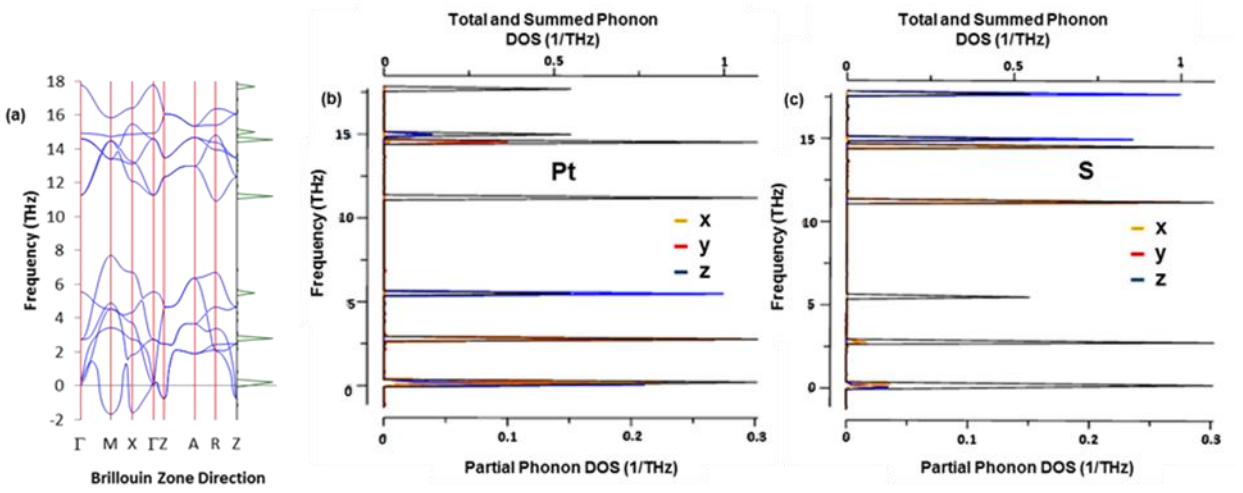

Figure 3.7.1. 4. (a) Phonon dispersion for $Pt_{50}S_{50}$ $P4_2/mmc$ at (40 GPa), Phonon density of states (b) Pt contribution and (c) S contribution.

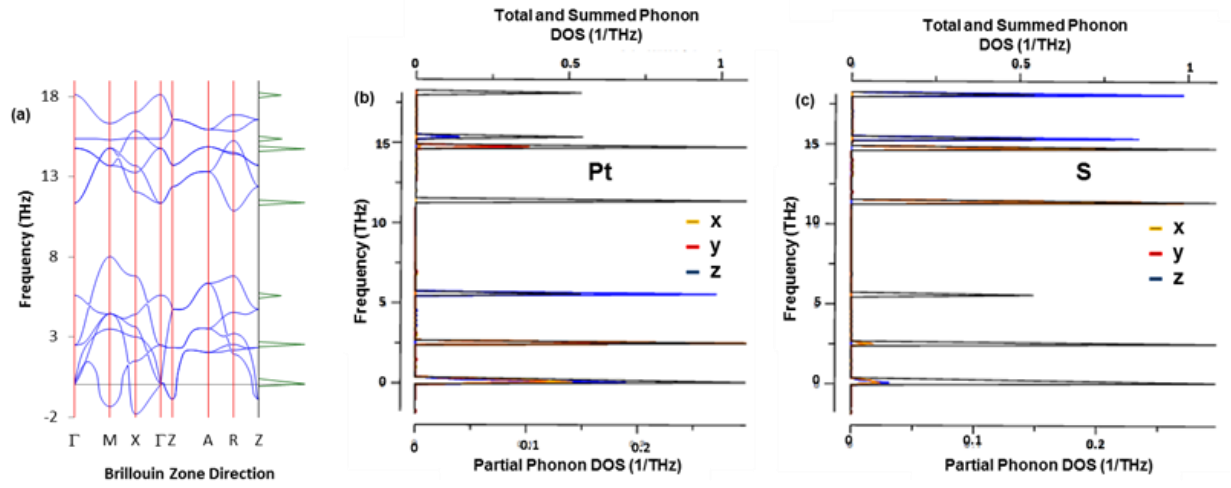

Figure 3.7.1. 5. Phonon dispersion for $Pt_{50}S_{50}$ $P4_2/mmc$ at (50 GPa) (a) Phonon density of states for $Pt_{50}S_{50}$ (b) Pt contribution and (c) S contribution

The analyses of the vibrational properties of $(Pt_{50-x}Pd_x)S_{50}$ and $(Pd_{50-x}Pt_x)S_{50}$ in regard to the phonon dispersion and partial phonon densities of states are shown above. Figure 3.4.1 shows phonon spectra of $Pt_{50}S_{50}$ $P4_2/mmc$ at (0 GPa). It was observed that all branches are positive, there are no soft modes detected from the structure. Figure 3.7.1.1, shows phonon spectra of 10 GPa, where imaginary frequencies were observed along M direction. The partial density of states (PDOS), shows platinum (Pt) and Sulphur (S) atoms vibrating at lower frequencies, below 0 THz and. It is evident that both Pt and S atoms to a limited extend are responsible for the soft modes, with x - z component contribution being dominant. The z component was observed to be dominant at around 5 THz in Pt, and 15 THz in S. The acoustic and optical branches of the lower bands emanate mainly from the Pt and S atoms and the optical branches of the upper bands emanate predominantly from the S atoms less from Pt atom. Figure 3.7.1.2, shows the phonon spectra of 20 GPa with soft modes at point M of the Brillouin zone extended more to negative frequencies. From the PDOS, it was observed that Pt and S atoms vibrate at lower frequencies, below 0 THz. It is clear that Pt atoms are mainly responsible for the soft modes, with x - z component being dominant. The contribution of S atoms towards the soft modes is small. The lower band of optical branches start at about 3.0 THz and end at 5.8 THz. Figure 3.7.1.3, shows phonon spectra of 30 GPa

with negative frequencies at point M - X of the Brillouin zone extended towards -2 THz. It is evident that the Pt atoms are mainly responsible for the soft modes. From the PDOS, it was noticed that Pt contributes significantly to the acoustic and optical branches in the lower band and the Pt and S atoms contributes to optical branches in the upper band. The z component was observed to be dominant at about 14 THz to 16 THz in S atoms. Figure 3.7.1.4, shows the phonon spectra of 40 GPa with negative frequencies along M - X - Z direction. Looking at the PDOS, Pt and S atoms are responsible for the soft modes observed with x - z component being dominant. The S atoms vibrate predominately at higher frequencies. Figure 3.7.1.5, shows phonon spectra of 50 GPa, where soft modes were observed at point M - X - Z of the Brillouin zone, where they extend towards -2 THz. From the PDOS, Pt and S atoms were observed to vibrate at lower frequencies, below 0 THz. It is clear that Pt atoms are predominantly responsible for the soft modes. The acoustic and optical branches in the lower band emanate from Pt atoms and optical branches in the upper band emanates from Pt and S atoms and the latter one dominant. It was observed that pressure increases the soft modes to different Brillioun zone direction.

3.7.2. Pressure variation of Phonon Dispersions – $Pt_{25}Pd_{25}S_{50}$– Phonon Density of States ($P4_2/mmc$)

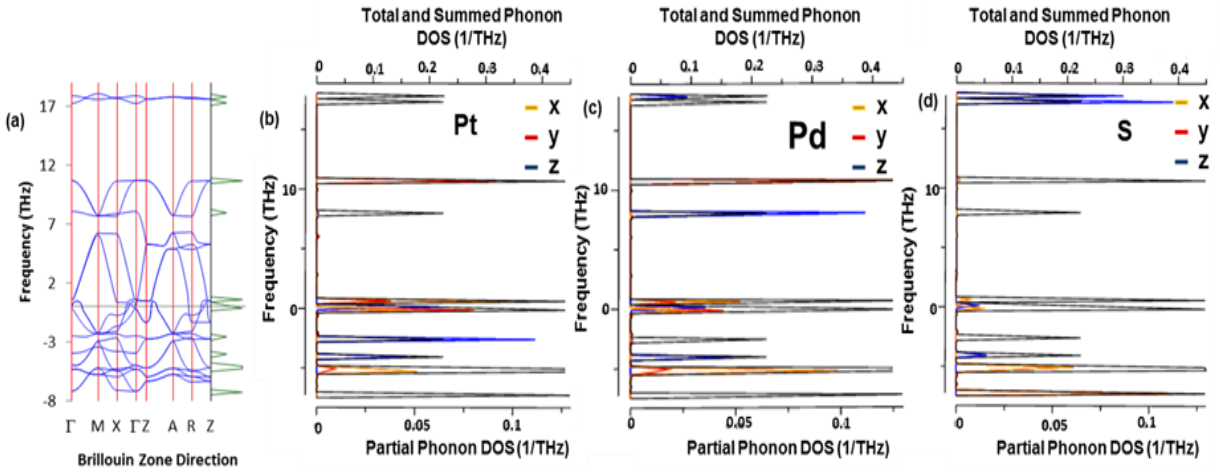

Figure 3.7.2. 1. (a) Phonon dispersion for $Pt_{25}Pd_{25}S_{50}$ $P4_2/mmc$ at (10 GPa), Phonon density of states (b) Pt contribution (c) Pd contribution and (d) S contribution

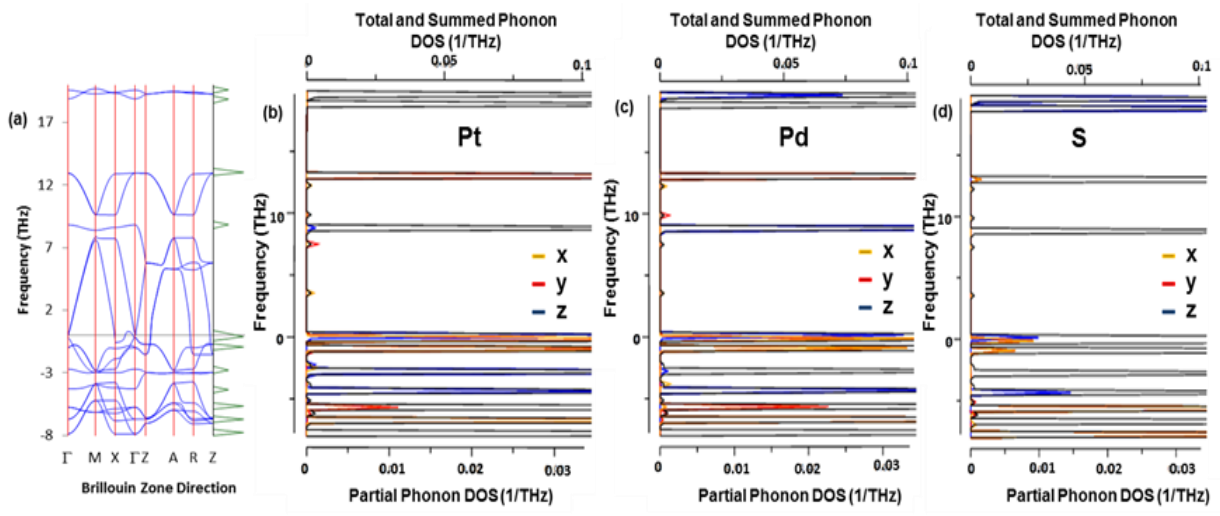

Figure 3.7.2. 2. (a) Phonon dispersion for $Pt_{25}Pd_{25}S_{50}$ $P4_2/mmc$ at (20 GPa), Phonon density of states (b) Pt contribution, (c) Pd contribution and (d) S contribution

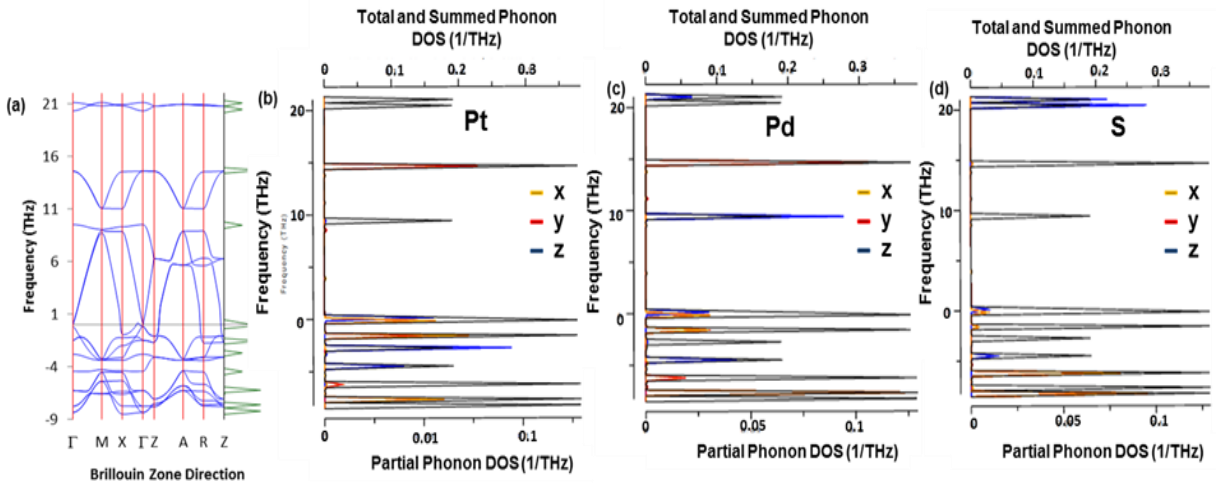

Figure 3.7.2. 3. (a) Phonon dispersion for $Pt_{25}Pd_{25}S_{50}$ $P4_2/mmc$ at (30 GPa), Phonon density of states (b) Pt contribution, (c) Pd contribution and (d) S contribution

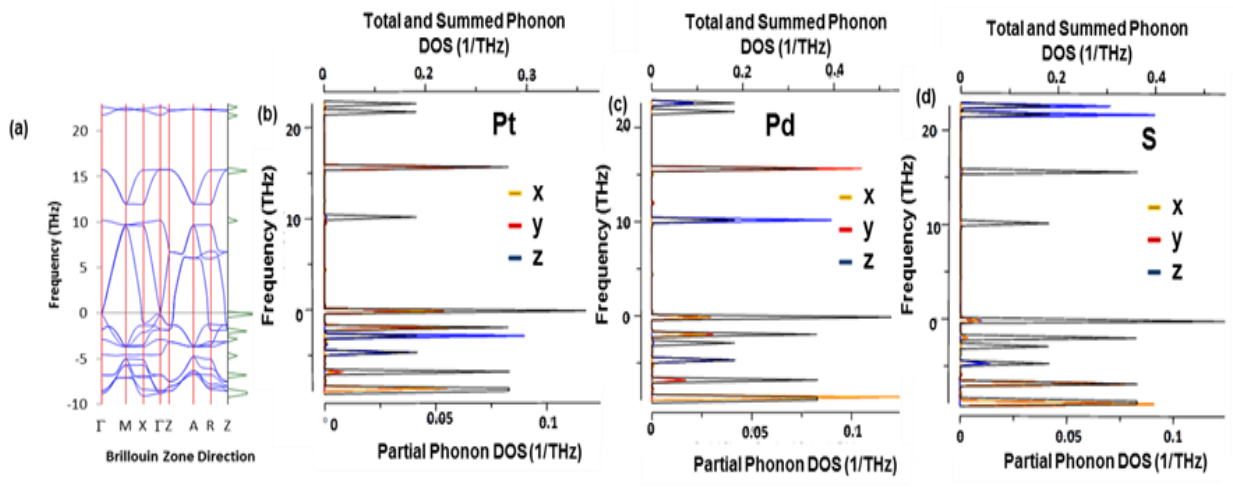

Figure 3.7.2. 4. (a) Phonon dispersion for $Pt_{25}Pd_{25}S_{50}$ $P4_2/mmc$ at (40 GPa), Phonon density of states (b) Pt contribution, (c) Pd contribution and (d) S contribution

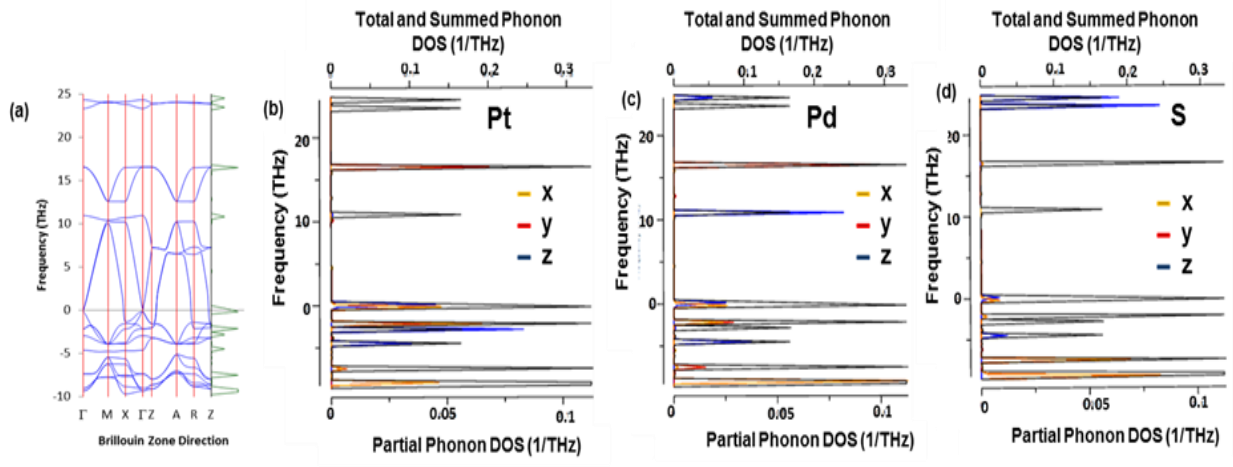

Figure 3.7.2. 5. Phonon dispersion for $Pt_{25}Pd_{25}S_{50}$ $P4_2/mmc$ at (50 GPa) (a) Phonon density of states for $Pt_{25}Pd_{25}S5_0$ (b) Pt contribution, (c) Pd contribution and (d) S contribution.

The $Pt_{25}Pd_{25}S_{50}$ $P4_2/mmc$ structure at 0 GPa (figure 3.4.2) was observed to have negative frequencies extended to -7 THz. Figure 3.7.2.1, shows phonon spectra of 10 GPa, where negative frequencies were observed. From the PDOS, it was noticed that Pt, Pd and S atoms are responsible for the soft modes. The soft modes are due to C_{44} and shear modulus being negative. The lower band of acoustic and optical branches emanates from Pd and S atom, the upper band of optical branches is associated with Pt, Pd and S atoms. Figure 3.7.2.2 gives the phonon spectra of 20 GPa. The soft modes were observed, it was noticed that Pt, Pd and S atoms are responsible for the soft modes. The z component in S was noticed to be dominant at about 17 THz. Pt, Pd and S atoms contributes towards the acoustic and optical branches in the lower bands and Pd and S atoms contributes towards the optical branches in the upper band. Figure 3.7.2.3, shows phonon spectra of 30 GPa, with negative frequency along M - X - Γ - Z - A - R directions of the Brillouin zone. Pt, Pd and S atoms are responsible for the soft modes, since they vibrate at lower frequencies, below 0 THz. The soft modes are due to C_{44} and shear modulus being negative which suggests instability. The z component is dominant at about 20 THz in S atoms. Figure 3.7.2.4 gives the phonon spectra of 40 GPa with soft modes. Looking at the PDOS, Pt, Pd and S atoms vibrate at lower frequencies, below 0 THz, which suggest that they are responsible for the soft modes. The z component in S is dominant at about 21 THz, in the upper band of optical branches. The z component in Pd is dominant at about 10 THz. Figure 3.7.2.5, shows the phonon spectra of 50 GPa, where soft modes were observed. From the PDOS, it was observed that the x and z components contribution from Pt, Pd and S atoms is responsible for the soft modes. It was observed that pressure extends the soft modes range to -10 THz.

3.7.3 Pressure variation of Phonon Dispersions – $Pd_{50}S_{50}$– Phonon Density of States ($P4_2/mmc$)

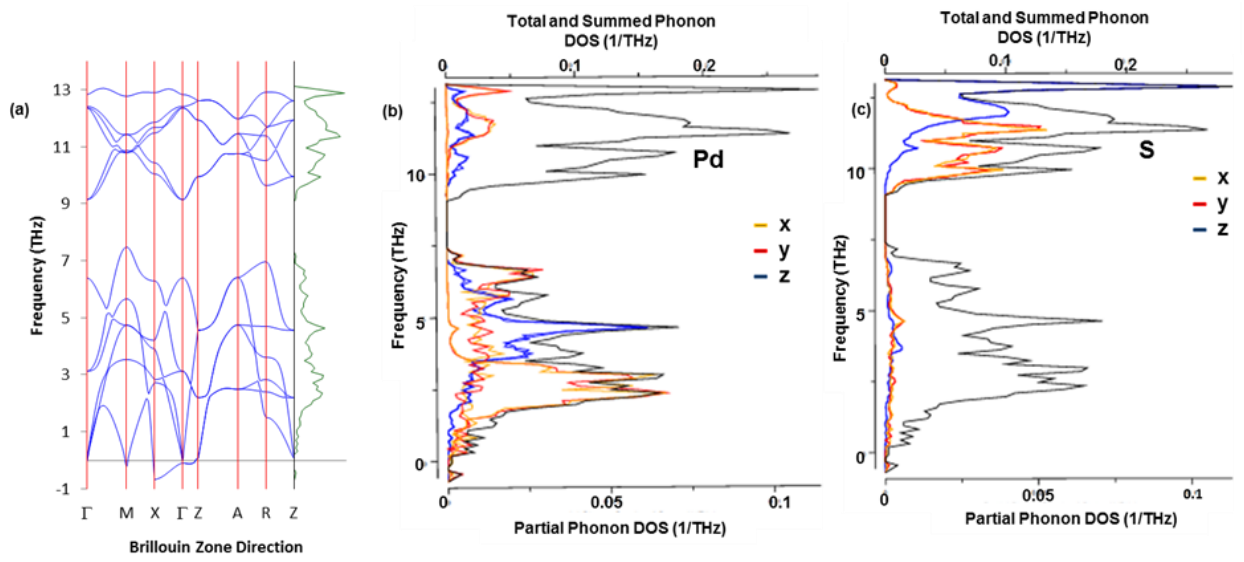

Figure 3.7.3. 1. (a) Phonon dispersion for $Pd_{50}S_{50}$ $P4_2/mmc$ at (10 GPa), Phonon density of states (b) Pd contribution, (c) S contribution

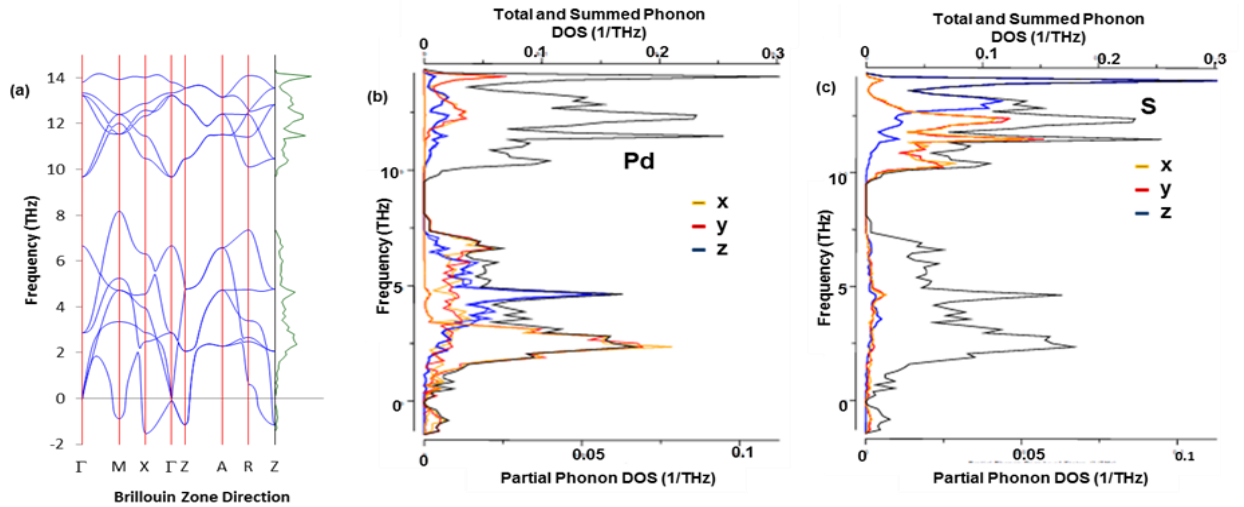

Figure 3.7.3. 2. (a) Phonon dispersion for $Pd_{50}S_{50}$ $P4_2/mmc$ at (20 GPa), Phonon density of states (b) Pd contribution, (c) S contribution

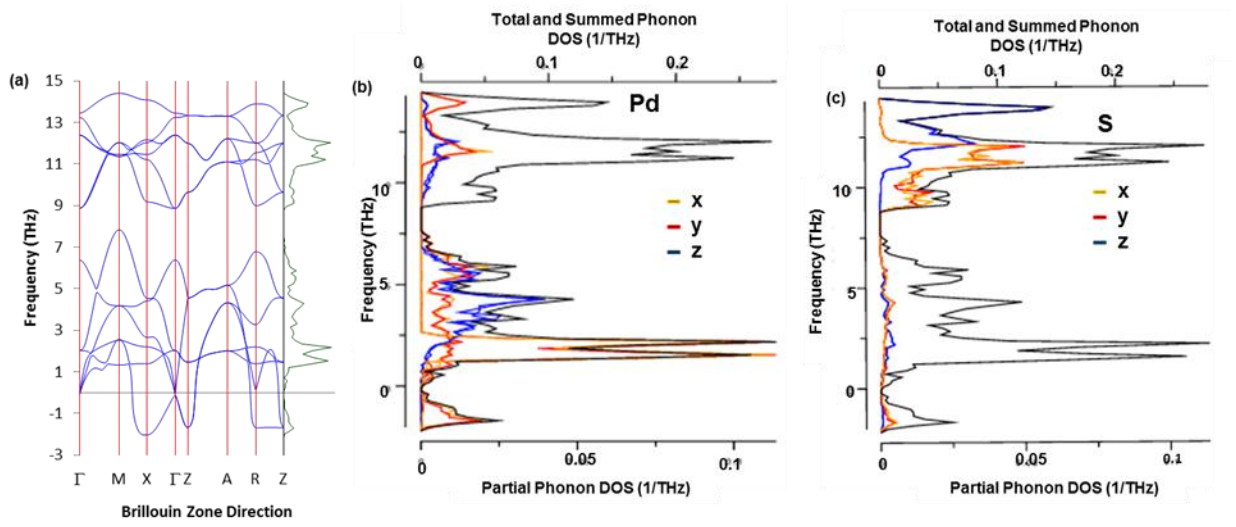

Figure 3.7.3. 3. (a) Phonon dispersion for $Pd_{50}S_{50}$ $P4_2/mmc$ at (30 GPa), Phonon density of states (b) Pd contribution, (c) S contribution

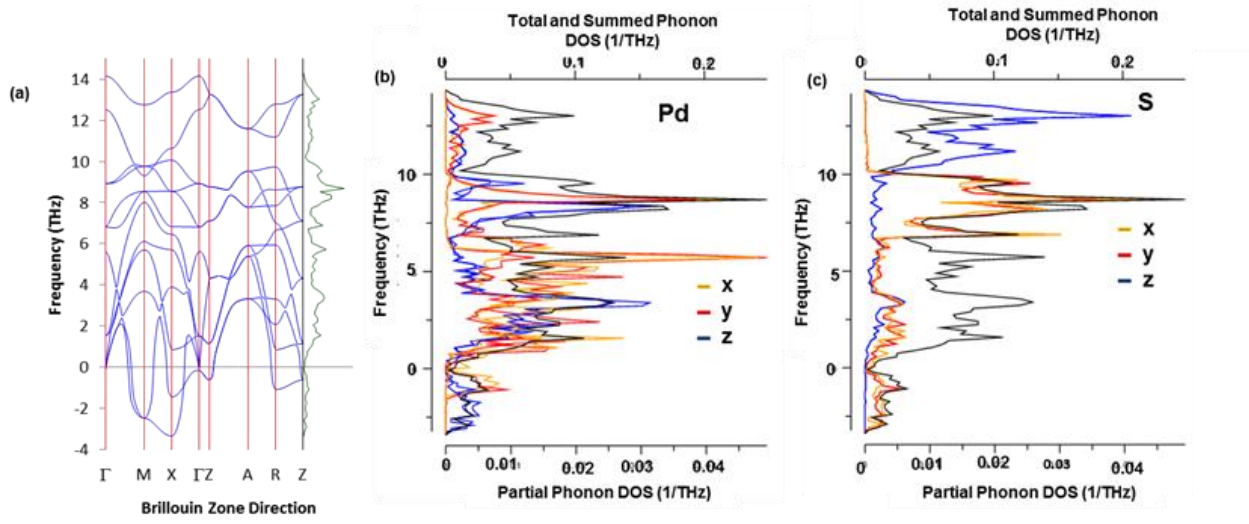

Figure 3.7.3. 4. (a) Phonon dispersion for $Pd_{50}S_{50}$ $P4_2/mmc$ at (40 GPa), Phonon density of states (b) Pd contribution (c) S contribution

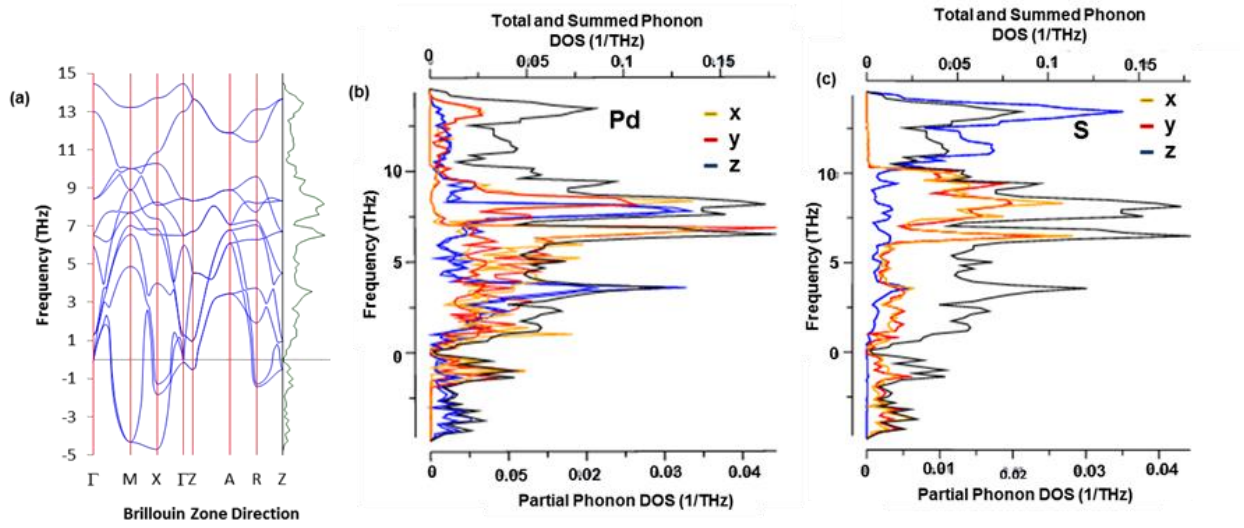

Figure 3.7.3. 5. (a) Phonon dispersion for $Pd_{50}S_{50}$ $P4_2/mmc$ at (50 GPa), Phonon density of states (b) Pd contribution, (c) S contribution.

The $Pd_{50}S_{50}$ with space group $P4_2/mmc$ at 0GPa (figure 3.4.4), shows no soft modes, all branches are positive. Figure 3.7.3.1, shows phonon spectra of 10 GPa, where negative frequencies were observed at point X - Γ - Z of the Brillioun zone. From the PDOS, it is evident that Pd and S atoms are responsible for the negative frequencies. The lower band of acoustic and optical branches emanates from Pd atoms and the upper band of optical branches emanates from Pd and S atoms. The z component in Pd was noticed to be dominant at around 11 - 13 THz. Contribution of S atoms is less towards the soft modes. Figure 3.7.3.2, shows the phonon spectra of 20 GPa, with negative frequencies at point M - X - Z of the Brillouin zone. It is clear that Pd and S atoms are responsible for the negative frequencies. The S atoms contribute less to the soft modes. The lower band of acoustic branches starts at about -1 THz and ends at 3 THz. The upper band of optical braches starts at about 9.8 THz and end at 14 THz. Figure 3.7.2.3, shows phonon spectra of 30 GPa, with soft modes observed along X - Z - R directions. Looking at the PDOS, the x - y component in Pd and S atoms contribute towards the soft modes. The lower band of acoustic and optical branches emanates from the Pd and S atoms and the upper bands of optical branches emanates from the S atoms. Contribution of S atoms to the soft modes is minimal. Figure 3.7.2.4 gives the phonon spectra of 40 GPa.

Looking at the PDOS, It is evident that Pd and S atoms are responsible for the soft modes. The lower band of acoustic and optical branches emanates from Pd and S atoms and the upper band of optical branches are associated with Pd and S atoms. Figure 3.7.2.5 gives the phonon spectra of 50 GPa, with soft modes at point M - X - Z - R of the Brillouin zone. From the PDOS, it was noted that Pd and S atoms are responsible for the soft modes, with z component of Pd and x - y component of S contributing to the soft modes. Pressure extends the soft modes to -5 THz. It was observed that as pressure increases the lower and upper bands mix.

3.7.4. Pressure variation of Phonon Dispersions – $Pd_{50}S_{50}$– Phonon Density of States ($P4_2/m$)

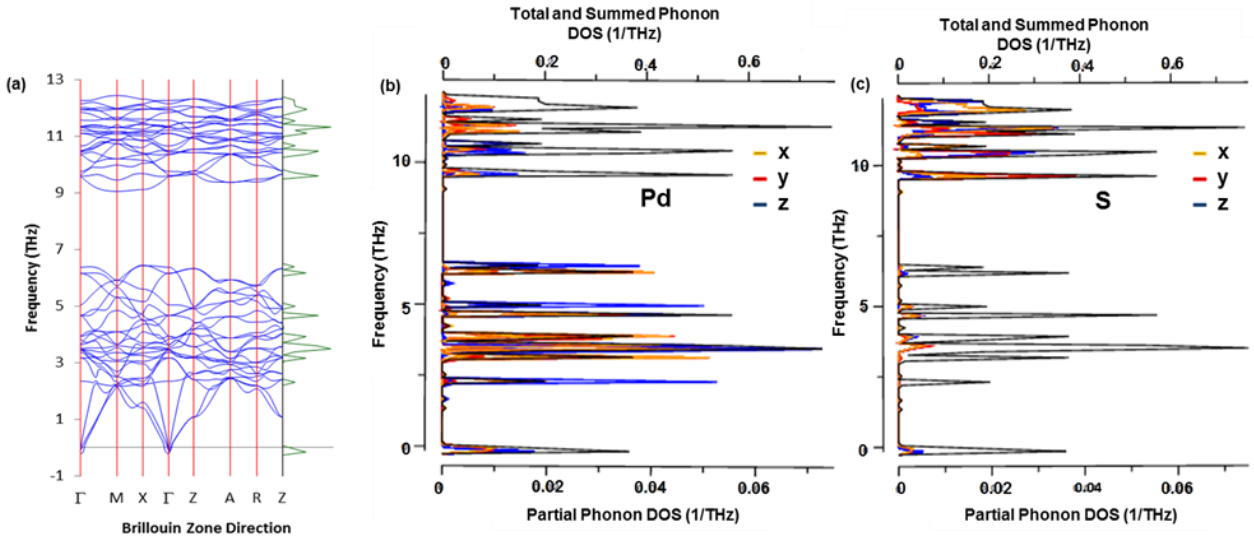

Figure 3.7.4. 1. (a) Phonon dispersion for $Pd_{50}S_{50}$ $P4_2/m$ at (10 GPa), Phonon density of states (b) Pd contribution and (c) S contribution

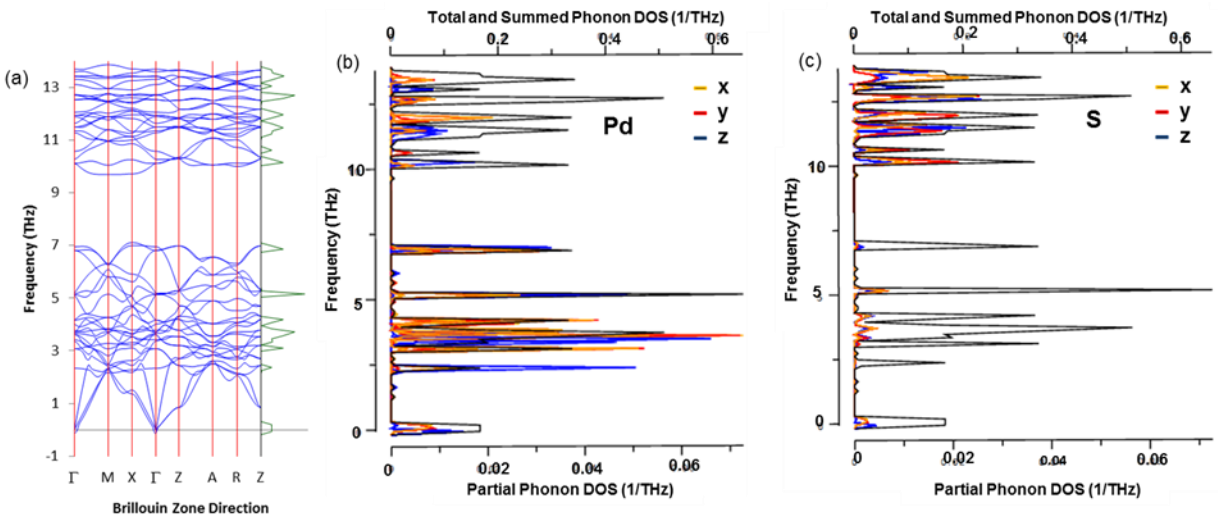

Figure 3.7.4. 2. (a) Phonon dispersion for $Pd_{50}S_{50}$ $P4_2/m$ at (20 GPa), Phonon density of states (b) Pd contribution and (c) S contribution

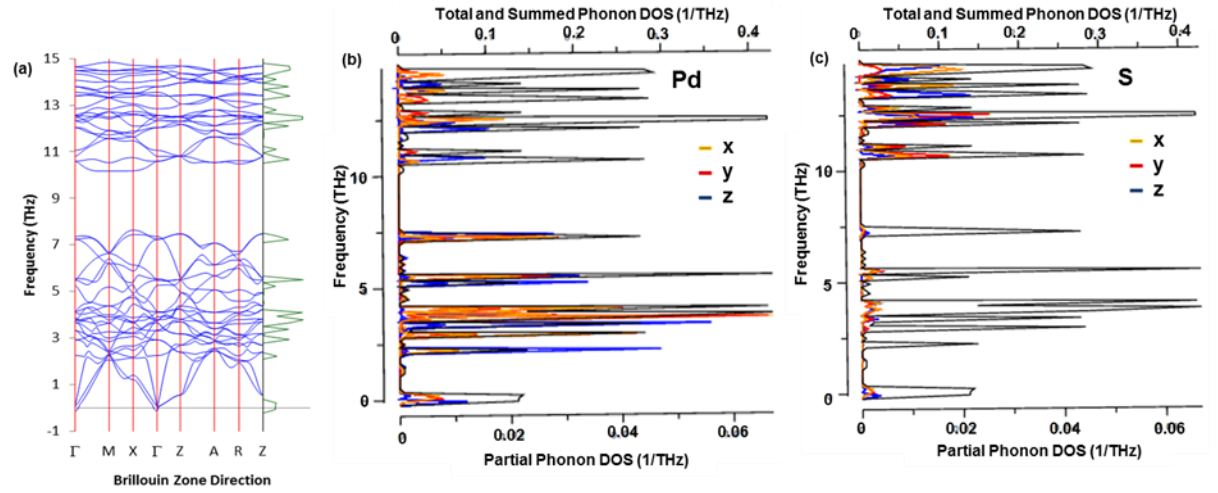

Figure 3.7.4. 3. (a) Phonon dispersion for $Pd_{50}S_{50}$ $P4_2/m$ at (30 GPa), Phonon density of states (b) Pd contribution and (c) S contribution

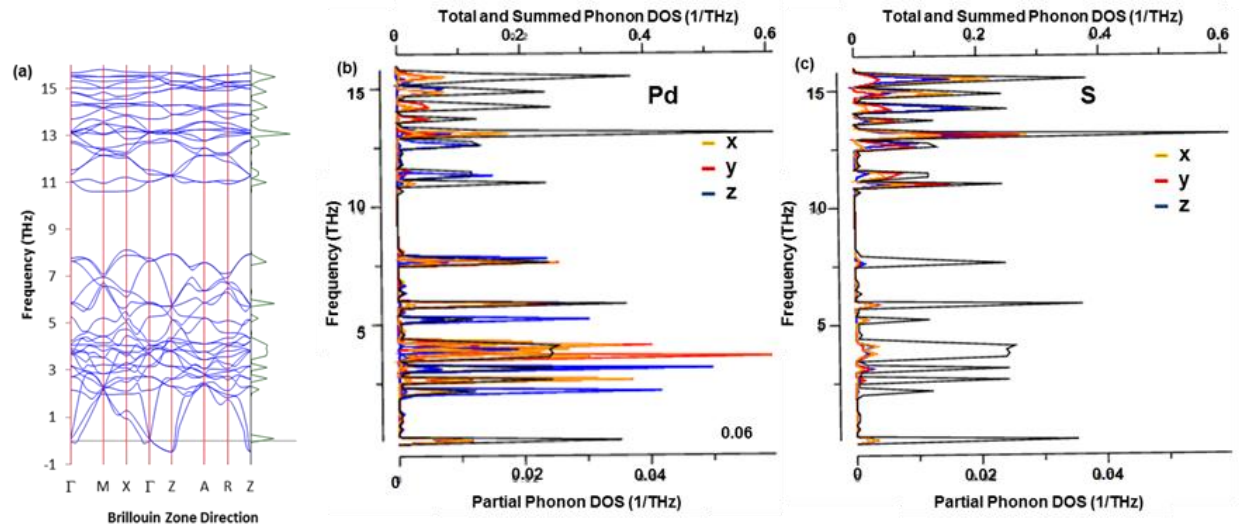

Figure 3.7.4. 4. (a) Phonon dispersion for $Pd_{50}S_{50}$ $P4_2/m$ at (40 GPa), Phonon density of states (b) Pd contribution and (c) S contribution

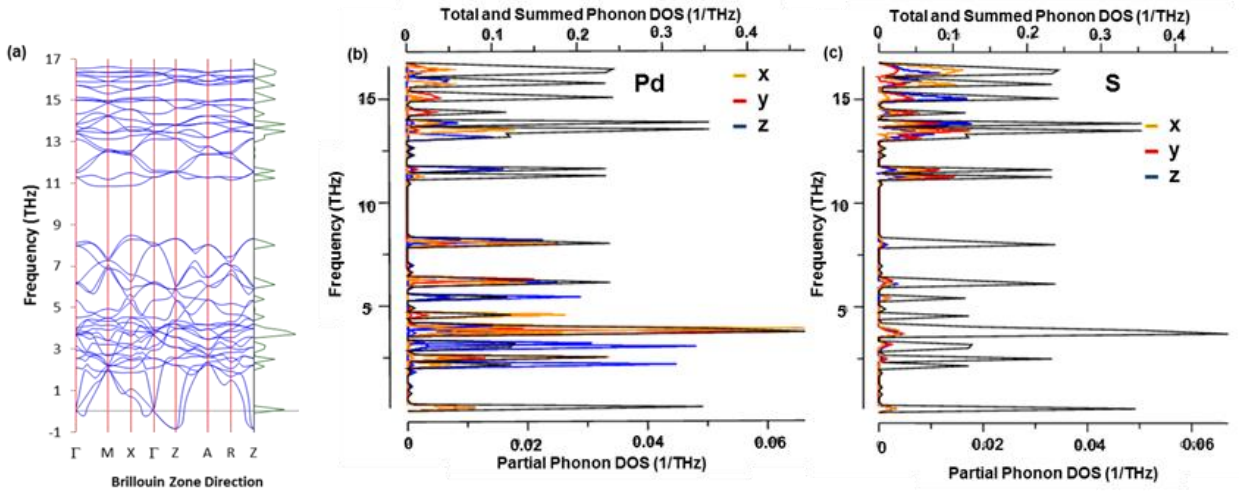

Figure 3.7.4. 5. (a) Phonon dispersion for $Pd_{50}S_{50}$ $P4_2/m$ at (50 GPa), Phonon density of states (b) Pd contribution and (c) S contribution

The $Pd_{50}S_{50}$ $P4_2/m$ at 0 GPa (figure 3.4.5), shows phonon spectra with small imaginary frequencies at point Γ of the Brillioun zone. Figure 3.7.4.1, shows the phonon spectra of 10 GPa with negative frequencies at point Γ of the Brillouin zone. It is clear that Pd and S atoms are responsible for the soft modes, with S atoms contributing minimally. The lower band of acoustic and optical branches emanates mainly from Pd and S atoms, the upper band of optical branches are associated with Pd and less from S atoms. Figure 3.7.4.2 gives the phonon spectra of 20 GPa, where all branches are positive. There are no soft modes observed. The lower band of acoustic and optical branches emanates from Pd and a minimal contribution from S atoms and the upper band of optical branches emanates from Pd and S atoms. Figure 3.7.4.3 gives the phonon spectra of 30 GPa. All branches are positive. The lower band of acoustic and optical branches start at about 0 THz and end at 3.5 THz and the upper band of optical branches starts at about 10.5 THz and ends at 15 THz. Figure 3.7.4.4, shows the phonon spectra of 40 GPa with imaginary soft modes at point Z of the Brillouin zone. It is evident that Pd and to a less extend S atoms are responsible for the soft modes. Contributions of S atoms are minimal towards the negative frequencies. The lower band of acoustic and optical branches emanates from Pd and S atoms and the upper band of optical branches is associated with Pd and S atoms. Figure 3.7.4.5, shows the phonon spectra of 50 GPa with soft modes along Z direction. From the PDOS, it is clear that Pd atoms are responsible for the soft modes. The negative frequencies are due to shear modulus being small. The lower band of acoustic and optical branches starts at about -2 THz and ends at 2 THz. The upper band of optical branches starts at about 11 THz and ends at 16.5 THz. It was observed that as more pressure is applied the DOS peaks in the lower and upper bands are broadened. Pressure extends the soft modes range to -1 THz.

3.7.5. Pressure variation of Phonon Dispersions – $Pd_{37.5}Pt_{12.5}S_{50}$– Phonon Density of States ($P4_2/m$)

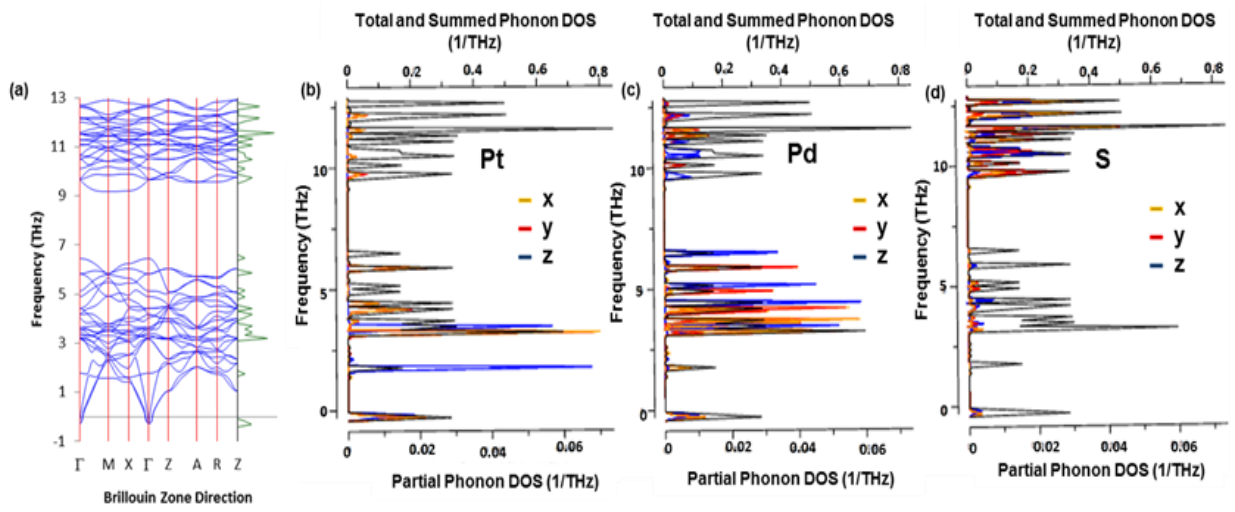

Figure 3.7.5. 1. (a) Phonon dispersion for $Pd_{37.5}Pt_{12.5}S_{50}$ $P4_2/m$ at (10 GPa), Phonon density of states (b) Pt contribution, (c) Pd contribution and (d) S contribution

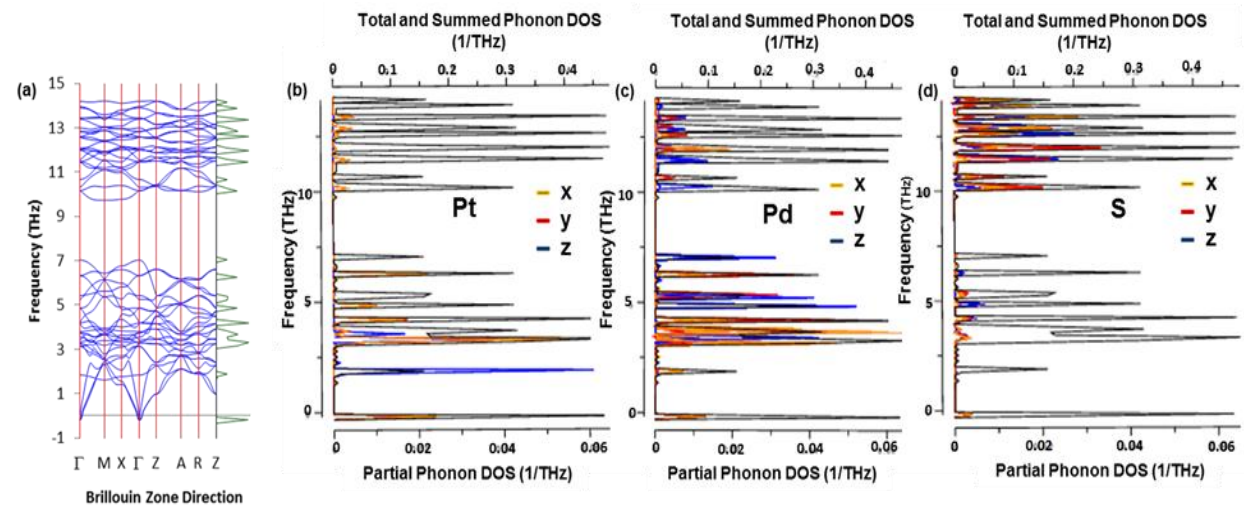

Figure 3.7.5. 2. (a) Phonon dispersion for $Pd_{37.5}Pt_{12.5}S_{50}$ $P4_2/m$ at (20 GPa), Phonon density of states (b) Pt contribution, (c) Pd contribution and (d) S contribution

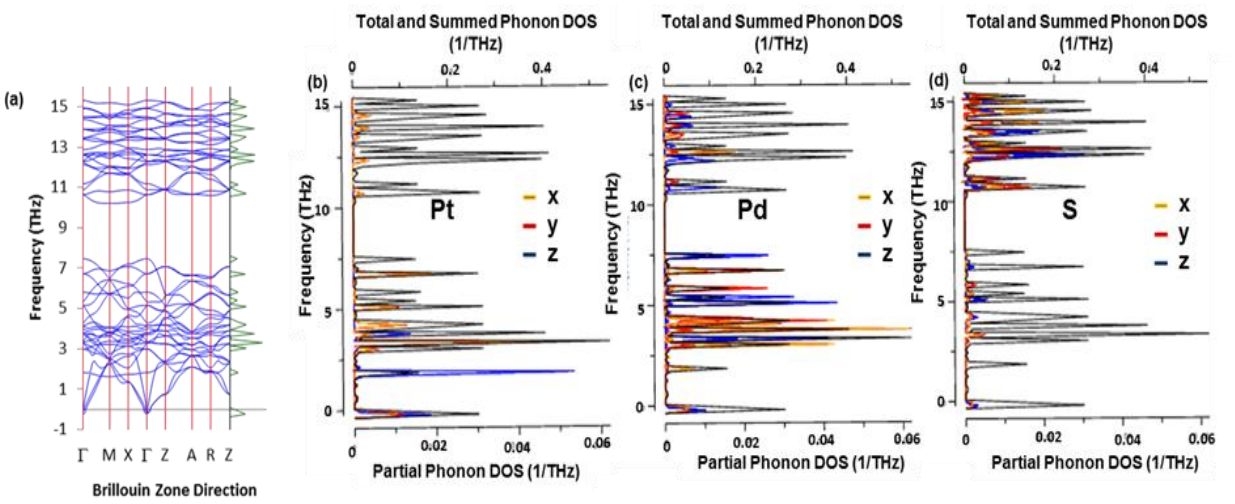

Figure 3.7.5. 3. (a) Phonon dispersion for $Pd_{37.5}Pt_{12.5}S_{50}$ $P4_2/m$ at (30 GPa), Phonon density of states (b) Pt contribution and (c) Pd contribution and (d) S contribution

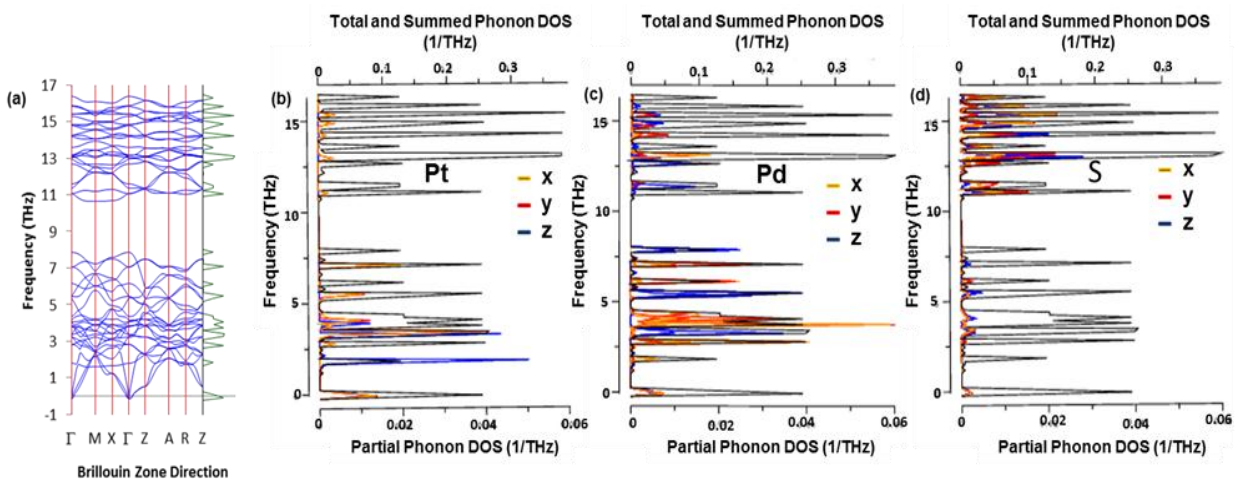

Figure 3.7.5. 4. (a) Phonon dispersion for $Pd_{37.5}Pt_{12.5}S_{50}$ $P4_2/m$ at (40 GPa), Phonon density of states (b) Pt contribution, (c) Pd contribution and (d) S contribution

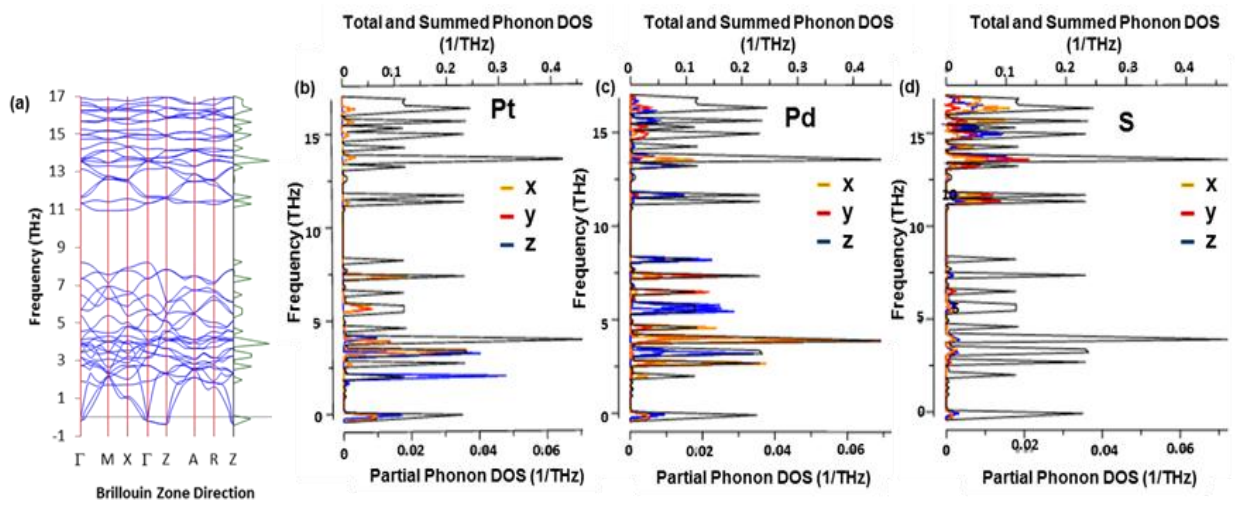

Figure 3.7.5. 5. (a) Phonon dispersion for $Pd_{37.5}Pt_{12.5}S_{50}$ $P4_2/m$ at (50 GPa), Phonon density of states (b) Pt contribution, (c) Pd contribution and (d) S contribution

The $Pd_{37.5}Pt_{12.5}S_{50}$ with space group $P4_2/m$ at 0 GPa (figure 3.4.6) shows soft modes at the Γ point. Figure 3.7.5.1, shows phonon spectra of 10 GPa with very limited soft modes along Γ. Looking at the PDOS, it was observed that Pt and Pd atoms are responsible for the negative frequencies. The S atoms contribute less towards the soft modes. The lower band of acoustic and optical branches starts at about -0.5 THz and ends at 6.5 THz, and the upper band of optical branches starts at about 9.5 THz and ends at 13 THz. All vibrational components in Pd was observed to be dominant at about 3 THz to 6.5 THz. Pd and S atoms are responsible for the upper band of optical branches. Figure 3.7.5.2, shows phonon spectra of 20 GPa with limited negative frequencies at point Γ of the Brillouin zone. From the PDOS, it was observed that the y – z component of Pt, Pd and S atoms are responsible for the soft modes, with S atoms contribution being small. The lower band of acoustic and optical branches emanate from the Pt, Pd and S atoms and the upper bands of optical branches are associated with Pd and S atoms, where x component of Pt atoms contributes minimal. Figure 3.7.5.3 gives the phonon spectra of 30 GPa. Looking at the PDOS, there are limited negative frequencies observed along Γ direction. The Pt and Pd atoms are responsible for the imaginary frequencies. The lower band of acoustic and optical branches starts at about -0.5 THz and

end at 7.3 THz and the upper band of optical branches starts at about 10.5 THz and ends at 15 THz. Figure 3.7.5.4 gives the phonon spectra of 40 GPa. All branches are positive, which suggests stability. The lower band of acoustic and optical branches starts at about 0 THz and ends at 8.5 THz. The upper band of optical branches starts at about 11 THz and ends at 16.5 THz. Figure 3.7.5.5 shows phonon spectra of 50 GPa with soft modes at points J and Z of the Brillioun zone. Looking at the PDOS, Pt and Pd atoms are responsible for the soft modes, with x - y contribution being dominant. The Pd and S atoms contributes in the upper band of optical branches. The contribution of S atoms is minimal to the soft modes. The range of lower and upper band increases with increasing pressure.

3.7.6. Pressure variation of Phonon Dispersions – $Pd_{25}Pt_{25}S_{50}$– Phonon Density of States ($P4_2/m$)

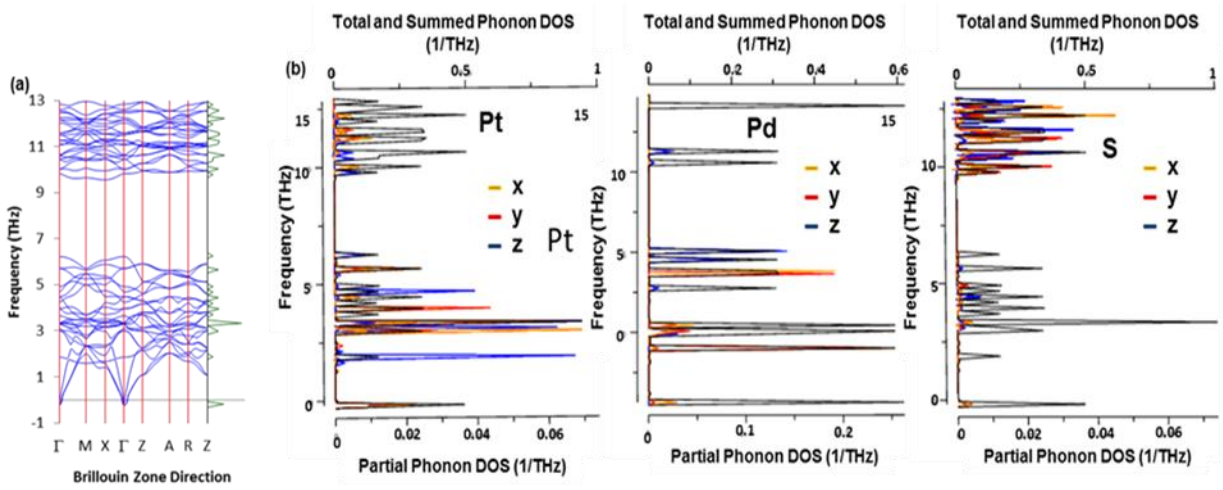

Figure 3.7.6. 1. (a) Phonon dispersion for $Pd_{25}Pt_{25}S_{50}$ $P4_2/m$ at (10 GPa), Phonon density of states (b) Pt contribution, (c) Pd contribution and (d) S contribution

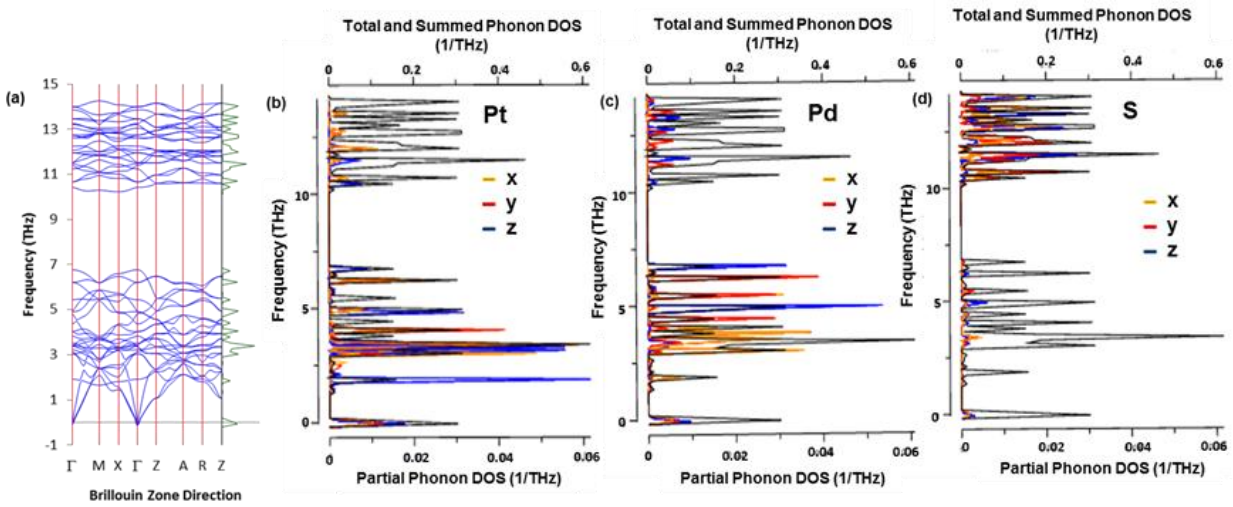

Figure 3.7.6. 2. (a) Phonon dispersion for $Pd_{25}Pt_{25}S_{50}$ $P4_2/m$ at (20 GPa), Phonon density of states (b) Pt contribution, (c) Pd contribution and (d) S contribution

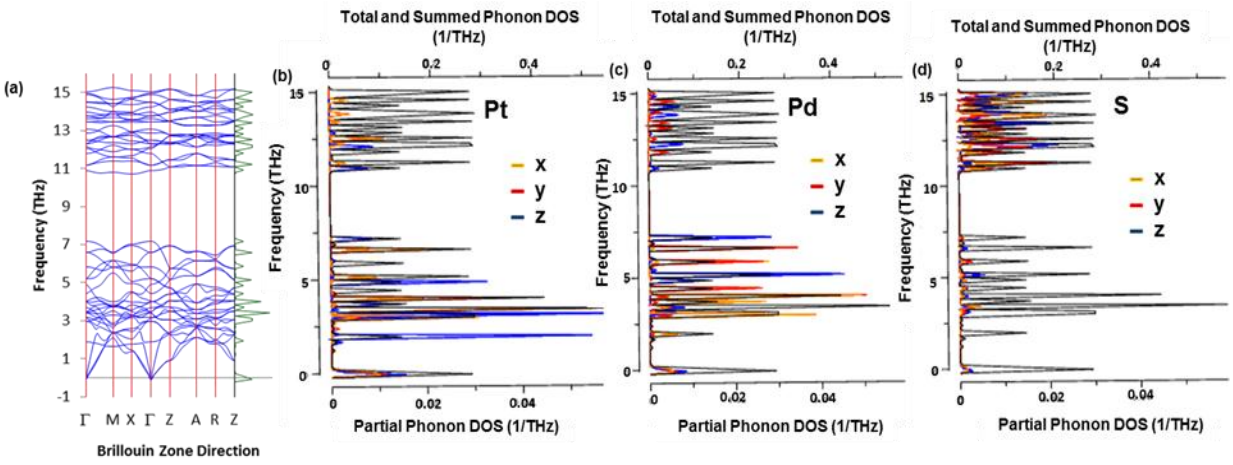

Figure 3.7.6. 3. (a)Phonon dispersion for $Pd_{25}Pt_{25}S_{50}$ $P4_2/m$ at (30 GPa), Phonon density of states (b) Pt contribution, (c) Pd contribution and (d) S contribution

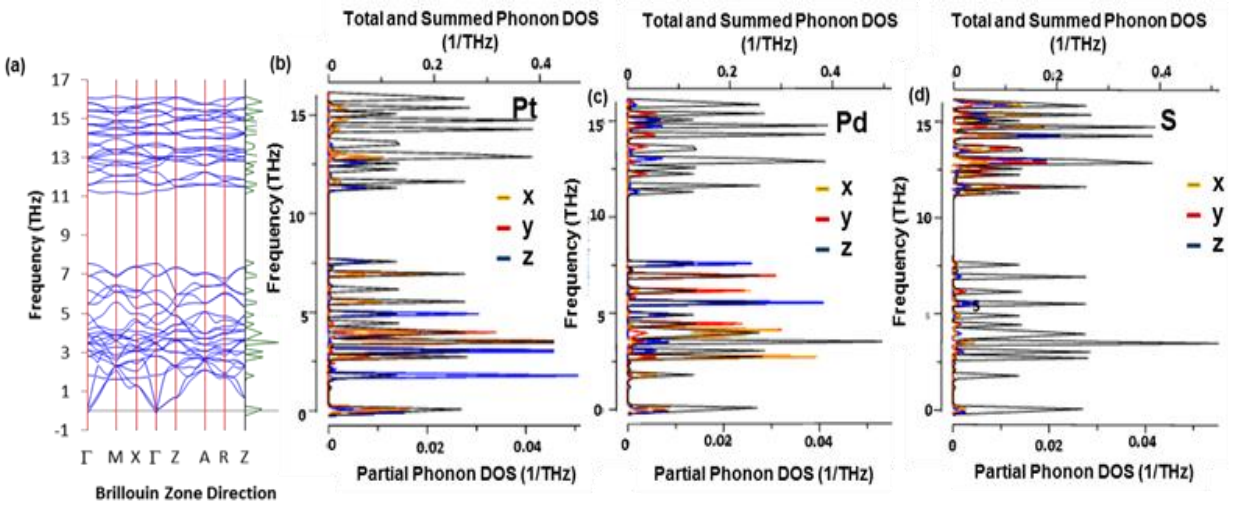

Figure 3.7.6. 4. (a) Phonon dispersion for $Pd_{25}Pt_{25}S_{50}$ $P4_2/m$ at (40 GPa), Phonon density of states (b) Pt contribution, (c) Pd contribution and (d) S contribution

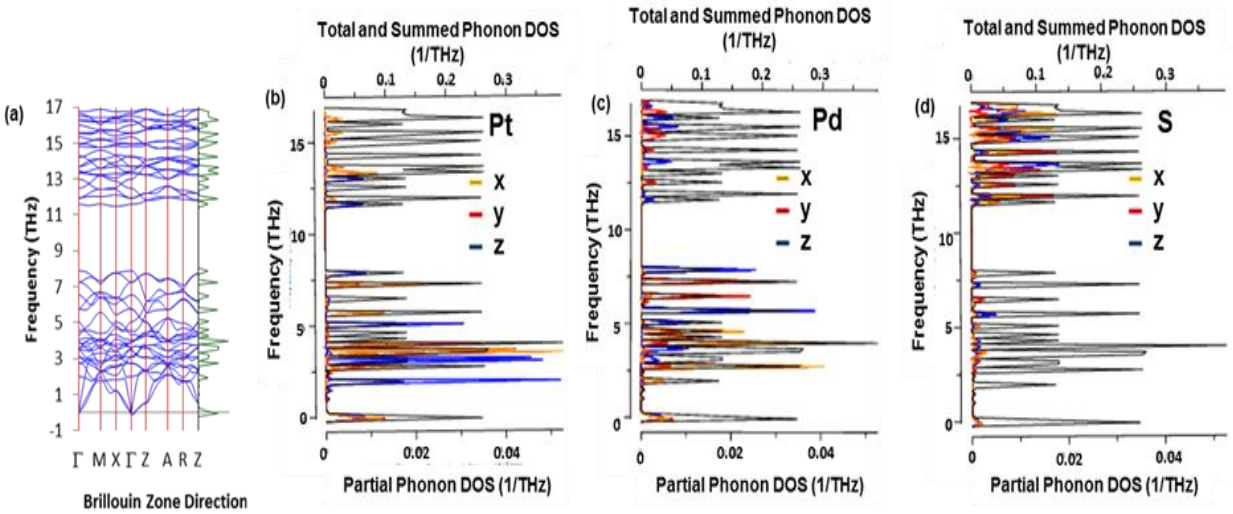

Figure 3.7.6. 5. (a) Phonon dispersion for $Pd_{25}Pt_{25}S_{50}$ $P4_2/m$ at (50 GPa), Phonon density of states (b) Pt contribution, (c) Pd contribution and (d) S contribution

The $Pd_{25}Pt_{25}S_{50}$ with space group $P4_2/m$ at 0 GPa (figure 3.4.7) shows soft modes at the Γ point. Figure 3.7.6.1, features phonon spectra of 10 GPa with limited negative frequencies at the Γ point of the Brillouin zone. From the PDOS, it is observed that Pt and Pd atoms are responsible for the imaginary frequencies with S atoms contribution being minimal. The lower band of acoustic and optical branches emanates from Pt and Pd atoms. The upper band of optical branches is associated with Pt, Pd and S atoms with the latter being dominant. Figure 3.7.6.2, gives the phonon spectra of 20 GPa. All branches are positive, which suggests stability. The lower band of acoustic and optical branches starts at about 0 THz and ends at 6.85 THz and the upper band of optical branches starts at about 10 THz and ends at 14 THz. Figure 3.7.6.3, shows the phonon spectra of 30 GPa. All branches are positive, there are no soft modes observed. The lower band of acoustic and optical branches emanate from Pt and Pd atoms and the upper band of optical branches are associated with Pt, Pd and S atoms and those of the latter are dominant. Figure 3.7.6.4 gives the phonon spectra of 40 GPa, where all branches corresponds to positive frequencies. The lower band of acoustic and optical branches starts at about 0 THz and ends at 7.4 THz and the upper band of optical branches starts at about 11 THz and ends at 16 THz. Figure 3.7.6.5, shows the phonon spectra of 50 GPa, with all branches being positive, which suggests stability. Looking at the PDOS, it was noticed that the lower band of acoustic branches emanates from the Pt and Pd atoms, with S atoms contribution being limited and the upper band of optical branches emanates from the Pt, Pd and S atoms. The z component in Pt was observed to be dominant at about 1.5THz to 5 THz. Pressure increases the lower and upper bands.

3.7.7. Pressure variation of Phonon Dispersions – $Pd_{12.5}Pt_{37.5}S_{50}$– Phonon Density of States ($P4_2/m$)

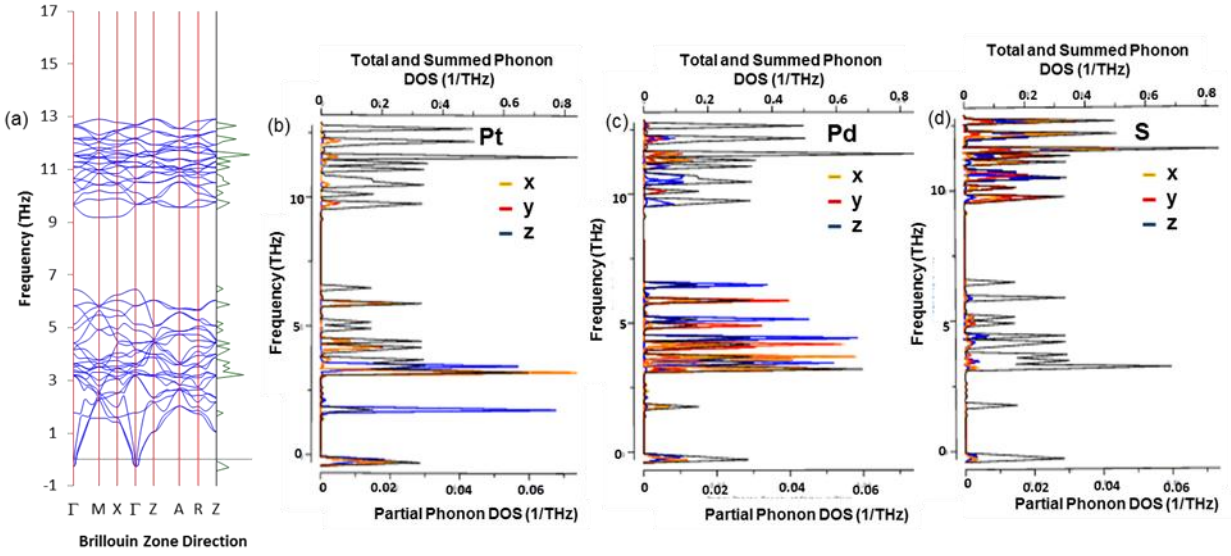

Figure 3.7.7. 1. (a) Phonon dispersion for $Pd_{12.5}Pt_{37.5}S_{50}$ $P4_2/m$ at (10 GPa), Phonon density of states for $Pd_{12.5}Pt_{37.5}S_{50}$ (b) Pt contribution, (c) Pd contribution and (d) S contribution

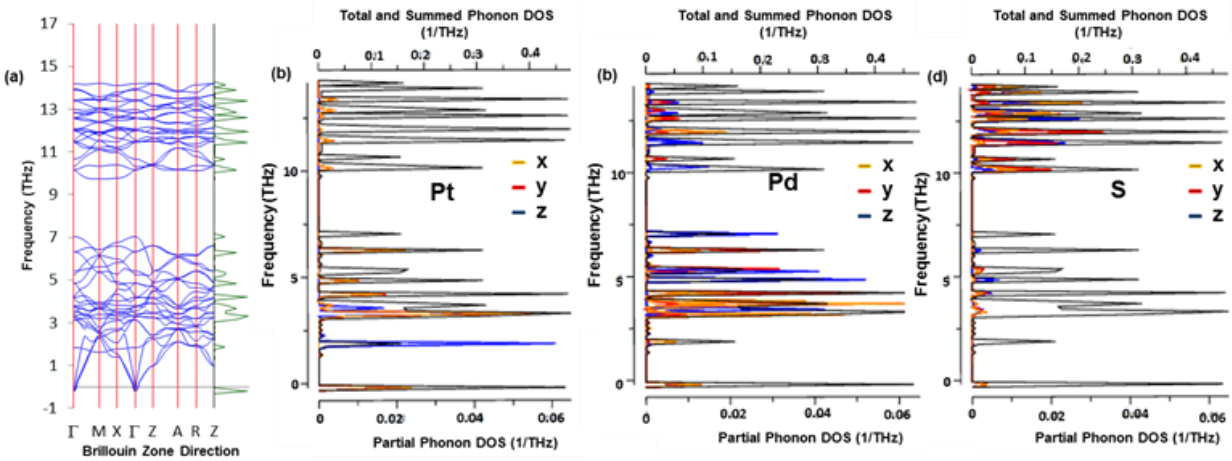

Figure 3.7.7. 2. (a) Phonon dispersion for $Pd_{12.5}Pt_{37.5}S_{50}$ $P4_2/m$ at (20 GPa), Phonon density of states (b) Pt contribution, (c) Pd contribution and (d) S contribution

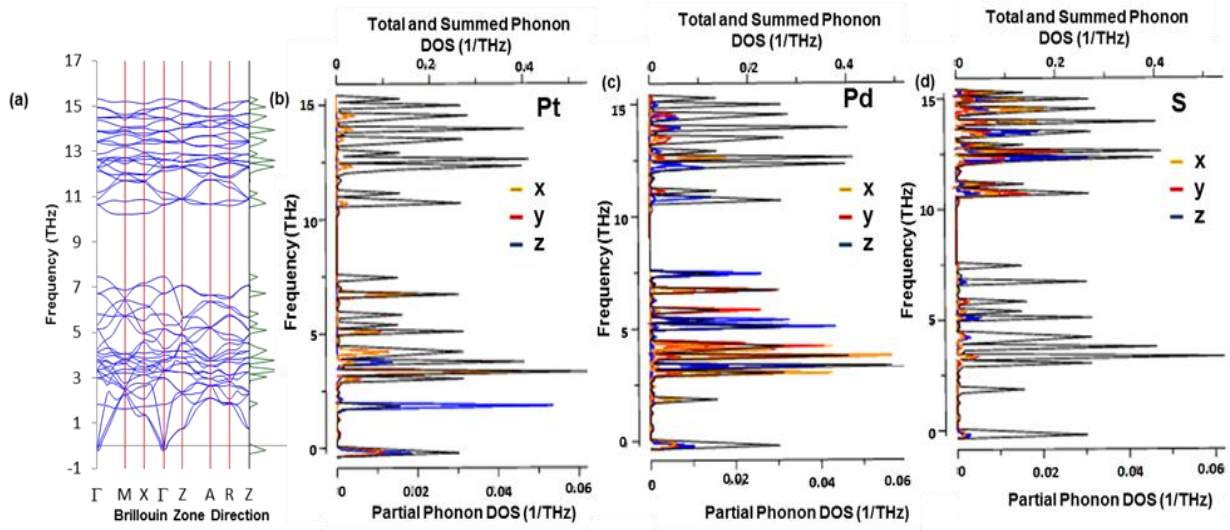

Figure 3.7.7. 3. (a) Phonon dispersion for $Pd_{12.5}Pt_{37.5}S_{50}$ $P4_2/m$ at (30 GPa), Phonon density of states (b) Pt contribution, (c) Pd contribution and (d) S contribution

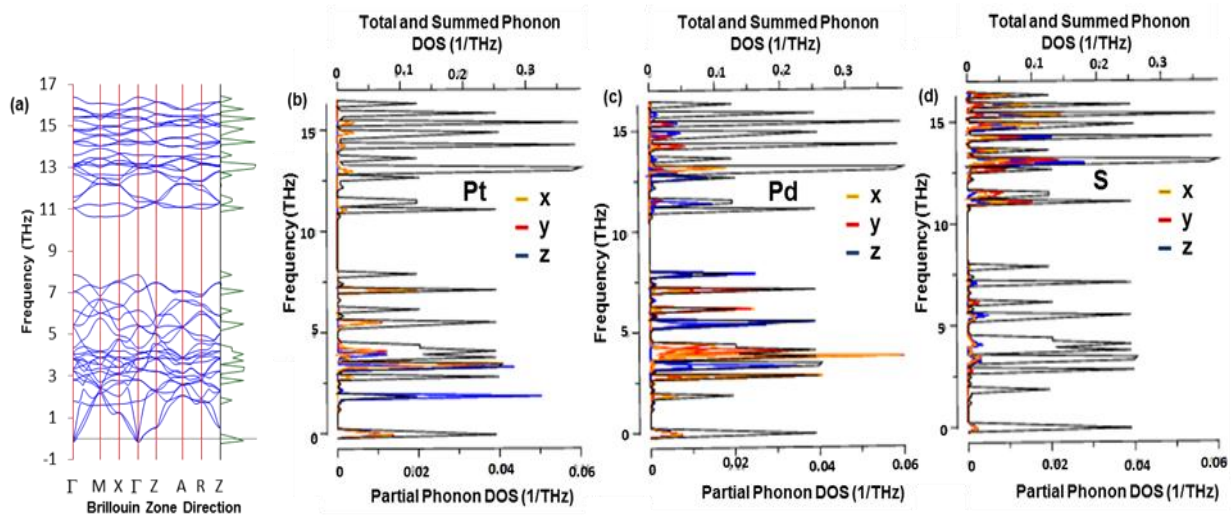

Figure 3.7.7. 4. (a) Phonon dispersion for $Pd_{12.5}Pt_{37.5}S_{50}$ $P4_2/m$ at (40 GPa), Phonon density of states (b) Pt contribution, (c) Pd contribution and (d) S contribution

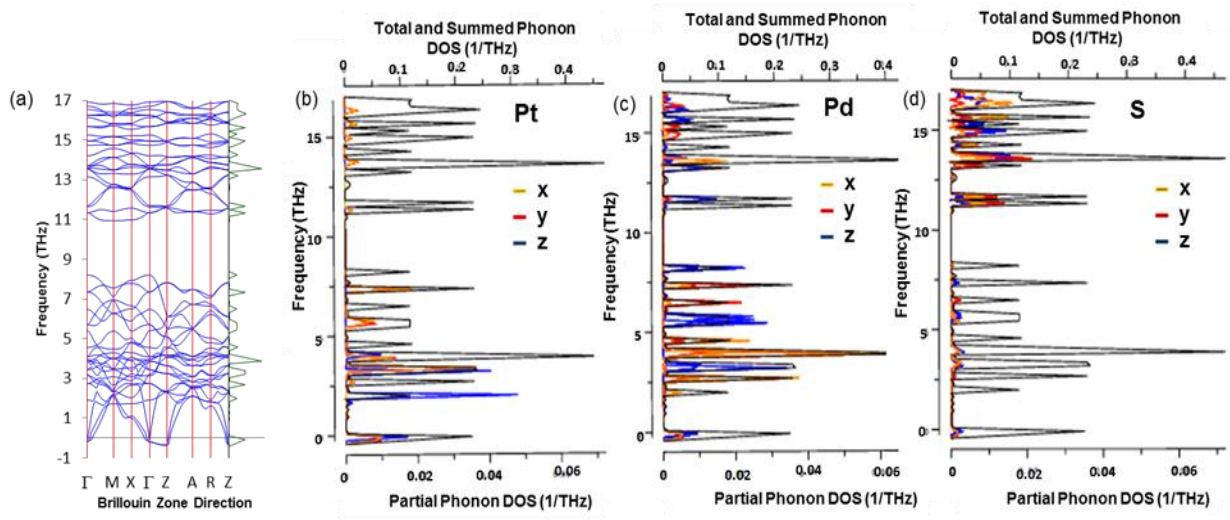

Figure 3.7.7. 5. (a) Phonon dispersion for $Pd_{12.5}Pt_{37.5}S_{50}$ $P4_2/m$ at (50 GPa), Phonon density of states (b) Pt contribution, (c) Pd contribution and (d) S contribution

The $Pd_{12.5}Pt_{37.5}S_{50}$ with space group $P4_2/m$ at 0 GPa (figure 3.4.8), shows no negative frequencies. Figure 3.7.7.1 gives the phonon spectra of 10 GPa, where negative frequencies were detected at point Γ of the Brillouin zone. From the PDOS, the Pt and Pd atoms are responsible for the soft modes, where S atoms contribute minimally. S atoms vibrate at higher frequencies. The lower band of acoustic and optical branches emanates from the Pt and Pd atoms. The upper band of optical branches is associated with Pd and S atoms with a limited contribution from Pt atoms. Figure 3.7.7.2, shows the phonon spectra of 20 GPa with slight negative frequencies along the Γ direction. Looking at the PDOS, Pt and Pd are responsible for the imaginary frequencies, since they vibrate at lower frequencies. The lower bands of acoustic and optical branches emanate from Pt and Pd atoms and the upper bands of optical branches are associated with Pd and S atoms, where Pt contribution is minimal. Figure 3.7.7.3, gives the phonon spectra of 30 GPa. The imaginary frequencies were detected at point Γ direction. Looking at the PDOS, it was observed that the y - z components of Pt and Pd atoms contribute to the negative frequencies. S atoms contribute less to the soft modes. The lower band of acoustic and optical branches starts at about -0.5 THz and ends at 7.4 THz, the upper

band of optical branches starts at about 10.5 THz and ends at 15.5 THz. Figure 3.7.7.4, shows the phonon spectra of 40 GPa with limited negative frequencies along Γ direction, with y contributions of Pt and Pd being dominant. The lower band of acoustic and optical branches starts at about -0.5 THz and ends at 7.5 THz, the upper bands of optical branches starts at about 10.5 THz and ends at 15.5 THz. From the PDOS, Pt and Pd vibrate at lower frequencies and the S atoms vibrate predominantly at frequencies greater than 0 THz. The z component is dominant at around 2.5 THz in Pt, 3 THz to 7.5 THz in Pd atoms. Figure 3.7.7.5 gives the phonon spectra of 50 GPa. Imaginary frequencies were detected at point Z of the Brillouin zone. Looking at the PDOS, it was observed that Pt and Pd atoms vibrate at lower frequencies, below 0 THz. The S atoms vibrate at frequencies greater than 0 THz. Furthermore, it is evident that the Pt and Pd atoms are responsible for the negative frequencies, with S atoms contributing minimally.

3.7.8. Pressure variation of Phonon Dispersions –$Pt_{50}S_{50}$– Phonon Density of States ($P4_2/m$)

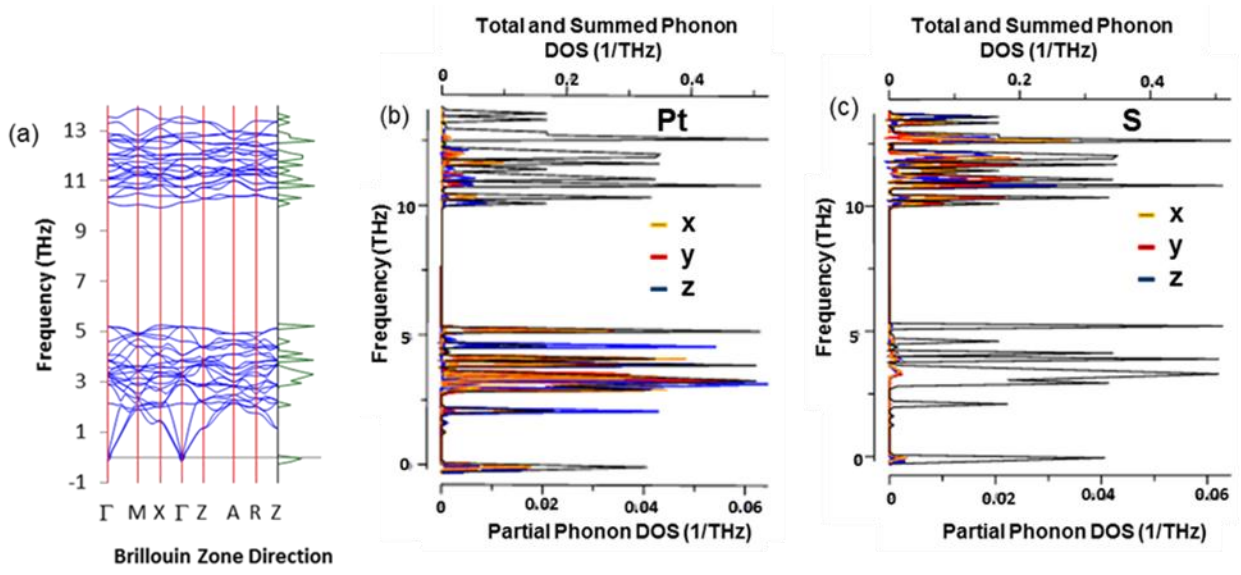

Figure 3.7.8. 1. (a) Phonon dispersion for $Pt_{50}S_{50}$ $P4_2/m$ at (10 GPa), Phonon density of states (b) Pt contribution, (c) S contribution

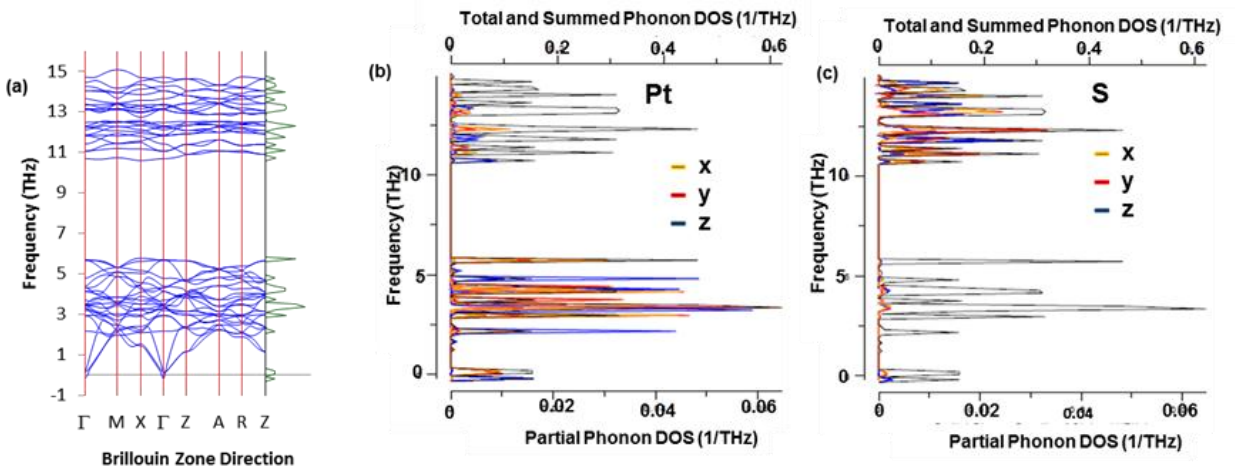

Figure 3.7.8. 2. (a) Phonon dispersion for $Pt_{50}S_{50}$ $P4_2/m$ at (20 GPa), Phonon density of states (b) Pt contribution and (c) S contribution

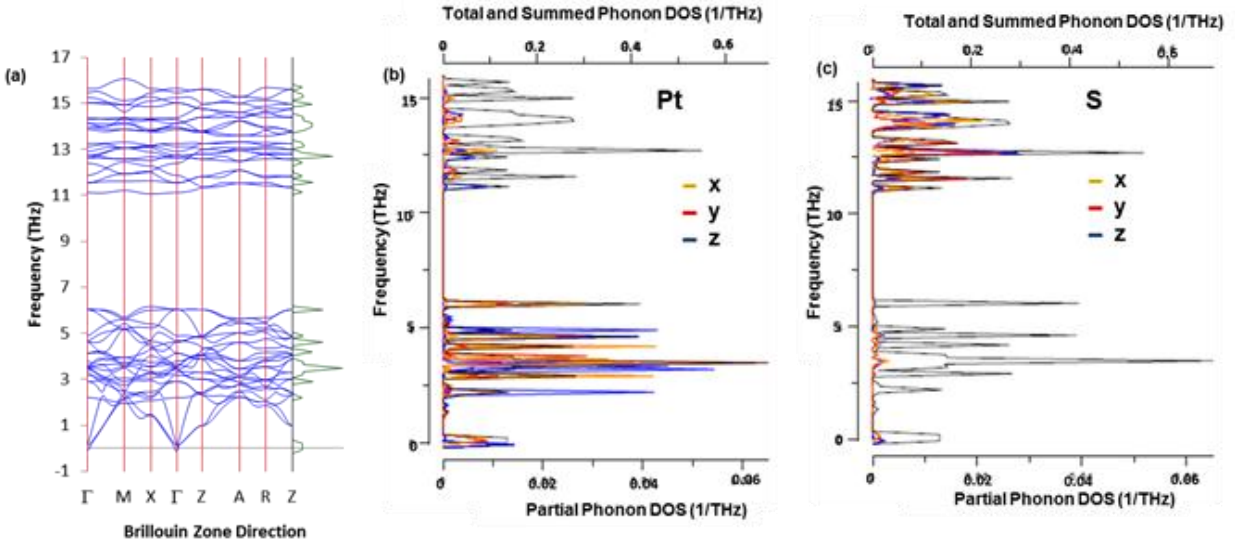

Figure 3.7.8. 3. (a) Phonon dispersion for $Pt_{50}S_{50}$ $P4_2/m$ at (30 GPa), Phonon density of states (b) Pt contribution and (c) S contribution

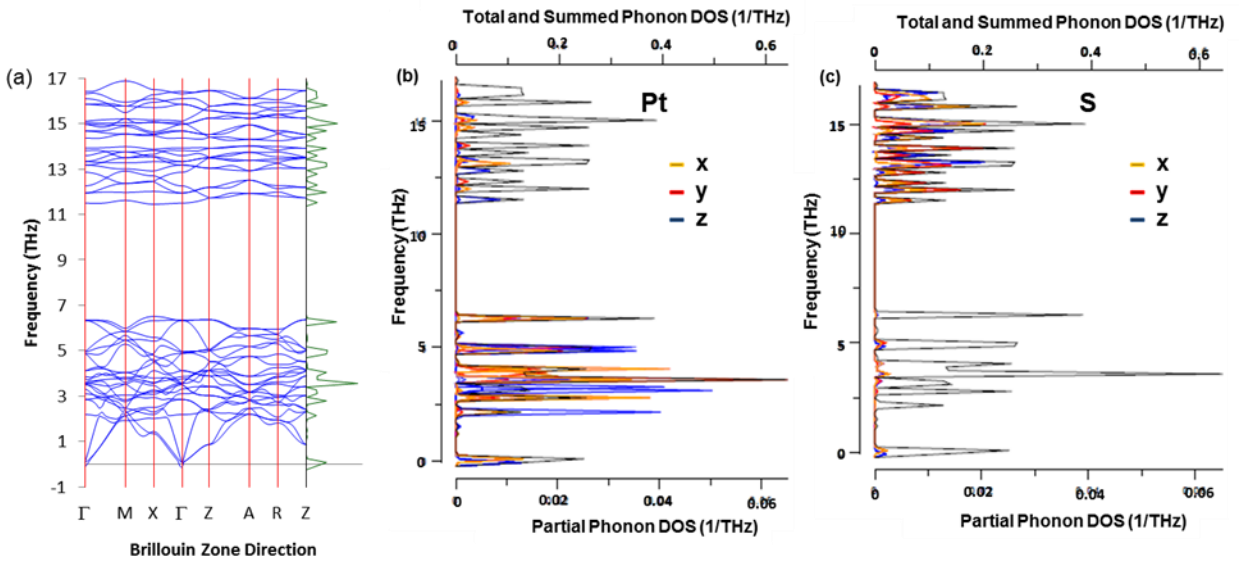

Figure 3.7.8. 4. (a) Phonon dispersion for $Pt_{50}S_{50}$ $P4_2/m$ at (40 GPa), Phonon density of states (b) Pt contribution and (c) S contribution

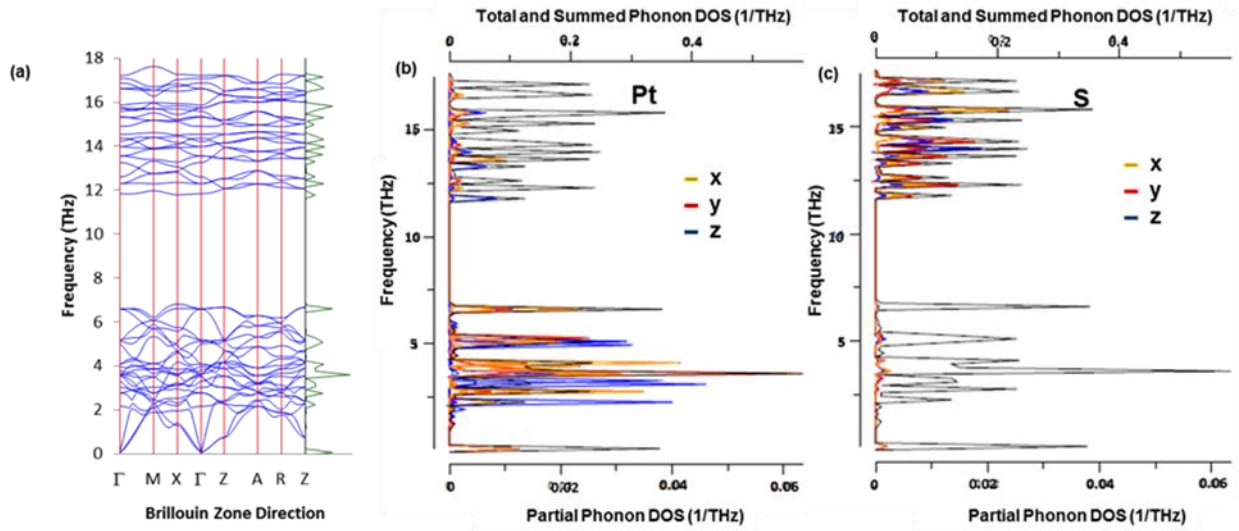

Figure 3.7.8. 5. Phonon dispersion for $Pt_{50}S_{50}$ $P4_2/m$ at (50 GPa) (a) Phonon density of states for $Pt_{50}S_{50}$ (b) Pt contribution and (c) S contribution

The $Pt_{50}S_{50}$ with space group $P4_2/m$ at 0 GPa (figure 3.4.8), shows no negative frequencies. Figure 3.7.8.1, shows the phonon spectra of 10 GPa, with limited negative frequencies at point Γ of the Brillouin zone. From the PDOS, it is evident that Pt atoms are responsible for the negative frequencies, with the x - y components dominant. The S atoms contribute less to the soft modes. The lower band of acoustic and optical branches emanates from Pt atoms and the upper band of optical branches is associated with Pt and S atoms. Figure 3.7.8.2, shows the phonon spectra of 20 GPa. Negative frequencies were detected. Looking at the PDOS, Pt is responsible for the negative frequencies, with the y component being dominant. The lower band of acoustic and optical branches starts at about -0.3 THz and ends at 5.5 THz, the upper band of optical branches starts at about 10.5 THz and ends at 14 THz. The S atoms contribution is very limited towards the negative frequencies. Figure 3.7.8.3 gives the phonon spectra of 30 GPa, where limited negative frequencies were observed along Γ direction. From the PDOS, it is evident that Pt atoms with contribution of the y - z components are responsible for the negative frequencies. The lower band of acoustic and optical branches emanates mainly from Pt atoms, the upper band of optical branches is derived from the Pt and S atoms with the latter one dominant. Figure 3.7.8.4 gives the phonon spectra of 40 GPa with limited negative frequencies along Γ direction. From the PDOS, it was noted that Pt atoms are responsible for the negative frequencies. The S atoms contribution is minimal towards the negative frequencies. Figure 3.7.8.5, shows the phonon spectra of 50 GPa, with no soft modes observed, where frequencies corresponding to all branches are positive. The lower band of acoustic and optical branches starts at about 0 THz and ends at 6.5 THz, the upper band of optical branches starts at about 12 THz and ends at 17 THz. The z component in Pt is dominant at around 3 THz to 5 THz. It was observed that the lower and upper band increases with increasing pressure.

3.7.9. Pressure variation of Phonon Dispersions –$Pt_{50}S_{50}$– Phonon Density of States P_1 (from $P4_2/mmc$)

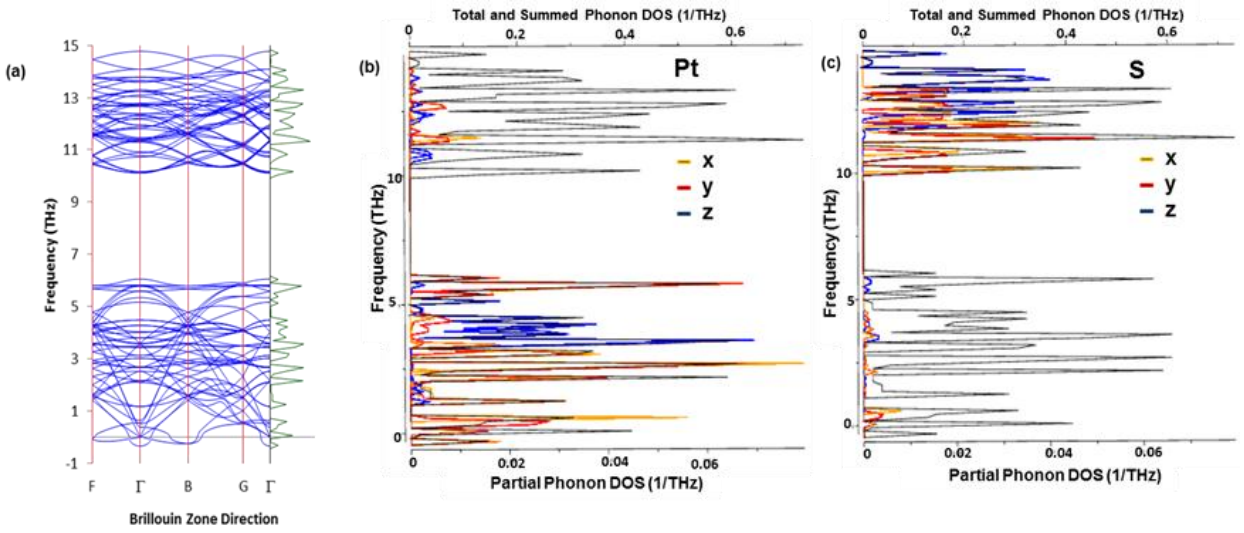

Figure 3.7.9. 1. (a) Phonon dispersion for $Pt_{50}S_{50}$ P_1 (from $P4_2/mmc$) at (10 GPa), Phonon density of states (b) Pt contribution and (c) S contribution

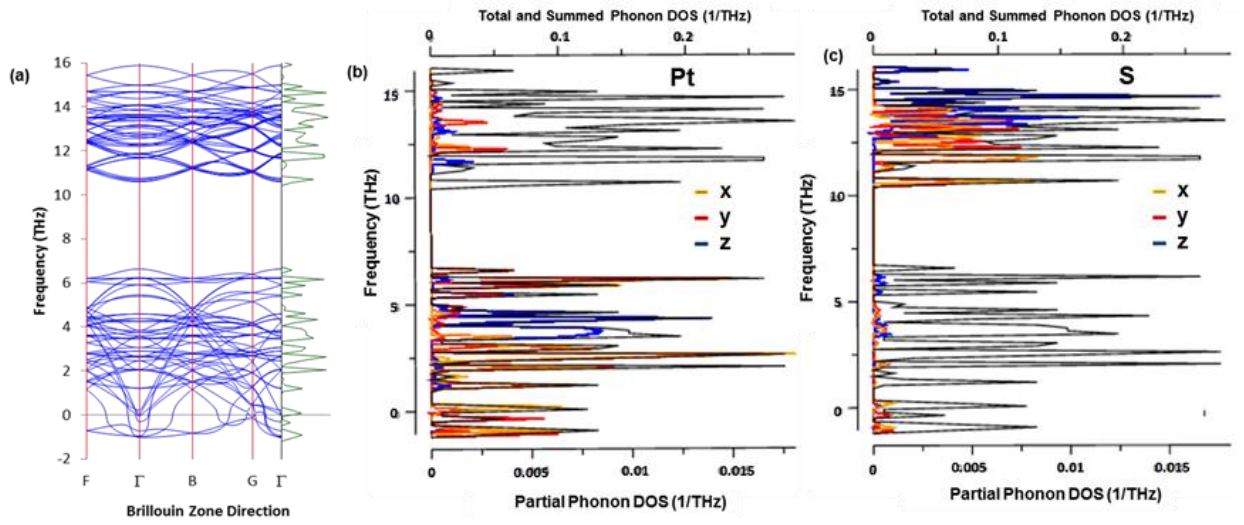

Figure 3.7.9. 2. (a) Phonon dispersion for $Pt_{50}S_{50}$ P_1 (from $P4_2/mmc$) at (20 GPa), Phonon density of states (b) Pt contribution and (c) S contribution

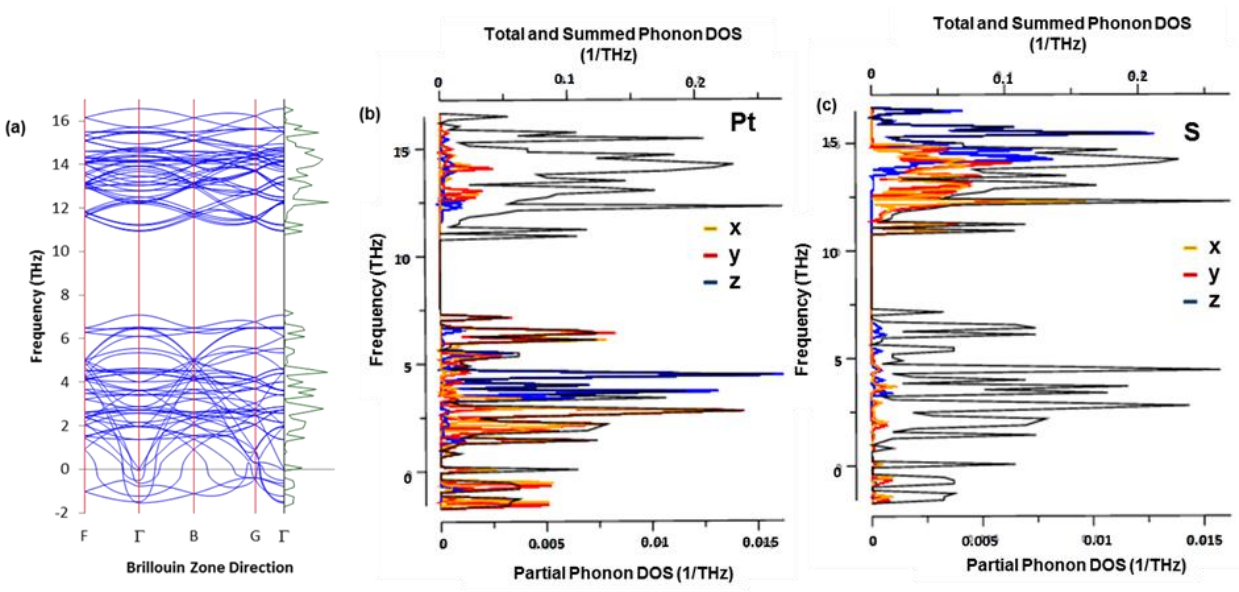

Figure 3.7.9. 3. (a) Phonon dispersion for $Pt_{50}S_{50}$ P_1 (from $P4_2/mmc$) at (30 GPa), Phonon density of states (b) Pt contribution and (c) S contribution

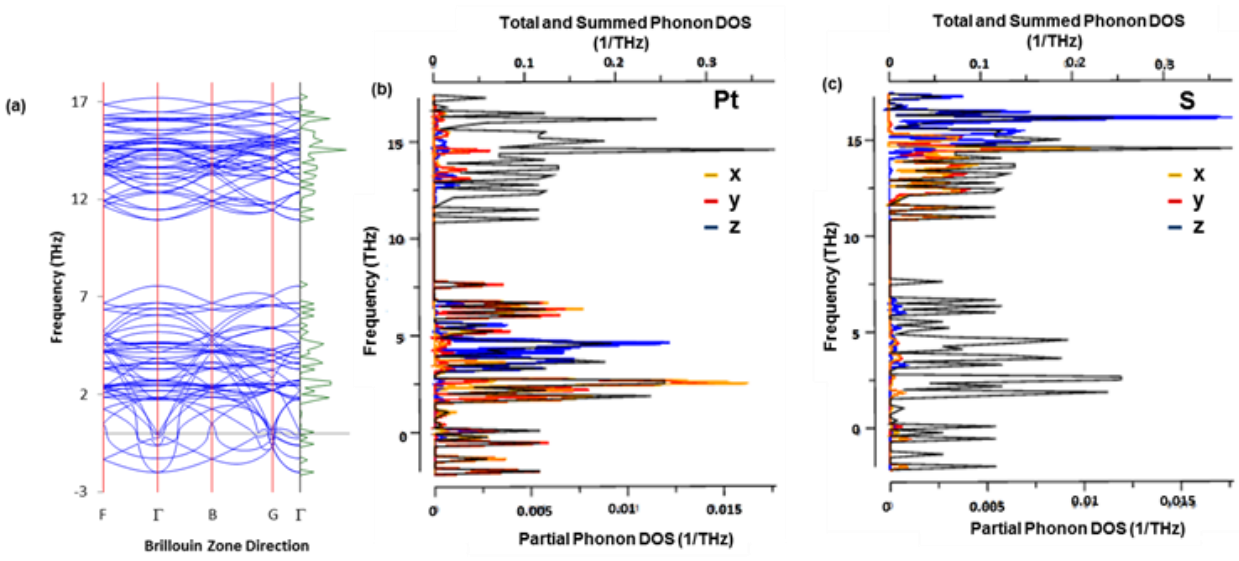

Figure 3.7.9. 4. (a) Phonon dispersion for $Pt_{50}S_{50}$ P_1 (from $P4_2/mmc$) at (40 GPa), Phonon density of states (b) Pt contribution and (c) S contribution

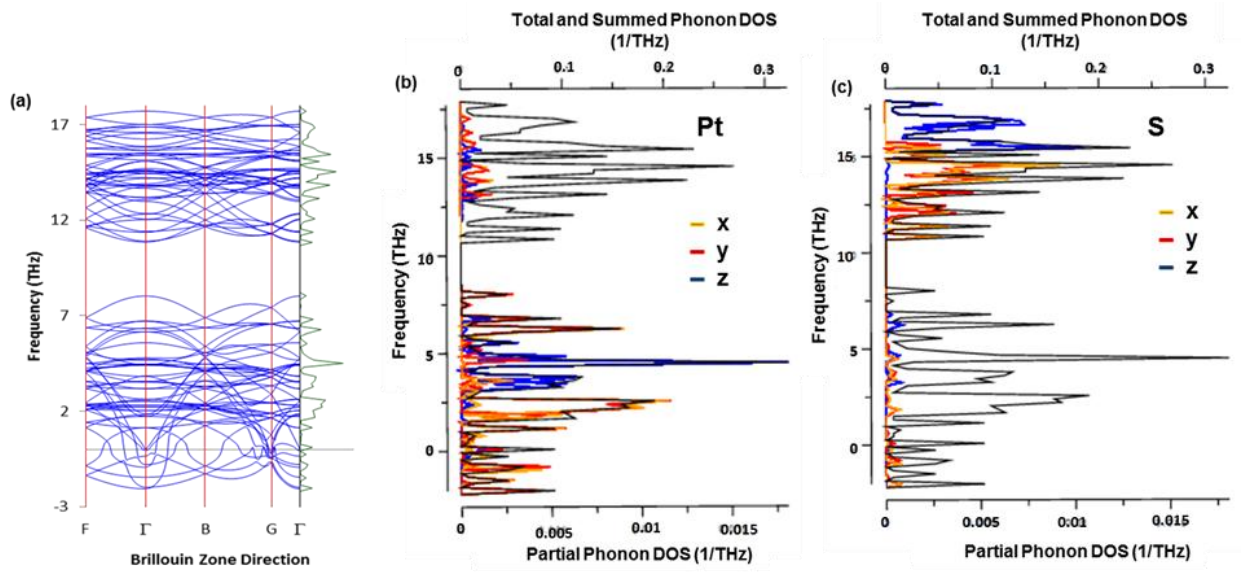

Figure 3.7.9. 5. (a) Phonon dispersion for $Pt_{50}S_{50}$ P_1 (from $P4_2/mmc$) at (50 GPa), Phonon density of states (b) Pt contribution and (c) S contribution

The analyses of the vibrational properties of $(Pt_{50-x}Pd_X)S_{50}$ with respect to the phonon dispersion and partial phonon densities of states are discussed below. The $Pt_{50}S_{50}$ with space group P_1 at 0 GPa (figure 3.4.9), shows phonon spectra with no soft modes. All branches have positive frequencies. Figure 3.7.9.1, shows phonon spectra for 10 GPa, where limited soft modes were observed along Γ - B of the Brillouin zone. The PDOS shows that Pt and S atoms are responsible for the soft modes, with x - y component being dominant. Looking at the PDOS for Pt, it was observed that the z- component is dominant at around 3.5 - 5 THz. The contribution of S atoms towards the negative frequencies is minimal. The z component of S atoms is dominant at around 11 - 15 THz. The lower band of acoustic and optical branches emanates from Pt atoms, where S atoms contribution is minimal and the upper band of optical branches is associated with Pt and S atoms. Figure 3.7.8.2, shows phonon spectra of 20 GPa with soft modes along Γ - B - G directions of the Brillouin zone. The Pt and S atoms are responsible for the soft

modes. The corresponding PDOS clearly indicate that the soft modes are due to the high vibrations of Pt atoms, with x - y component being dominant. S atoms contribution is minimal towards the soft modes. From the PDOS of Pt, It was noted that z component is dominant at around 4 - 5 THz. Pt and S atoms are responsible for the lower band of acoustic and optical branches and Pt and S atoms are responsible for the upper band of optical branches. Furthermore, z component of vibration for the S atoms is dominant at 14 - 15 THz. Figure 3.7.8.3, shows phonon spectra of 30 GPa with soft modes along Γ- B - G high symmetry directions. Pt and S atoms are responsible for the soft modes, since they vibrates at frequencies below 0 THz. S atoms contributes less towards the soft modes. The lower band of acoustic and optical branches emanates from Pt and S atoms with the latter contributing very less and the upper band of optical branches are associated with Pt and S atoms. Figure 3.7.8.4, the soft modes were observed along F - Γ - B - G of the Brillouin zone. It is evident that Pt and S atoms are responsible for the soft modes and the vibrations were along x - y component. The z component in Pt was noticed to be dominant at 4 - 5 THz, whereas in S atoms it was dominant at 14 – 17 THz. The lower band of acoustic and optical branches emanates mainly from Pt and S atoms, whereas upper band of optical branches are associated with Pt and S atoms. Figure 3.7.8.5, shows phonon spectra of 50 GPa with soft modes along F - Γ - B - G of the Brillouin zone. From the PDOS, Pt and S atoms are responsible for the soft modes and they vibrate along x - y component with S contributing minimally to the soft modes. The z component of Pt being dominant at 4 - 5 THz, the x - y components of S is dominant at 10.2 - 16 THz.

3.7.10. Phonon Dispersions –$Pt_{37.5}Pd_{12.5}S_{50}$– Phonon Density of States P_1 (from $P4_2/mmc$)

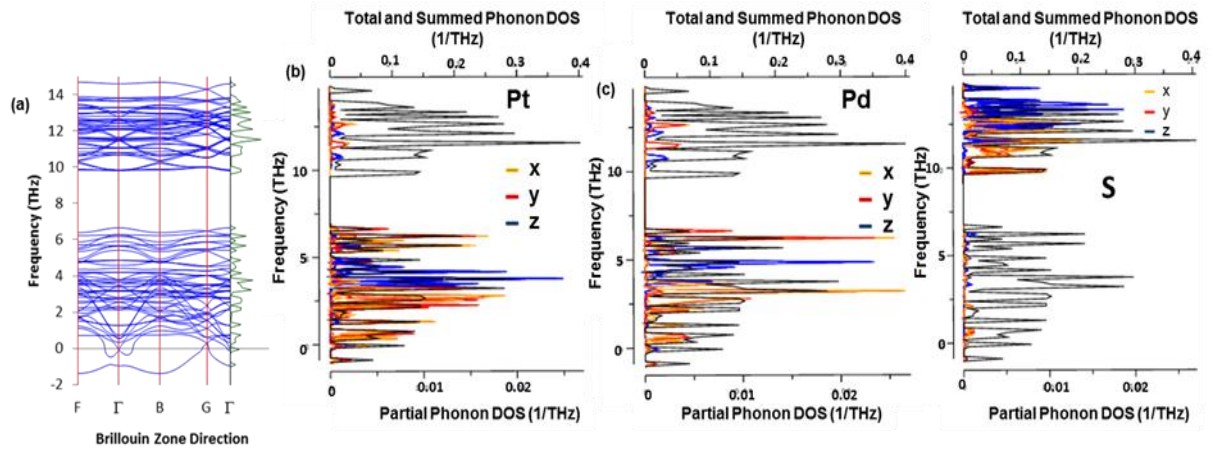

Figure 3.7.10. 1. (a) Phonon dispersion for $Pt_{37.5}Pd_{12.5}S_{50}$ P_1 (from $P4_2/mmc$) at (10 GPa), Phonon density of states (b) Pt contribution, (c) Pd contribution and (d) S contribution

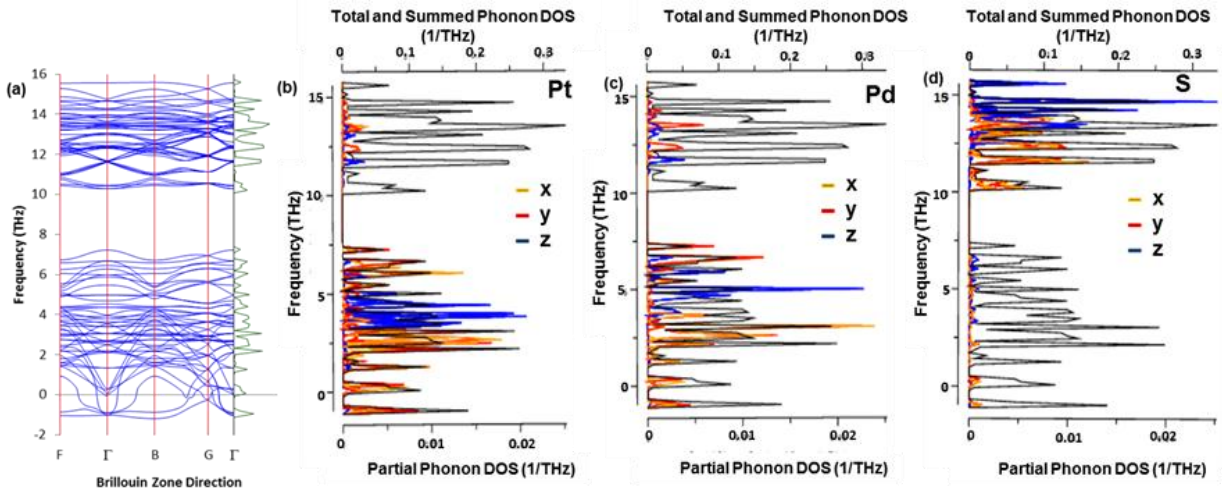

Figure 3.7.10. 2. (a) Phonon dispersion for $Pt_{37.5}Pd_{12.5}S_{50}$ P_1 (from $P4_2/mmc$) at (20 GPa), Phonon density of states (b) Pt contribution, (c) Pd contribution and (d) S contribution

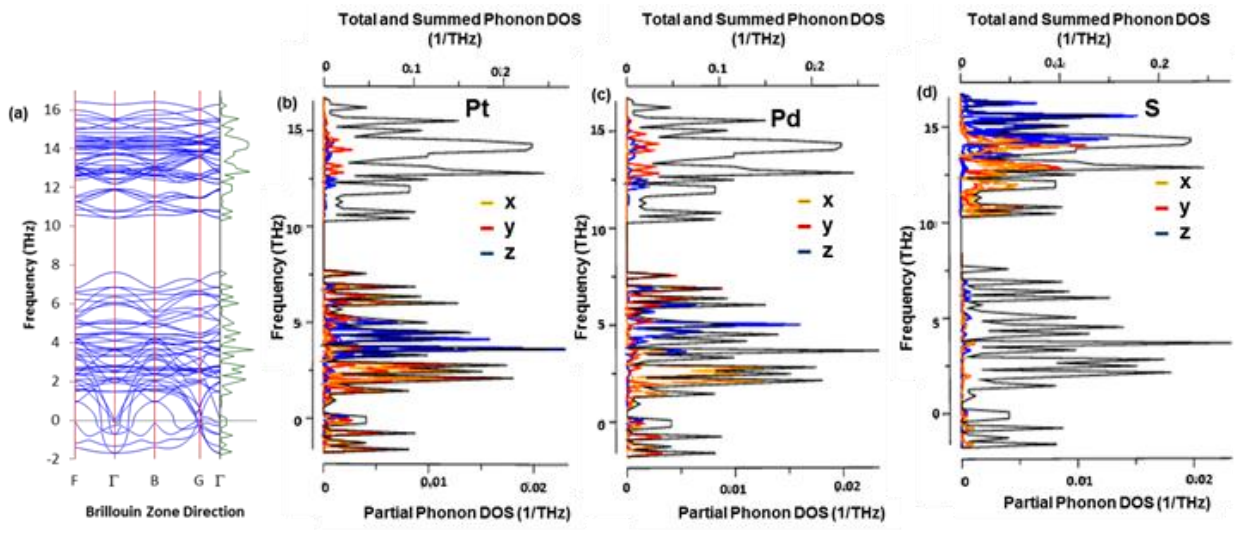

Figure 3.7.10. 3. (a) Phonon dispersion for $Pt_{37.5}Pd_{12.5}S_{50}$ P_1 (from $P4_2/mmc$) at (30 GPa), Phonon density of states (b) Pt contribution, (c) Pd contribution and (d) S contribution

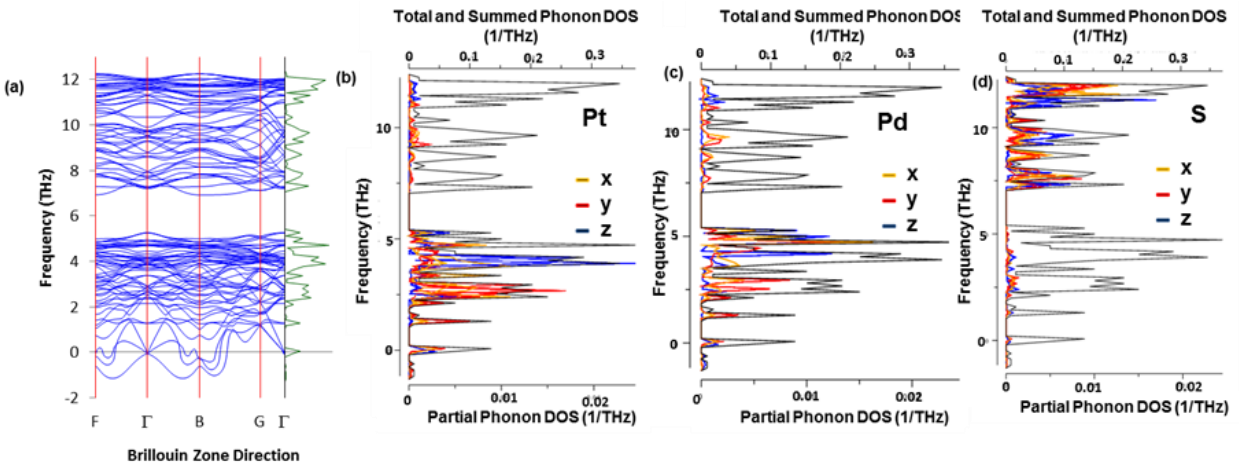

Figure 3.7.10. 4. (a) Phonon dispersion for $Pt_{37.5}Pd_{12.5}S_{50}$ P_1 (from $P4_2/mmc$) at (40 GPa), Phonon density of states (b) Pt contribution, (c) Pd contribution and (d) S contribution

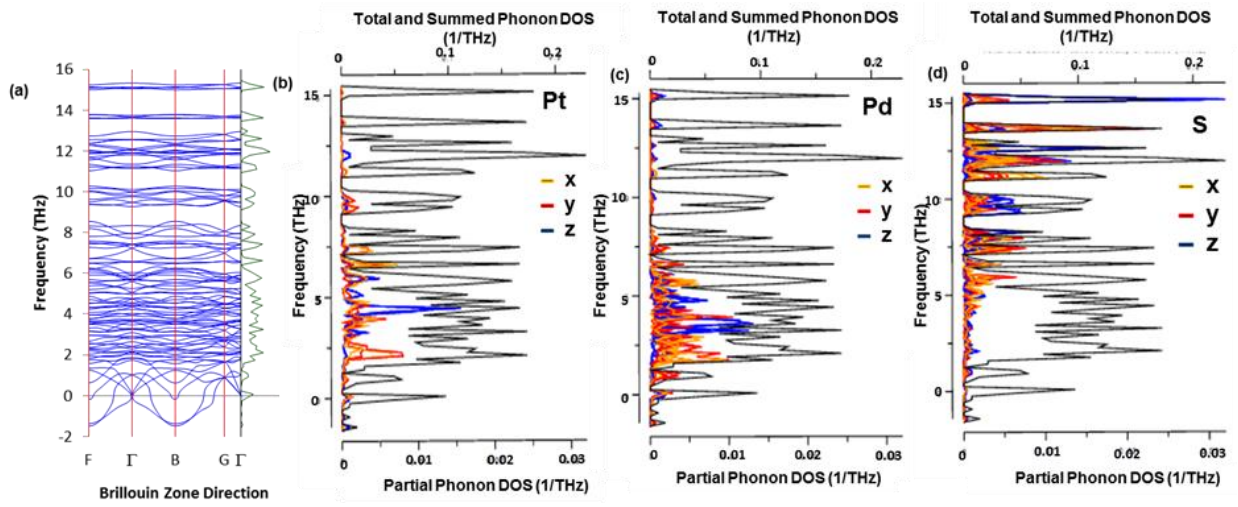

Figure 3.7.10. 5. (a) Phonon dispersion for $Pt_{37.5}Pd_{12.5}S_{50}$ P_1 (from $P4_2/mmc$) at (50 GPa), Phonon density of states (b) Pt contribution, (c) Pd contribution and (d) S contribution

The $Pt_{37.5}Pd_{12.5}S_{50}$ with space group P_1 at 0 GPa (figure 3.4.11), shows phonon spectra with soft modes along F – B direction of the Brillioun zone. Figure 3.7.10.1, shows phonon spectra of 10 GPa with soft modes along Γ - B high symmetry directions. The corresponding PDOS clearly indicates that the soft modes are due to significant vibrations of Pt and Pd atoms. S atoms vibrate at frequencies greater than 0 THz and they contribute less towards the soft modes. It was noted that z component is dominant in both Pt and Pd with magnitude around 4 - 5 THz and in S atoms its dominant at 11 - 14THz. The lower band of acoustic and optical branches emanates mainly from Pt and Pd atoms and the upper band of optical branches are associated mainly with the S atoms. Figure 3.7.10.2, shows phonon dispersion of 20 GPa with soft modes along Γ - B - G directions of the Brillouin zone. The PDOS shows that Pt, Pd and S atoms are responsible for the soft modes, with x - y component being dominant. The z component is dominant at 3 - 5 THz in Pt and Pd atoms and in S atoms it was dominant at around 13 – 16 THz. The upper band of optical branches starts at approximately 10 THz and ends at 16 THz and the lower band of acoustic branches ends at around 2 THz. Figure 3.7.10.3, shows phonon spectra of 30 GPa with soft modes along Γ - B - G directions of

the Brillioun zone. It is evident that Pt, Pd and S atoms are responsible for the soft modes, with S atoms contributing minimally. The lower band of acoustic and optical branches is mainly from Pt and Pd vibrations, the upper band of optical branches are associated with Pt, Pd and S contribution. The vibrations are along x - y component, where the z component is dominant at 13 - 16 THz in S atoms. The S atoms contribute less towards the soft modes. Figure 3.7.10.4, shows phonon spectra of 40 GPa with soft modes observed along F - B of the Brillioun zone. It is clear that Pt and Pd are responsible for the negative frequencies. The lower band of acoustic and optical branches starts at about -2.0 THz and ends at 5.2 THz and the upper band of optical branches starts at 11 THz and ends at 16.5 THz. Figure 3.7.10.5 gives the phonon spectra of 50 GPa. Negative frequencies were detected along F - B direction. The lower band of acoustic and optical branches emanates from the Pt and Pd atoms and the upper band of optical branches emanates from S atoms.

3.7.11. Phonon Dispersions –$Pt_{25}Pd_{25}S_{50}$– Phonon Density of States P_1 (from $P4_2/mmc$)

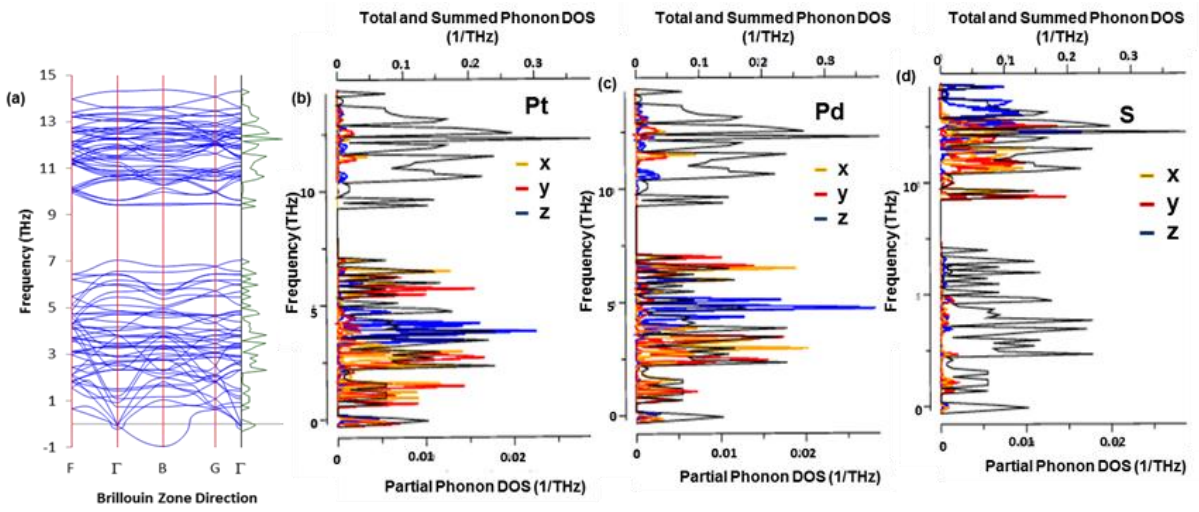

Figure 3.7.11. 1. (a) Phonon dispersion for $Pt_{25}Pd_{25}S_{50}$ P_1 (from $P4_2/mmc$) at (10 GPa), Phonon density of states (b) Pt contribution, (c) Pd contribution and (d) S contribution

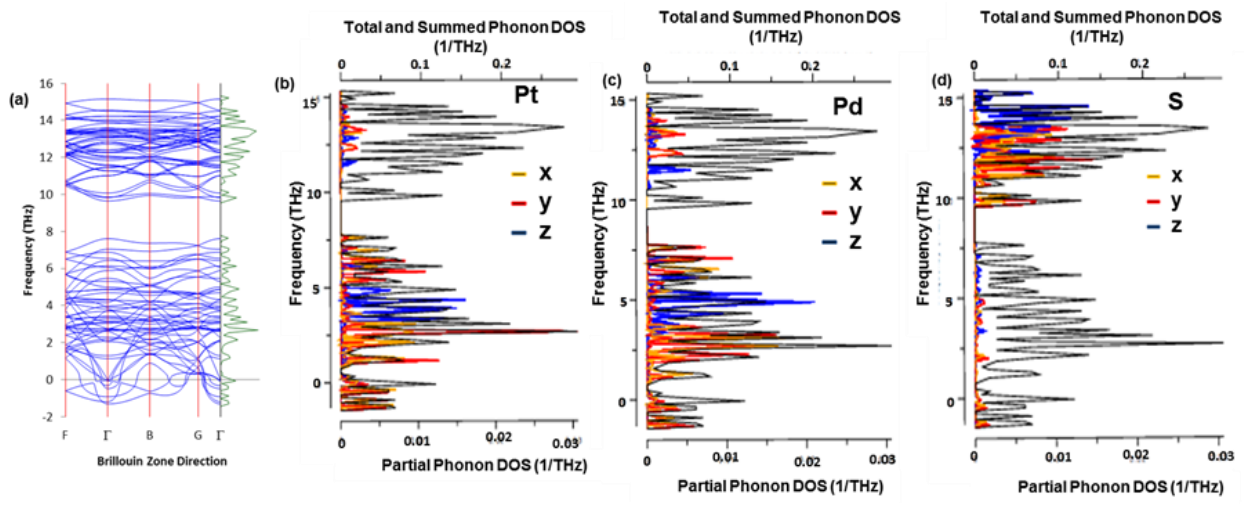

Figure 3.7.11. 2. (a) Phonon dispersion for $Pt_{25}Pd_{25}S_{50}$ P_1 (from $P4_2/mmc$) at (20 GPa), Phonon density of states (b) Pt contribution, (c) Pd contribution and (d) S contribution

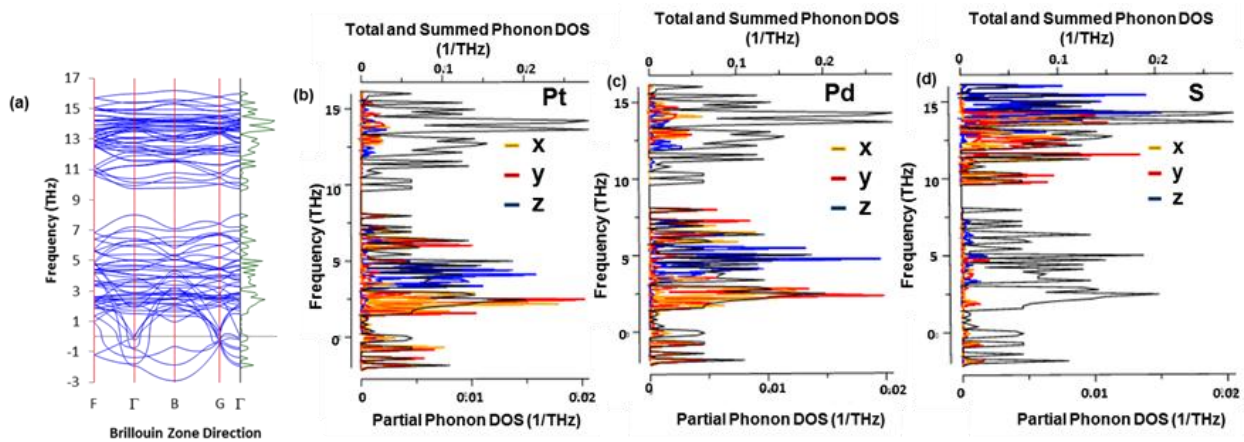

Figure 3.7.11. 3. (a) Phonon dispersion for $Pt_{25}Pd_{25}S_{50}$ P_1 (from $P4_2/mmc$) at (30 GPa), Phonon density of states (b) Pt contribution, (c) Pd contribution and (d) S contribution

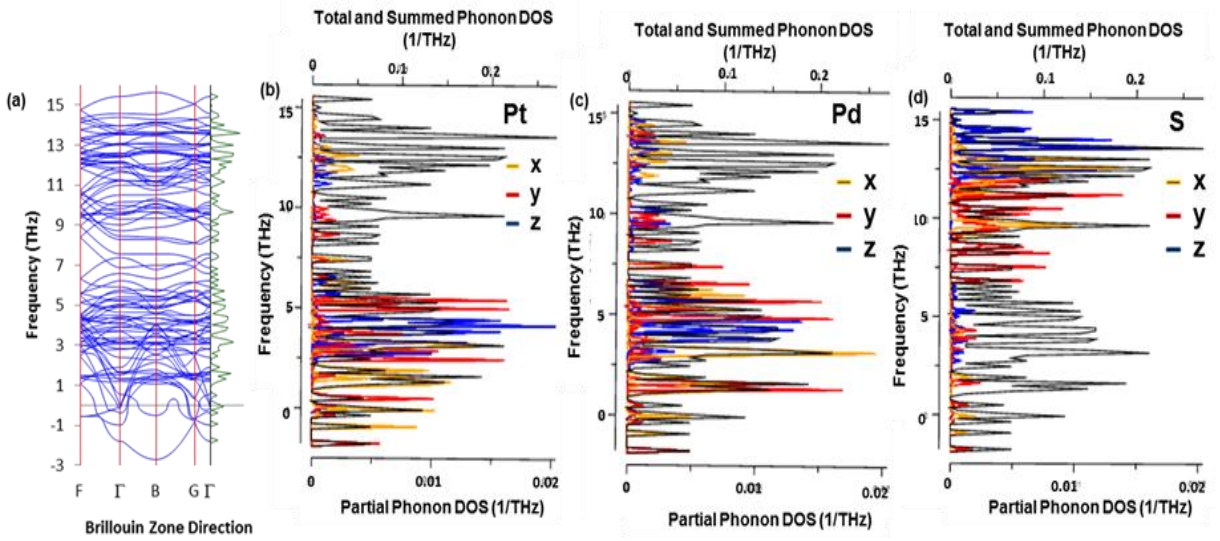

Figure 3.7.11. 4. (a) Phonon dispersion for $Pt_{25}Pd_{25}S_{50}$ P_1 (from $P4_2/mmc$) at (40 GPa), Phonon density of states (b) Pt contribution, (c) Pd contribution and (d) S contribution

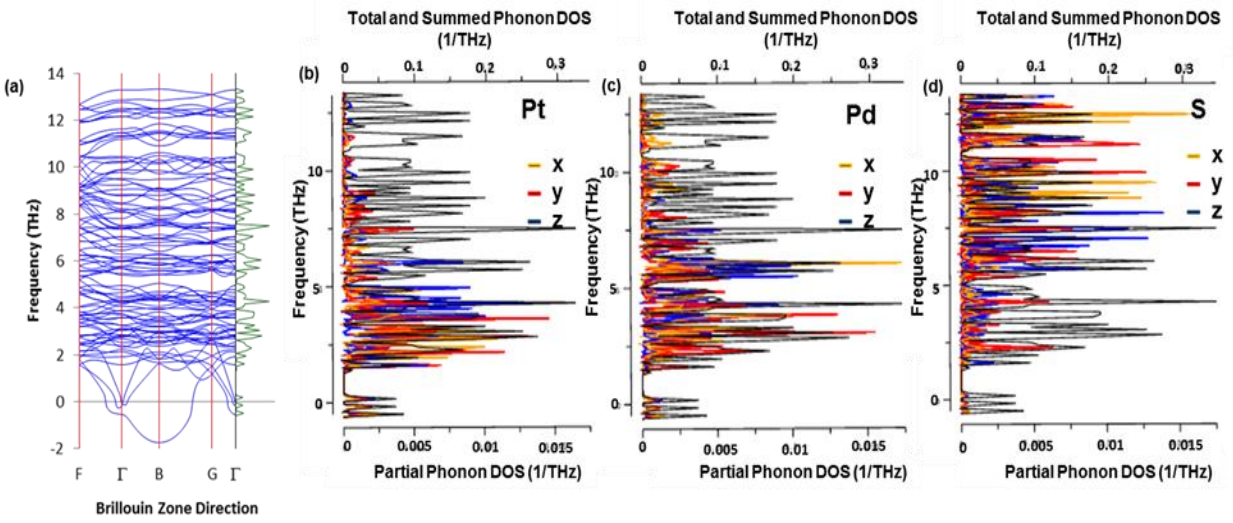

Figure 3.7.11. 5. (a) Phonon dispersion for $Pt_{25}Pd_{25}S_{50}$ P_1 (from $P4_2/mmc$) at (50 GPa), Phonon density of states (b) Pt contribution, (c) Pd contribution and (d) S contribution

The $Pt_{25}Pd_{25}S_{50}$, space group P_1 structure at 0 GPa (figure 3.4.12), gives phonon spectra with soft modes in the B direction. Figure 3.7.11.1, shows a phonon spectra of 10 GPa with negative frequencies at point B of the Brillouin zone. The PDOS shows that Pt and Pd atoms are responsible for the soft modes. The upper band of optical branches starts at about 10 THz and ends at 14 THz and the lower band of acoustic and optical branches starts at about -0.5 THz and end at 7.0 THz. The x and z vibrations of Pt and Pd are prevalent at 3.0 - 5 THz and for S atoms it was dominant at 13 – 15 THz. S atoms contribution towards the imaginary soft modes is negligible. Figure 3.7.11.2, shows phonon dispersion for 20 GPa with soft modes along Γ and B directions of the Brillouin zone. From the PDOS, it is observed that Pt, Pd and S atoms are responsible for the soft modes. The lower band of acoustic and optical branches emanates from Pt and Pd atoms and the upper band of optical branches are associated mainly with vibrations of S atoms. Figure 3.7.11.3, shows phonon spectra of 30 GPa with soft modes at F - Γ - B directions. From the PDOS, it was noted that Pt, Pd and S atoms are responsible for the soft modes, since they vibrate at lower frequencies. The z component is dominant at 3 – 5 THz in both Pt and Pd atoms and in S atoms it is dominant at 14 - 16 THz. The x - y components are dominant at 1.5 - 3 THz in Pt and 2 - 3 THz in Pd. Pt and Pd are responsible for the lower band of acoustic branches and S atoms are responsible for the upper band of optical branches. Figure 3.7.11.4, shows phonon spectra with negative frequencies at point Γ - B of the Brillioun zone. The PDOS shows that Pt, Pd and S atoms are responsible for the soft modes. The lower band of acoustic and optical branches emanates mainly from Pt and Pd S atoms and the upper band of optical branches are associated mainly with S atoms which have now merged with no gaps between them. Figure 3.7.11.5, shows phonon spectra of 50 GPa with negative frequencies at point B of the Brillouin zone. It is observed that the Pt, Pd and S atoms are responsible for the soft modes. As pressure increases, the lower and upper bands of acoustic and optical branches mix.

3.7.12. Phonon Dispersions –$Pt_{12.5}Pd_{37.5}S_{50}$– Phonon Density of States P_1 (from $P4_2/mmc$)

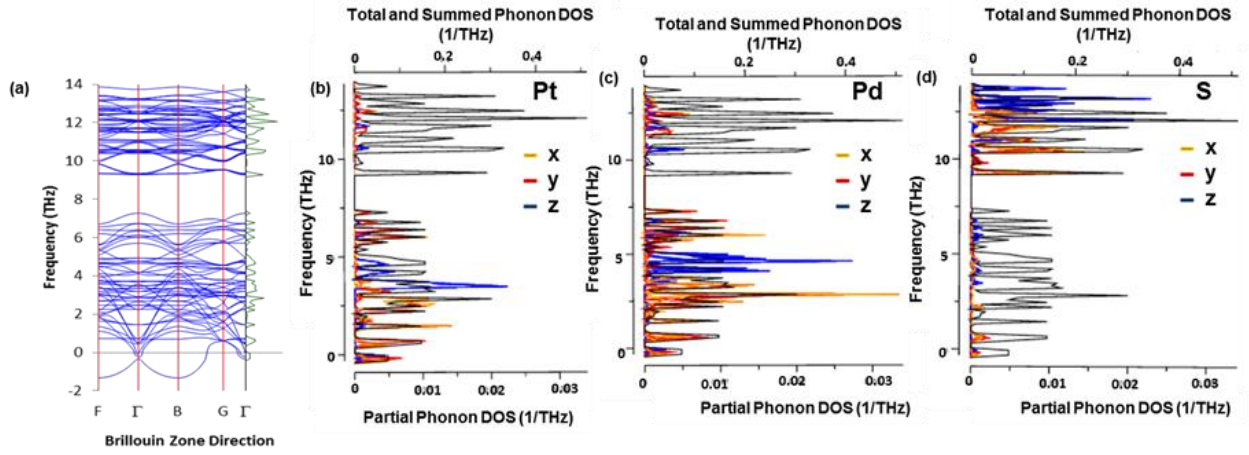

Figure 3.7.12. 1. (a) Phonon dispersion for $Pt_{12.5}Pd_{37.5}S_{50}$ P_1 (from $P4_2/mmc$) at (10 GPa), Phonon density of states (b) Pt contribution, (c) Pd contribution and (d) S contribution

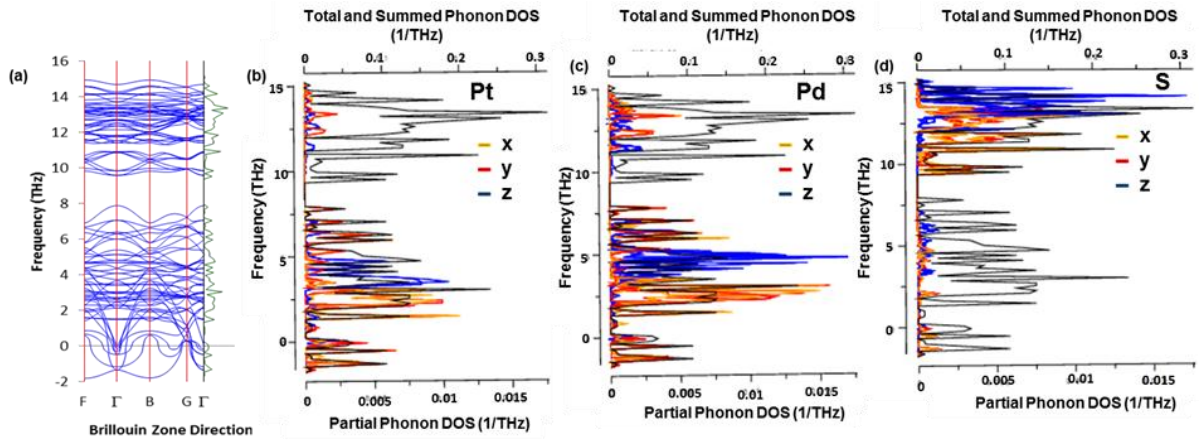

Figure 3.7.12. 2. (a) Phonon dispersion for $Pt_{12.5}Pd_{37.5}S_{50}$ P_1 (from $P4_2/mmc$) at (20 GPa), Phonon density of states (b) Pt contribution, (c) Pd contribution and (d) S contribution

The $Pt_{12.5}Pd_{37.5}S_{50}$ with space group P_1 at 0 GPa (figure 3.4.13), depicts no negative frequencies, all branches are positive. Figure 3.7.12.1, shows phonon spectra for 10 GPa, where negative frequencies are observed at Γ- B of the Brillioun zone. It was not-

ed that Pt, Pd and S atoms are responsible for the soft modes. The lower band of acoustic and optical branches starts at about -1.5 THz and ends at 7.5 THz, the upper band of optical branches starts at 9 THz and ends at 14 THz. Looking at the PDOS, x - z vibrations are dominant at -2 - 0 THz in both Pt and Pd atoms and the z vibration in S is dominant at 12 - 14 THz. Figure 3.7.12.2 gives the phonon spectra of 20 GPa, with soft modes along Γ- B direction, with x - y vibrations of Pt and Pd being dominant. It was observed that Pt, Pd and S atoms are responsible for the soft modes. Pt and Pd atoms vibrate preferentially at lower frequencies. The x - y vibrations of Pt and Pd are dominant at -2 - 0 THz and the z vibration of Pd is dominant at 3.5 THz to 5 THz and in S it is dominant at 12 THz to 14 THz. The lower band of acoustic and optical branches emanate from Pt, Pd and S atoms and the upper band of optical branches are associated with Pt, Pd and S atoms. The 30, 40 and 50 GPa could not run due to the structure changing its symmetry and did not converge.

3.7.13. Phonon Dispersions –$Pd_{50}S_{50}$– Phonon Density of States P_1 (from $P4_2/mmc$)

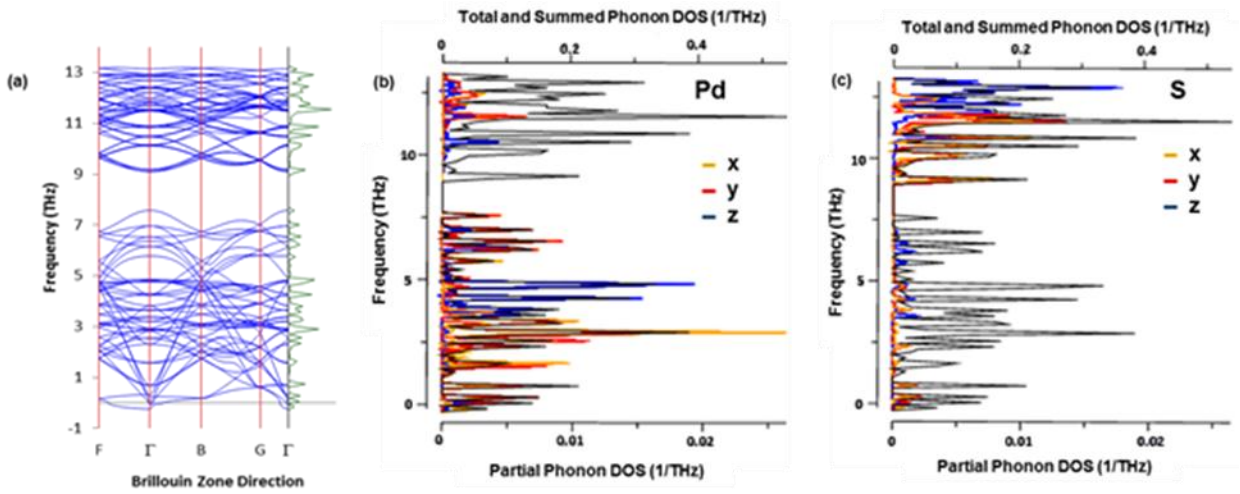

Figure 3.7.13. 1. (a) Phonon dispersion for $Pd_{50}S_{50}$ P_1 (from $P4_2/mmc$) at (10 GPa), Phonon density of states (b) Pd contribution and (c) S contribution

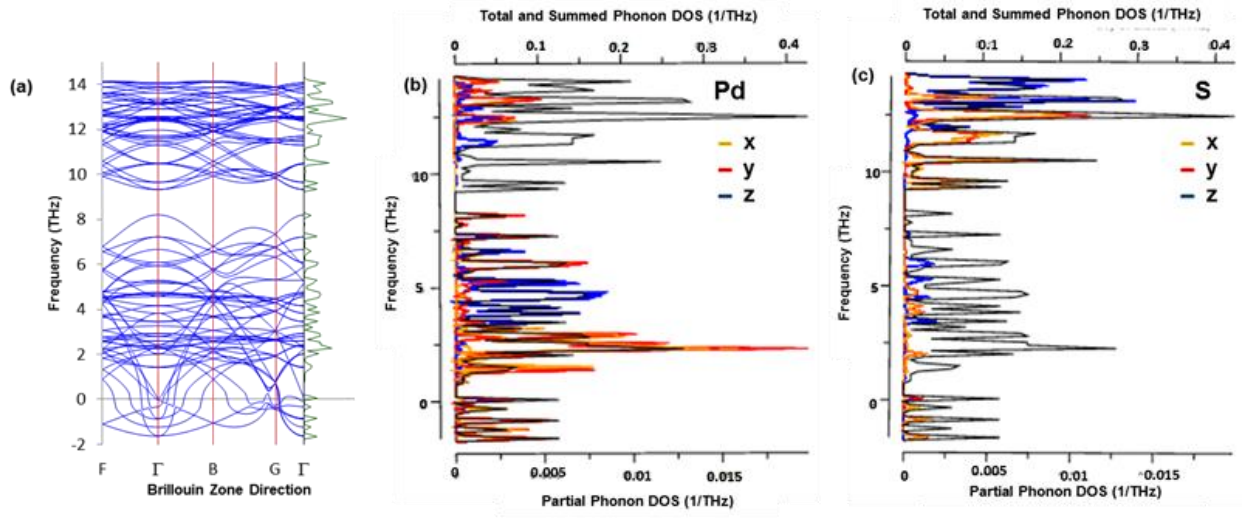

Figure 3.7.13. 2. (a) Phonon dispersion for $Pd_{50}S_{50}$ P_1 (from $P4_2/mmc$) at (20 GPa), Phonon density of states (b) Pd contribution and (c) S contribution

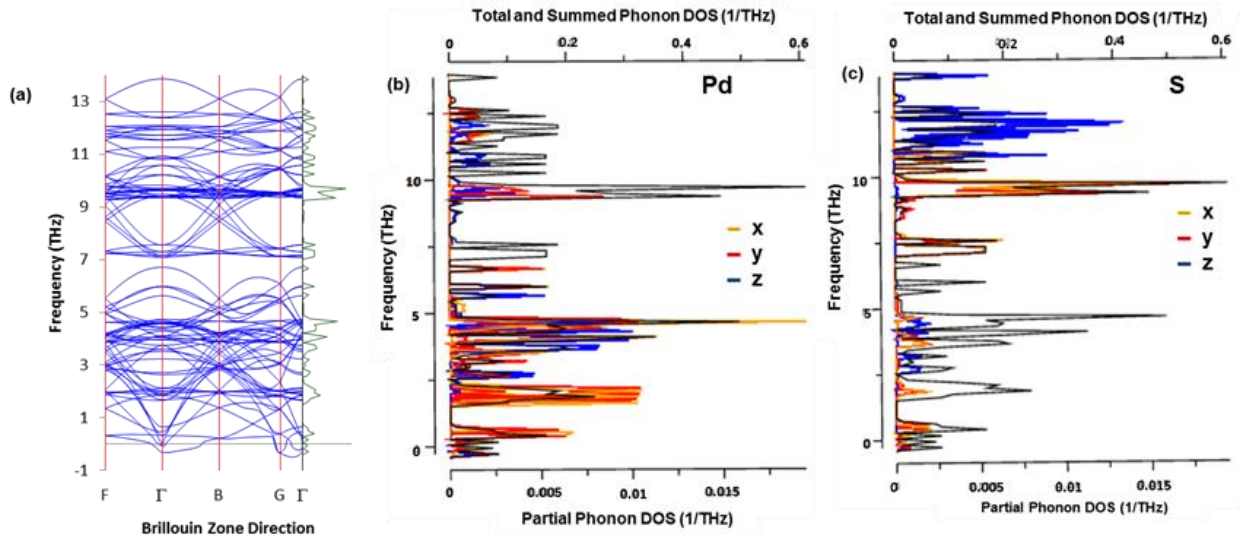

Figure 3.7.13. 3. (a) Phonon dispersion for $Pd_{50}S_{50}$ P_1 (from $P4_2/mmc$) at (30 GPa), Phonon density of states (b) Pd contribution and (c) S contribution

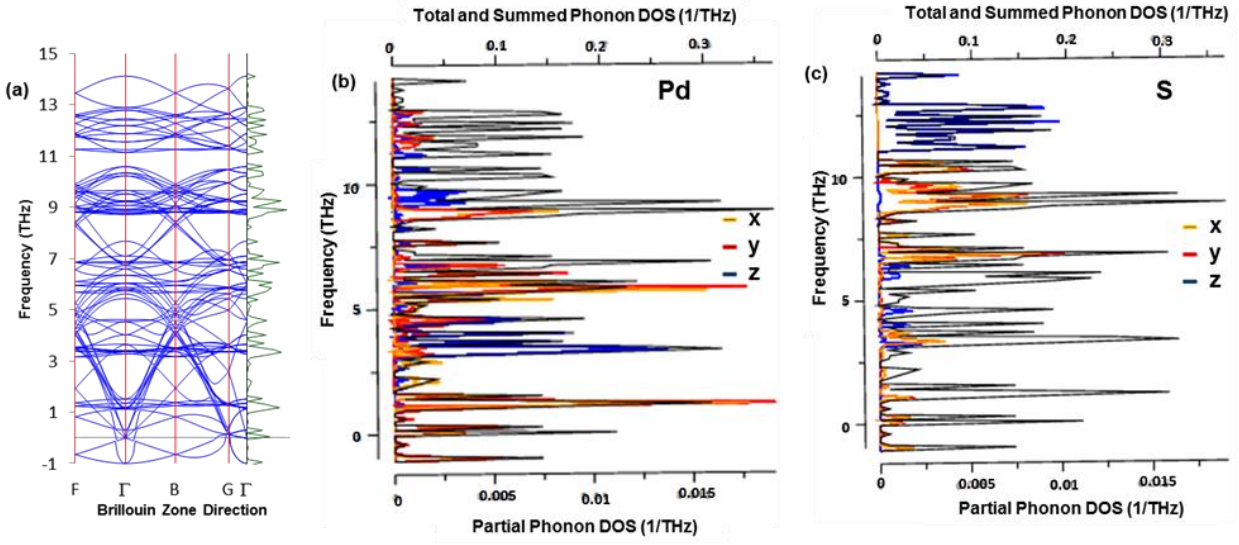

Figure 3.7.13. 4. (a) Phonon dispersion for $Pd_{50}S_{50}$ P_1 (from $P4_2/mmc$) at (40 GPa), Phonon density of states (b) Pd contribution and (c) S contribution

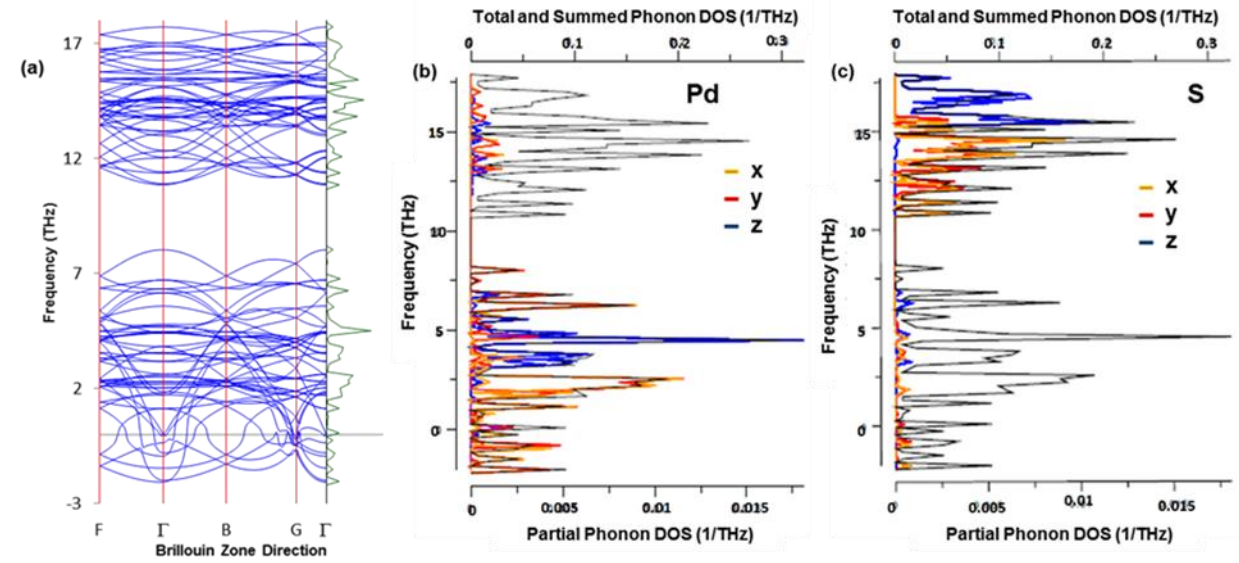

Figure 3.7.13. 5. (a) Phonon dispersion for $Pd_{50}S_{50}$ P_1 (from $P4_2/mmc$) at (50 GPa), Phonon density of states (b) Pd contribution and (c) S contribution

The $Pd_{50}S_{50}$ with space group P_1 at 0 GPa (figure 3.4.14), shows no soft modes as all branches have positive frequencies. Figure 3.7.13.1, shows the calculated phonon DOS and dispersion curves at 10 GPa. There are soft modes along Γ direction. The PDOS indicate that Pd and S atoms are responsible for the soft modes. The lower band of acoustic and optical branches emanates from Pd and S atoms and the upper band of optical bands are associated with Pd and S atoms. The lower band of acoustic and optical branches starts at about -0.5 THz and ends at 7.2 THz, the upper band of optical branches starts at about 9.5 THz and ends at 13 THz. Figure 3.7.13.2, shows phonon spectra of 20 GPa with soft modes along F - Γ - B - G direction, with x - y component being dominant. Pd and S atoms are responsible for the soft modes, since they vibrate at lower frequencies. The x - y vibrations of Pd and S are dominant at -2 - 3THz and z vibration of Pd is dominant at 3 THz to 5 THz. S it is dominant at around 12 THz to 14 THz. The lower band of acoustic and optical branches emanates from Pd and S atoms and the upper bands of optical branches emanate from the Pd and S atoms. Figure 3.7.13.3 gives the phonon spectra of 30 GPa with soft modes along Γ- B - G direction. The soft modes are due to Pt and S atoms vibrating at frequencies, below 0 THz. The lower band of acoustic and optical branches starts at about -0.5 THz and ends at 5.5 THz, the upper band of optical branches starts at about 7.2 THz and ends at 13 THz. The z component in S is dominant at around 11.7 THz to 13 THz. Figure 3.7.13.4, shows phonon spectra of 40 GPa with soft modes along Γ- B - G direction. From the PDOS, it was observed that Pd and S atoms are responsible for the soft modes. The lower band of acoustic and optical branches emanates from Pd and S atoms and the upper band of optical branches are associated with Pd and S atoms. Figure 3.7.13.5 gives the phonon spectra of 50 GPa with soft modes at Γ- B - G of the Brillouin zone. From the PDOS, it is evident that Pd and S atoms are responsible for the soft modes. The x - y vibrations of Pd and S atoms is dominant at -2 - 1.8 THz and z vibration of Pd is dominant at 3 THz to 5 THz. Contribution of the S atoms is less towards the soft modes. It was observed that as pressure increases the soft modes extends to -1 THz. The two bands, which were separated by a gap at lower pressures, have now merged. It is noted that tle lower and upper frequencies bands separate as the pressure is

increased from 40 to 50 GPa. This could approximately be ascribed to change in the structure.

3.8. Pressure dependence on density of states of $Pd_{50-x}Pt_xS_{50}$ and $Pt_{50-x}Pd_xS_{50}$

3.8.1. Density of States –$Pd_{50}S_{50}$ – ($P4_2/m$)

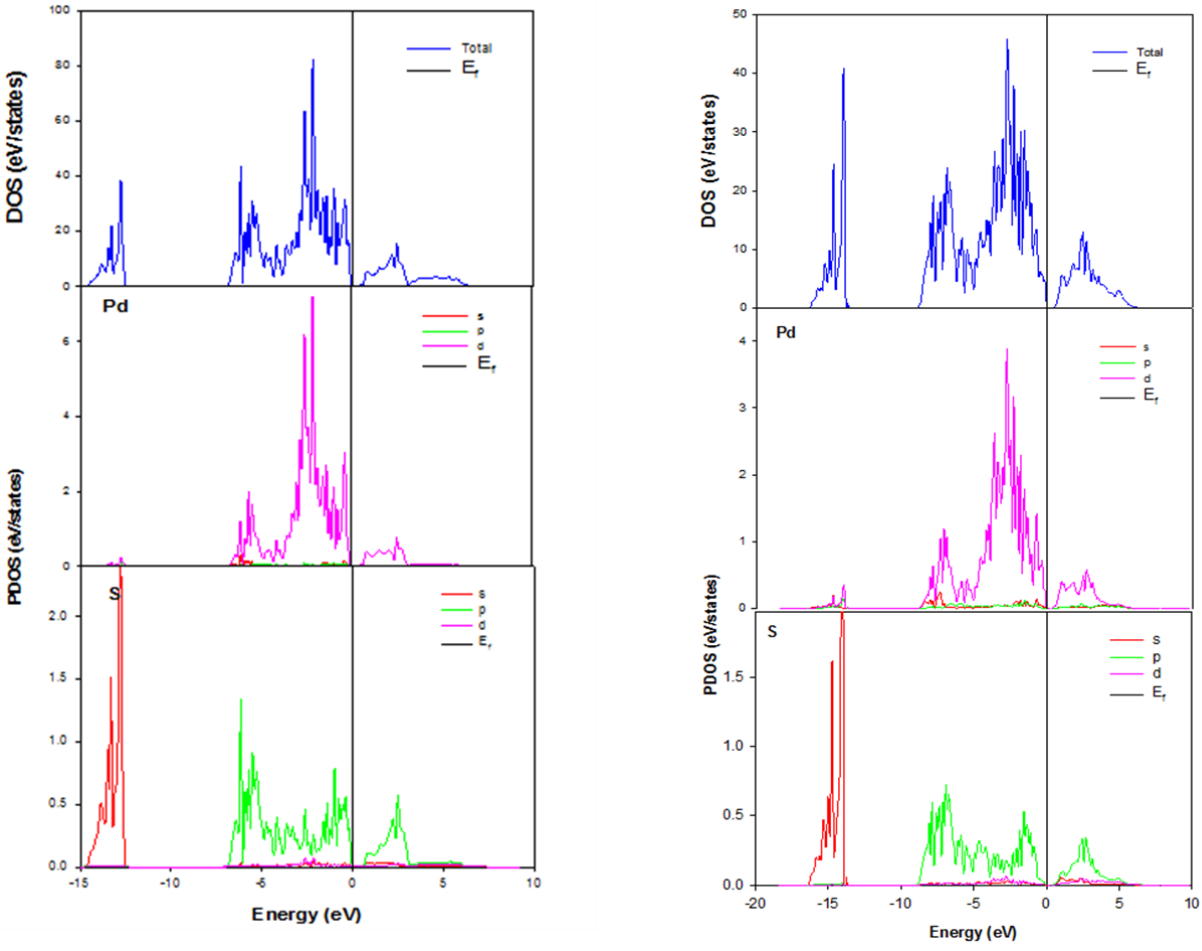

(a) (b)

Figure 3.8.1. 1. Total and partial density of states of $Pd_{50}S_{50}$ ($P4_2/m$) (a) 10 GPa and (b) 20 GPa

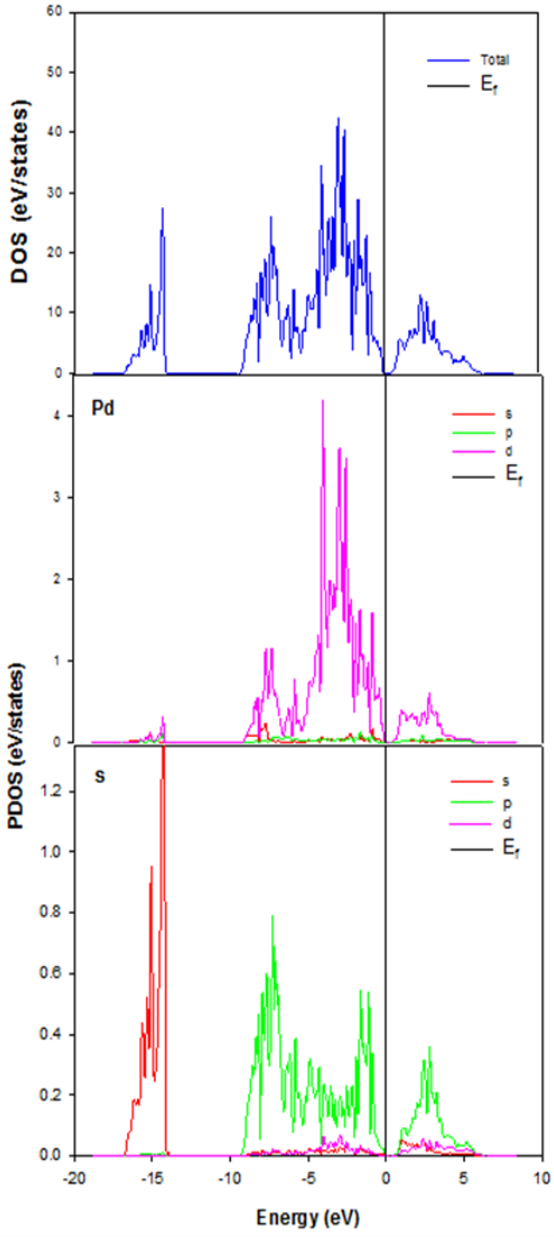

(c)

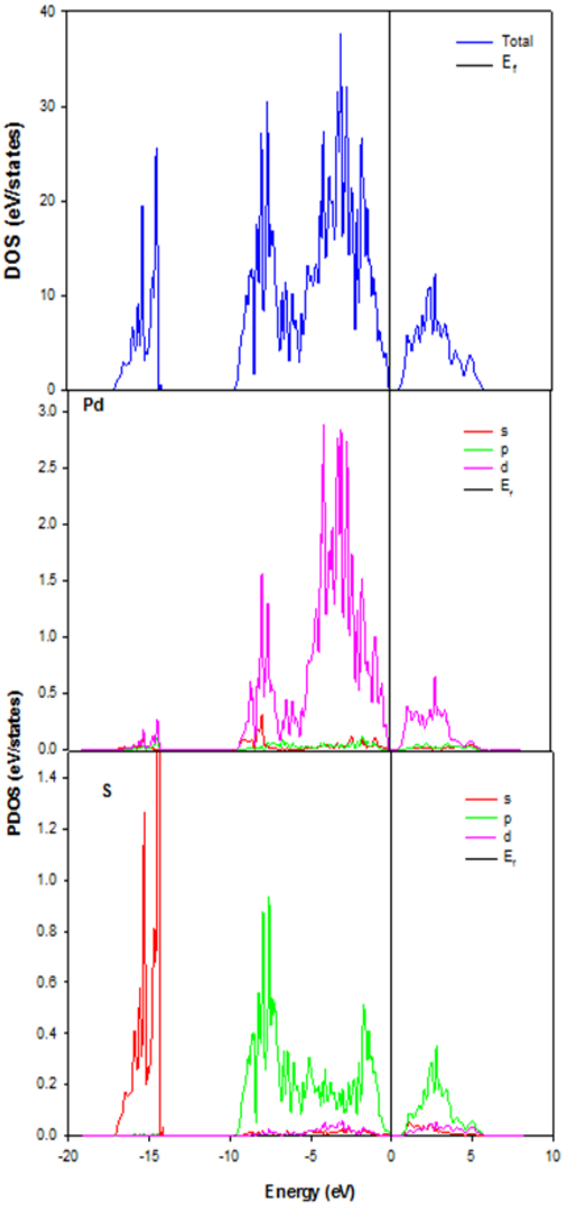

(d)

Figure 3.8.1. 2. Total and partial density of states of $Pd_{50}S_{50}$ ($P4_2/m$), (c) 30 GPa and (d) 40 GPa

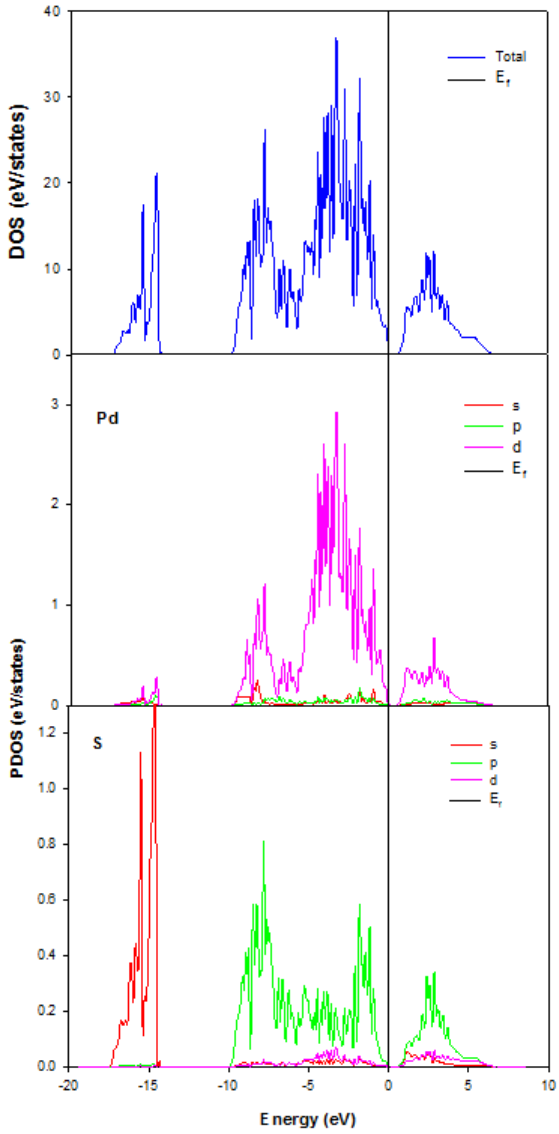

Figure 3.8.1. 3. Total and partial density of states of $Pd_{50}S_{50}$ ($P4_2/m$) at 50 GPa

Total and partial density of states for $Pd_{50-x}Pt_xS_{50}$ will be presented at different pressures ranging from 10 - 50 GPa to check how pressure affect the stability of the structures. Figure 3.8.1.1 (a), gives the total density of states (DOS) and partial density of states (PDOS) of $Pd_{50}S_{50}$ at 10 GPa. The peak, in the total DOS, ranging from -14 eV to 12.5 eV emanates mainly from the 3s states of Sulphur. The peak stretching from -6.5 eV to the top of the valence band (VB) originates from the 3p states of S and the domi-

nant 4d states of Pd. The hybridisation of 3p S and 4d Pd states leads to the Pd-S covalent bond. The calculations have shown that PdS has an indirect band gap of 1.0 eV. The conduction band consists of the anti-bonding d states of Pd and p states of S. The distribution of peaks in the total DOS of $Pd_{50}S_{50}$ at 20, 30, 40 and 50 GPa are reflected in figures (a) 3.8.1.1, (b), 3.8.1.2 (a), 3.8.1.4 (b) and 3.8.1.5 respectively and all emanates from the same states as those of 3.7.1.1. However, the band gaps at different pressures are depicted as 0.5, 0.6, 0.8 and 0.9 eV for 20, 30, 40 and 50 GPa respectively. It was observed that as pressure increases the band gap also increases.

3.8.2. Density of States –$Pd_{37.5}Pt_{12.5}S_{50}$ – ($P4_2/m$)

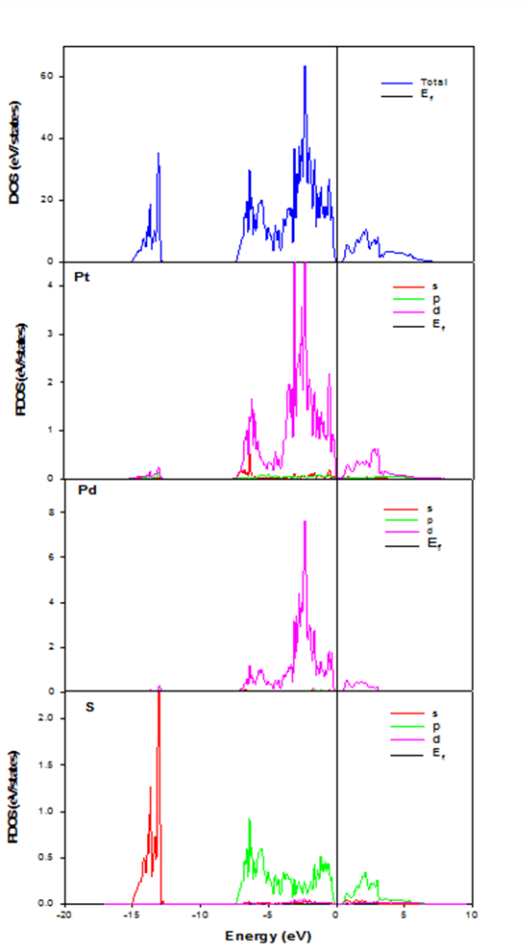

(a)

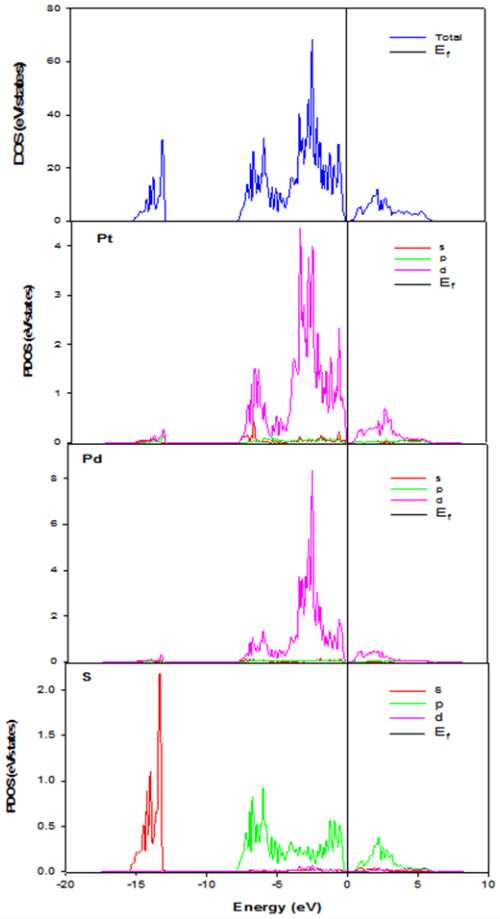

(b)

Figure 3.8.2. 1. Total and partial density of states of $Pd_{37.5}Pt_{12.5}S_{50}$ ($P4_2/m$) (a) 10 GPa and (b) 20 GPa

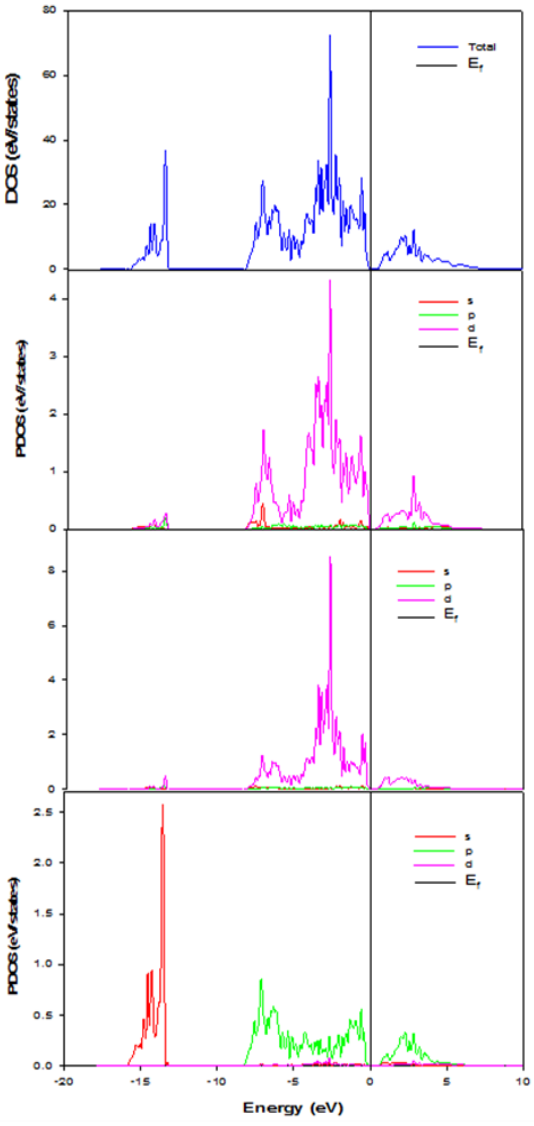

(c)

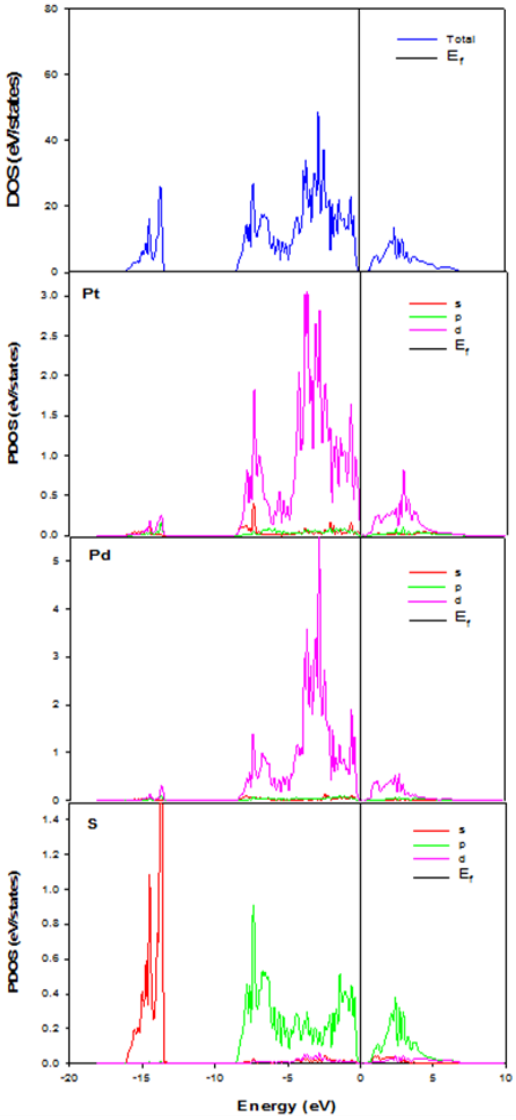

(d)

Figure 3.8.2. 2. Total and partial density of states of $Pd_{37.5}Pt_{12.5}S_{50}$ ($P4_2/m$) (c) 30 GPa and (d) 40 GPa

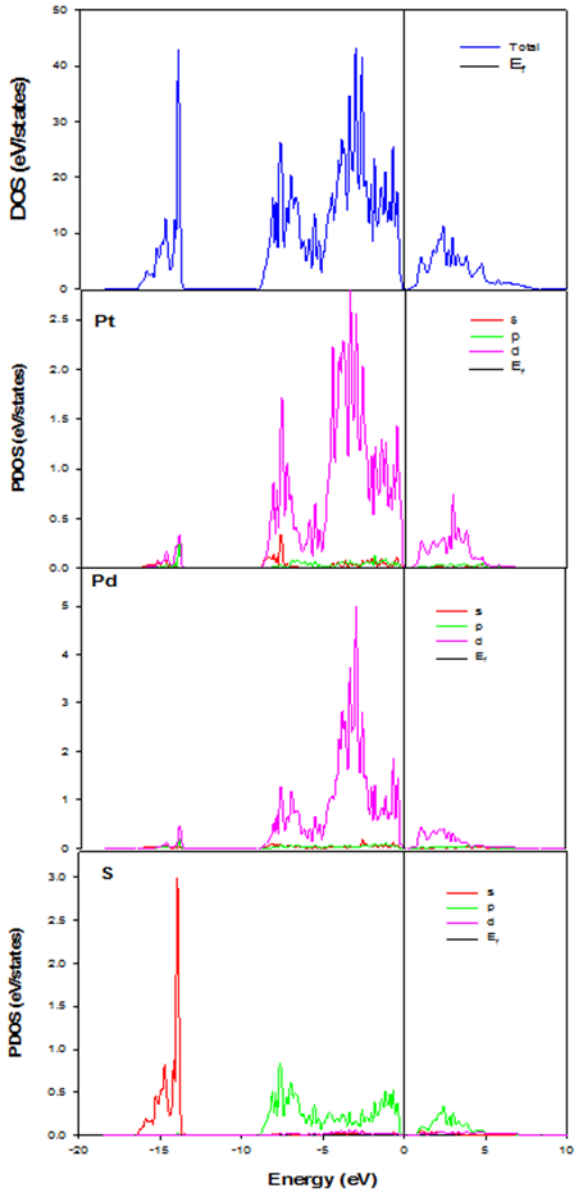

Figure 3.8.2. 3. Total and partial density of states of $Pd_{37.5}Pt_{12.5}S_{50}$ ($P4_2/m$) at (50 GPa)

Figure 3.8.2.1(a) shows total DOS and PDOS of $Pd_{37.5}Pt_{12.5}S_{50}$ $P4_2/m$ at 10 GPa. A psuedogab observed was estimated as 0.2 eV. The peak, in the total DOS, ranging from -15 eV to -12 eV emanates mainly from the 3s states of S. The peak stretching from -6.5 eV to the valence band originates from the 3p states of S, the dominant 3d states of Pt and 4d states of Pd. A hybridisation of 3p S, Pt and 4d of Pd states were observed. The conduction band consists of the anti-bonding d states of Pt and Pd and p states of

S. The distribution of peaks in the total DOS of $Pd_{37.5}Pt_{12.5}S_{50}$ at 20, 30, 40 and 50 GPa are reflected in figures 3.8.2.2(b), 3.8.2.3 (a), 3.8.2.4 (b), and 3.8.2.5 respectively and all emanates from the same states as those of 3.8.4. However, the psuedogaps at different pressures are depicted as follows, 0.3, 0.5, 0.5 and 0.5 eV for 20, 30, 40 and 50 GPa respectively. As pressure increases the band gap stays the same.

3.8.3. Density of States –$Pt_{25}Pd_{25}S_{50}$ – ($P4_2/m$)

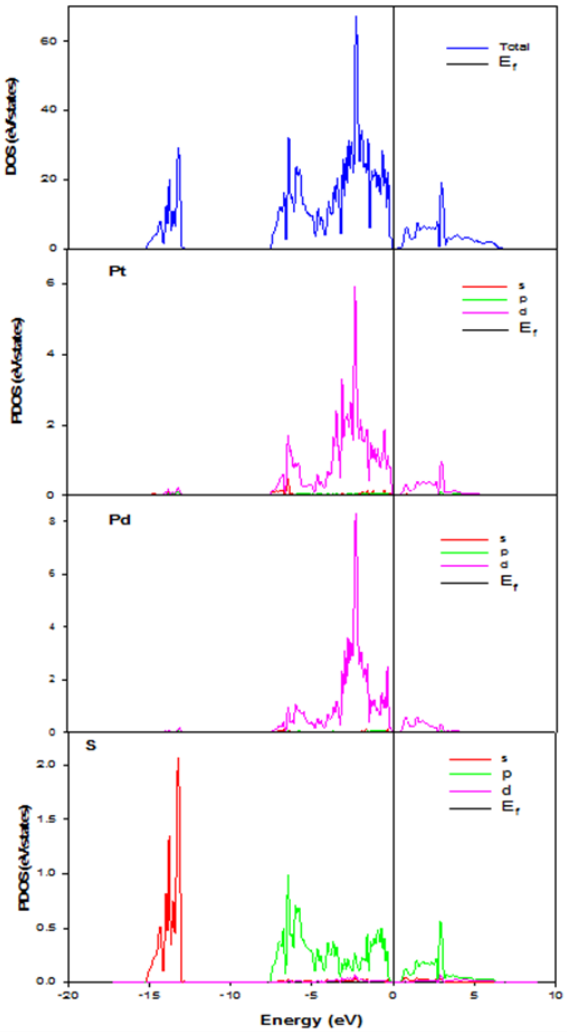

(a)

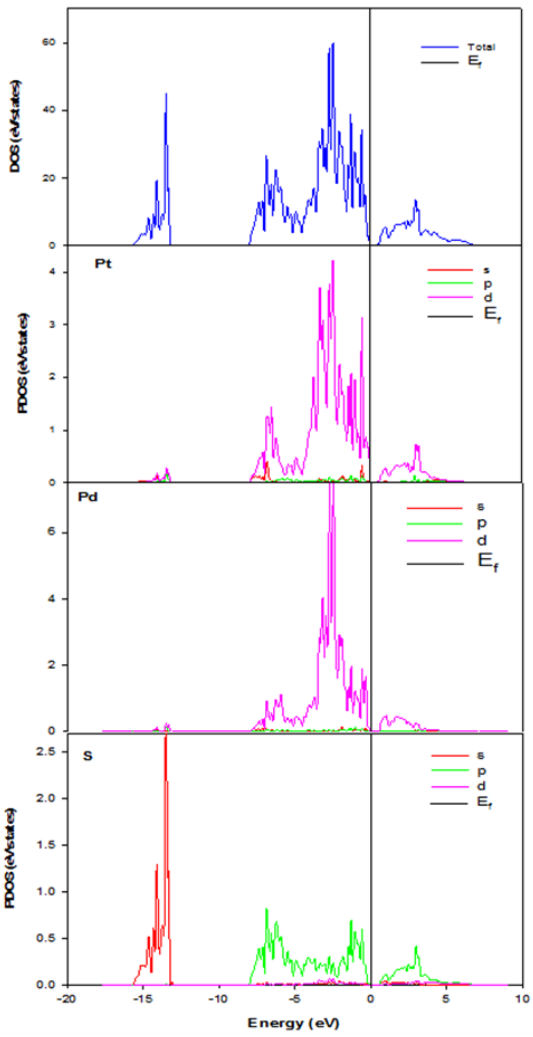

(b)

Figure 3.8.3. 1. Total and partial density of states of $Pd_{25}Pt_{25}S_{50}$ ($P4_2/m$), (a) 10 GPa and (b) 20 GPa

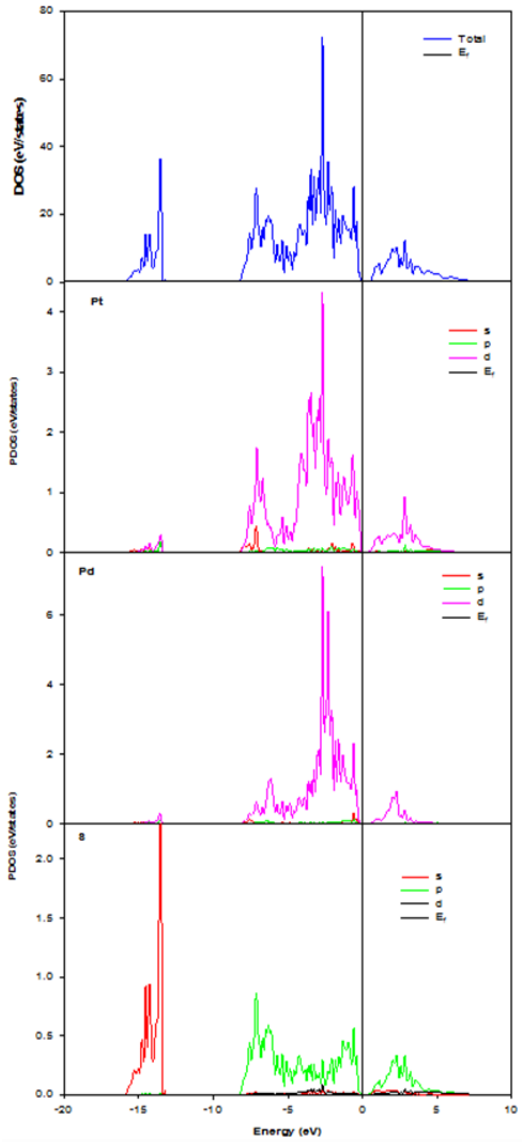

(c)

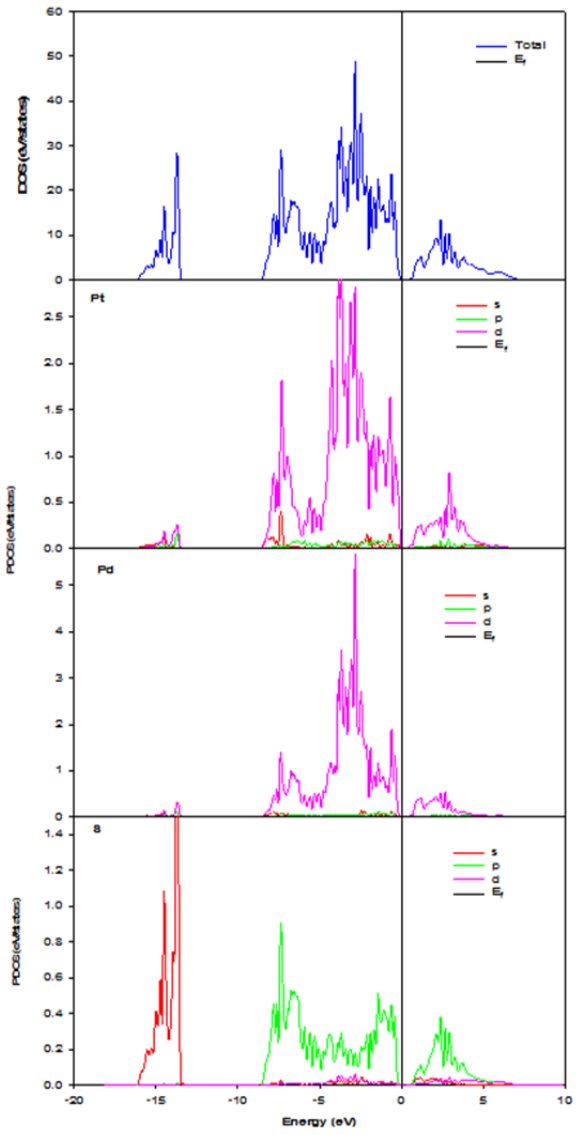

(d)

Figure 3.8.3. 2. Total and partial density of states of $Pd_{25}Pt_{25}S_{50}$ ($P4_2/m$), (c) 30 GPa and (d) 40 GPa.

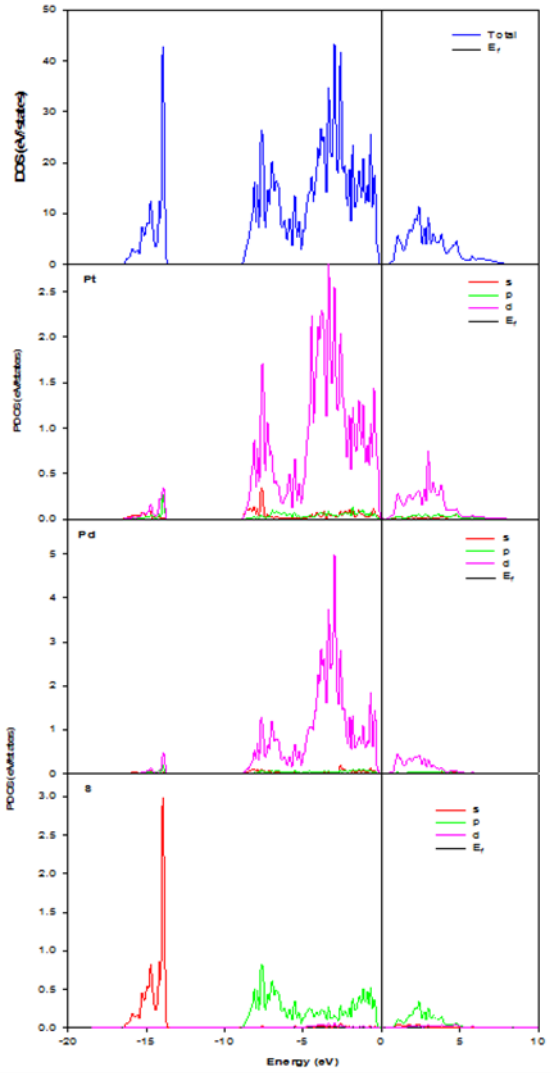

Figure 3.8.3. 3. Total and partial density of states of $Pd_{25}Pt_{25}S_{50}$ ($P4_2/m$) at 50 GPa

Figure 3.8.3.1(a), shows the total DOS and PDOS of $Pd_{25}Pt_{25}S_{50}$ $P4_2/m$ at 10 GPa. The d states of both Pt and Pd contribute more to the total DOS. The peak ranging from -15.6 eV to -12.5 eV emanated mainly from the 3s states of S. The peak stretching from -6.5 eV to the top of the VB originates from the 3p states of S and the dominant 3d of Pt and 4d of Pd. The hybridisation of 3p S, 3d Pt and 4d Pd states leads to Pd-Pt-S covalent bond. The calculations have shown that $Pd2_5Pt_{25}S5_0$ has a band gap of 0.4 eV. The conduction band consists of the anti-bonding d states of Pt and Pd and p states of S. The distribution of peaks in the total DOS at 20, 30, 40 and 50 GPa are reflected in fig-

ure 3.8.3.1(b), 3.8.3.2 (a), 3.8.3.2 (b) and 3.8.3.3 respectively. Moreover, the band gaps at different pressures are depicted as follows, 0.5, 0.8, 0.9 and 1.0 eV for 20, 30, 40 and 50 GPa respectively. However, it was noted that pressure increases the band gap.

3.8.4. Density of States – $Pd_{37.5}Pt_{12.5}S_{50}$ – ($P4_2/m$)

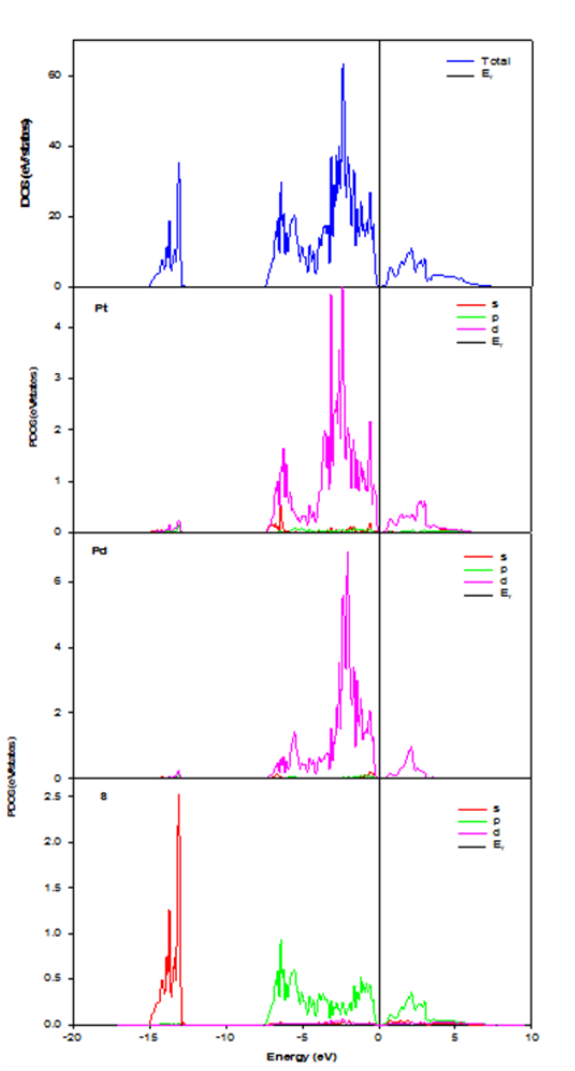

(a)

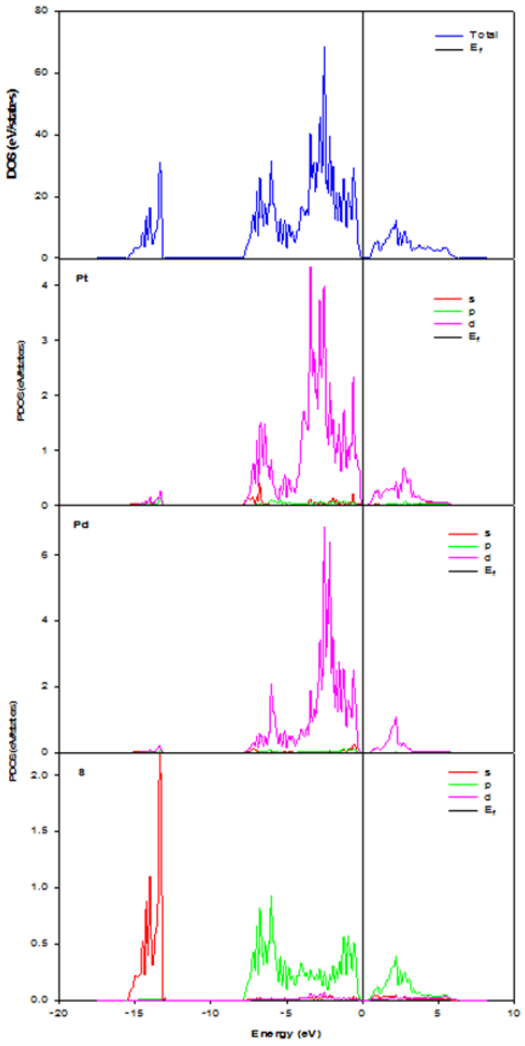

(b)

Figure 3.8.4. 1. Total and partial density of states of $Pd_{12.5}Pt_{37.5}S_{50}$ ($P4_2/m$), (a) 10 GPa and (b) 20 GPa

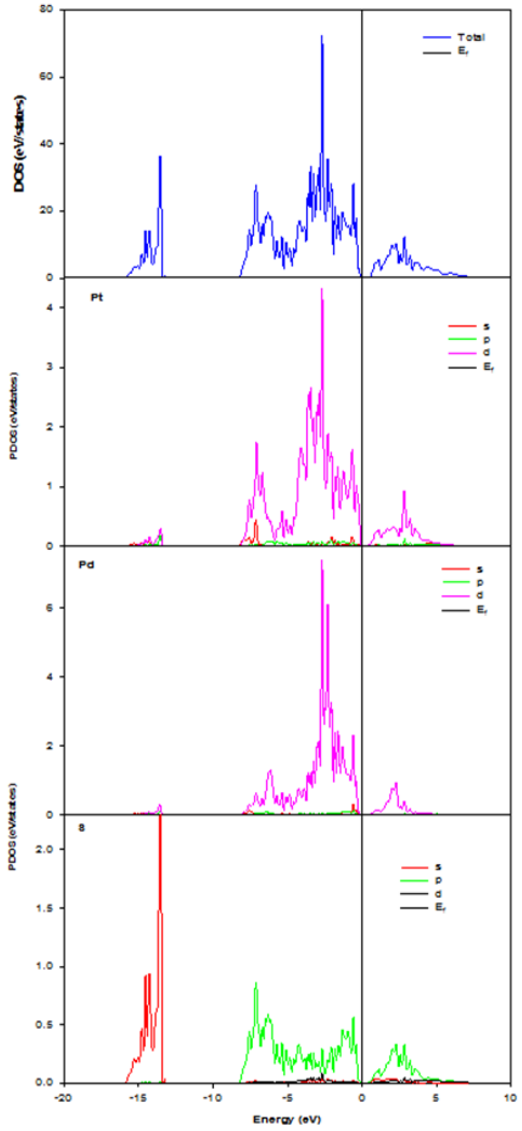

(c)

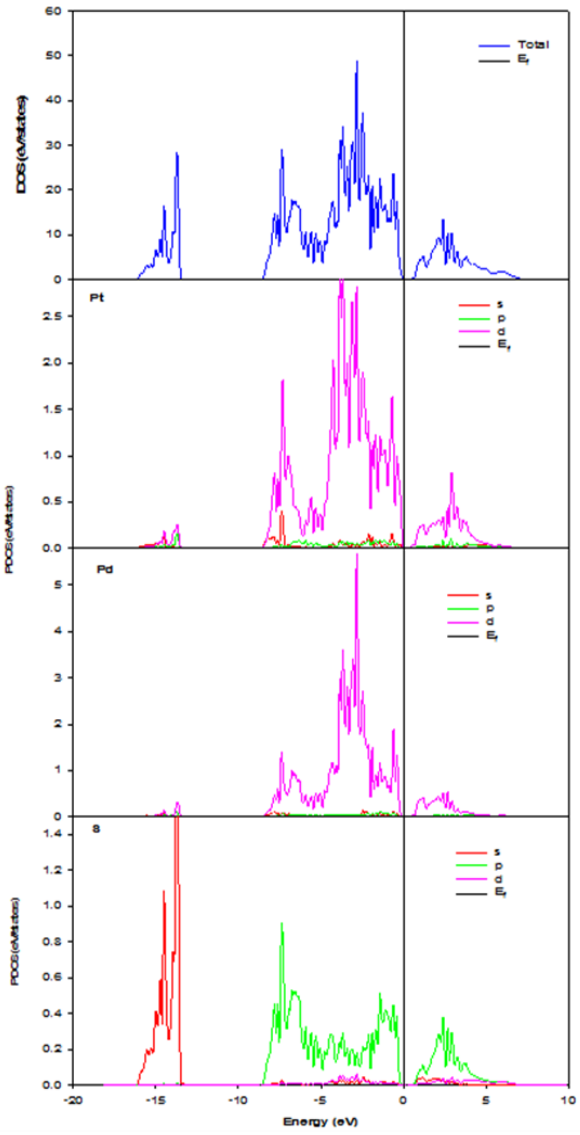

(d)

Figure 3.8.4. 2. Total and partial density of states of $Pd_{12.5}Pt_{37.5}S_{50}$ ($P4_2/m$), (c) 30 GPa and (d) 40 GPa

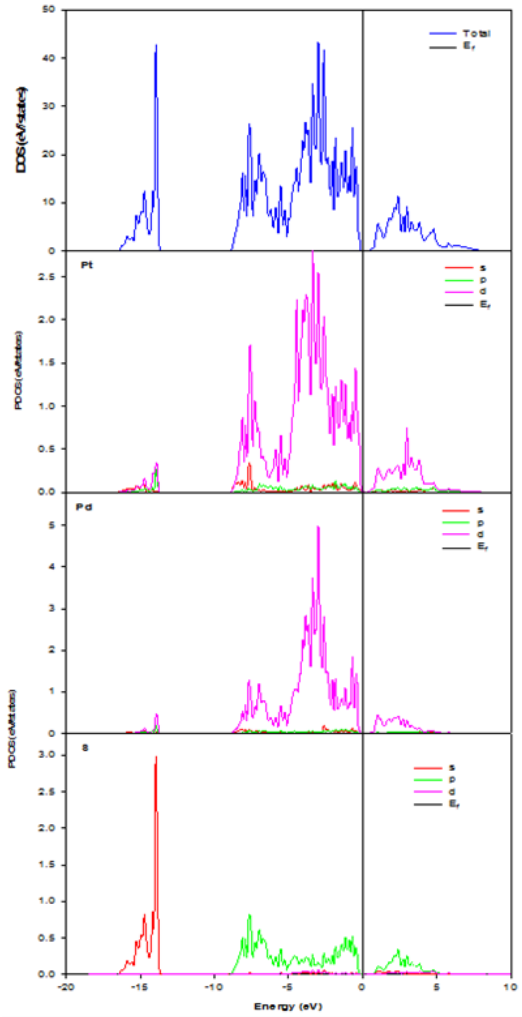

Figure 3.8.4. 3. Total and partial density of states of $Pd_{12.5}Pt_{37.5}S_{50}$ ($P4_2/m$) at 50 GPa

Figure 3.8.4.1(a) shows the total DOS and PDOS of $Pd_{37.5}Pt_{12.5}S_{50}$ $P4_2/m$ at 10 GPa. It was noted that the d states of Pt contributes more to the total DOS. The peak ranging from -15 eV to -14.5 eV emanates from the 3s states of S and the peak ranging from -7 eV to the VB is associated with the 3p states of S the dominant 3d states of Pt and 4d of Pd. The hybridization of 3p S 3d Pt and 4d of Pd was noted. The calculations have shown that $Pd_{37.5}Pt_{12.5}S_{50}$ has a band gap of 0.5 eV. The conduction band consists of the anti-bonding d states of Pt and Pd and p states of S. The distribution of peaks in the total DOS at 20, 30, 40 and 50 GPa are reflected in figures 3.8.4.1(b), 3.8.4.2(a), 3.8.4.2(b) and 3.8.4.3 respectively and all emanates from the same states as those of

3.8.4.1. However, the band gaps at different pressures are depicted as follows, 0.5, 0.6, 0.8 and 0.9 eV respectively. As pressure increases, the band gap also increases.

3.8.5. Density of States –$Pt_{50}S_{50}$ – ($P4_2/m$)

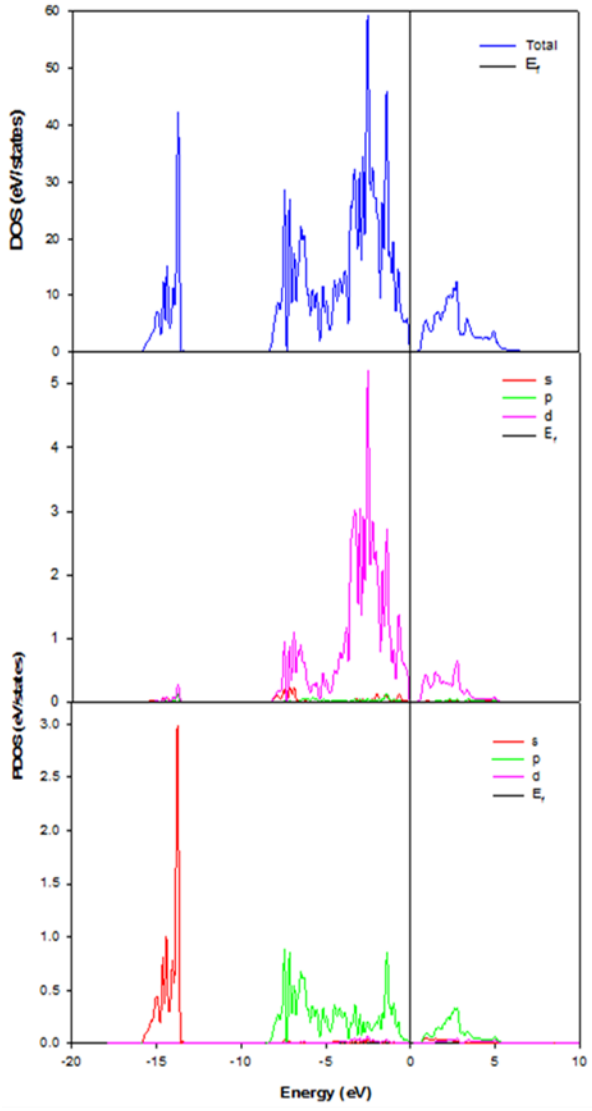

(a)

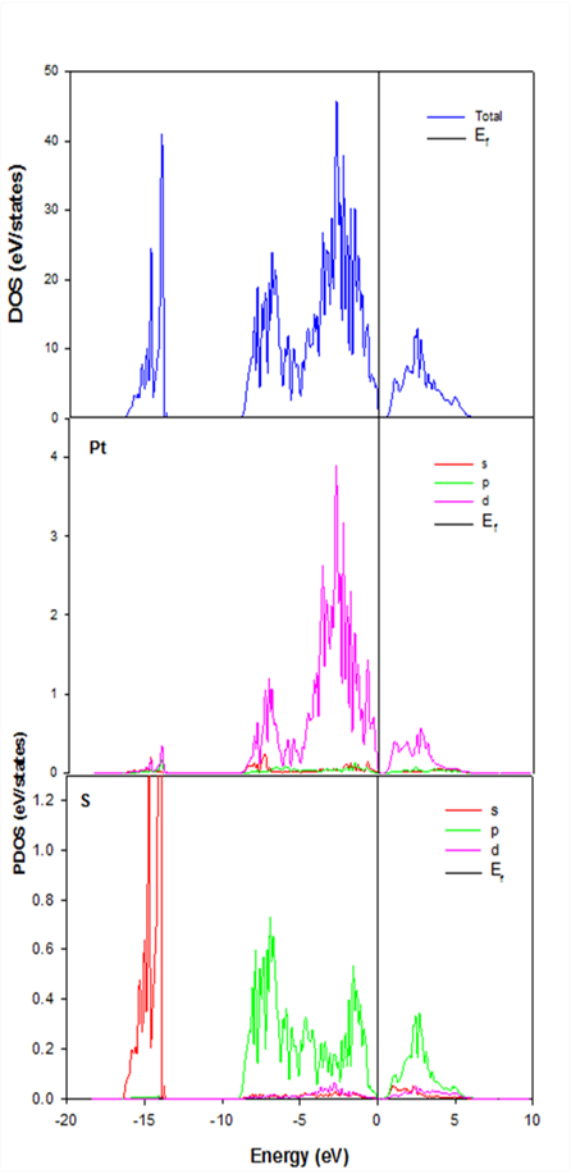

(b)

Figure 3.8.5. 1. Total and partial density of states of $Pt_{50}S_{50}$ ($P4_2/m$) (a) 10 GPa and (b) 20 GPa

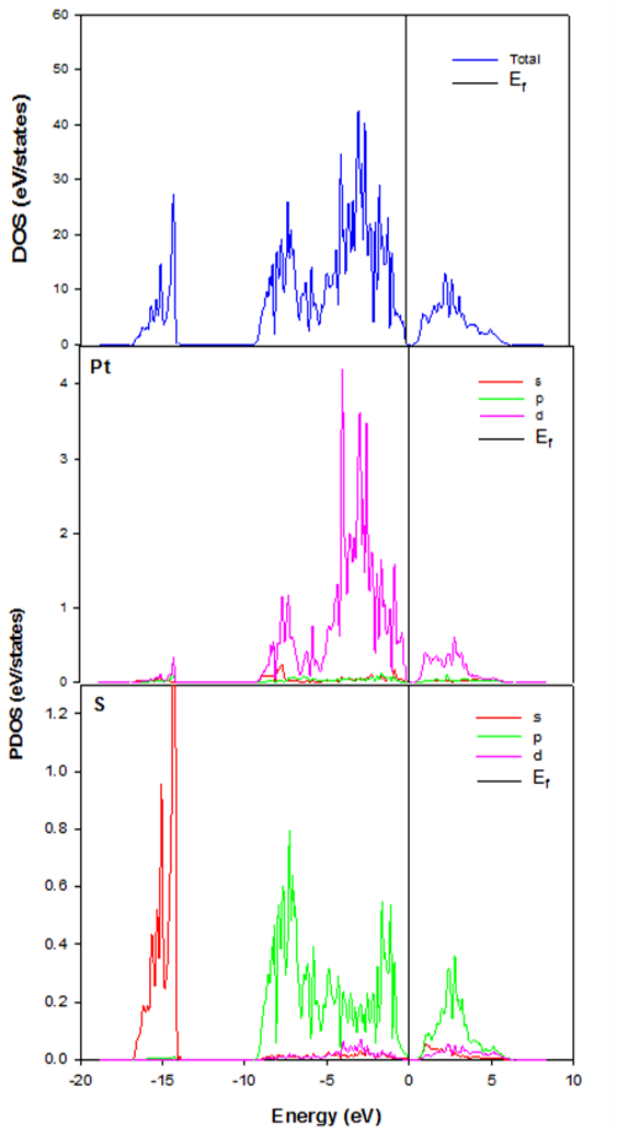

(c)

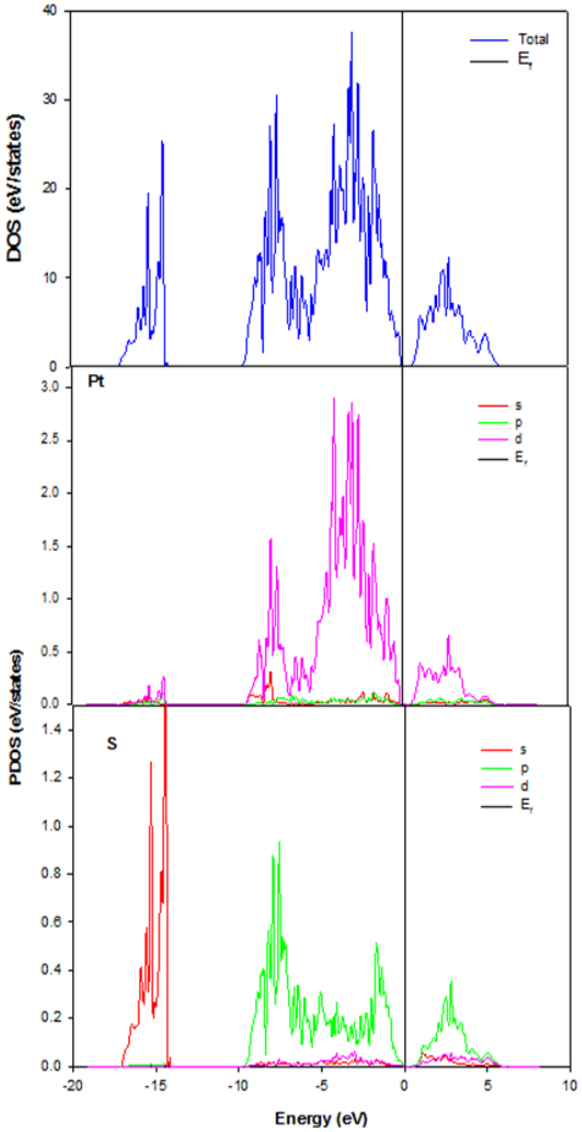

(d)

Figure 3.8.5. 2. Total and partial density of states of $Pt_{50}S_{50}$ ($P4_2/m$) (c) 30 GPa and (d) 40 GPa

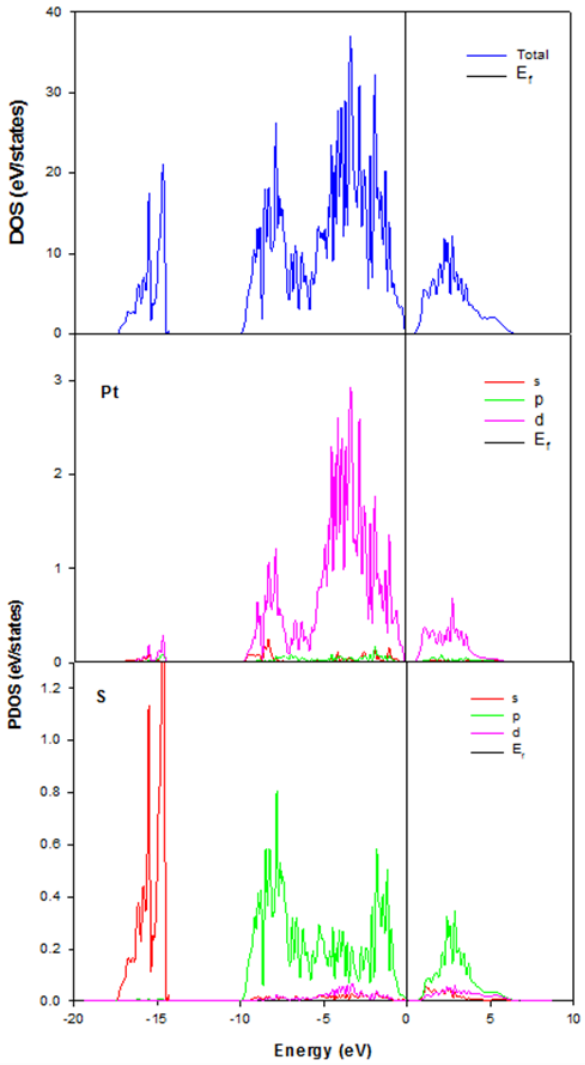

Figure 3.8.5. 3. Total and partial density of states of $Pt_{50}S_{50}$ ($P4_2/m$) at 50 GPa

Figure 3.8.5.1(a), gives the total DOS and PDOS of $Pt_{50}S_{50}$ $P4_2/m$ at 10 GPa, where a band gap was observed, which is estimated as 0.5 eV. The total DOS of $Pt_{50}S_{50}$ is the contribution of both Pt and S states. The s and p states contribution is almost the same. The peak ranging from -16 eV to -14.2 eV emanates mainly from the 3s of S. The peak stretching from -12.5 eV to the top of the VB originates from the 3p states of S and the dominant 3d states of Pt. The hybridisation of 3p S and 3d Pt states leads to the Pt-S covalent bond. The conduction band consists of the anti-bonding d states of Pt and p

states of S. The distribution of peaks in the total DOS of $Pt_{50}S_{50}$ at 20, 30, 40 and 50 GPa are reflected in figures 3.8.5.1(b), 3.8.5.3(a), 3.8.5.2(b) and 3.8.5.3 respectively and all from the same states as those in 3.8.5.1(a). Moreover, the band gabs at different pressures are depicted as follows, 0.6, 0.8, 0.9 and 1.0 eV for 20, 30, 40 and 50 GPa. It was observed that as pressure increases the band gap also increases

3.8.6. Density of States –$Pt_{50}S_{50}$ – P_1 (from $P4_2/mmc$)

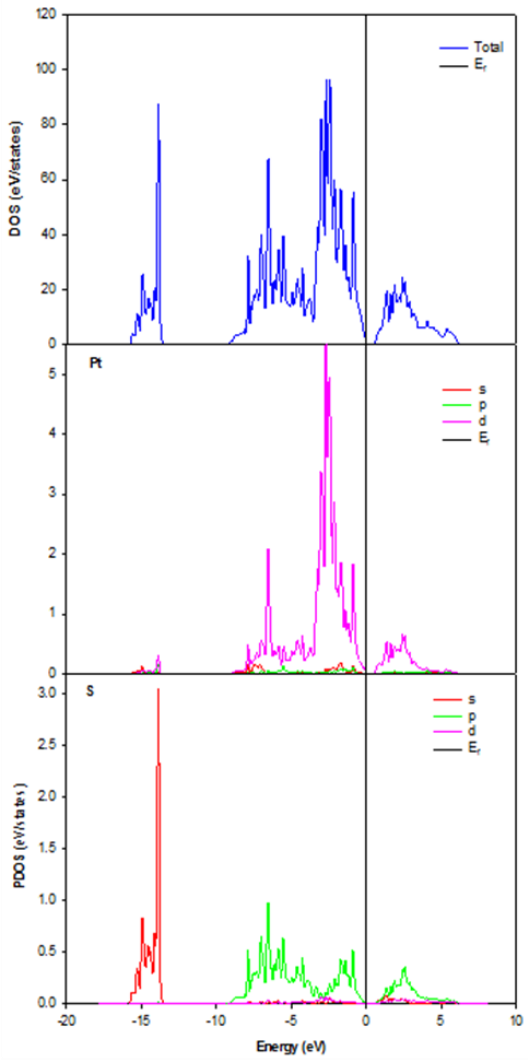

(a)

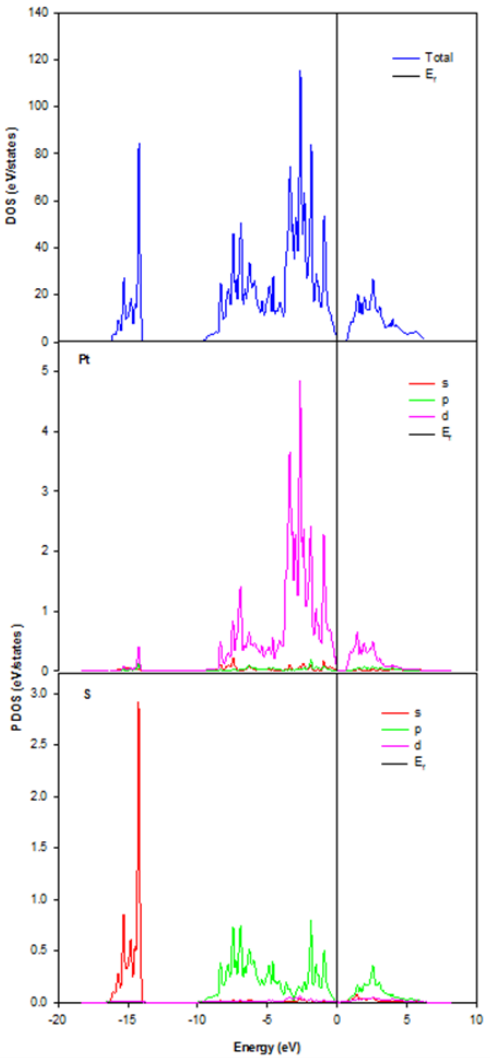

(b)

Figure 3.8.6. 1. Total and partial density of states of $Pt_{50}S_{50}$ P_1 (from $P4_2/mmc$), (a) 10 GPa and (b) 20 GPa

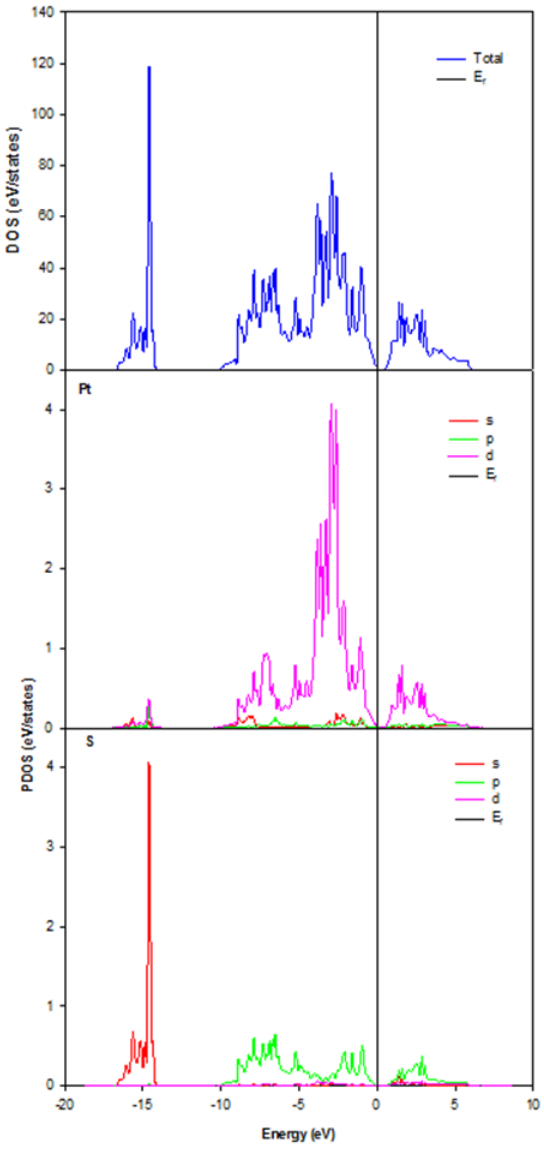

(c)

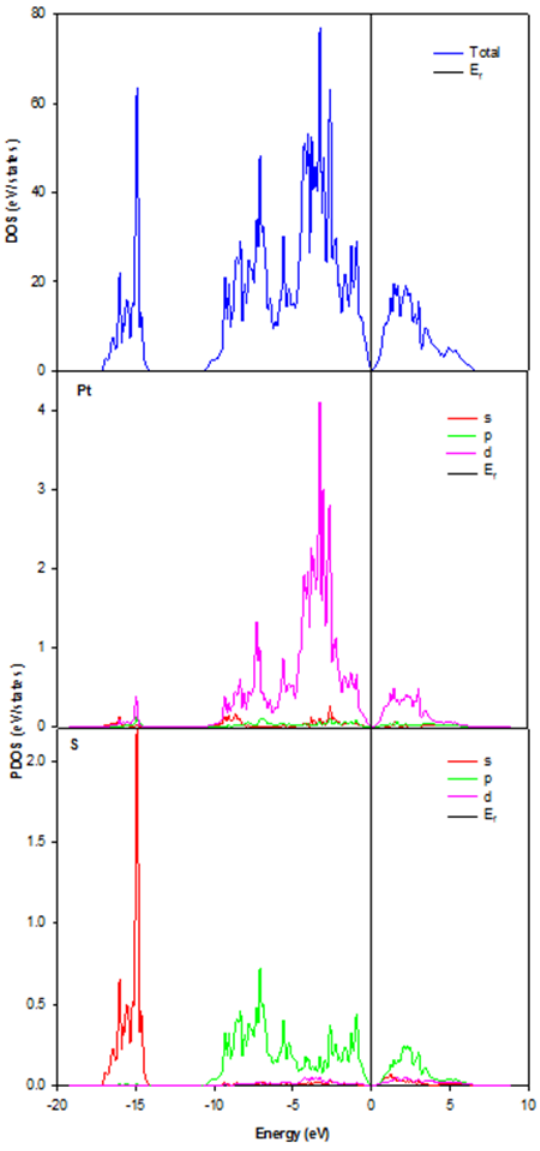

(d)

Figure 3.8.6. 2. Total and partial density of states of $Pt_{50}S_{50}$ P_1 (from $P4_2/mmc$), (c) 30 GPa and (d) 40 GPa

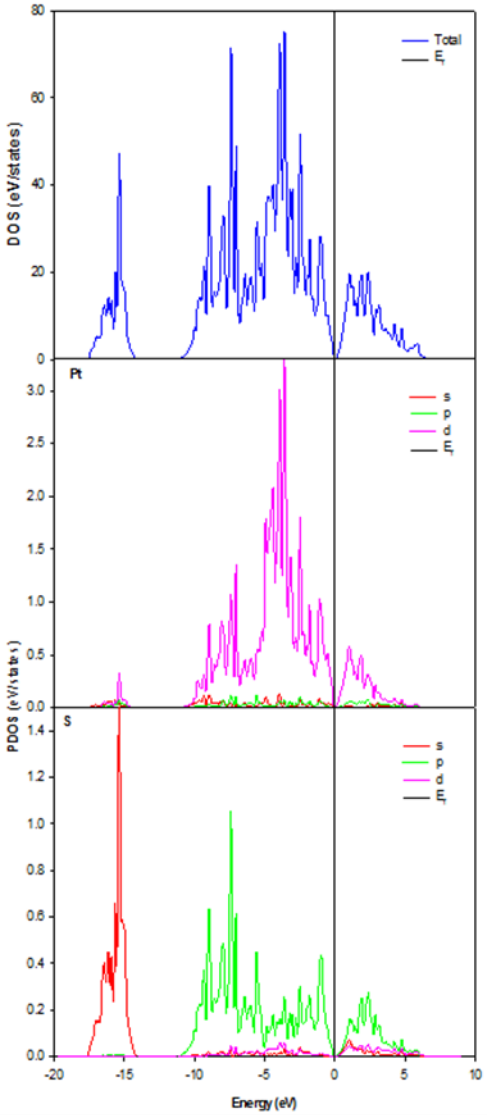

Figure 3.8.6. 3. Total and partial density of states of $Pt_{50}S_{50}$ P_1 (from $P4_2/mmc$) at 50 GPa

Figure 3.8.6.1(a) shows the total DOS and PDOS of $Pt_{50}S_{50}$ P_1 (from $P4_2/mmc$) at 10 GPa. The d states of Pt contribute more to the total DOS and the contribution of s and p states are almost the same. The peak ranging from -15.5 eV to -14 eV corresponds mainly to the 3s states of S. The peak stretching from -9.0 eV to the top of the VB originates from the 3p states of S and the dominant 3d of Pt. The hybridisation of 3p S and 3d Pt states were noted. The calculations have shown that $Pt_{50}S_{50}$ has a band gap of

0.5 eV. The conduction band consists of the anti-bonding d states of Pt and p states of S. The distribution of peaks in the total DOS of $Pt_{50}S_{50}$ at 20, 30, 40 and 50 GPa are reflected in figures 3.8.6.1(b), 3.8.6.2(a), 3.8.6.2(b) and 3.8.6.3 respectively. However, the band gaps at different pressures are depicted as follows, 0.6, 0.7, 0.9 and 1.0 eV for 20, 30, 40 and 50 GPa respectively. It was noted that pressure increases the band gap.

3.8.7. Density of States – $Pt_{37.5}Pd_{12.5}S_{50}$ – P_1 (from $P4_2/mmc$)

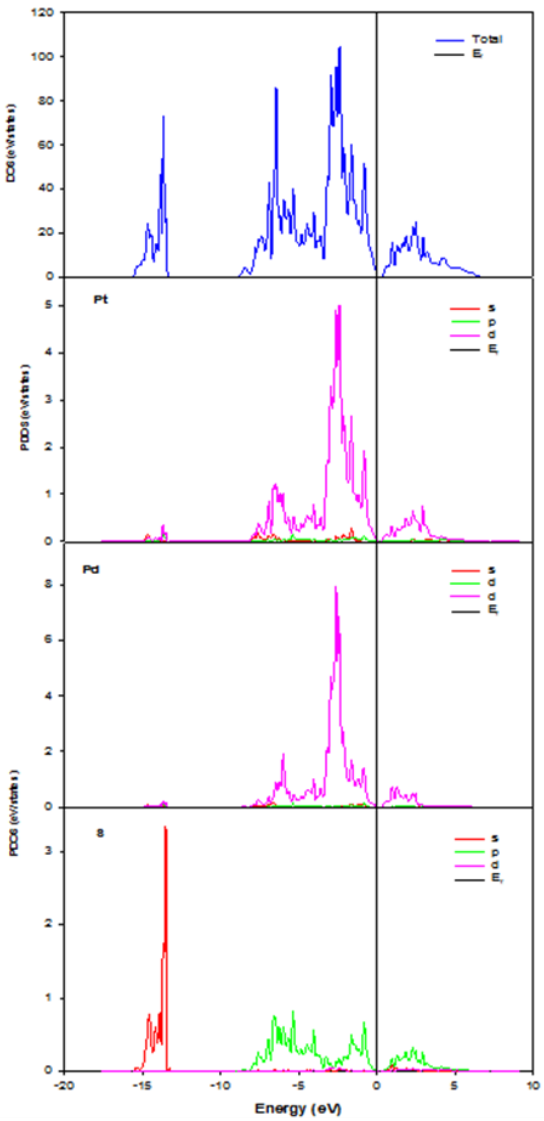

(a)

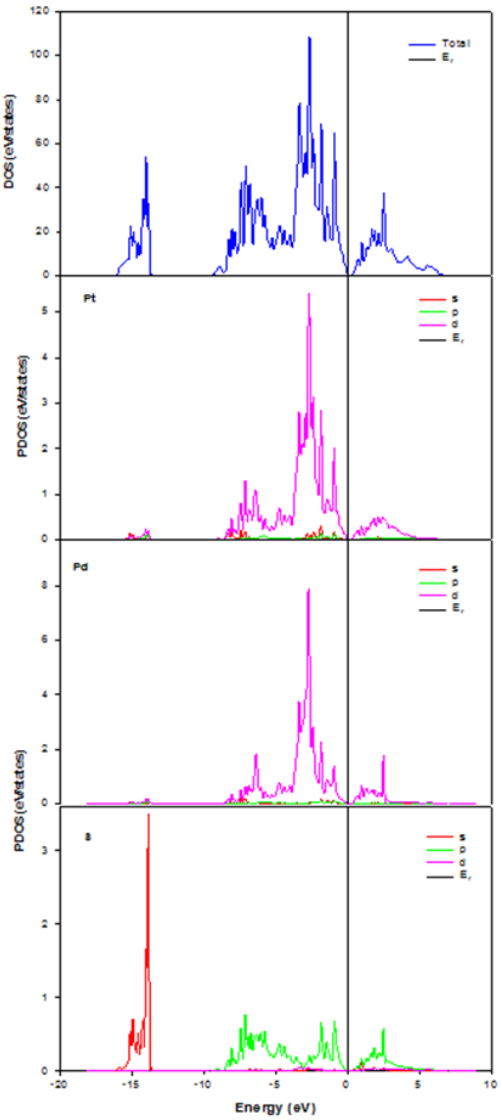

(b)

Figure 3.8.7. 1. Total and partial density of states of $Pt_{37.5}Pd_{12.5}S_{50}$ P_1 (from $P4_2/mmc$), (a) 10 GPa and (b) 20 GPa

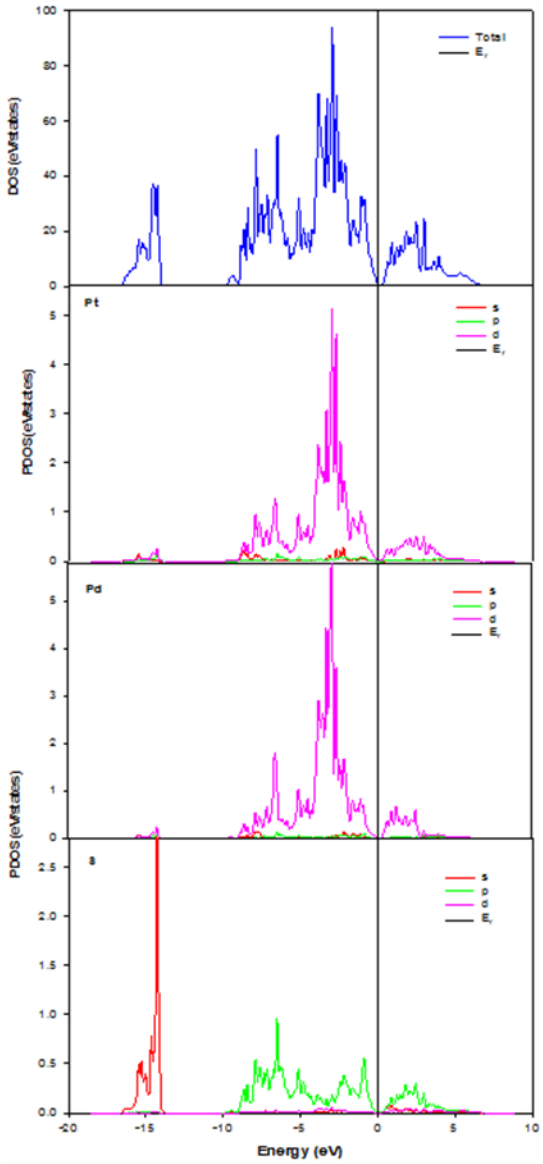

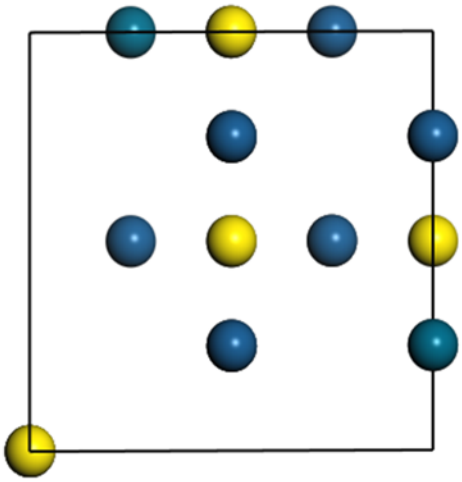

Figure 3.8.7. 2. Total and partial density of states of $Pt_{37.5}Pd_{12.5}S_{50}$ P_1 (from $P4_2/mmc$) at 30 GPa

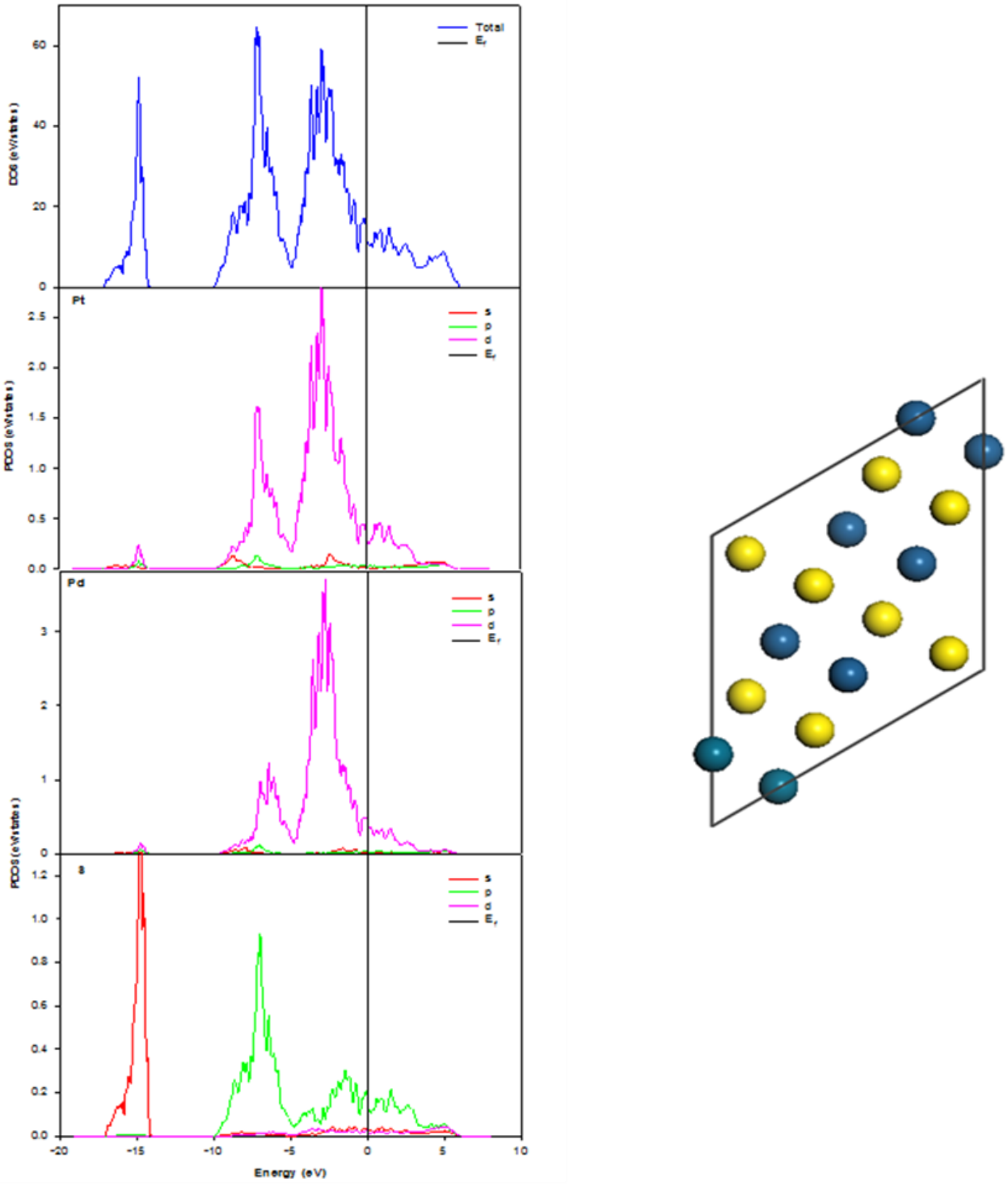

Figure 3.8.7. 3. Total and partial density of states of $Pt_{37.5}Pd_{12.5}S_{50}$ P_1 (from $P4_2/mmc$) at 40 GPa

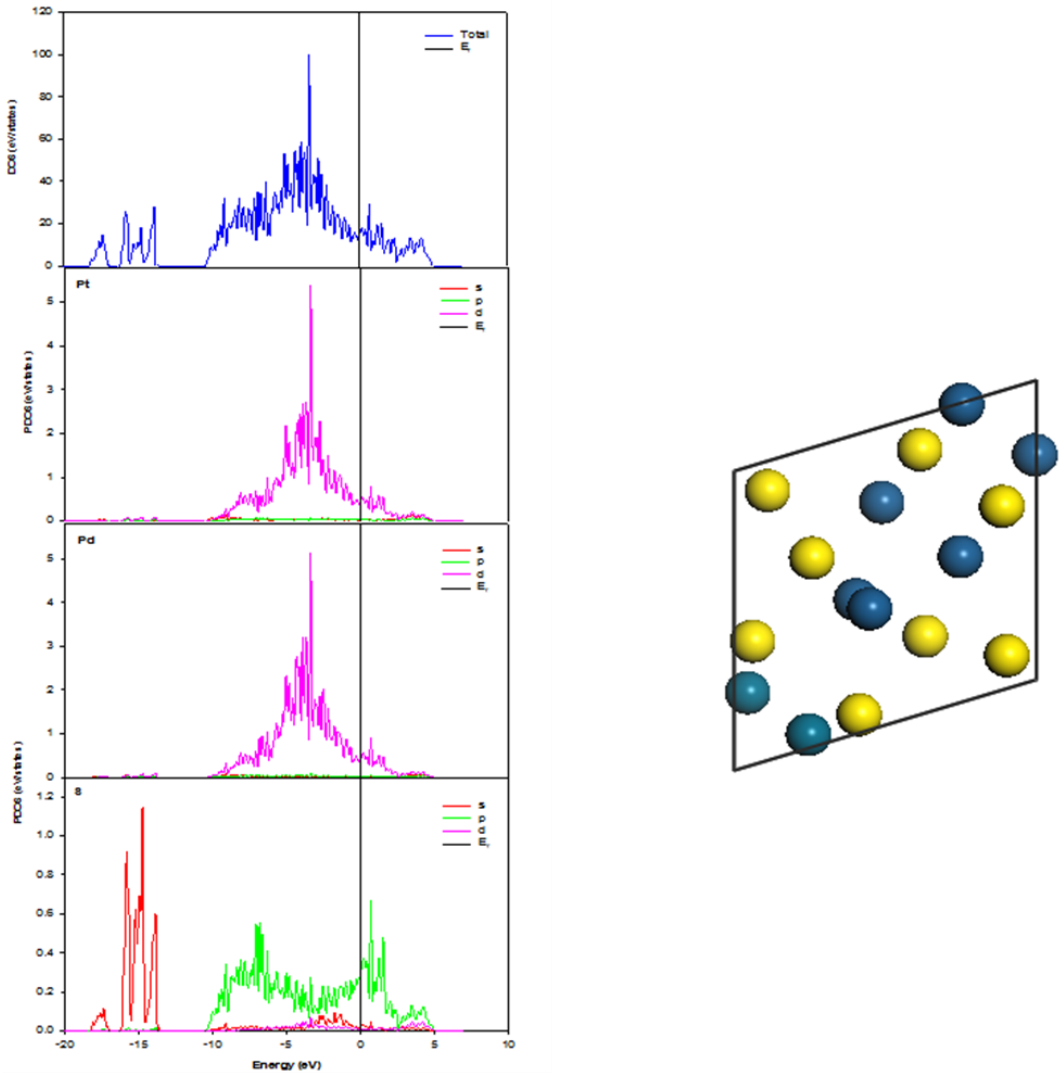

Figure 3.8.7. 4. Total and partial density of states of $Pt_{37.5}Pd_{12.5}S_{50}$ P_1 (from $P4_2/mmc$) at 50 GPa

Figure 3.8.7.1(a) shows the total DOS and PDOS of $Pd_{37.5}Pt_{12.5}S_{50}$ P_1 (from $P4_2/mmc$) at 10 GPa. From the PDOS, it was observed that the d states of both Pt and Pd contribute more to the total DOS. The s and p states contribution is almost the same. The peak ranging from -15 eV to -14.5 eV emanates mainly from the 3s states of S. The broader distribution between -8 eV and VB emanates predominately from the 3p states S, the dominant 3d states of Pt and 4d states of Pd. The hybridisation of 3p S, 3d Pt and 4d Pd states were observed. The calculations have shown that $Pd_{37.5}Pt_{12.5}S_{50}$ has a band

gap of 0.4 eV. The conduction band consists of the anti-bonding d states of Pt and Pd and p states of S. The distribution of peaks in the total DOS of $Pd_{37.5}Pt_{12.5}S_{50}$ at 20, 30, 40 and 50 GPa are reflected in figures 3.8.7.1(b), 3.8.7.2, 3.8.7.3 and 3.8.7.4 respectively and all emanates from the same states as those in 3.8.7.1(a). However, the band gabs at different pressures are depicted as follows 0.4, and 0.3 eV for 20 and 30 GPa. A band gap was noted to have closed in the 40 and 50 GPa structures. Furthermore, rearrangement of atoms in $Pd_{37.5}Pt_{12.5}S_{50}$ corresponds to that of figure 3.8.7.4 (at 50 GPa).

3.8.8. Density of States – $Pd_{25}Pt_{25}S_{50}$ – P_1 (from $P4_2/mmc$)

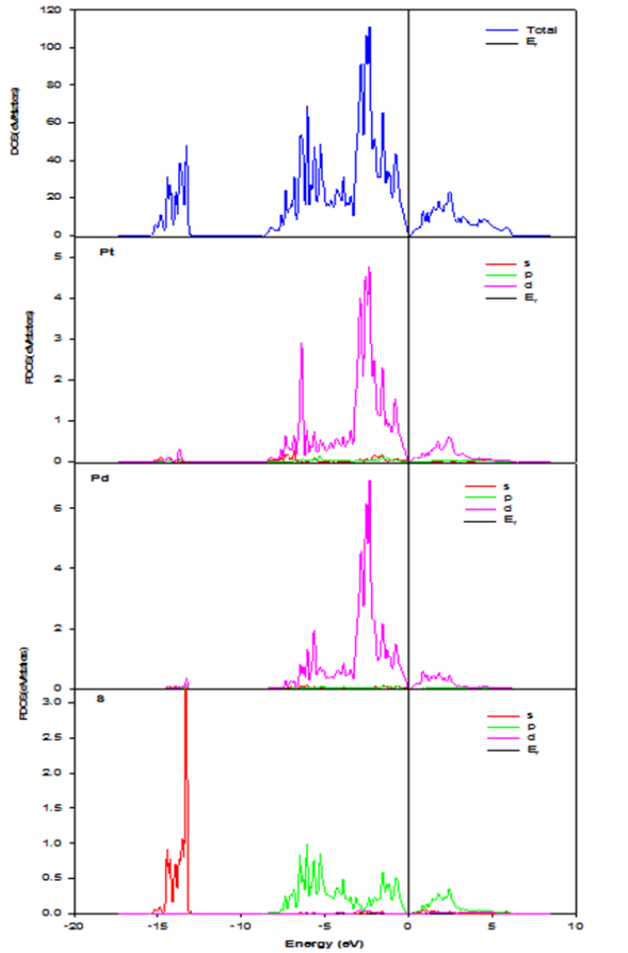

(a)

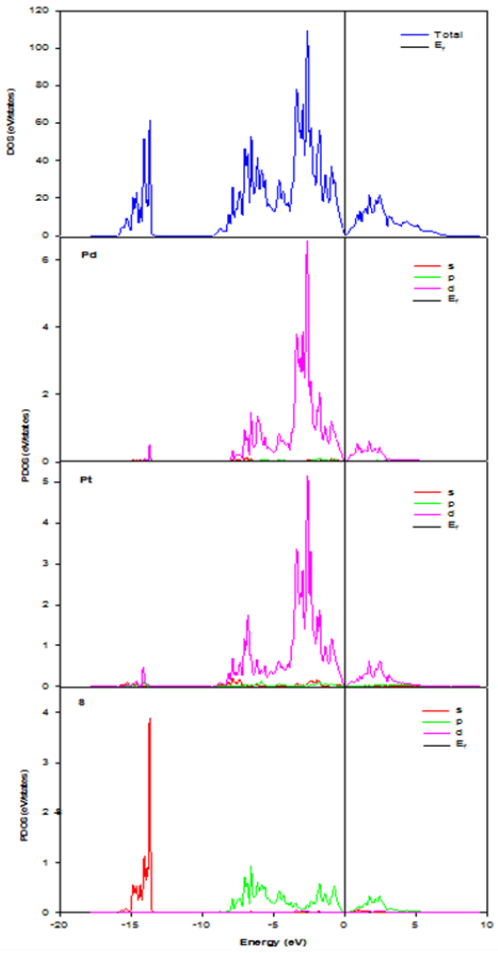

(b)

Figure 3.8.8. 1. Total and partial density of states of $Pd_{25}Pt_{25}S_{50}$ P_1 (from $P4_2/mmc$), (a) 10 GPa and (b) 20 GPa

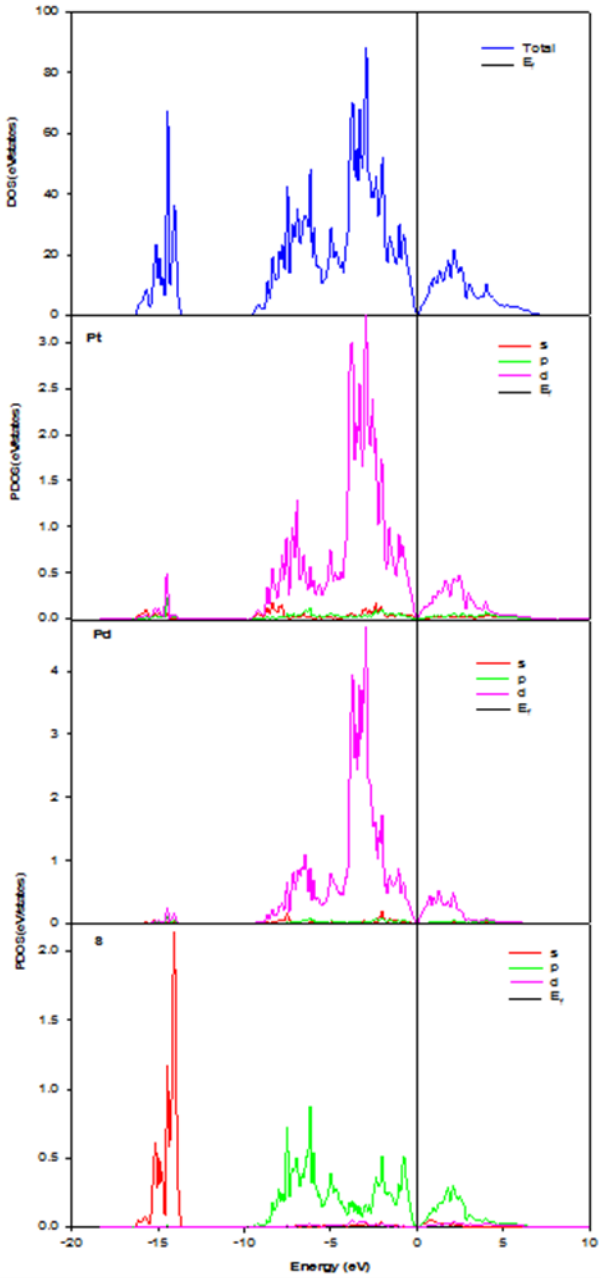

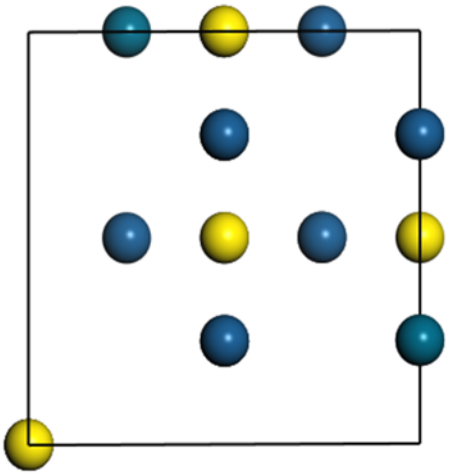

Figure 3.8.8. 2. Total and partial density of states of $Pd_{25}Pt_{25}S_{50}$ P_1 (from $P4_2/mmc$) at 30 GPa

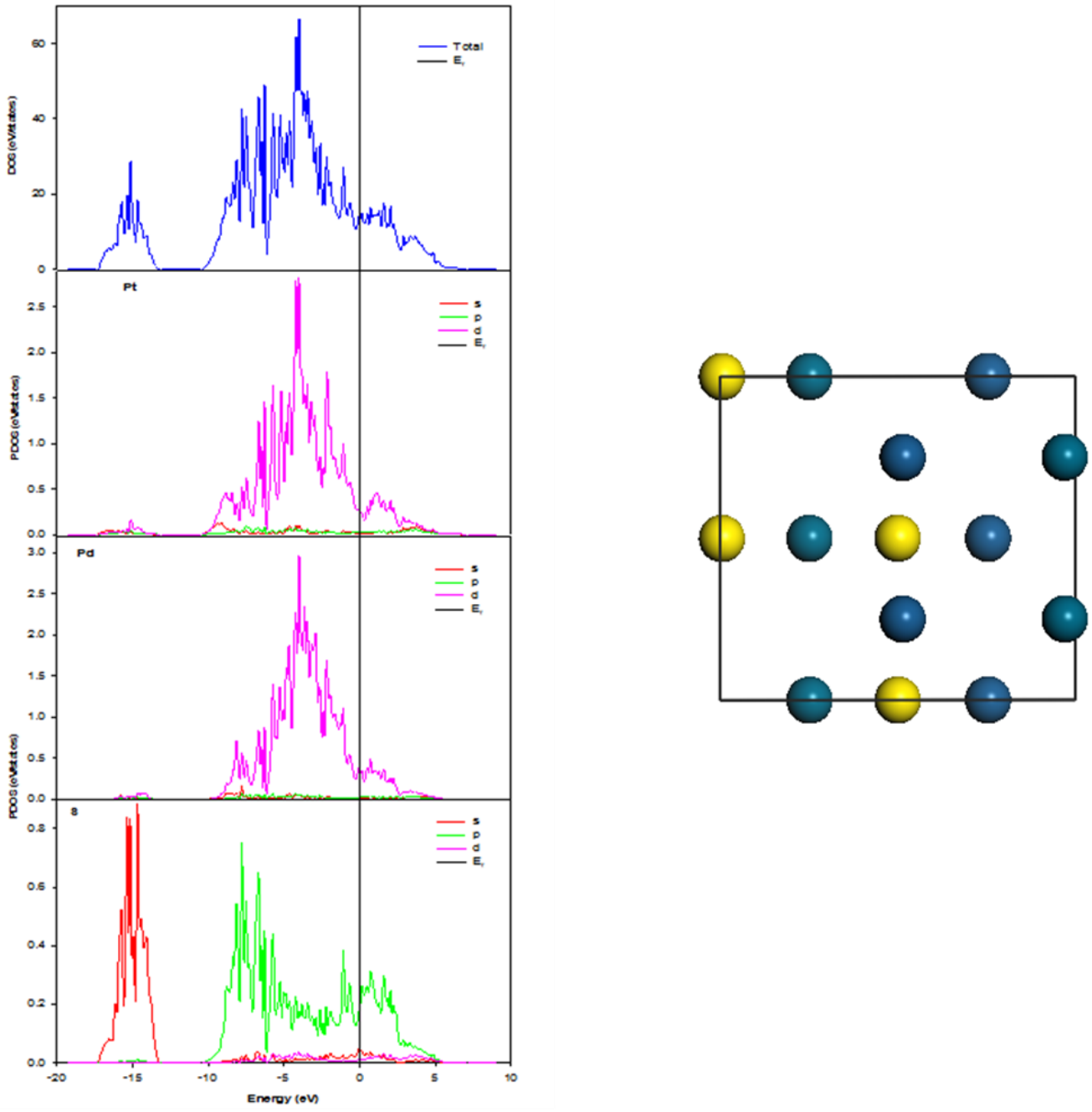

Figure 3.8.8. 3. Total and partial density of states of $Pd_{25}Pt_{25}S_{50}$ P_1 (from $P4_2/mmc$) at 40 GPa

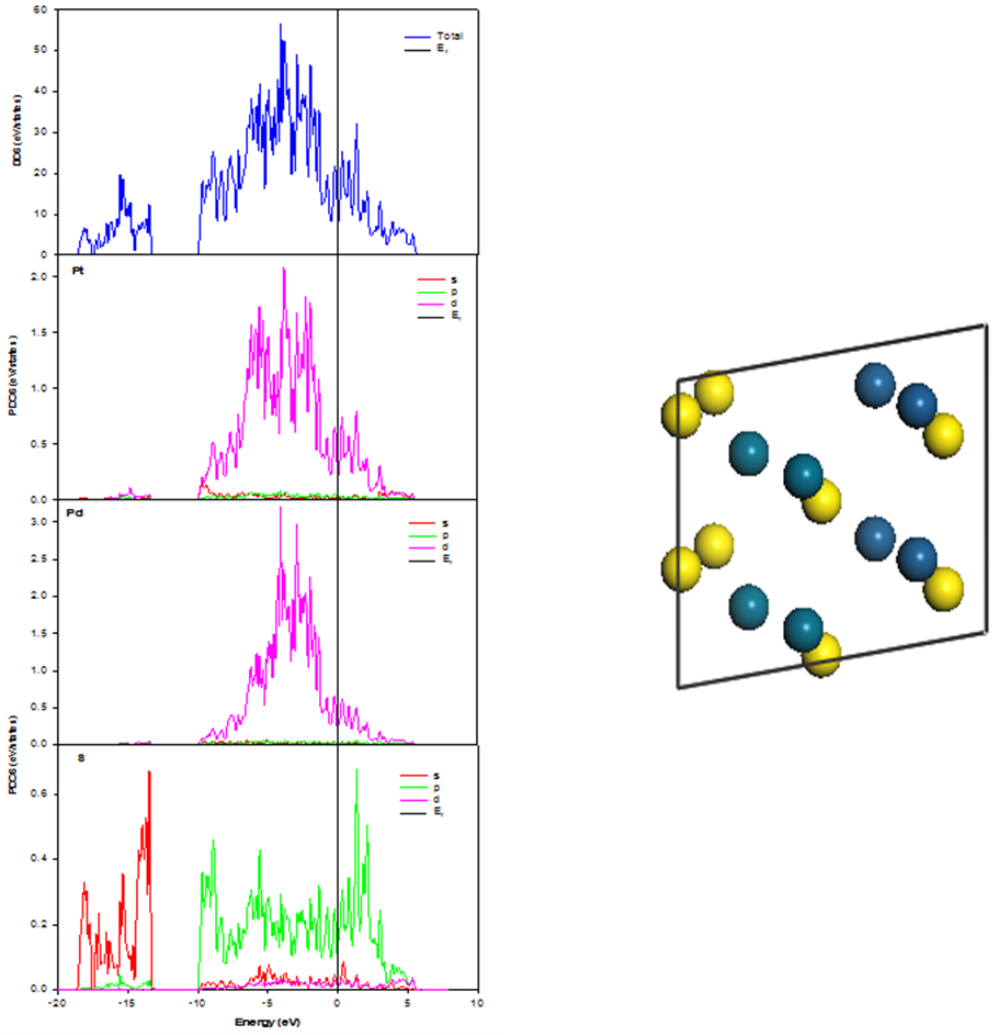

Figure 3.8.8. 4. Total and partial density of states of $Pd_{25}Pt_{25}S_{50}$ P_1 (from $P4_2/mmc$) at 50 GPa

Figure 3.8.8.1(a) shows the total DOS and PDOS of $Pt_{25}Pd_{25}S_{50}$ P_1 (from $P4_2/mmc$) at 10 GPa. The d states in Pt contribute more to the total DOS and the s and p states contribution is almost the same. The peak ranging from -15.2 eV to -14 eV emanates mainly from the 3s states of S. The broader distribution between -8.5 eV and VB emanates predominately from the 3p states of S, the dominant 3d states of Pt and 4d states of Pd. The hybridization of 3p S, 3d Pt and 4d Pd states were observed. The calculations have shown that $Pt_{25}Pd_{25}S_{50}$ has a band gap of 0.6 eV. The conduction band consists of the

anti-bonding d states of Pt and Pd and p states of S. The distribution of peaks in the total DOS of $Pt_{25}Pd_{25}S_{50}$ at 20, 30, 40 and 50 GPa are reflected in figures 3.7.8.1(b), 3.8.8.2, 3.8.8.3 and 3.8.8.4, respectively and all emanates from the same states as those in 3.8.8.1(a). However, the band gaps at different pressures are depicted as follows, 0.8 and 0.5 eV for 20 and 30 GPa. The band gap decrease with increasing pressure. It was observed that the band gap has closed at 40 and 50 GPa and the orientation of the structure at 50 GPa has changed. A metallic behavior was observed.

3.8.9. Density of States – $Pd_{12.5}Pt_{37.5}S_{50}$ – P_1 (from $P4_2/mmc$)

Figure 3.8.9.1(a) gives the total DOS and PDOS of $Pd_{12.5}Pt_{37.5}S_{50}$ P_1 (from $P4_2/mmc$) at 10 GPa. A band gap of 0.4 eV was observed. Contribution of s and p states in Pt and Pd is almost the same and the d states contribution is more to the total DOS. The peak ranging from -15.2 eV to -14 eV emanates from mainly from the 3s states of S. The broader distribution between -8 eV and VB emanates predominately from the 3p states of S, the dominant 3d of Pt and the 4d of Pd. The hybridisation of 3p S, 3d Pt and 4d Pd states were noted. The conduction band consists of the anti-bonding d states of Pt and Pd and the p states of S The distribution of peaks in the total DOS of $Pd_{12.5}Pt_{37.5}S_{50}$ at 20 GPa as reflected in figure 3.8.9.1(b) However, the band gap at 20 GPa is depicted as 0.5 eV. The 30, 40 and 50 GPa could not run since the structure changes symmetry. It was noted that pressure increases the band gap.

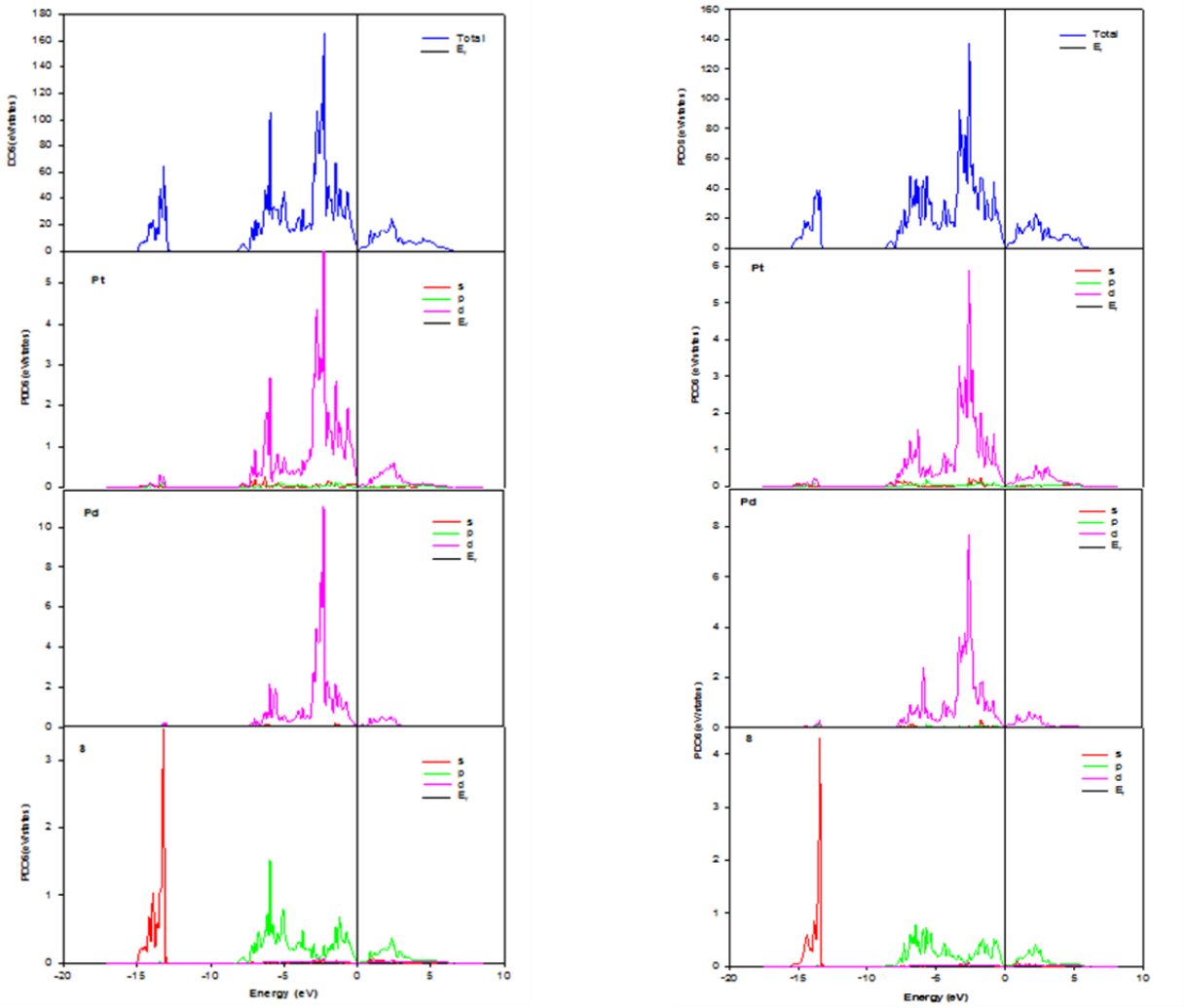

(a) (b)

Figure 3.8.9. 1. Total and partial density of states of $Pd_{12.5}Pt_{37.5}S_{50}P_1$ (from $P4_2/mmc$), (a) 10 GPa and (b) 20 GPa

3.8.10. Density of States –$Pd_{50}S_{50}$ – P_1 (from $P4_2/mmc$)

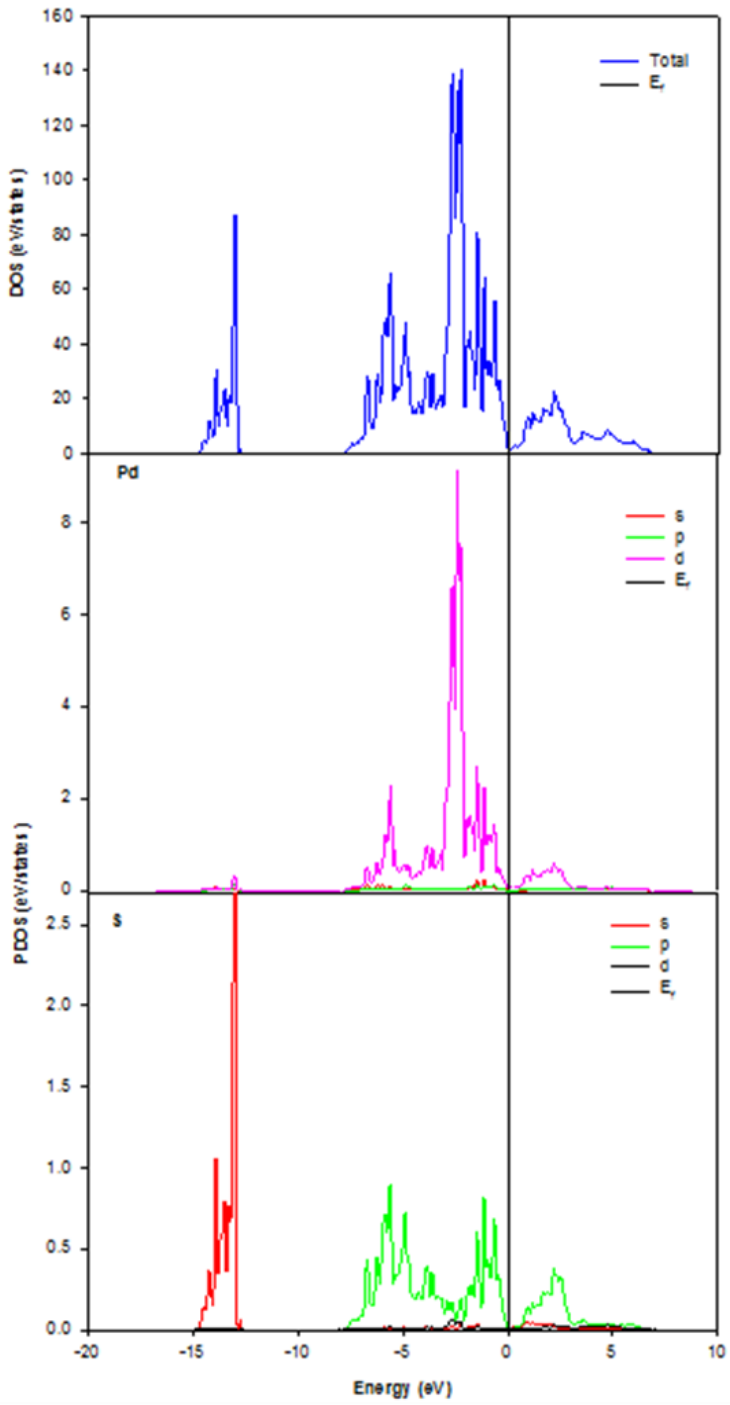

Figure 3.8.10. 1. Total and partial density of states of $Pd_{50}S_{50}$ P_1 (from $P4_2/mmc$) at 10 GPa

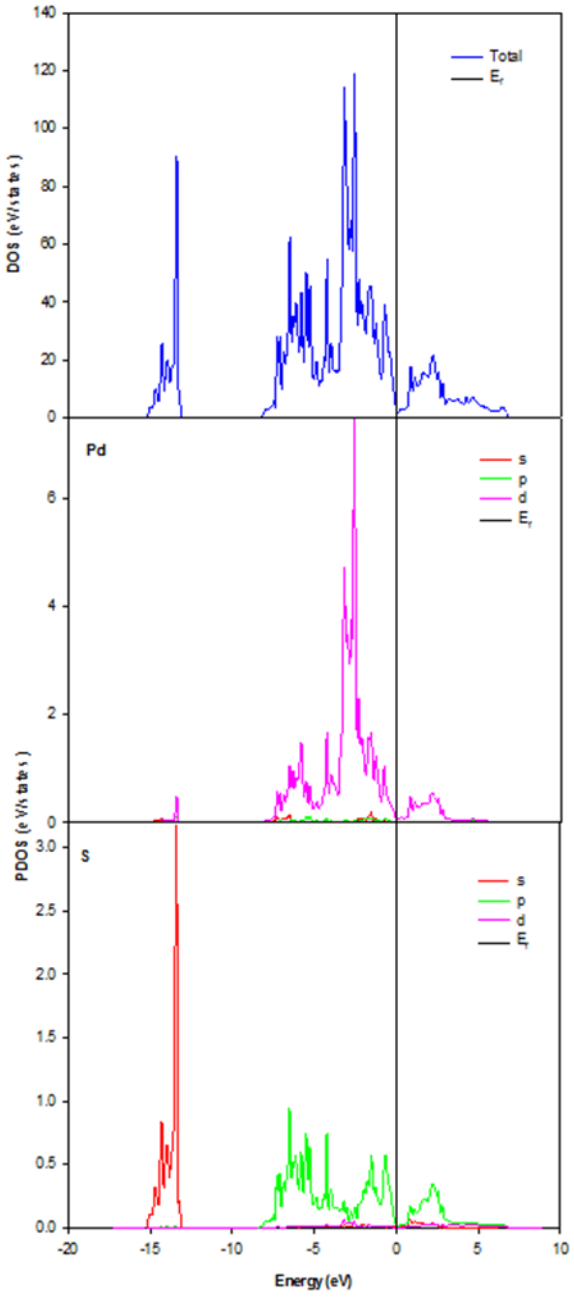

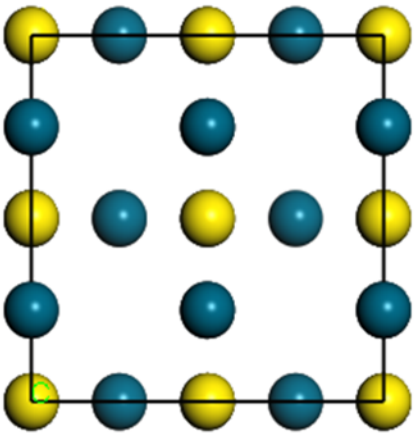

Figure 3.8.10. 2. Total and partial density of states of $Pd_{50}S_{50}$ P_1 (from $P4_2/mmc$) at 20 GPa

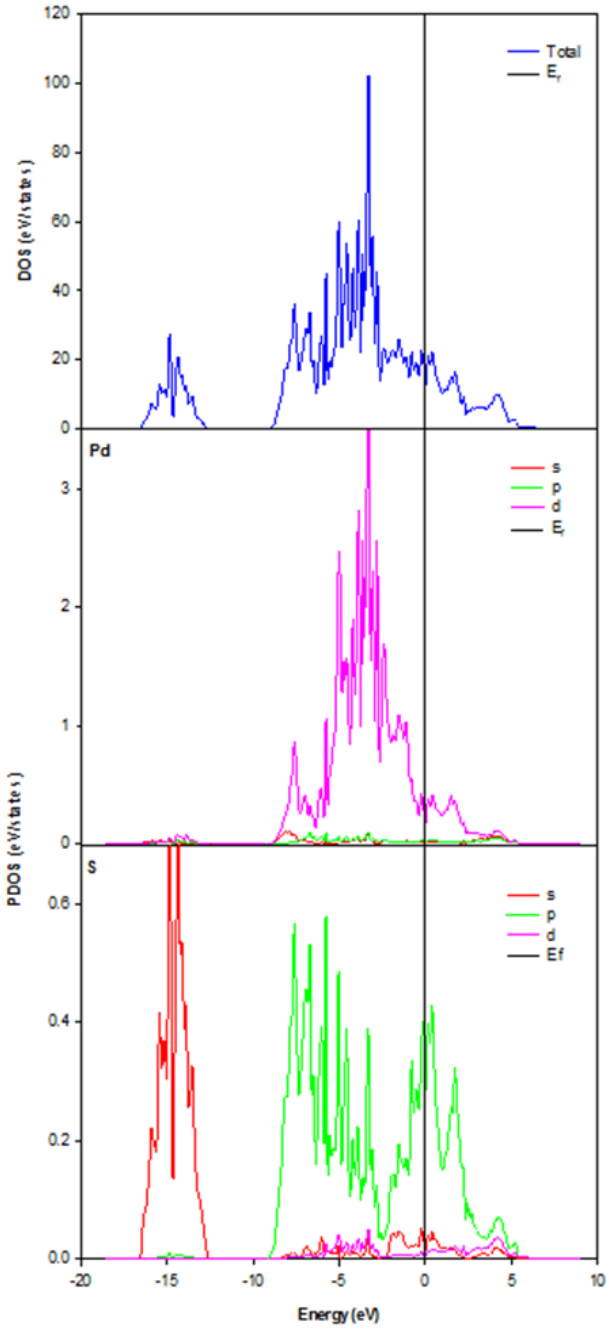

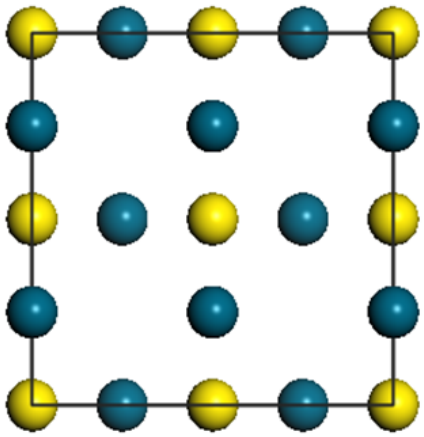

Figure 3.8.10. 3. Total and partial density of states of $Pd_{50}S_{50}$ P_1 (from $P4_2/mmc$) at 30 GPa

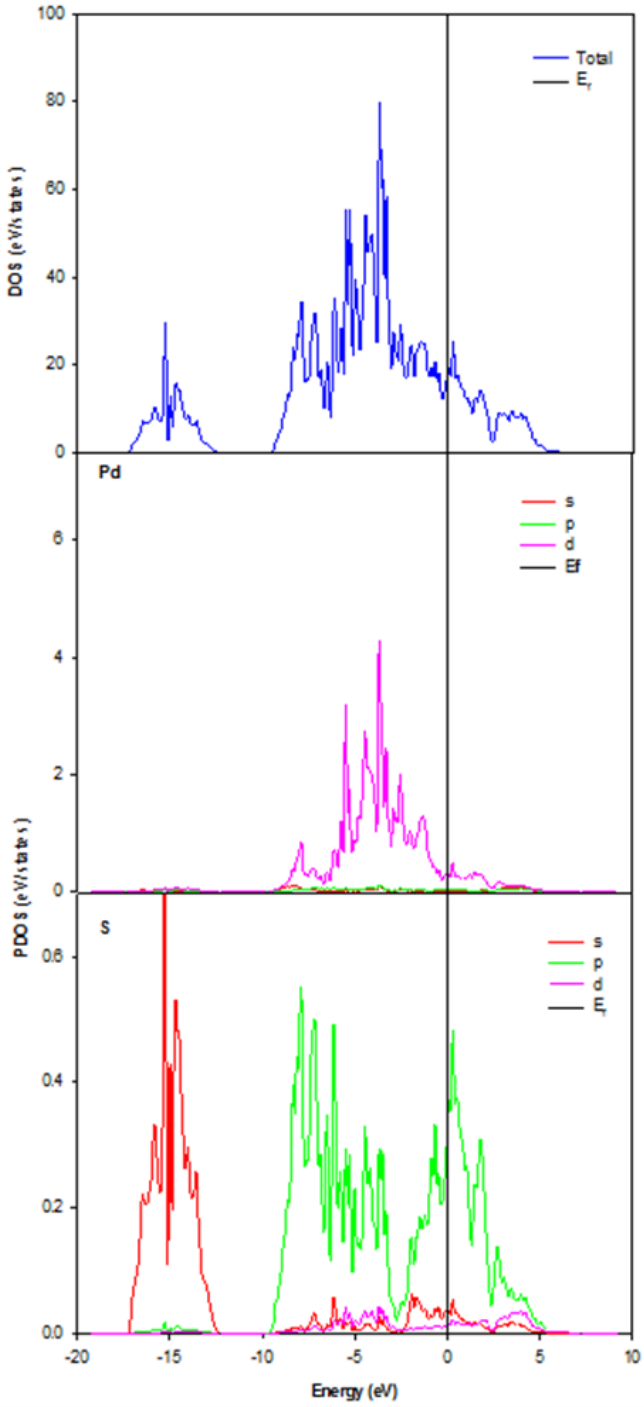

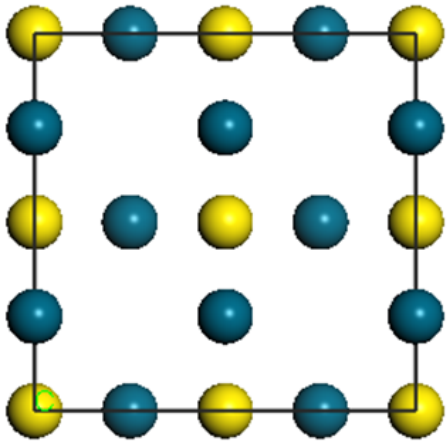

Figure 3.8.10. 4. Total and partial density of states of $Pd_{50}S_{50}$ P_1 (from $P4_2/mmc$) at 40 GPa

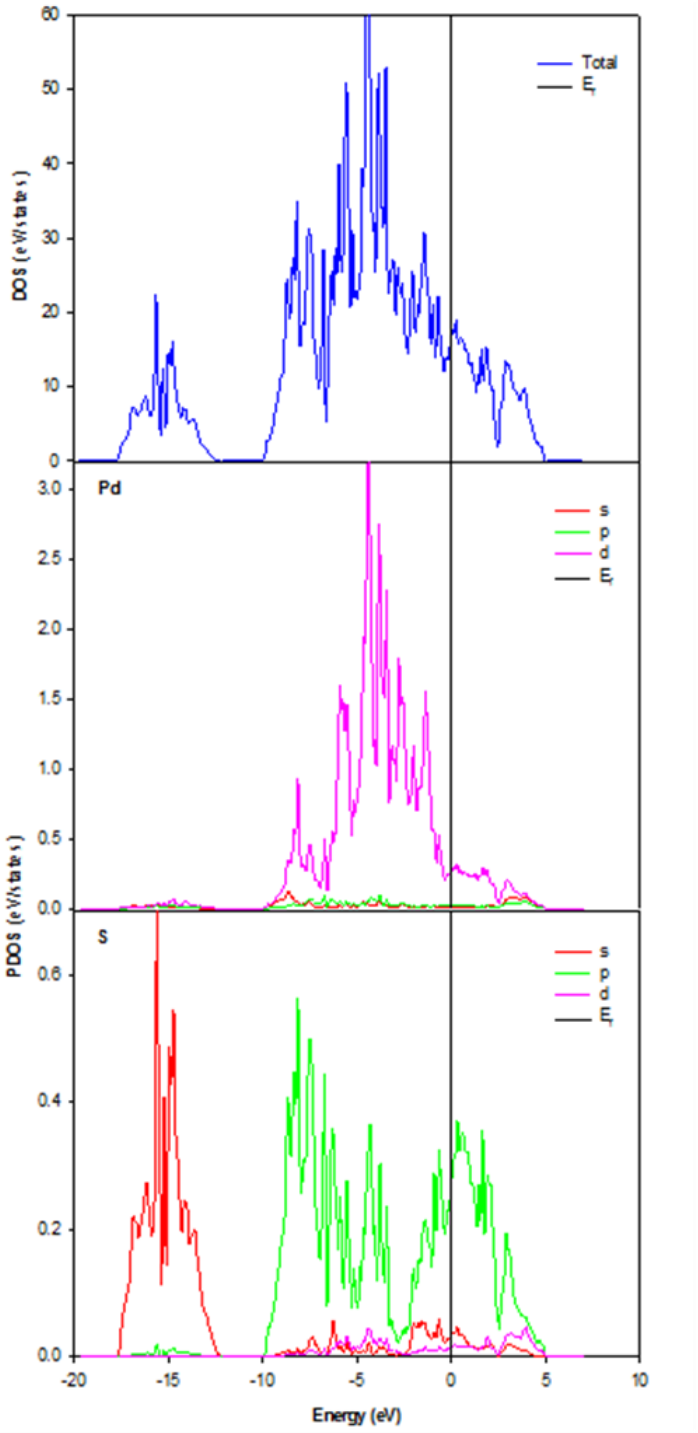

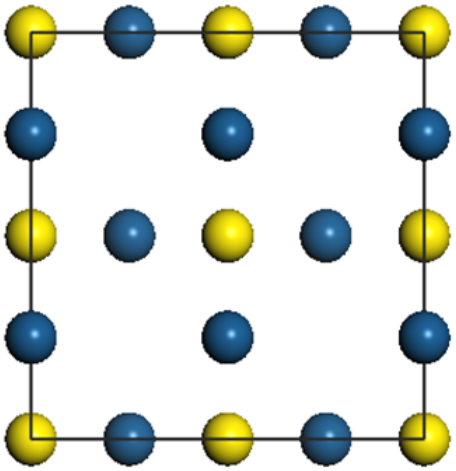

Figure 3.8.10. 5. Total and partial density of states of $Pd_{50}S_{50}$ P_1 (from $P4_2/mmc$) at 50 GPa

Figure 3.8.10.1, shows the total DOS and PDOS of $Pd_{50}S_{50}$ P_1 (from $P4_2/mmc$) at 10 GPa. The d states of Pd contribute more to the total DOS and the s and p states contribution is almost the same. Looking at the PDOS, the peak in the total DOS, ranging from -15 eV to -13 eV emanates mainly from the 3s states of S. The peak stretching from -7.5 eV to the top of the VB originates from the 3p states of S and the dominant 4d of Pd. The hybridisation of 3p S and 4d Pd states lead to the Pd-S covalent bond. The calculations have shown that $Pd_{50}S_{50}$ has an indirect band gap of 0.5 eV. The conduction band consists of the anti-bonding d states of Pd and p states of S. The distribution of peaks in the total DOS of $Pd_{50}S_{50}$ at 20, 30,40 and 50 GPa are reflected in figures 3.8.10.2, 3.8.10.3, 3.8.10.4 and 3.8.10.5 respectively and all emanate from the same states as those of 3.8.10.1. However, the band gap of 20 GPa is 0.5 eV. It was noted that starting at 30 GPa – 50 GPa, the structures do not differ in orientation. As pressure increases a metallic behaviour is observed. The 50 GPa pressure did not converge, it was observed that the structure do not withstand high pressures.

Chapter 4

Summary and conclusion

Density functional methods have been successfully used to investigate the structural, electronic, mechanical and vibrational properties from PtS to PdS and PdS to PtS using planewave pseudopotential methods embodied in the VASP code. The transformation from platinum sulphide to palladium sulphide and palladium sulphide to platinum sulphide was successfully modelled. Three symmetries, the PtS $P4_2/mmc$, PdS $P4_2/m$ and PtS P_1 were used in the study. The P_1 symmetry was generated from $P4_2/mmc$, to allow for finer concentration changes. The equilibrium lattice constants and the heats of formation were calculated, and it was observed that lattice parameters increase steadily with increasing Pd concentration for both $P4_2/m$ and P_1 symmetry. The results were in good agreement with available experimental values, within 1.9%. The dependence of lattice parameters on pressure has been evaluated for 0 – 50 GPa. Generally lattice parameters decreased with increasing pressure. Striking features of lattice parameters were noted at $Pt_{50}S_{50}$, $Pd_{50}S_{50}$ $P4_2/mmc$ and in P_1 (from $P4_2/mmc$) structures where the lattice parameter increases with increasing pressure, which is in agreement with previous studies, Marnier et al. We performed electronic DOS on all compositions. We noted a good correlation in electronic properties. They predict bandgaps in the range 0.5 - 0.9 eV which is within the experimental measured values of 0.02 eV to 2 eV [67, 68, 69, 8]. The phonon DOS's of $Pd_{50}S_{50}$ $P4_2/mmc$ subjected to pressure was observed to be different to other phonon DOS's, since $Pd_{50}S_{50}$ $P4_2/mmc$ does not occur naturally. It occurs in a form $Pd_{50}S_{50}$ $P4_2/m$. The band gap was changed under variation of pressure and for most structures they increased with increasing pressure. In the case of $Pt_{37.5}Pd_{12.5}S_{50}$ and $Pt_{25}Pd_{25}S_{50}$ P_1, the band gap closed at 40 GPa. The $Pt_{12.5}Pd_{37.5}S_{50}$ P_1 could not run at 30, 40 and 50 GPa, owing to significant structural changes. A metallic behaviour was noted in $Pd_{50}S_{50}$ P_1 from 30 GPa. Interestingly, the $Pt_{50}S_{50}$ P_1 and $P4_2/m$ did not go completely metallic above 30 GPa. The P_1 (from $P4_2/mmc$) is a known symmetry for PtS, hence Pd appears to be introducing instability into this symmetry. Furthermore, we performed calculations on vibrational and mechanical properties of

studied systems, i.e. phonon dispersion curves and elastic properties. The phonon dispersion curves show that palladium addition stabilizes the structure in $Pt_{50-x}Pd_xS_{50}$ $P4_2/mmc$. In the $Pd_{50-x}Pt_xS_{50}$ $P4_2/m$, platinum addition stabilizes the structure noted as $Pd_{12.5}Pt_{37.5}S_{50}$ $P4_2/m$. Pressure related studies, suggest that an increase in pressure mostly render structures unstable as indicated by the presence of soft modes, mostly attributable to Pt and Pd vibrations. It was observed that the lower and upper frequency bands do not mix at high pressures for $Pt_{50}S_{50}$ and $Pt_{25}Pd_{25}S_{50}$ $P4_2/m$ symmetry. It was shown that the bands tend to mix at high pressures for $Pt_{50}S_{50}$ $P4_2/mmc$. However, it was noted that the bands for $Pt_{37.5}Pd_{12.5}S_{50}$ $P4_2/mmc$ mixed at 50 GPa, whereas for the $Pt_{25}Pd_{25}S_{50}$ $P4_2/mmc$, they mix from 40 GPa. In the case of $Pt_{12.5}Pd_{37.5}S_{50}$ $P4_2/mmc$, only calculations related 10 and 20 GPa pressures could run similarly to what was noted in electronic DOS. The elastic properties at 0 GPa satisfy all necessary conditions for mechanical stability. As pressure was applied, the elastic constants showed negative values, which suggest instability of the structures, particularly in the $P4_2/mmc$ and P_1 symmetries. It was noted that the $Pt_{25}Pd_{25}S_{50}$ P_1 is the most unstable structure due to C_{44} and shear modulus being negative and also as depicted by phonon dispersions. The stable structure in P_1 symmetry is $Pt_{37.5}Pd_{12.5}S_{50}$ since it has a high value of C_{44} and the least stable being $Pt_{12.5}Pd_{37.5}S_{50}$ due to C_{44} being smaller compared to other concentrations. The $Pt_{12.5}Pd_{37.5}S_{50}$ composition could not run as pressure was increased, which suggests that it could not withstand high pressure. The composition $Pt_{37.5}Pt_{12.5}S_{50}$ exists in nature with s symmetry $P4_2/m$, and is called braggite [4]. Hence, the observed stability of $Pt_{37.5}Pd_{12.5}S_{50}$ with P_1 symmetry, even under highly pressure could be partly ascribed to such natural occurrence. In conclusion, cluster expansion could shed valuable insights on stabilities of $Pt_{50-x}Pd_xS_{50}$ systems, under different symmetries.

Appendix

Papers presented at conferences

M. A. Masenya et al., “Computational studies of Palladium/Platinum Sulfide using solid-solution approach”. Presented at South African Institute of Physics (SAIP) 57th Annual Conference, held at University of Pretoria, in July 2012

M. A. Masenya et al., “Computational modelling studies of precious mixed metal sulphides”. Presented at Post-graduate Research Day in the Faculty of Science and Agriculture (PGRD - FSA), held at Bolivia lodge, in October 2012

M. A. Masenya et al., “Computational study of structural, electronic and mechanical properties of Platinum sulphide”. Presented at Centre of High Performance Computing (CHPC) National Meeting, held at Durban International Convention Centre (Durban ICC), in December 2012

M. A. Masenya et al., “Computational modelling studies of structural, electronic and mechanical properties of Palladium Sulphide”. Presented at South African Institute of Physics (SAIP) 58th Annual Conference, held at University of Zululand, in July 2013

Bibliography

[1] D.J. Vaughan and J.R. Craig, Mineral chemistry of metal sulphides, Cambridge University Press, Cambridge: Transactions of the Institution of Mining and Metallurgy, 1978.

[2] A. J. Stanley and C. J. Criddle , “Characteristic optical data for cooperite, braggite and vysotskite,” *The Canadian Mineralogist,* vol. 23, pp. 149-162, 1985.

[3] L. J. Cabri, “The mineralogy of the platinum-group elements,” *Minerals Science and Engineering,* vol. 4, pp. 3-29, 1972.

[4] L.J. Cabri, J.M. Stewart, K. Turner and B.J. Skinner, “On cooperite, braggite, and vysotskite,” *American Mineralogist,* vol. 63, pp. 832-839, 1978.

[5] S. Draggan, “Mineral Information Institute,” In Encyclopedia of Earth, Washington, D.C, 2008.

[6] F. Grønvold and E. Røst, “On the Sulfides, selenides, and tellurides of palladium.,” *Acta Chemica Scandinavica,* vol. 10, pp. 1620-1634, 1956.

[7] D. Nguyen-Manh, P. S. Ntoahae, D. G. Pettifor and P. E. Ngoepe, , “Electronic structure of platinum-group minerals. Prediction of semiconductor band gaps,” *Molecular simulation,* vol. 22, pp. 23-30, 1999.

[8] P. Raybaud, G. Kresse, J. Hafner and H. Toulhoat, , *Ab initio density functional studies of transition-metal sulphides, I. Crystal structure and cohesive properties. Journal of Physics: Condensed Matter ,* vol. 9, pp. 11085-11106 , 1997.

[9] M.H. Tsai and K.C Hass, “First-principles studies of NO chemisorption on rhodium, palladium, and platinum surfaces.,” *Physical Review B ,* vol. 51, pp. 14616-14625 , 1995.

[10] F. A. Cotton and G. Wilkinson, Advanced Inorganic Chemisry, New York: John Wiley and Sons, 1980.

[11] F. A. Bannister and M. H. Hey, “Determination of Minerals in Platinum Concentrates from the Transvaal by X-Ray Methods,” *Mineralogical Magazine,* vol. 23, pp. 188-206, 1932.

[12] A. D. Genkin and O. E. Zvyagintsev, “Vysotskite, a new sulfide of palladium and nickel,” *Zapiski Vses Mineralog. Obshch,* vol. 91, pp. 718-725, 1962.

[13] N. E. Brese, P.J. Squattrito and J. A. Ibers , “Reinvestigation of the structure of PdS,” *Acta Crystallographica,* vol. C41, pp. 1829-1830, 1985.

[14] I. P. Laputina, and A D. Genkin , “ Minerals of the braggitevysotskite series,” *Izomorpizm Mineraly, Izdat. Nauka,* pp. 146-150, 1975.

[15] H J Brynard, J. P. R. De Villiers and E. A. Viljoen, “A mineralogicali nvest igat iono f the MerenskyR eef at theWestern, Platinum mine, near Marikana,” *South Africa. Economic. Geology,* vol. 71, pp. 1299-1307, 1976.

[16] J. S. I. Schwellnus, S. A. Hiemstra and E. Gasparrini, “The Merensky Reef at the Atok Platinum mine and its environs,” *Economic Geology,* vol. 71, pp. 249-260, 1976.

[17] A. Marmier, P.S. Ntoahae, P.E. Ngoepe, D.G. Pettifor and S.C. Parker , “Negative compressibility in platinum sulfide using density-functional theory,” *Physical Review B,* vol. 71, pp. 172102-1 - 172102-4, 2010.

[18] S. B. Tlali, B. A. Mathe, L. M. Kotane, F.R.L. Schoning, J.D. Comins, A.G. Every, H.M. Sithole, P.E. Ngoepe, and K.V. Wright, “Brillouin scattering studies and computational simulations of the elastic properties of pyrite (FeS2) at high temperatures,” *Physica Status Solidi,* vol. 1, pp. 3073 - 3076, 2004.

[19] “http://www.ndt-ed.org/EducationResource/CommunityCollege/Materials/Mechanical/Mechanical.htm,” [Online]. [Accessed 06 05 2013].

[20] S. Kazanc and S. Ozgen, “Pressure Effect on Phonon Frequencies in Some Transition Metals: A molecular Dynamics study,” *Physica B,* vol. 365, pp. 185-192, 2005.

[21] M. T. Yin and M. L. Cohen, “Microscopic Theory of the Phase Transformation and Lattice Dynamics of Si,” *Physical Review Letters,* vol. 45, pp. 1004-1007, 1980.

[22] I. Efthimiopoulos, K. Kunc, S. Karmakar, K. Syassen, M. Hanfland and G. Vajenine, “Structural Transformation and Vibrational Properties of BaO2,” *Physical Review B,* vol. 82, pp. 134125-1-134125-10, 2010.

[23] H. M. Sithole, P. E. Ngoepe, and K. Wright, “Atomistic simulation of the structure and elastic properties of pyrite (FeS2) as a function of pressure,” *Physics and Chemistry of Minerals ,* vol. 30, pp. 615-619, 2003.

[24] P. Hohenberg and W. Kohn, “Inhomogeneous electron gas,” *Physical Review,* vol. 136, pp. 864-871, 1964.

[25] W. Kohn and L.J. Sham, “Self-consistent equations including exchange and correlation

effects," *Physical Review A,* vol. 140, pp. 1133-1138 , 1964.

[26] E. Wimmer, A.J. Freeman, C.-L. Fu, P.-L. Cao, Chou and B. Delley, in K.F. Jensen and D.G. Truhlar , "Supercomputer research in chemistry and chemical engineering," *ACS symposium series,* vol. 353, pp. 49-68, 1987.

[27] L.H. Thomas , "The calculation of atomic field," *Mathematical Proceedings of the Cambridge Philosophical Society,* vol. 23 , pp. 542-548 , 1926.

[28] E. Fermi , "Statistical methods of investigating electrons in atoms," *Zeitschrift für physik hadrons and nuclei,* vol. 48, pp. 73-79, 1928.

[29] J. C. Slater, "A simplification of the Hartree-Fock method," *Physical Review,* vol. 81, pp. 385-390 , 1951.

[30] J.C. Slater, Quantum Theory of Molecules and Solids: The self-consistent field for molecules and solids., New York: McGraw-Hill , 1974.

[31] R. M. Martin , Electronic Structure: Basic Theory and Practical Methods, Cambridge, UK: Cambridge University Press, 2004.

[32] J. P. Perdew and A. Zunger, "Self-interaction correction to density-functional approximations for many-electron systems," *Physical Review B,* vol. 23, pp. 5048-5071, 1981.

[33] J.P. Perdew, K. Burke and M. Ernzerhof , " Generalized gradient approximation made simple," *Physical Review Letters,,* vol. 77 , pp. 3865-3868 , 1996.

[34] J.P. Perdew, J. A. Chevary, S. H. Vosko, K. A. Jackson, M. R. Pederson, D. J. Singh and C. Fiolhais, "Atoms molecules, solids and surfaces: applications of the generalized gradient approximation for exchange and correlation," *Physical Review B,* vol. 46, pp. 6671-6682, 1992.

[35] R. Lesar, Introduction to Computational Materiala Sciences: Fundamentals, UK: Cambridge University Press, 2013.

[36] M. L. Cohen and V. Heine, "The fitting of pseudopotentials to experimental data and their subsequent application," *Solid State Physics: Advances in Research and Application,* vol. 24, pp. 37-248, 1970.

[37] J. C. Phillips, "Energy-band interpolation scheme based on a pseudopontial," *Physical. Review,* vol. 112, pp. 685-695, 1958.

[38] M. T. Yin and M. L. Cohen, "Theory of ab initiopseudopotential calculatioms," *Physical. Review, B,* vol. 25, pp. 7403-7412, 1982.

[39] W. A. Harrison, Electronic Structure and the Properties of Solids, New York: San Francisco, 1980.

[40] D. J. Chadi and M.L. Cohen, “Special Points in the Brillouin zone,” *Physical. Review, B,* vol. 8, pp. 5747-5753, 1973.

[41] H.J. Monkhorst and J.D. Pack, “Special points for Brillouin-zone integration,” *Physical. Review. B ,* vol. 13, pp. 5188-5198, 1976.

[42] G. Kresse and J. Furthmueller, “Efficiency of ab-initio total energy calculations for metals and semiconductors using plane-wave basis set,” *Computational. Materials. Science,* vol. 6, pp. 15-50, 1996.

[43] G. Kresse, M. Marsman and J. Furthmuller, VASP the Giude, Vienna: Computational Physics, 2013.

[44] P. Pulay, “Convergence Acceleration of Iterative Sequences. The Case of SCF Iteration,” *Chemical Physics Letters,* vol. 73, pp. 393-398, 1980.

[45] C. G. Broyden, “A class of methods for solving nonlinear simultaneous equations,” *Journal of Computational Mathematics,* vol. 19, pp. 577-593, 1965.

[46] R. Car and M. Parrinello , “Unified Approach for Molecular Dynamics and Density. Functional Theory,” *Physical. Review. Letters,* vol. 55, pp. 2471-2474, 1985.

[47] D. Vanderbilt, “Soft self-consistent pseudopotentials in a generalized eigenvalue formalism,” *Physical. Review. B,* vol. 41, pp. 7892-7895, 1990.

[48] F. Schwabel, Advanced Quantum Mechanics, Germany: Springer, 2008.

[49] B. Arie, “http://www.wisegeek.com/in-physics-what-is-a-phonon.htm,” [Online]. [Accessed 22 05 2013].

[50] T. Garl, Ultrafat Dynamics of coherent optical phonons in Bismuth, Germany : Institute for Laser Physics, 2008.

[51] A. Cottrell, An introduction to Metallurgy, London: Edward Arnold, 1975.

[52] M. Born and K. Huang K, Dynamical Theory of Crystal Lattices, Amen House, London: Oxford: Clarendon, 1954.

[53] J. Wang, S. Yip, S. R. Phillpot and D. Wolf, “Crystal Instabilities at Finite Strain,” *Physical.Review. Letters ,* vol. 71, pp. 4182-4185, 1993.

[54] N. W. Ashcroft and N. D. Mermin, Solid State Physics, Holt-Saunders, Philadelphia:

International Editions, 1976.

[55] J. F. Nye, Physical Properties of Crystals, London: Clarendon, Oxford, 1957.

[56] P. Ravindran, L. Fast, P. A. Korzhavyi, B. Johansson, J. Willis, and O. Eriksson, “Density functional theory for calculation of elastic properties of orthorhombic crystals: Application to equation font face='verdana'TiSi 2 equation,” *Journal of applied physics,* vol. 84, pp. 4891-4904, 1998.

[57] D. Iotova, N. Kioussis, and S.P. Lim, “Electronic Structure and Elastic Constants of the Ni3 X (X = Mn, Al,Ga, Si, Ge) Intermetallics,” *Physical. Review. B ,* vol. 54, pp. 14413-14422, 1996.

[58] V. Milman and M. C. Warren, “Elastic properties of TiB2 and MgB2,” *Journal of Physics: Condensed Matter,* vol. 13, pp. 5585-5595, 2001.

[59] V. Milman and M. C. Warren, “Elasticity of hexagonal BeO,” *Journal of Physics: Condensed Matter,* vol. 13, pp. 241-245, 2001.

[60] V. Milman, B.Winkler and M. I. J. Probert, “Stiffness and thermal expansion of ZrB2: an ab initio study,” *Journal of Physics: Condensed Matter,* vol. 17, p. 2233–2241, 2005.

[61] O. Beckstein, J. E. Klepeis, G. L. W. Hart and O. Pankratov, “First principles elastic constants and electronic structure of α-Pt2Si and PtSi,” *Physical. Review, B,* vol. 63, pp. 134112-134125, 2001.

[62] “http://www.nano-ou.net/files/3D%20Density%20of%20States.doc,” [Online]. [Accessed 15 05 2013].

[63] J. D. Joannopoulos and M. L. Cohen, “New insight into the optical properties of amorphous Ge and Si,” *Solid State Communications,* pp. 1115-1118, 1973.

[64] R. A. Evarestov and V. A. Lovchikov, “Special points of the Brillioun zone and their uses in the solid state theory,” *Physica status solidi B,* pp. 9-40, 1983.

[65] J. D. C. a. S. R. Hall, “The crystal structure of braggite, (Pt, Pd, Ni)S,” *Acta Crystallographica Section B,* pp. 1446-1451, 1973.

[66] P. Giannozzi, S. de Gironcoli, P. Pavone and S. Baroni, “Ab initio calculation of phonon dispersions in semiconductors,” *Physical. Review. B,* vol. 43, pp. 7231-7243, 1991.

[67] I. J. Ferrer, P. Díaz-Chao, A. Pascual, and C. Sánchez, “An Investigation on Palladium Sulphide (PdS) Thin Films as a Photovoltaic Material,” *Thin Solid Films,* vol. 515, p. 5783–5786, 2007.

[68] J. C. W. Folmer, J. A. Turner and B. A. Parkinson, “Palladium Chalcogenide and Pnictide Semiconductors and Their Photoelectrochemical Behavior,” *Journal of Solid State Chemistry,* vol. 68, pp. 28-37, 1987.

[69] S. Dey and V. K. Jain, “ Platinum Group Metal Chalcogenides,” *Platinum Metals Review,* vol. 48, pp. 16-29, 2004.